

# Higher-Order Corrections in Extended Higgs Sectors

Zur Erlangung des akademischen Grades eines  
DOKTORS DER NATURWISSENSCHAFTEN  
von der Fakultät für Physik des  
Karlsruher Instituts für Technologie (KIT)

genehmigte

DISSERTATION

von

Dipl.-Phys. Hanna Ziesche  
aus Pforzheim

Tag der mündlichen Prüfung: 21. Oktober 2016

Referentin: Prof. Dr. Margarete Mühlleitner

Korreferent: Prof. Dr. Rui Santos



This document is licensed under the Creative Commons Attribution – Share Alike 3.0 DE License (CC BY-SA 3.0 DE): <http://creativecommons.org/licenses/by-sa/3.0/de/>

# To my parents



## Abstract

Many questions left unanswered by the Standard Model (SM) of particle physics call for the investigation of models beyond the SM (BSM). These models often feature an extended Higgs sector. In this thesis we study higher-order corrections within the enlarged Higgs sectors of two specific extensions of the SM.

First we deal with the Higgs sector of the Two-Higgs-Doublet Model (2HDM). The focus is on the development of a renormalization scheme for three 2HDM-specific parameters, the mixing angles  $\alpha$  and  $\beta$  as well as the soft- $Z_2$ -breaking parameter  $m_{12}^2$ . In our study we aim for a renormalization scheme that is at the same time gauge independent, process independent and numerically stable. We discuss the significance of the treatment of the tadpoles for the issue of gauge dependence and present a dedicated study of numerical stability.

Afterwards, we turn to the complex Next-to-Minimal-Supersymmetric Standard Model (NMSSM) and calculate the corrections of  $\mathcal{O}(\alpha_t\alpha_s)$  to the trilinear Higgs self-couplings within its framework. The calculation is performed using the Feynman diagrammatic approach in the gaugeless limit and in the approximation of vanishing external momentum. In the subsequent numerical study, we address the remaining theoretical uncertainty due to missing higher-order corrections and the convergence of the perturbative series. We also consider Higgs-to-Higgs decays and discuss the limitations of the used approximations in this context.

## Zusammenfassung

Viele Fragen, die das Standardmodell (SM) der Teilchenphysik unbeantwortet lässt, verlangen nach einer Untersuchung von Modellen jenseits des SM. Diese Modelle weisen oft einen erweiterten Higgs-Sektor auf. In dieser Arbeit untersuchen wir Korrekturen höherer Ordnung in den vergrößerten Higgs-Sektoren zweier bestimmter Erweiterungen des SM.

Zunächst befassen wir uns mit dem Zwei-Higgs-Dublett Modell (2HDM). Der Schwerpunkt liegt auf der Entwicklung eines Renormierungs-Schemas für drei 2HDM-spezifische Parameter, die beiden Mischungswinkel  $\alpha$  und  $\beta$  sowie den soft- $Z_2$ -brechenden Parameter  $m_{12}^2$ . Hierbei streben wir nach einem Renormierungs-Schema, welches gleichzeitig eichunabhängig, prozessunabhängig und numerisch stabil ist. Wir diskutieren die Bedeutung der Behandlung der Tadpoles für die Thematik der Eichabhängigkeit und führen eine Untersuchung der numerischen Stabilität durch.

Anschließend wenden wir uns dem komplexen Nächst-Minimalen Supersymmetrischen Standardmodell (NMSSM) zu und berechnen die Korrekturen der Ordnung  $\mathcal{O}(\alpha_t\alpha_s)$  zu den trilinearen Higgs-Selbstkopplungen. Die Rechnung wird im Rahmen des Feynman-diagrammatischen Ansatzes im eichfreien Grenzfall und in der Näherung verschwindender äußerer Impulse durchgeführt. In der sich anschließenden numerischen Untersuchung diskutieren wir die theoretische Unsicherheit aufgrund fehlender Korrekturen höherer Ordnung und die Konvergenz der Störreihe. Außerdem betrachten wir Higgs-nach-Higgs Zerfälle und thematisieren die Grenzen der verwendeten Näherungen in diesem Zusammenhang.



# Contents

<b>1. Introduction</b>	<b>11</b>
<b>I. Theoretical Foundations</b>	<b>15</b>
<b>2. The Standard Model of Particle Physics and Models beyond</b>	<b>17</b>
2.1. The Standard Model of Particle Physics and its Shortcomings . . . . .	17
2.2. Supersymmetry . . . . .	20
2.3. Two Higgs Doublet Models . . . . .	22
<b>3. Selected Concepts of Perturbative QFT</b>	<b>25</b>
3.1. Regularization and Renormalization . . . . .	25
3.1.1. Regularization . . . . .	26
3.1.2. Renormalization . . . . .	27
3.2. LSZ Reduction, the $\mathcal{S}$ -matrix and Physical Observables . . . . .	28
3.2.1. LSZ Reduction and the $\mathcal{S}$ -matrix . . . . .	28
3.2.2. The Invariant Matrix Element $\mathcal{A}$ and Physical Observables . . . . .	31
3.3. Gauge Dependence and the Pinch Technique . . . . .	34
<b>II. Gauge-Independent Renormalization of the 2HDM</b>	<b>37</b>
<b>4. Outline of Part II</b>	<b>39</b>
<b>5. Introduction to the 2HDM</b>	<b>41</b>
5.1. The Lagrangian of the 2HDM . . . . .	41
5.2. The Scalar Potential . . . . .	42
5.3. Independent Parameters of the Scalar Potential . . . . .	45
5.4. The Yukawa Sector . . . . .	46
5.5. The Gauge Fixing and the Ghost Sector . . . . .	47
<b>6. General Remarks on the Renormalization of the 2HDM</b>	<b>49</b>
6.1. Renormalization of Mixing Fields . . . . .	49
6.2. Introduction of Counterterms . . . . .	52
6.3. Treatment of the Tadpoles . . . . .	54
6.4. On-Shell Renormalization of the Scalar Masses and Fields . . . . .	56
6.5. On-Shell Renormalization of the Gauge and Fermion Sector . . . . .	58
6.6. Renormalization of $\alpha$ and $\beta$ . . . . .	58
6.7. Renormalization of $m_{12}^2$ . . . . .	59
<b>7. Renormalization in Tadpole Scheme I</b>	<b>61</b>
7.1. On-Shell Renormalization of the Scalar Sector in Tadpole Scheme I . . . . .	61

7.2. On-Shell Renormalization of the Gauge Sector in Tadpole Scheme I . . . . .	63
7.3. On-Shell Renormalization of the Fermion Sector in Tadpole Scheme I . . . . .	64
7.4. A Process-Independent Definition of $\alpha$ and $\beta$ and its Gauge Dependence . . . . .	64
7.4.1. $\alpha$ and $\beta$ in the KOSY Scheme . . . . .	65
7.4.2. The Origin of the Gauge Dependence . . . . .	66
<b>8. Renormalization in Tadpole Scheme II</b>	<b>69</b>
8.1. Tadpole Renormalization as the Origin of Gauge Dependence . . . . .	69
8.2. Implementation of Tadpole Scheme II in the Framework of the 2HDM . . . . .	72
8.3. Transformation of the On-Shell Counterterms in Tadpole Scheme II . . . . .	77
8.4. Transformation of the Couplings in Tadpole Scheme II . . . . .	79
8.5. Process-Independent Definition of $\alpha$ and $\beta$ in Tadpole Scheme II . . . . .	81
<b>9. A Process-Dependent Scheme for <math>\alpha</math> and <math>\beta</math></b>	<b>85</b>
9.1. Process Selection . . . . .	85
9.2. Determination of $\delta\beta$ from $A_0 \rightarrow \tau\tau$ . . . . .	86
9.3. Determination of $\delta\alpha$ from $H \rightarrow \tau\tau$ . . . . .	88
9.4. Discussion of the Gauge Dependence of $\delta\alpha$ and $\delta\beta$ . . . . .	88
9.5. $\overline{\text{MS}}$ Definition of $\delta\alpha$ and $\delta\beta$ . . . . .	89
<b>10. Different Renormalization Schemes for <math>m_{12}^2</math></b>	<b>91</b>
10.1. $\overline{\text{MS}}$ Definition of $\delta m_{12}^2$ . . . . .	91
10.2. Process-Dependent Definition of $\delta m_{12}^2$ . . . . .	92
<b>11. Overview of the Discussed Renormalization Schemes</b>	<b>95</b>
<b>12. Investigation of Numerical Stability</b>	<b>97</b>
12.1. Tools and Software . . . . .	97
12.2. Input Parameter Sets . . . . .	98
12.3. Numerical Analysis of the Decay $H^\pm \rightarrow W^\pm h$ . . . . .	100
12.4. Numerical Analysis of the Decay $H \rightarrow ZZ$ . . . . .	104
12.5. Numerical Analysis of the Decay $H \rightarrow hh$ . . . . .	106
<b>13. Conclusion of Part II</b>	<b>113</b>
<b>III. The <math>\mathcal{O}(\alpha_t\alpha_s)</math> Corrections to the Trilinear Higgs Self-Couplings in the Complex NMSSM</b>	<b>115</b>
<b>14. Outline of Part III</b>	<b>117</b>
<b>15. Preliminaries on Used Approximations and the Structure of the Corrections</b>	<b>121</b>
<b>16. Introduction to the NMSSM</b>	<b>123</b>
16.1. Motivations for and Particle Content of the NMSSM . . . . .	123
16.2. The Lagrangian of the NMSSM . . . . .	127
16.3. The NMSSM Higgs Potential . . . . .	128
16.4. Independent Parameters of the NMSSM Higgs Potential . . . . .	131
16.5. The Stop Sector of the NMSSM . . . . .	132
<b>17. Renormalization</b>	<b>133</b>
17.1. Renormalization of the Top-Stop Sector . . . . .	133
17.2. Wave Function Renormalization . . . . .	135

17.3. Renormalization of the Higgs Potential . . . . .	136
<b>18. The Corrections of <math>\mathcal{O}(\alpha_t)</math></b>	<b>139</b>
18.1. The Effective Potential Approach . . . . .	140
18.2. The Virtual $\mathcal{O}(\alpha_t)$ Corrections to the Trilinear Higgs Self-Couplings . . . . .	142
18.3. The Counterterm of $\mathcal{O}(\alpha_t)$ . . . . .	143
<b>19. The Corrections of <math>\mathcal{O}(\alpha_t\alpha_s)</math></b>	<b>145</b>
19.1. The Genuine Two-Loop Corrections to the Trilinear Higgs Self-Couplings . . . . .	145
19.2. Diagrams with Counterterms from the Top-Stop Sector . . . . .	147
19.3. The Counterterm of $\mathcal{O}(\alpha_t\alpha_s)$ . . . . .	148
<b>20. Numerical Analysis of the Corrections</b>	<b>149</b>
20.1. Different Mass Bases . . . . .	149
20.2. Software Tools and Numerical Setup . . . . .	151
20.3. Comparison between Full One-Loop-Corrected and Effective $\mathcal{O}(\alpha_t)$ Couplings . . . . .	154
20.4. Numerical Analysis of the $\mathcal{O}(\alpha_t\alpha_s)$ Corrections . . . . .	157
20.5. Higgs-to-Higgs Decays . . . . .	162
<b>21. Conclusion of Part III</b>	<b>165</b>
<b>22. Conclusion</b>	<b>169</b>
<b>A. Parameters and Couplings</b>	<b>171</b>
A.1. Shifts in the 2HDM Parameters . . . . .	171
A.2. Couplings of the 2HDM . . . . .	172
A.3. Trilinear Higgs Self-Couplings of the NMSSM at Tree Level . . . . .	173
<b>B. Explicit Expressions for Selected Loop Corrections</b>	<b>175</b>
B.1. The Width $\Gamma_{H^+ \rightarrow W^+h}^{\mathcal{O}(1\text{-loop})}$ . . . . .	175
B.2. Trilinear Higgs Self-Couplings of the NMSSM at $\mathcal{O}(\alpha_t)$ . . . . .	176
B.3. The Coupling Counterterms $\Delta\lambda_{\phi_i\phi_j\phi_k}^{\mathcal{O}(\alpha_t),\text{ct}}$ and $\Delta\lambda_{\phi_i\phi_j\phi_k}^{\mathcal{O}(\alpha_t\alpha_s),\text{ct}}$ . . . . .	177
<b>C. Loop Functions</b>	<b>181</b>
C.1. Reduction of the Scalar Loop Functions . . . . .	181
C.2. Splitting of Gauge-Dependent $A_0$ and $B_0$ Functions . . . . .	183
<b>D. RGEs and Approximations</b>	<b>185</b>
D.1. The Running of $m_t^{\overline{\text{DR}}}$ . . . . .	185
D.2. Approximation of the Two-Loop RGEs for the Parameters of the NMSSM Higgs Sector . . . . .	186
<b>Acknowledgments</b>	<b>189</b>



# CHAPTER 1

---

## Introduction

---

*“Similarly, when Charles Darwin named his book “On the Origin of Species”, he was going far beyond taxonomy by giving the logical explanation for the diversity of animals in nature. What is needed in physics is a counterpart of this book, to be called “On the Origin of Symmetry”, which explains the reasons why certain symmetries are found in nature .”*

Michio Kaku

(Hyperspace, A Scientific Odyssey through parallel universes, time warps, and the tenth dimension)

For decades the main objective of numerous experimental collaborations and facilities, among which the Large Electron Positron collider (LEP), the Tevatron and the Large Hadron Collider (LHC), has been the discovery of all particles predicted by the Standard Model (SM) of particle physics [1–9] as well as a precise determination of their properties. Countless experimental investigations have contributed to the effort of testing and approving the predictions of the SM with high accuracy, the positive results of which have established the SM as the foundation of modern elementary particle physics.

However, despite its tremendous success in multitudinous tests, the SM leaves unanswered many questions concerning fundamental properties of our universe and can therefore not be considered as the ultimate description of nature. On the one hand it fails in explaining various experimental observations like e.g. dark matter, on the other hand it is plagued by theoretical shortcomings, one of which is constituted by the hierarchy problem.

Hence the discovery of the Higgs boson in July 2012 [10, 11] is of two-fold interest. While up to now all measurements of its properties and couplings are in good agreement with the SM expectations and thus with it being the long-sought last missing piece of the SM [12–15], the Higgs boson might as well be the harbinger of new physics.

Many extensions of the SM, striving to procure solutions to its deficiencies, feature an enlarged Higgs sector. Therefore, the particle discovered at the LHC could serve as the entrance to these models beyond the SM (BSM).

One of the simplest possibilities of constructing a model exhibiting an augmented Higgs sector is to add one additional complex scalar doublet to the particle content of the SM. The

resulting models are known as Two Higgs Doublet Models (2HDMs) [16–18]. Apart from being capable of solving some of the problems the SM is fraught with, 2HDMs show an interesting and rich phenomenology. Furthermore, many more complicated extensions of the SM incorporate a 2HDM as Higgs sector, which adds to the attractiveness of 2HDMs.

Perhaps the most prominent representative of models comprising a 2HDM is the Minimal Supersymmetric Standard Model (MSSM). As the name suggests, the MSSM constitutes the simplest realization of a supersymmetric (SUSY) [19–29] extension of the SM. Within the framework of SUSY, a symmetry between fermionic and bosonic degrees of freedom is established through the graduation of the Poincaré algebra of space-time symmetry by anti-commuting operators. In its simplest realization, this symmetry requires the extension of the SM Higgs sector by a second complex scalar doublet as well as the addition of one supersymmetric partner for each SM degree of freedom to the particle content of the SM. Although the MSSM is the most economic realization of SUSY, which at the same time provides solutions to many of the problems of the SM, it is also afflicted with certain shortcomings, like the so-called  $\mu$ -problem or the issue of fine-tuning. These can be overcome by the introduction of one further complex scalar singlet and its SUSY partner to the particle spectrum of the MSSM, resulting in the Next-to-Minimal Supersymmetric Standard Model, the NMSSM [30–37].

An extension of the SM Higgs sector can become manifest in different ways. On the one hand, the additional Higgs bosons might themselves be detected. On the other hand, the existence of extra Higgs bosons may result in an alteration of observables and of the couplings of SM particles to the Higgs boson already discovered. As the measurements of the Higgs properties and couplings at the LHC seem to converge to the SM expectations, a detection of possible deviations requires both accurate measurements and precise predictions. Hence, the importance of higher-order calculations concerning BSM Higgs sectors is growing. With this thesis, we intend to contribute to the objective of providing higher-order predictions for the Higgs sectors of BSM models, concentrating on two specific extensions, the 2HDM and the NMSSM.

The thesis is subdivided into three parts. Part I has the purpose of introducing the most important notions and concepts, which will be dealt with in this work. We will begin in Ch. 2 with a brief introduction to the SM and a discussion of its limitations. Subsequently, we will present the basic ideas and motivations for SUSY and the 2HDM. Ch. 3 will familiarize the reader with selected fundamental concepts of perturbative quantum field theory (QFT). We will concisely elucidate the subject of regularization and renormalization, introduce the notion of the  $\mathcal{S}$ -matrix and the LSZ formalism and explain the construction of physical observables. Moreover, we will touch on the topic of gauge fixing and briefly highlight the principle of the pinch technique (PT).

Part II of this thesis is devoted to the development of a complete and suitable renormalization scheme for the 2HDM. A consistent renormalization scheme, i.e. a prescription of treating divergences appearing in loop calculations, is an important prerequisite for higher-order predictions. As the efforts to establish a complete renormalization scheme for the 2HDM have been scarce in the past and to our knowledge all schemes proposed so far do either not strive for completeness [38, 39] or are plagued with gauge dependences [40], a thorough investigation of this topic is essential<sup>1</sup>. Our research will be guided by the three criteria of a good renormalization scheme, given by gauge independence, process independence and numerical stability. We will in particular focus on the formulation of renormalization prescriptions for the three 2HDM specific parameters, the mixing angles  $\alpha$  and  $\beta$  and the soft- $Z_2$ -breaking parameter  $m_{12}^2$ . Concerning the subject of gauge dependence, the treatment of the tadpoles will turn out to be crucial. Therefore, we will examine in detail two different tadpole schemes, i.e. two approaches to dealing with the tadpoles. While the first scheme requires the introduction of

<sup>1</sup>Only recently, after the publication of our own results, the subject was also addressed in Ref. [41].

tadpole counterterms to comply with the minimum conditions of the 2HDM Higgs potential to all orders, no such counterterms are necessary within the second tadpole scheme. Instead, tadpole diagrams have to be taken into account explicitly in all Green's functions within the second approach.

We will explore various renormalization schemes for the three 2HDM specific parameters within both tadpole schemes and investigate their capability of satisfying the three guiding criteria for a good renormalization scheme. In order to study numerical stability we will consider three test processes and analyze the behaviour of the radiative corrections within the different proposed schemes.

As we will show, a definition of the angular counterterms that is at the same time process independent, numerically stable and leads to gauge-independent expressions for physical observables is possible only within the framework of the second tadpole scheme.

The results of this part have been published in Refs. [42] and [43].

In Part III we will present the calculation of the corrections of  $\mathcal{O}(\alpha_t\alpha_s)$  to the trilinear Higgs self-couplings in the complex NMSSM. We will adopt the Feynman diagrammatic approach and work in the approximation of vanishing external momentum and in the gaugeless limit. Trilinear Higgs self-couplings play an important role both in the SM and in BSM Higgs sectors. They enter interesting observables and processes like Higgs-to-Higgs decays and Higgs pair production and their determination would be an important step towards a better understanding of the mechanism of EWSB. Moreover, they are closely connected to the masses of the Higgs bosons, present in the respective Higgs sectors, since both masses and trilinear self-couplings derive from the Higgs potential. For that reason, a consistent treatment of the NMSSM Higgs sector requires the corrections to both, masses and trilinear couplings, to be of the same order. As the masses are known up to  $\mathcal{O}(\alpha_t\alpha_s)$  in the complex NMSSM [44]<sup>2</sup>, while the trilinear couplings have been determined only to full one-loop order [46], the corrections presented in this thesis constitute a missing ingredient for consistent higher-order predictions. The determination of the  $\mathcal{O}(\alpha_t\alpha_s)$  corrections entails the reduction of two-loop integrals to master integrals as well as the renormalization of the NMSSM Higgs sector at  $\mathcal{O}(\alpha_t\alpha_s)$  and of the top-stop sector at  $\mathcal{O}(\alpha_s)$ . All calculational steps will be exhibited in detail.

Furthermore, we will also present the calculation of the corrections of  $\mathcal{O}(\alpha_t)$ , subject to the same approximations as those of  $\mathcal{O}(\alpha_t\alpha_s)$ , i.e. in the gaugeless limit and at vanishing external momentum, which will allow us a consistent definition of effective trilinear Higgs self-couplings at  $\mathcal{O}(\alpha_t\alpha_s)$ . In addition, a comparison of the  $\mathcal{O}(\alpha_t)$  corrections to the available full one-loop corrections will give us access to an estimation of the goodness of our approximations.

We will close with the numerical analysis of the calculated corrections, discussing the convergence of the perturbative expansion, the theoretical uncertainty due to missing higher orders and the impact of the corrections on Higgs-to-Higgs decays.

The results of this part have been published in [47].

<sup>2</sup>Since recently also corrections beyond  $\mathcal{O}(\alpha_t\alpha_s)$  are available, published in Ref. [45].



**Part I.**

**Theoretical Foundations**



---

## The Standard Model of Particle Physics and Models beyond

---

In this chapter, we introduce and illustrate three important models of particle physics, which this thesis will build upon and be concerned with. Sec. 2.1 is devoted to the *Standard Model* (SM) of particle physics, which can be considered as *the* basis of current elementary particle physics. After a presentation of its particle content and underlying symmetries, we will discuss its limitations. Subsequently, we will introduce two possible extensions of the SM, which are capable of solving some of the problems the SM is plagued with. First, in Sec. 2.2, we will outline the concept of *Supersymmetry* (SUSY) and advocate its virtues. In doing so we will heavily draw on Ref. [48], an excellent introduction into the subject. Afterwards, we will present and motivate *2-Higgs-Doublet Models* (2HDMs), the second type of SM extensions we will study in detail in this thesis.

### 2.1. The Standard Model of Particle Physics and its Shortcomings

The Standard Model of particle physics [1–9] constitutes the foundation of modern elementary particle theory. Its origins date back to the early 1960s, when Glashow succeeded in unifying the electromagnetic and weak interactions [1], and it was finalized from the theoretical side in the mid-1970s, when the theory of strong interactions assumed its current formulation [3, 9]. Subsequent experimental discoveries of particles predicted by the SM, like the detection of the massive weak gauge bosons in 1983 by the UA1 and UA2 collaborations at CERN<sup>1</sup> or of the top quark in 1995 at the Tevatron, have increased its credibility and manifested its role as the fundament of modern particle physics. Upon the discovery of the Higgs boson at the LHC in 2012 [10, 11], the SM can be considered as complete also from the experimental side. The SM is a relativistic quantum field theory (QFT) based on the principles of Lorentz invariance and local gauge invariance. It comprises three out of the four known fundamental forces in nature, namely the weak, the strong and the electromagnetic interaction, in terms of a non-abelian renormalizable gauge theory with an underlying  $SU(3)_C \otimes SU(2)_L \otimes U(1)_Y$  symmetry group. Gravity in turn, the fourth fundamental force, has up to now resisted any attempt of a consistent formulation in the form of a QFT. However, due to its weakness at the subatomic level, our lack of understanding the basic principles of this force does not have

---

<sup>1</sup>The European Organization for Nuclear Research.

type	field	$(SU(3)_C \otimes SU(2)_L \otimes U(1)_Y)$
quarks	$Q_L = (u_L, d_L)^T$	$(\mathbf{3}, \mathbf{2}, \frac{1}{6})$
	$u_R$	$(\bar{\mathbf{3}}, \mathbf{1}, -\frac{2}{3})$
	$d_R$	$(\bar{\mathbf{3}}, \mathbf{1}, \frac{1}{3})$
leptons	$L_L = (\nu_L, e_L)^T$	$(\mathbf{1}, \mathbf{2}, -\frac{1}{2})$
	$e_R$	$(\mathbf{1}, \mathbf{1}, 1)$
Higgs	$\Phi = (\phi^+, \phi^0)^T$	$(\mathbf{1}, \mathbf{2}, \frac{1}{2})$
gluon	$g$	$(\mathbf{8}, \mathbf{1}, 0)$
$W$ boson	$W = (W_1, W_2, W_3)^T$	$(\mathbf{1}, \mathbf{3}, 0)$
$B$ boson	$B$	$(\mathbf{1}, \mathbf{1}, 0)$

**Table 2.1.:** Matter particles and force carriers of the SM and their transformation properties under the underlying gauge groups. The fermions come in three generations.  $u$  stands collectively for  $u, c, t$ , and  $d$  for  $d, s, b$  and  $e$  for  $e, \mu, \tau$ . The gauge bosons are given in the symmetric phase, i.e. before EWSB.

practical consequences for the accuracy of our predictions on elementary particles and their interactions. Each of the other three fundamental forces is represented within the SM via one of the underlying gauge groups. Quantum Chromodynamics, the theory of the strong interaction, is based on the group  $SU(3)_C$  and incorporates eight gluons as elementary force carriers. The fundamental charge characterizing the strong interaction is called color and comes in three different variants. All particles carrying color can take part in strong interactions. The electromagnetic and weak interaction, combined into the electroweak interaction, are described by the product  $SU(2)_L \otimes U(1)_Y$  and the corresponding force carriers are given by the  $SU(2)$ -triplet  $W = (W_1, W_2, W_3)$  and the  $U(1)$ -singlet field  $B$ . This symmetry is broken down spontaneously to  $U(1)_{\text{em}}$ , the group of the electromagnetic interactions, via Electroweak Symmetry Breaking (EWSB), which will be explained below. After EWSB the electromagnetic force is mediated by the photon, coupling to the electric charge of the particles, whereas the weak interactions are conveyed by the weak gauge bosons, the  $W$  and the  $Z$  boson. The fundamental charge of the weak interaction is the weak isospin  $I_w$ . All force mediators of the SM exhibit a spin quantum number of one and therefore belong to the group of bosons, i.e. the group of particles with integer spin. Due to their role in gauge theory, they are called *gauge bosons*.

Apart from these force carriers, mediating the basic interactions of nature, the SM comprises the quarks and leptons, the fundamental constituents of matter. Unlike the gauge bosons, all matter particles hold a spin quantum number  $1/2$  and thus belong to the group of *fermions*, defined as particles with half-integral spin. As such they are represented by *spinors*, which consist of a left- and a right-handed component, called *Weyl fermions*.

The matter particles can be characterized by their transformation properties w.r.t. the underlying symmetry groups of the SM. Conventionally this is achieved by specifying their representation with respect to the  $SU(3)_C$  and the  $SU(2)_L$  gauge group as well as their hypercharge  $Y$ , defined as

$$Q_{\text{em}} = I_w^3 + Y, \quad (2.1)$$

where  $Q_{\text{em}}$  denotes the electric charge of the particle and  $I_w^3$  the third component of the weak isospin. The corresponding classification of all SM particles can be found in Tab. 2.1. Both, the quarks and the leptons can be grouped into three generations such that the members of

the different generations feature identical quantum numbers but differ in mass.

All quarks are charged under  $SU(3)_C$  and therefore take part in the strong interaction. In addition, they carry the electric charge  $Q_{\text{em}} = 2/3$  or  $Q_{\text{em}} = -1/3$ , where the first case applies to the *up-type* quarks (*up, charm, top*) and the second to the *down-type* quarks (*down, strange, bottom*). Due to their charge, quarks participate in the electromagnetic interaction. Finally, the weak force only couples to the left-handed components of the quark fields. According to their transformation properties, these are grouped into  $SU(2)_L$  doublets consisting of one up-type and one down-type quark, whereas the right-handed field components constitute singlets under  $SU(2)_L$ .

In contrast to the quarks, the leptons of the SM do not carry color charge and therefore transform trivially under  $SU(3)_C$ . Their left-handed components form doublets under  $SU(2)_L$ , the right-handed fields do not take part in the weak interaction and hence are represented by  $SU(2)_L$ -singlets. The lower components of the  $SU(2)_L$  doublets are formed by charged leptons ( $e, \mu, \tau$ ) with  $Q_{\text{em}} = -1$ , whereas the upper components contain neutral leptons, the *neutrinos* ( $\nu_e, \nu_\mu, \nu_\tau$ ). According to the original formulation of the SM, the neutrinos are strictly massless and only occur as left-handed fields. However, the observation of neutrino oscillations constitutes an unambiguous evidence of the fact, that neutrinos have to possess a non-vanishing mass. While the true nature of the neutrino is a subject of current research, we will not explicate this any further and only want to point out that the SM can in principle be extended to incorporate right-handed and massive neutrinos.

In the SM, the mechanism of EWSB, alluded to above, is realized by the introduction of a scalar  $SU(2)_L$  doublet, which acquires a non-vanishing vacuum expectation value (vev). Apart from breaking the  $SU(2)_L \otimes U(1)_Y$  gauge group spontaneously down to  $U(1)_{\text{em}}$ , this mechanism, called Higgs mechanism [4], generates masses for the fermions and the  $W$  and  $Z$ -bosons in a gauge-invariant way. As a direct mass term for the SM fermions and gauge bosons would violate the principle of gauge invariance, the Higgs mechanism is indispensable for the validity of the SM. The Higgs boson is the directly observable physical remnant of this process and therefore its discovery serves as a first step towards the validation of the Higgs mechanism.

Currently, the properties of the Higgs boson, in particular its couplings to the other SM particles, are under thorough investigation at the LHC. So far, all measurements are compatible with the Higgs boson predicted by the SM [12–15]. Nevertheless, experimental data still leave room for deviations. From a theoretical point of view, there is no reason, why the scalar sector of the particle spectrum should be realized in the minimal form as proposed by the SM and not attain a more complicated structure. Indeed, many extensions of the SM predict an enlarged Higgs sector, comprising several scalar doublets, singlets or even higher representations of  $SU(2)_L$ . Some of these extensions will be presented in the following sections and studied in more detail in the course of this thesis.

In spite of its success in describing and predicting most phenomena of elementary particle physics to high accuracy and although it has excelled in numerous high precision experiments, the SM is not capable of explaining all aspects of nature. Furthermore it is plagued by some theoretical issues.

Apart from the fact, that it lacks a description of gravity, the SM also does not offer an explanation for dark matter and dark energy. Cosmological observations have revealed, that these forms of energy account for 26.8% or 68.3%, respectively, of the total amount of the energy content of the universe, whereas the ordinary matter, described by the SM, only represents about 4.9% [49].

Moreover, the SM fails in providing a source of CP violation that is strong enough to explain the dominance of matter over antimatter we observe in today's universe. The only manifestation of CP violation present in the SM, the complex phase of the CKM matrix, is not sufficient

to fulfill one of the three Sakharov conditions, prerequisites for a successful baryogenesis [50]. Besides these obvious deficiencies, the SM is flawed by some weaknesses which are of a more theoretical nature. For instance, within the SM, the three fundamental forces, described by gauge theories, cannot be unified. Although their gauge couplings approach each other when they are evolved to high energy scales, they do not intersect in a single point, as required for a description of the three forces by *one* originating force.

Another frequently discussed issue is the *hierarchy problem*. This phrase refers to fact that, unlike the masses of fermions and gauge boson, which are protected by chirality or gauge symmetry, the mass of an elementary scalar, as the SM Higgs boson, is subject to huge radiative corrections. These result from virtual particles that are constantly created out of and re-annihilated back into the vacuum. In perturbative QFT these virtual processes are described by loop-corrections, which are mathematically expressed in terms of integrals over the phase space of the virtual particles. Often these integrals exhibit divergences in the region of high loop momenta (called the ultraviolet (UV) region) and one possibility to regularize these is to introduce a hard *cut-off* scale  $\Lambda_{UV}$  for the integration (cf. Subs. 3.1.1). Proceeding in this way for  $\Delta m_h^2$ , the radiative corrections to the mass of the Higgs boson, leads to terms which are quadratic in  $\Lambda_{UV}$ . The dominant contribution, evoked by loops containing the top quark, is given by

$$\Delta m_h^2 = -\frac{y_t^2}{8\pi} [\Lambda_{UV}^2 + \dots] + \dots \quad (2.2)$$

Here  $y_t$  denotes the top Yukawa coupling, i.e. the coupling of the top quark to the Higgs boson, and the dots inside the brackets represent terms proportional to  $m_t^2$ , the top mass squared, which grow at most logarithmically in  $\Lambda_{UV}$ . Those outside the brackets stand for the contributions of other particles. Adopting the view that the SM is valid up to the Planck scale, i.e. equating  $\Lambda_{UV} = M_{Pl} \sim 10^{18}$  GeV, these huge corrections require an enormous amount of *fine-tuning*, to adjust the counterterm  $\delta m_H^2$  such that the Higgs mass attains the measured value of  $m_h \approx 125$  GeV [51].

Even if one refrains from any physical interpretation of  $\Lambda_{UV}$ , the hierarchy problem remains. Any heavy particle  $S$  of mass  $m_S$  will lead to a term in  $\Delta m_h^2$ , which is proportional to  $m_S^2$ , even if  $S$  couples to the Higgs boson only indirectly [48]. Very generically the corresponding contributions have the form

$$\Delta m_h^2 = a \left[ \Lambda_{UV}^2 - b m_S^2 \ln \left( \frac{\Lambda_{UV}}{m_S} \right) + \dots \right] + \dots, \quad (2.3)$$

where  $a$  and  $b$  denote combinations of couplings, group theory and loop factors. Hence, the Higgs mass is sensitive to any new physics at an arbitrarily high scale and receives corrections from the masses of the heaviest existing particles. Due to experimental evidence of phenomena the SM fails to describe, it appears ill-advised to deny the existence of any high-mass particles that couple (even if only indirectly) to the Higgs boson. These particles, however, immediately necessitate fine-tuning of the Higgs mass counterterm  $\delta m_h^2$ .

All these deficiencies clearly show that the SM cannot be the ultimate description of nature. Striving for a more profound understanding of the universe, particle physicists are thus driven to embark on journeys to new shores and study models beyond the SM (BSM).

## 2.2. Supersymmetry

In the development of the SM, symmetries have turned out to be a valuable guideline. Therefore, it appears promising to make use of this approved tool also in the development of

<sup>2</sup>The notion of a counterterms will be explained below in chapter 3.1, dealing with the subject of renormalization.

extensions to the SM. The principle of symmetry is brought to perfection in *Supersymmetry* (SUSY) [19–29], as within the framework of SUSY, the maximal non-trivial combination of symmetries, consistent with relativistic QFT, into one Lie superalgebra is realized. This is achieved by extending the Poincaré algebra of space-time symmetry through the introduction of anti-commuting spinorial generators  $Q$  and  $Q^\dagger$ , the so-called *supercharges*. By means of these fermionic operators, the restrictions of the Coleman-Mandula theorem [52] are circumvented and, in contradiction to the implication of this theorem, a non-trivial combination of internal symmetries with the space-time symmetries of the Poincaré algebra is accomplished. This is the essence of the Haag-Lopuszański-Sohnius theorem [53], which emphasizes that only the inclusion of SUSY leads to the maximal possible symmetry of a consistent QFT. Due to their fermionic nature, the operators  $Q$  and  $Q^\dagger$ , carrying spin  $1/2$ , turn bosonic states into fermionic states and vice versa

$$Q|\text{Boson}\rangle = |\text{Fermion}\rangle, \quad Q|\text{Fermion}\rangle = |\text{Boson}\rangle. \quad (2.4)$$

The single particle states emerging from one another via this relation are called *superpartners*. They are grouped together into a *supermultiplet*, i.e. an irreducible representation of the SUSY algebra. Since the operators  $Q$  and  $Q^\dagger$  commute with the generators of other internal symmetries, like gauge symmetries, all members of a supermultiplet share the same quantum numbers, apart from their spin. Moreover, the spinorial operators commute with  $-P^2$ , the squared mass operator, leading to mass degeneracy within the supermultiplets. Given the fact that up to date experimental evidence for any superpartner of an SM particle is still missing, SUSY cannot be manifest in nature but has to be broken in the accessible energy range. In order to prevent the loss of its endowments, the breaking of SUSY must be realized in a soft way, i.e. by the introduction of SUSY-violating terms of *positive* mass dimension into the Lagrangian. These only affect the masses of the SUSY particles and leave the SUSY relations between the couplings intact.

SUSY offers a solution to all pending issues of the SM discussed in the previous section. Maybe the most frequently discussed example is the natural emergence of a solution to the hierarchy problem. In SUSY every fermionic degree of freedom is accompanied by a bosonic one, sharing the same quantum numbers and, if SUSY is exact, the same mass. Due to the fact, that the contributions of fermionic and bosonic particles to  $\Delta m_h^2$ , as the one in Eq. (2.2), differ by a sign, the effects of two superpartners identically cancel, provided SUSY is unbroken. Taking into consideration, that SUSY has to be violated in nature, this cancellation is no longer exact. However, the quadratic dependence of  $m_h^2$  on an arbitrarily large scale is still precluded. Instead of Eq. (2.2) or Eq. (2.3),  $\Delta m_h^2$  now contains terms of the form

$$\begin{aligned} \Delta m_h^2 &= \frac{1}{8\pi^2} (\lambda - \lambda) \Lambda_{\text{UV}}^2 + m_{\text{soft}}^2 \left[ \frac{\lambda}{16\pi^2} \ln \left( \frac{\Lambda_{\text{UV}}}{m_{\text{soft}}} \right) + \dots \right] \\ &= m_{\text{soft}}^2 \left[ \frac{\lambda}{16\pi^2} \ln \left( \frac{\Lambda_{\text{UV}}}{m_{\text{soft}}} \right) + \dots \right], \end{aligned} \quad (2.5)$$

where  $\lambda$  represents a generic dimensionless coupling constant (e.g.  $y_t$ ) and  $m_{\text{soft}}$  denotes the soft-SUSY-breaking scale, above which SUSY is exact. Apparently, as long as  $m_{\text{soft}}$  is not too large ( $\lesssim 1\text{TeV}$ ), unnaturally huge contributions to  $\Delta m_h^2$  are prohibited and the hierarchy problem does not occur. A crucial prerequisite for this is the equality of the coupling constants  $\lambda$  of the superpartners to the Higgs boson, which is unaffected by soft SUSY breaking.

Although the procurement of a solution to the hierarchy problem is often stated as its main motivation, SUSY also offers other benefits. For instance, SUSY can provide a solution to the dark matter puzzle. Many SUSY models are based on a discrete symmetry called *R-parity* or *matter parity*, originally introduced to prevent proton decay. Each particle of the SUSY model is assigned a multiplicative *R-parity* quantum number, according to

$$R_P = (-1)^{3(B-L)+2s}, \quad (2.6)$$

where  $B$  and  $L$  denote the baryon and lepton number and  $s$  stands for the spin of the particle. According to these definitions, all SM particles obtain  $R_P = +1$ , whereas their superpartners are assigned  $R_P = -1$ . As an immediate consequence of  $R$ -parity conservation, SUSY particles (sparticles) can only be produced in pairs and their decay must always involve an odd number of lighter sparticles. Consequently, the lightest SUSY particle (LSP) must be stable and hence, if electrically neutral and weakly interacting, constitutes an excellent candidate for dark matter.

Finally, by the introduction of a large amount of potentially complex new parameters, SUSY models also offer new sources of CP violation and thus may allow for a successful baryogenesis in the early universe.

We will come back to SUSY in Part III of this thesis, which deals with the Next-to-Minimal Supersymmetric Standard Model (NMSSM), one specific realization of a SUSY model. There, we will also elaborate in more detail on the particle content of SUSY theories. However, we already want to mention one important characteristic in this introduction, which will serve us as motivation for the next section. In order to prevent the occurrence of gauge anomalies and in order to preserve holomorphy of the superpotential, SUSY theories necessitate the introduction of at least *two* Higgs doublets. These are conventionally denoted as  $H_u$  and  $H_d$ , emphasizing the fact that, as far as the SM fermions are concerned,  $H_u$  only couples to up-type quarks, whereas  $H_d$  only interacts with down-type quarks and charged leptons. Therefore, the Higgs sector of a SUSY model constitutes, in the simplest case, a Two Higgs Doublet Model (2HDM). This fact has, among others, led to an increased interest in 2HDMs in the recent years and also motivated our own studies of these models, which represent a major part of this thesis.

### 2.3. Two Higgs Doublet Models

Another possibility to construct an extensions of the SM is to first concentrate on the scalar sector. The scalar sector is the least well studied and constrained part of the SM and hence offers many possibilities of incorporating new physics. With the current run 2, the LHC has launched a closer investigation of the Higgs boson, the only elementary scalar particle known up to now<sup>3</sup>, however before we can enter the high-precision era in the scalar sector, a new particle collider, like e.g. the International Linear Collider (ILC) will have to be built. As mentioned above, from a theoretical point of view, nothing prohibits the scalar sector from attaining a more complicated structure than the minimal form proposed by the SM. There are some restrictions, of course any extension has to fulfill. One of the most severe constraints comes from electroweak precision measurements and is often expressed in terms of the  $\rho$  parameter, given by

$$\rho = \frac{M_W^2}{M_Z^2 c_W^2}. \quad (2.7)$$

Here  $M_W$  and  $M_Z$  denote the masses of the weak gauge bosons and  $c_W = \cos(\theta_W)$ , where  $\theta_W$  is the Weinberg angle. Experimentally the  $\rho$  parameter is determined to be very close to one [54]

$$\rho = 1.00040 \pm 0.0024. \quad (2.8)$$

<sup>3</sup>Note that it is also possible, that the Higgs boson is a composite object. In this thesis, however, we will always assume the Higgs boson to be an elementary particle.

The theoretical prediction of the  $\rho$  parameter depends on the realization of the scalar sector and can at tree level, i.e. at the lowest order of perturbation theory, be expressed as [17, 55]<sup>4</sup>

$$\rho = \frac{\sum_{i=1}^n (I_i(I_i + 1) - Y_i^2) v_i^2}{2 \sum_{i=1}^n Y_i^2 v_i^2}, \quad (2.9)$$

for a model containing  $n$  scalar  $SU(2)_L$  multiplets of a respective hypercharge  $Y_i$ , a weak isospin  $I_i$  and a vev  $v_i$ . In the SM and in any model featuring only singlets and doublets in the scalar sector,  $\rho = 1$  exactly at tree-level and no artificial arrangement of the individual quantum numbers and vevs in Eq. (2.9) is necessary to comply with the strict experimental bounds.

A further constraint results from severe experimental limits on flavor changing neutral currents (FCNCs). For the minimal Higgs sector of the SM, these are automatically precluded at tree level, since a diagonalization of the fermion mass matrices simultaneously leads to a diagonalization of the corresponding matrices of Yukawa, i.e. fermion-Higgs, couplings. However, in extended scalar sectors, this is no longer necessarily fulfilled and care has to be taken to enforce the absence of tree-level FCNCs or at least suppress them such that they are in accordance with experiment. In the case of 2HDMs, i.e. models whose scalar sector comprises two scalar  $SU(2)_L$  doublets, the occurrence of tree-level FCNCs can be prevented by imposing a  $Z_2$  symmetry on the 2HDM Lagrangian. We will elaborate on this in Sec. 5.4.

The fact that 2HDMs automatically fulfill the tree-level constraints of the  $\rho$ -parameter and can be constructed in such a way, that tree-level FCNCs are absent, is an important motivation to study these models. Furthermore, they are of particular interest, since, apart from singlet extensions, they constitute the simplest generalization of the SM scalar sector and still show a rich phenomenology, featuring e.g. charged and CP-odd scalars.

Due to the enlarged scalar sector, containing several potentially complex parameters, 2HDMs moreover offer the possibility of explicit or spontaneous CP-violation. This in turn may provide a basis for successful baryogenesis.

Special realizations of the 2HDM, the *Inert 2HDMs* (IDMs), besides offer a solution to the dark matter problem as first discussed in [56, 57]. Within these models, only one of the two doublets, denoted by  $\Phi_1$ , receives a vev in the course of EWSB, while the other, called the *inert* doublet  $\Phi_2$ , remains without. As a consequence, the  $Z_2$ -symmetry, which is imposed on the Lagrangian in such a way that only  $\Phi_2$  transforms non-trivially, remains unbroken. Hence, the lightest inert particle is rendered stable and, if electrically neutral, represents a candidate for dark matter.

Finally, many extensions of the SM incorporate a 2HDM as Higgs sector, among which axion models and SUSY models. Especially the fact that the simplest realization of SUSY, the Minimal Supersymmetric Standard Model (MSSM), comprises a 2HDM, has triggered increased scientific activity in the field.

<sup>4</sup>Note that our definition of the hypercharge differs from the one used in [17].



---

## Selected Concepts of Perturbative QFT

---

The purpose of this chapter is to introduce important notions and concepts of QFT, we will make use of in this thesis. We do not strive for rigorous derivations and do not claim completeness. Instead, we will refer the reader to the literature at some points, where this appears appropriate. Furthermore, we assume the reader to be familiar with the basic concepts of special relativity, gauge invariance and Feynman diagrammatic calculations, which we will not repeat in this introduction. These topics are comprehensively covered in any textbook on QFT, e.g. in Refs. [58, 59].

Since a major part of this thesis will deal with the subject of renormalization, we will start in Sec. 3.1 with an illustration of the ideas of *regularization* and *renormalization*. Subsequently in Sec. 3.2, we will introduce the  $\mathcal{S}$ -matrix as one of *the* central objects of QFT and present some important properties and relations, we will take advantage of in this thesis. Finally, Sec. 3.3 is devoted to the topic of gauge fixing and *gauge dependence* and throws a first glance on the *pinch technique*, which will be important for our discussion on gauge-independent renormalization in Part II.

### 3.1. Regularization and Renormalization

All along in perturbative QFT we have to deal with higher-order loop-corrections, which are caused by quantum fluctuations, i.e. by virtual particles, which permanently emerge from and disappear back into the vacuum. As already mentioned in the previous chapter, these are parametrized by loop-integrals, i.e. integrals over the phase space of the virtual particles. Frequently, these integrals diverge in the limit of either vanishing or very high loop momenta, resulting in infrared (IR) or ultraviolet (UV) divergences. While the IR divergences arising from loop-integrals are, according to the Kinoshita-Lee-Nauenberg theorem, cancelled by a summation over all degenerate initial and final states [60, 61], the UV divergences require a particular treatment referred to as *renormalization*. The machinery of renormalization is based on a two-step procedure. In the first step, called *regularization*, the divergences are extracted and parametrized in a convenient way. Afterwards, the actual *renormalization* is performed, in the course of which all UV divergences are disposed of.

In this section we briefly want to outline these two steps.

### 3.1.1. Regularization

A typical example for a UV divergent integral, appearing in the calculation of higher-order corrections, has the form

$$\int_0^\infty \frac{d^4q}{(2\pi)^4} \frac{1}{q^2 + m^2}. \quad (3.1)$$

This integral develops a quadratic divergence for high loop momenta, i.e. in the limit  $|q| \rightarrow \infty$ . In Sec. 2.1 we have already encountered the possibility to isolate this divergence by the introduction of a hard cut-off

$$\int_0^{\Lambda_{\text{UV}}} \frac{d^4q}{(2\pi)^4} \frac{1}{q^2 + m^2} \propto \left[ \frac{\Lambda_{\text{UV}}^2}{m^2} - \ln \left( \frac{\Lambda_{\text{UV}}^2}{m^2} \right) \right] + \mathcal{O}((\Lambda_{\text{UV}})^0). \quad (3.2)$$

The divergences are now separated and parametrized in terms of  $\Lambda_{\text{UV}}$ . For actual calculations, the regularization via a hard cut-off, however, turns out to be impractical, since it destroys translational invariance.

Another method of regularization, which leaves both translational invariance intact and has the further desirable property of respecting gauge and Lorentz invariance, comes in the form of dimensional regularization (DReg) [62, 63]. This method is based on the idea of changing the measure of integration by allowing the dimension of the integral to take a value  $D = 4 - 2\epsilon$ , where  $\epsilon$  is chosen such that the integration can be performed formally. Schematically, this change amounts to

$$\int_0^\infty \frac{d^4q}{(2\pi)^4} \rightarrow \mu_r^{4-D} \int_0^\infty \frac{d^Dq}{(2\pi)^D}. \quad (3.3)$$

In order to preserve the correct mass dimension of the integral, the unphysical mass scale  $\mu_r$ , called the renormalization scale, has to be introduced. After the integration the divergence is contained in the universal term

$$\Delta_{\overline{\text{MS}}} = \frac{1}{\epsilon} - \gamma_E + \ln(4\pi), \quad (3.4)$$

which diverges in the physical limit  $\epsilon \rightarrow 0$ . Here  $\gamma_E$  denotes the Euler-Mascheroni constant. Particular care has to be taken, if the integrand contains  $\gamma_5$  since the continuation of this Dirac matrix to  $D$  dimensions is non-trivial. As we will not encounter this subtlety in this thesis, we do not elaborate on that topic and instead refer the reader to the literature (see [64, 65] and references therein).

Due to its attractive features and general ease in application, DReg is one of the most widely used regularization schemes for non-SUSY higher-order calculations. However, DReg has been shown to violate SUSY [66]. The violation can be traced back to a mismatch between bosonic and fermionic degrees of freedom resulting from the continuation of the polarization vectors of the gauge bosons to  $D$  dimensions. Thus, employing DReg in a SUSY calculation, SUSY has to be re-established by the introduction of *SUSY restoring counterterms* [67–70]. Alternatively, one can make use of a different regularization procedure referred to as *dimensional reduction* (DRed) [71–73]. Although the theory behind DRed is involved, its practical application is straightforward in most cases. In short it amounts to continuing the measure of integration and loop momenta to  $D$  dimensions but keeping all polarization vectors and the Dirac algebra four-dimensional. Again, care has to be taken concerning a consistent treatment of  $\gamma_5$  and furthermore in view of the fact that Fierz identities no longer apply. While a general all-order proof is still missing, DRed was shown to respect SUSY at one-loop order. For higher loop orders only a few dedicated studies have been performed, which all turned out affirmative [74–76].

### 3.1.2. Renormalization

As physical observables are finite, measurable quantities, the divergences extracted by a suitable regularization prescription must not appear in the final result for a physical observable. Hence, a neat cancellation of various divergences has to take place among the different contributions to a physical quantity. The occurrence of this cancellation rests upon a reinterpretation of the parameters of the Lagrangian. Regarding the original parameters as unphysical and unobservable quantities, all divergences can be absorbed into these so-called *bare* parameters. This procedure, called *renormalization*, renders all physical observables and relations among them finite, renormalizability of the theory provided. On the other hand, the bare parameters and the relation between these and physical observables become UV-divergent and any physical interpretation of the Lagrangian parameters is lost.

In order to restore a physical meaning of the bare Lagrangian parameters and to simplify the bookkeeping of UV-divergent contributions, an elegant formalism, the *counterterm formalism*, has been introduced and is widely used nowadays. This formalism is based on the idea of redefining the original parameters of the Lagrangian, such that all UV-divergent terms are absorbed into unphysical shifts, the *counterterms*. For an arbitrary bare Lagrangian parameter  $p_b$  this amounts to

$$p_b = p_r + \delta p = p_r + \delta^{(1)}p + \delta^{(2)}p + \dots, \quad (3.5)$$

where the superscripts schematically indicate the loop-order of the counterterm. Both, the bare parameter  $p_b$  and the counterterm  $\delta p$  are UV-divergent and lack any physical meaning. In contrast, the *renormalized* parameter  $p_r$  is finite and allows for a physical interpretation. Proceeding in this way for all bare parameters results in a splitting of the Lagrangian into a renormalized and a counterterm part

$$\mathcal{L}_b = \mathcal{L}_r + \delta\mathcal{L}, \quad (3.6)$$

where  $\mathcal{L}_r$  has the same form as  $\mathcal{L}_b$  and  $\delta\mathcal{L}$  comprises all counterterms. Using this Lagrangian to derive the Feynman rules results in additional rules for the counterterms, which thus enter the expressions for physical observables. In a renormalizable QFT, the counterterms can be adjusted such, that they cancel all divergences in any physical observable order by order in perturbation theory.

While this parameter renormalization is sufficient to render physical quantities finite, it is often convenient to redefine also the fields by the introduction of *wave function renormalization constants* (WFRCs). These are conventionally established according to

$$\begin{aligned} \phi_b &= \sqrt{Z_\phi} \phi_r = \sqrt{1 + \delta^{(1)}Z_\phi + \delta^{(2)}Z_\phi + \dots} \phi_r \\ &= \left( 1 + \frac{1}{2}\delta^{(1)}Z_\phi - \frac{1}{8}\left(\delta^{(1)}Z_\phi\right)^2 + \frac{1}{2}\delta^{(2)}Z_\phi + \dots \right) \phi_r \end{aligned} \quad (3.7)$$

for each bare field  $\phi_b$  of the theory. In the last step we have performed an expansion in the loop-order.

If the theory under consideration contains particles with identical quantum numbers, these will in general mix through higher-order corrections. In order to account for this, it is necessary to introduce matrix valued WFRCs. For  $n$  species  $\phi_i$  with identical quantum numbers,  $Z_\phi$  has to be defined as complex  $n \times n$  matrix resulting in

$$\phi_{b,i} = (Z_\phi)_{ij}^{1/2} \phi_{r,j}. \quad (3.8)$$

The benefit of introducing WFRCs is two-fold. On the one hand they render all Green's functions finite and can be defined in such a way, that no external leg corrections or LSZ-factors<sup>1</sup>

<sup>1</sup>The notion of Green's functions and LSZ-factors will be introduced in section 3.2.

have to be taken into account. On the other hand, they greatly simplify the definition of parameter counterterms, especially of mass counterterms in the case of mixing particles [77]. After the counterterms have been introduced, they need to be fixed by a suitable procedure. The requirement of UV finiteness only poses limits on the divergent parts of the counterterms, whereas the finite parts can be chosen freely within the boundaries enjoined on them by symmetries. Different possible choices of the counterterms are denoted as different *renormalization schemes*.

Subsequent to the development of the counterterm formalism, two schemes emerged, which nowadays enjoy wide popularity both in SM and in BSM calculations: the *on-shell* (OS) scheme [78–80] and the  $\overline{\text{MS}}$  or  $\overline{\text{DR}}$  scheme [81, 82]. Note that the terms MS and DR refer to the same renormalization scheme and differ only by the underlying prescription of regularization. While the MS scheme is based on DReg, the DR scheme rests on DRed.

The OS scheme follows the philosophy to define the counterterms for the Lagrangian parameters in such a way that the corresponding renormalized parameters can be interpreted as physical observables. For instance in the case of a mass parameter  $m$  this amounts to adjusting the counterterm  $\delta m$  such, that the renormalized mass  $m_r$  corresponds to the pole of the propagator of the respective particle. This is tantamount to saying that  $m_r$  represents the physical mass of an *on-shell* particle, explaining the origin of the nomenclature. In particle physics, a particle with four momentum  $p$  and mass  $m$  is termed *on-shell* if it satisfies the relativistic energy-momentum relation  $p^2 = m^2$  and *off-shell* otherwise.

The  $\overline{\text{MS}}$  or  $\overline{\text{DR}}$  scheme takes a different view. Instead of striving for physically meaningful renormalized parameters, these schemes focus on simplicity and ease of the calculation. To this end, in the MS or the DR scheme the counterterms are defined as purely divergent with the only purpose to cancel the divergences arising from radiative corrections. The MS or DR scheme can therefore be regarded as *minimal*. A slight modification of these schemes leads to the *modified minimal* schemes  $\overline{\overline{\text{MS}}}$  or  $\overline{\overline{\text{DR}}}$ . These schemes rely on the fact that in DReg or DRed the divergences are always accompanied by the universal finite terms  $-\gamma_E + \ln(4\pi)$ . Absorbing these finite terms together with the divergence into the counterterms, i.e. absorbing the term  $\Delta_{\overline{\text{MS}}}$  defined in Eq. (3.4), simplifies the expressions for the final results.

Since both regularization and renormalization constitute auxiliary means of the computation, a physical observable must not depend on the scheme choice for either of both. Due to the fact that in a perturbative calculation we can only take into account a finite number of terms, a residual dependence on the chosen renormalization scheme remains. In the case of  $\overline{\text{MS}}$  or  $\overline{\text{DR}}$  the result furthermore depends on the unphysical renormalization scale  $\mu_r$ . These dependences on both the scheme and the scale choice can be used as a measure for missing higher-order corrections and therefore for the theoretical uncertainty due to the latter.

## 3.2. LSZ Reduction, the $\mathcal{S}$ -matrix and Physical Observables

### 3.2.1. LSZ Reduction and the $\mathcal{S}$ -matrix

Due to its importance and since in the following we will need to refer to it in several places, we briefly want to introduce the notion of the  $\mathcal{S}$ -matrix, one of *the* central objects in perturbative QFT. However, we will not give rigorous proofs of the relations stated in this section but instead refer the reader to the literature [58, 80], in particular to Ref. [59], which we will make ample use of.

Let  $|p_1, \dots, p_s\rangle_{\text{in}}$  and  $\langle -p_{s+1}, \dots, -p_n|$  denote asymptotic *in* and *out* states of definite momentum, as introduced in detail e.g. in the textbook by Peskin and Schroeder [58]. Then, the  $\mathcal{S}$ -matrix is defined via

$$\langle -p_{s+1}, \dots, -p_n | p_1, \dots, p_s \rangle_{\text{in}} = \langle -p_{s+1}, \dots, -p_n | \mathcal{S} | p_1, \dots, p_s \rangle_{\text{in}}. \quad (3.9)$$

According to this, the  $\mathcal{S}$ -matrix describes the transition amplitude between in the *in* and *out* states. In practice, we are interested only in the non-trivial part of the  $\mathcal{S}$ -matrix, which is the part actually representing interactions. For the purpose of isolating the interesting parts, one usually introduces the  $\mathcal{T}$ -matrix, given by

$$\mathcal{S} = \mathbb{1} + i\mathcal{T}. \quad (3.10)$$

Finally, in order to account for momentum conservation, one extracts from  $\mathcal{T}$  the four dimensional delta-distribution  $\delta^{(4)}(p_1 + \dots + p_n)$  and defines the invariant matrix element  $\mathcal{A}$  as

$$\langle -p_{s+1}, \dots, -p_n | i\mathcal{T} | p_1, \dots, p_s \rangle_{\text{in}} = (2\pi)^4 \delta^{(4)}(p_1 + \dots + p_n) i\mathcal{A}(p_1, \dots, p_n). \quad (3.11)$$

We will often refer to  $\mathcal{A}$  as *the amplitude*. Furthermore, we will drop the subscripts “in” in the following.

The importance of the  $\mathcal{S}$ -matrix in QFT is two-fold: On the one hand, it has nice theoretical properties, e.g. it is unitary and can be proven to be gauge invariant and gauge independent [83–89] (cf. Sec. 3.3). On the other hand, the relation in Eq. (3.11) allows an extraction of the amplitude  $\mathcal{A}$ , which appears in the calculation of physical observables like cross-sections and decay rates. For our purposes it will be of particular importance, that the gauge independence of the  $\mathcal{S}$ -matrix is directly transferred to  $\mathcal{A}$  via Eq. (3.11).

When it comes to calculating  $\mathcal{S}$ -matrix elements, we have to invoke the so-called LSZ-formalism (thus denoted as contribute to its inventors Lehmann, Symanzik, Zimmermann) [90], which establishes a direct connection between  $\mathcal{S}$ -matrix elements and n-particle correlation functions (also called Green's functions). The latter can be expressed in terms of Feynman diagrams and are thus calculable with the help of the corresponding Feynman rules. According to the LSZ-formalism, the following relation holds

$$\begin{aligned} & \langle -p_{s+1}, \dots, -p_n | \mathcal{S} | p_1, \dots, p_s \rangle \\ &= (-i)^n \tilde{Z}_{\varphi_1}^{-1/2} (p_1^2 - m_1^2) \dots \tilde{Z}_{\varphi_n}^{-1/2} (p_n^2 - m_n^2) \tilde{G}_{\varphi_1 \dots \varphi_n}(p_1, \dots, p_n) \Big|_{p_i^2 = m_i^2}, \end{aligned} \quad (3.12)$$

with  $i = 1, \dots, n$ . Here we have assumed the incoming and outgoing particles to be scalars. In the case of fermions or vector bosons, we would have to take into account the more complicated Lorentz structure and attach suitable polarization vectors or spinors.  $\tilde{G}_{\varphi_1 \dots \varphi_n}(p_1, \dots, p_n)$  denotes the Fourier transform of the n-scalar correlation function  $G_{\varphi_1 \dots \varphi_n}(x_1, \dots, x_n)$

$$\begin{aligned} \tilde{G}_{\varphi_1 \dots \varphi_n}(p_1, \dots, p_n) &= \int d^4x_1 \dots d^4x_n e^{-i(p_1x_1 + \dots + p_nx_n)} G_{\varphi_1 \dots \varphi_n}(x_1, \dots, x_n) \\ &= (2\pi)^4 \delta^{(4)}(p_1 + \dots + p_n) G_{\varphi_1 \dots \varphi_n}(p_1, \dots, p_n). \end{aligned} \quad (3.13)$$

Furthermore, we have introduced the LSZ factors  $\tilde{Z}_{\varphi_i}^{1/2}$ , which are defined as the residuum of the two-point correlation function, i.e. the propagator, of the scalar field  $\varphi_i$  at the pole

$$\tilde{Z}_{\varphi_i} = -i(p_i^2 - m_i^2) G_{\varphi_i \varphi_i}(p_i, -p_i) \Big|_{p_i^2 = m_i^2}. \quad (3.14)$$

Again, straightforward modifications are necessary for fermions or vector bosons. Inserting Eq. (3.14) into Eq. (3.12), we arrive at

$$\begin{aligned} & \langle -p_{s+1}, \dots, -p_n | \mathcal{S} | p_1, \dots, p_s \rangle \\ &= \tilde{Z}_{\varphi_1}^{1/2} G_{\varphi_1 \varphi_1}^{-1}(p_1, -p_1) \dots \tilde{Z}_{\varphi_n}^{1/2} G_{\varphi_n \varphi_n}^{-1}(p_n, -p_n) \tilde{G}_{\varphi_1 \dots \varphi_n}(p_1, \dots, p_n) \Big|_{p_i^2 = m_i^2} \\ &= \tilde{Z}_{\varphi_1}^{1/2} \dots \tilde{Z}_{\varphi_n}^{1/2} \tilde{G}_{\varphi_1 \dots \varphi_n}^{\text{trunc}}(p_1, \dots, p_n) \Big|_{p_i^2 = m_i^2}. \end{aligned} \quad (3.15)$$

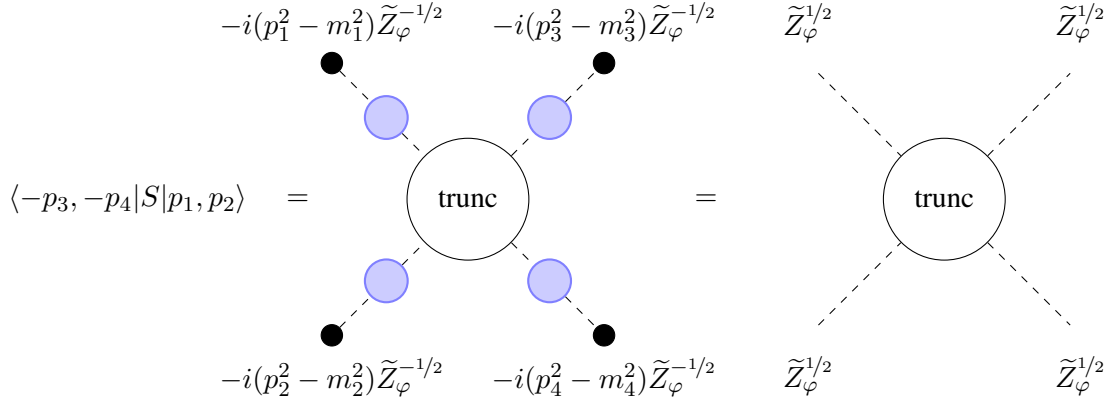


**Figure 3.1.:** Diagrammatic representation of the LSZ formula. Blue (grey) circles represent the full propagator, i.e. the propagator with resummed corrections. The circles labeled as *trunc* contain all possible truncated Feynman diagrams, contributing to the process under consideration

Hence,  $\mathcal{S}$ -matrix elements can be expressed in terms of truncated Green's functions  $\tilde{G}_{\varphi_1 \dots \varphi_n}^{\text{trunc}}(p_1, \dots, p_n)$  taken on-shell, i.e.  $n$ -particle correlation functions, whose external propagators have been “amputated” by operating on them with corresponding inverse two-point functions. The term *on-shell* is used to express the fact that all external particles satisfy the relativistic energy-momentum relation as explained in Subs. 3.1.2.

Pictorially the formula in Eq. (3.15) can be represented as shown in Fig. 3.1. Here and in the following the blue (grey) circles represent the full propagator, i.e. the propagator with resummed corrections, whereas the circles labeled as *trunc* contain all possible truncated Feynman diagrams, contributing to the process under consideration.

Up to this point, we have worked with unrenormalized Green's functions  $\tilde{G}_{\varphi_1 \dots \varphi_n}$ . However, we can also derive a connection between  $\mathcal{S}$ -matrix elements and renormalized Green's functions  $\tilde{G}_{\varphi_1 \dots \varphi_n}^r$ . The latter are obtained from the corresponding unrenormalized ones by multiplication with suitable WFRs  $Z_\varphi^{1/2}$  for each external field appearing in  $\tilde{G}_{\varphi_1 \dots \varphi_n}$  [59]

$$\tilde{G}_{\varphi_1 \dots \varphi_n}^r(p_1 \dots p_n) = Z_{\varphi_1}^{-1/2} \dots Z_{\varphi_n}^{-1/2} \tilde{G}_{\varphi_1 \dots \varphi_n}(p_1 \dots p_n). \quad (3.16)$$

Renormalizing all Lagrangian parameters  $g_0$  appearing in the expressions for  $\tilde{G}_{\varphi_1 \dots \varphi_n}$  and  $\tilde{G}_{\varphi_1 \dots \varphi_n}^r$  as illustrated in Subs. 3.1.2, both  $\tilde{G}_{\varphi_1 \dots \varphi_n}$  and  $\tilde{G}_{\varphi_1 \dots \varphi_n}^r$  depend on renormalized parameters  $g$  and counterterms  $\delta g$ . In order to derive from Eq. (3.16) a relation for *truncated* Green's functions, we have to amputate all external legs with renormalized propagators, leading us to

$$\tilde{G}_{\varphi_1 \dots \varphi_n}^{r, \text{trunc}}(p_1 \dots p_n) = Z_{\varphi_1}^{1/2} \dots Z_{\varphi_n}^{1/2} \tilde{G}_{\varphi_1 \dots \varphi_n}^{\text{trunc}}(p_1 \dots p_n). \quad (3.17)$$

Inserting Eq. (3.17) into Eq. (3.15), we arrive at

$$\begin{aligned} \langle -p_{s+1}, \dots, -p_n | \mathcal{S} | p_1, \dots, p_s \rangle &= \tilde{Z}_{\varphi_1}^{1/2} \dots \tilde{Z}_{\varphi_n}^{1/2} \tilde{G}_{\varphi_1 \dots \varphi_n}^{\text{trunc}}(p_1, \dots, p_n) \Big|_{p_i^2 = m_i^2} \\ &= \tilde{Z}_{\varphi_1}^{1/2} Z_{\varphi_1}^{-1/2} \dots \tilde{Z}_{\varphi_n}^{1/2} Z_{\varphi_n}^{-1/2} \tilde{G}_{\varphi_1 \dots \varphi_n}^{r, \text{trunc}}(p_1, \dots, p_n) \Big|_{p_i^2 = m_i^2}. \end{aligned} \quad (3.18)$$

Obviously, choosing  $Z_{\varphi_i} = \tilde{Z}_{\varphi_i}$  the LSZ-factors for renormalized Green's functions vanish. This choice corresponds to OS renormalization of the fields (cf. Sec. 6.4). It should be noted, however, that although no LSZ-factors are needed in the OS scheme, the WFRs do appear as part of the counterterm Feynman rules.

Before closing this discussion, we want to generalize these results to the case of mixing scalars,

as we will heavily draw on these relations in the following. Since a rigorous deduction would be beyond the scope of this thesis, we will only state the results. For details of the derivation see [80]. If mixing between scalars is considered, Eq. (3.15) takes the form (summation over recurring indices implied)

$$\begin{aligned} & \langle -p_{s+1}, \dots, -p_n | \mathcal{S} | p_1, \dots, p_s \rangle \\ &= \tilde{Z}_{\varphi_j \varphi_1}^{1/2} G_{\varphi'_1 \varphi_j}^{-1}(p_1, -p_1) \dots \tilde{Z}_{\varphi_k \varphi_n}^{1/2} G_{\varphi'_n \varphi_k}^{-1}(p_n, -p_n) \tilde{G}_{\varphi'_1 \dots \varphi'_n}(p_1, \dots, p_n) \Big|_{p_i^2 = m_i^2} \\ &= \tilde{Z}_{\varphi_j \varphi_1}^{1/2} \dots \tilde{Z}_{\varphi_k \varphi_n}^{1/2} \tilde{G}_{\varphi_j \dots \varphi_k}^{\text{trunc}}(p_1, \dots, p_n) \Big|_{p_i^2 = m_i^2}. \end{aligned} \quad (3.19)$$

In this equation, both the LSZ-factors and the propagator  $G_{\varphi_i \varphi_j}(p, -p)$  are to be considered as elements of  $m \times m$  matrices  $\tilde{Z}$  and  $G$ , respectively, where  $m$  is the number of mixing fields. Introducing matrix valued WFRCs  $Z_{\varphi_i \varphi_j}$  leads to

$$\begin{aligned} & \langle -p_{s+1}, \dots, -p_n | \mathcal{S} | p_1, \dots, p_s \rangle \\ &= \tilde{Z}_{\varphi_j \varphi_1}^{1/2} Z_{\varphi_s \varphi_j}^{-1/2} \dots \tilde{Z}_{\varphi_k \varphi_n}^{1/2} Z_{\varphi_t \varphi_k}^{-1/2} \tilde{G}_{\varphi_s \dots \varphi_t}^{r, \text{trunc}}(p_1, \dots, p_n) \Big|_{p_i^2 = m_i^2}, \end{aligned} \quad (3.20)$$

which becomes in the OS scheme

$$\begin{aligned} & \langle -p_{s+1}, \dots, -p_n | \mathcal{S} | p_1, \dots, p_s \rangle \\ & \stackrel{\text{OS}}{=} \underbrace{\tilde{Z}_{\varphi_j \varphi_1}^{1/2} Z_{\varphi_s \varphi_j}^{-1/2}}_{\delta_{1s}} \dots \underbrace{\tilde{Z}_{\varphi_k \varphi_n}^{1/2} Z_{\varphi_t \varphi_k}^{-1/2}}_{\delta_{nt}} \tilde{G}_{\varphi_s \dots \varphi_t}^{r, \text{trunc}}(p_1, \dots, p_n) \Big|_{p_i^2 = m_i^2} \\ &= \tilde{G}_{\varphi_1 \dots \varphi_n}^{r, \text{trunc}}(p_1, \dots, p_n) \Big|_{p_i^2 = m_i^2}. \end{aligned} \quad (3.21)$$

Due to Eq. (3.21) mixing between different scalars on the external legs does not have to be considered, if the particles are renormalized according to OS conditions. The same is true for gauge bosons and fermions.

### 3.2.2. The Invariant Matrix Element $\mathcal{A}$ and Physical Observables

In practice, we are often interested in calculating an amplitude  $\mathcal{A}$  up to some order in the perturbative expansion. This is achieved by taking into account in Fig. 3.1 only those diagrams, leading to contributions of the desired order. The resulting amplitude will then be composed of tree-level, virtual correction and counterterm contributions, denoted by  $\mathcal{A}_{\text{tree}}$ ,  $\mathcal{A}_{\text{virt}}$  and  $\mathcal{A}_{\text{ct}}$ , respectively. Assuming on-shell renormalization of the fields, this decomposition is schematically illustrated in Fig. 3.2 for the case of three scalars. For simplicity, we do not consider mixing in this picture. In the first row, the big crossed circle indicates, that this diagram comprises the full vertex counterterm, including the coupling counterterm as well as the WFRCs of the respective fields. The latter have been separated from the remaining counterterm amplitude in the second row. If we do not introduce WFRCs, which are not necessary in order to obtain finite  $\mathcal{S}$ -matrix elements, the diagrams in the last row can be interpreted as contributions from LSZ-factors (or “external leg corrections”). In general these diagrams will contain both contributions from LSZ-factors and WFRCs as can be read off Eq. (3.18). Of course, the contributions of these diagrams stay the same in any scheme, however, their distribution among LSZ-factors and WFRCs changes depending on the choice of the wave function renormalization. Furthermore, the diagram with the grey circle is supposed to incorporate all possible virtual corrections to the process under consideration.

The amplitude  $\mathcal{A}$  is a complex valued quantity and therefore cannot be a physical observable by itself. Like in quantum mechanics, it is rather to be interpreted as a transition amplitude and only the square of its absolute value can be associated with a transition probability at

$$\begin{aligned}
i\mathcal{A}(p_1, p_2, p_3) &= S_1 \text{---tree} + \text{---virt} + \text{---ct} \\
&= \text{---tree} + \text{---virt} + \text{---ct} \\
&+ \frac{1}{2}\delta Z_{S_1 S_1} + \frac{1}{2}\delta Z_{S_2 S_2} + \frac{1}{2}\delta Z_{S_3 S_3}
\end{aligned}$$

**Figure 3.2.:** Decomposition of a generic amplitude into tree-level, virtual and counterterm contributions. For simplicity, we consider the case of three non-mixing scalars. In the second row, the WFRs have been split off the vertex counterterm, as explained in the text.

a given point in phase space. Consequently, only  $|\mathcal{A}|^2$  will enter physical observables, like cross-sections and decay rates. In this thesis we will mainly be interested in decays of one heavier scalar into two lighter particles. Therefore, we state here the generic expression for the corresponding decay width in the rest frame of the decaying scalar

$$\Gamma_{\phi \rightarrow f_1 f_2} = \frac{\sigma}{2m_\phi} \int d\Pi_2 \sum_{\lambda_1 \lambda_2} |\mathcal{A}_{\phi \rightarrow f_1 f_2}|^2. \quad (3.22)$$

$\lambda_1$  and  $\lambda_2$  denote additional quantum numbers of the outgoing particles (e.g. their color or polarization) and  $\sigma$  is a symmetry factor, which takes the value  $1/2$  for identical particles in the final state and 1 otherwise. Furthermore, we have introduced the two-body phase space  $\Pi_2$

$$\begin{aligned}
\int d\Pi_2 &= \left( \prod_{i=1,2} \int \frac{d^3 p_i}{(2\pi)^3} \frac{1}{2E_i} \right) (2\pi)^4 \delta^{(4)}(p_\phi - p_1 - p_2) \\
&= \int d\Omega \frac{|\vec{p}_1|}{(4\pi)^2 m_\phi^2} \\
&= \frac{1}{8\pi m_\phi^2} \lambda(m_\phi^2, m_{f_1}^2, m_{f_2}^2),
\end{aligned} \quad (3.23)$$

with the Källén function

$$\lambda(a, b, c) = (a^2 + b^2 + c^2 - 2ab - 2bc - 2ca)^{1/2}. \quad (3.24)$$

Since we will always assume the external particles to be on-shell in this thesis, the integrands  $\sum_{\lambda_1 \lambda_2} |\mathcal{A}_{\phi \rightarrow f_1 f_2}|^2$  of all scalar decays we consider are independent of the four momenta  $p_1$  and  $p_2$  and can hence be pulled in front of the integral.

Calculating  $\Gamma_{\phi \rightarrow f_1 f_2}$  up to some desired loop order  $n$ , denoted as  $\mathcal{O}(n\text{-loop})$ , we have to expand  $|\mathcal{A}|^2$  and consider only terms, which contribute at that order. For instance at  $\mathcal{O}(1\text{-loop})$  we

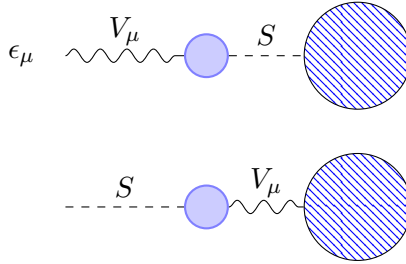


**Figure 3.3.:** Illustration of external leg corrections arising from the mixing between charged or pseudoscalar Higgs bosons with vector bosons. The blob on the right stands for an arbitrary rest amplitude.

have to take into account

$$\begin{aligned}
 |\mathcal{A}|_{\mathcal{O}(1\text{-loop})}^2 &= \left| \mathcal{A}_{\text{tree}} + \sum_{i=1}^{\infty} \mathcal{A}^{(i)} \right|_{\mathcal{O}(1\text{-loop})}^2 & (3.25) \\
 &= |\mathcal{A}_{\text{tree}}|^2 + \mathcal{A}_{\text{tree}}^* \mathcal{A}^{(1)} + \mathcal{A}^{*(1)} \mathcal{A}_{\text{tree}} \\
 &= |\mathcal{A}_{\text{tree}}|^2 + \mathcal{A}_{\text{tree}}^* \left( \mathcal{A}_{\text{virt}}^{(1)} + \mathcal{A}_{\text{ct}}^{(1)} \right) + \left( \mathcal{A}_{\text{virt}}^{(1)} + \mathcal{A}_{\text{ct}}^{(1)} \right)^* \mathcal{A}_{\text{tree}} \\
 &= |\mathcal{A}_{\text{tree}}|^2 + 2\text{Re} \left[ \mathcal{A}_{\text{tree}}^* \left( \mathcal{A}_{\text{virt}}^{(1)} + \mathcal{A}_{\text{ct}}^{(1)} \right) \right],
 \end{aligned}$$

where the superscript  $(i)$  denotes the loop order and the tree-level amplitude is supposed to be free of loops<sup>2</sup>. Moreover, we have split the one-loop amplitude into a virtual part  $\mathcal{A}_{\text{virt}}^{(1)}$ , containing the virtual one-loop corrections, and a counterterm amplitude  $\mathcal{A}_{\text{ct}}^{(1)}$ , which consists of the corresponding counterterm contributions.

One further comment is in order concerning the mixing between vector particles and scalars. Many extensions of the SM, like 2HDMs and SUSY models, feature an extended scalar sector, which contains charged and CP-odd Higgs bosons. Since these possess the same quantum numbers as the  $W$ - or  $Z$ -boson, they can mix with the gauge bosons. Therefore the question arises, how these mixing contributions have to be treated correctly, when appearing on external legs. Generically, two different situations can appear, which are depicted in Fig. 3.3. The contribution of the first generic diagram always vanishes. This is due to the transversality of the external gauge boson and to the fact, that the vector-scalar mixing propagator is proportional to the incoming four-momentum  $p^\mu$ . Contracting  $p^\mu$  with the polarization vector  $\epsilon(p)_\mu$  of the gauge boson yields  $\epsilon(p) \cdot p = 0$ .

For the second case we can exploit a Slavnov-Taylor identity, which allows us to connect the contribution of the scalar-vector mixing to an equivalent contribution, where the gauge boson is replaced by the corresponding Goldstone boson [91]. In an OS scheme, the latter vanishes if the external momenta are taken on-shell and scalar-vector mixing does not need to be considered. However, for general non-OS schemes these contributions have to be taken into account when calculating  $\mathcal{A}_{\text{virt}}$ .

In addition, if the process under considerations exhibits IR divergences, caused by internal massless propagators of a species  $f_i^0$ , a meaningful result for the decay width requires the inclusion of all possible processes with degenerate initial and final states [60, 61] of the appropriate order. There are two types of IR divergences given by *soft* and *collinear* divergences. Since we do not consider processes exhibiting the latter type of IR divergences in this thesis, we restrict our discussion here to the first type. Soft IR divergences can be cured by taking into account processes with additional soft, i.e. low-energy, massless particles  $f_i^0$  in the final state, which are called *real corrections*. These exhibit the same IR divergences with an opposite sign as those appearing in the virtual corrections. A physically meaningful partial decay

<sup>2</sup>Note that in this representation, the expansion of any loop-induced process, whose leading order amplitude is of one-loop order, would start with  $\mathcal{A}^{(1)}$  and the lowest order term in Eq. (3.25) would be  $|\mathcal{A}^{(1)}|^2$ .

width is consequently obtained as an incoherent sum of the widths  $\Gamma_{\phi \rightarrow f_1 f_2}^{\mathcal{O}(n\text{-loop})}$  from above and  $\Gamma_{\phi \rightarrow \sum_i f_1 f_2 f_i^0}^{\text{soft},(n)}$ , containing the real corrections, i.e

$$\Gamma_{\phi \rightarrow f_1 f_2}^{\mathcal{O}(n\text{-loop}),\text{phys}} = \Gamma_{\phi \rightarrow f_1 f_2}^{\mathcal{O}(n\text{-loop})} + \Gamma_{\phi \rightarrow \sum_i f_1 f_2 f_i^0}^{\text{soft},(n)}. \quad (3.26)$$

The superscript *soft* refers to the fact, that only the low-energy part of the integrals over the phase space of the additional massless particle  $f_i^0$  is to be included in  $\Gamma_{\phi \rightarrow \sum_i f_1 f_2 f_i^0}^{\text{soft},(n)}$ . Furthermore it is understood, that the real corrections have to match the order of the virtual corrections in  $\Gamma_{\phi \rightarrow f_1 f_2}^{\mathcal{O}(n\text{-loop})}$ , which we indicate by the superscript  $(n)$ . As the IR divergences exactly cancel between  $\Gamma_{\phi \rightarrow \sum_i f_1 f_2 f_i^0}^{\text{soft},(n)}$  and  $\Gamma_{\phi \rightarrow f_1 f_2}^{\mathcal{O}(n\text{-loop})}$ , the final result  $\Gamma_{\phi \rightarrow f_1 f_2}^{\mathcal{O}(n\text{-loop}),\text{phys}}$  is IR finite.

### 3.3. Gauge Dependence and the Pinch Technique

When quantizing a gauge theory, one is faced with the difficulty of coping with unphysical degrees of freedom. These are inherent in the formulation of a gauge theory in terms of vector fields containing unphysical modes. The problem, which can be traced back to the gauge invariance of the Lagrangian, becomes immediately apparent within the path-integral formalism [58, 59]. Schematically, this formalism introduces the generating functional  $\mathcal{Z}[\mathbf{J}]$ , which for a gauge theory with vector fields  $\mathbf{A} \equiv A_\mu^a(x)$ , the corresponding sources  $\mathbf{J} \equiv J_\mu^a(x)$  and an action  $S\{\mathbf{A}\}$  is given by

$$\mathcal{Z}[\mathbf{J}] = \int \mathcal{D}[\mathbf{A}] \exp \left( iS\{\mathbf{A}\} + i \int d^4x J^{\mu,a}(x) A_\mu^a(x) \right), \quad (3.27)$$

Here the measure  $\mathcal{D}[A] = \prod_{x,\mu,a} dA_\mu^a(x)$  incorporates a product over all components of the four vector and all group elements at each space-time point  $x$ . Within the path integral formalism, the thus defined generating functional serves as starting point for the derivation of Green's functions and Feynman rules. However, the functional integral in Eq. (3.27) is badly divergent since the integration runs over a continuous infinity of physically equivalent configurations of  $\mathbf{A}$ , which are related by gauge transformations. For a meaningful quantization of a gauge theory, this redundancy has to be disposed of, such that each physical configuration is taken into account exactly once. This can be achieved by a procedure introduced by L. D. Faddeev and V. N. Popov [92], which is referred to as *gauge fixing*. By imposing a particular gauge condition, exactly one representative of all physically equivalent configurations is singled out and the integration over the continuous infinity reduces to an overall factor, that drops out in Green's functions and  $\mathcal{S}$ -matrix elements. However, the invariance of the Lagrangian under gauge transformations is explicitly broken by selecting a particular gauge condition. Furthermore, the procedure introduces arbitrary unphysical parameters, the gauge fixing parameters, which appear in the intermediate steps of a calculation. Nonetheless, the final result for  $\mathcal{S}$ -matrix elements (cf. Sec. 3.2) and hence all physical observables can be shown to be gauge invariant and gauge independent<sup>3</sup> [83–89].

In some cases, though, it is desirable to work with gauge-independent building blocks already in intermediate steps of the calculation. The elementary building blocks in a perturbative expansion of the  $\mathcal{S}$ -matrix are given by off-shell Green's functions and since these are unphysical objects, they show, in general, an explicit dependence on the gauge fixing parameters. Yet, there is a method, called the *Pinch Technique* (PT), that allows to redistribute individual terms among the conventional Green's functions such that the resulting objects are gauge independent. In addition they show further characteristics, usually attributed to physical

<sup>3</sup>Note, however, that an unsuitably chosen, unphysical renormalization scheme can destroy this property. Moreover, note that we carefully distinguish the two terms of gauge invariance, i.e. the invariance under gauge transformations, and gauge independence, i.e. independence of gauge fixing parameters.

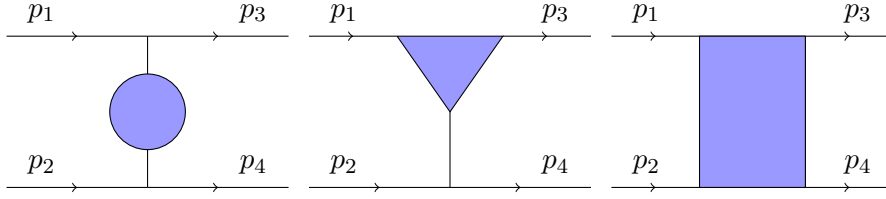


**Figure 3.4.:** Diagrams contributing to the  $\mathcal{S}$ -matrix, grouped into self-energy, triangle and box topologies. The Mandelstam variables  $s$ ,  $t$ ,  $u$  are defined as  $s = (p_1 + p_2)^2$ ,  $t = (p_1 - p_3)^2$ ,  $u = (p_1 - p_4)^2$ .

observables, e.g. they satisfy simple Ward Identities (WIs) instead of merely Slavnov-Taylor identities (STIs), they involve no unphysical thresholds and show a well-defined high-energy behaviour [93, 94].

The basic idea of the PT in constructing gauge-independent *pinched* Green's functions, is to exploit the vast cancellation of gauge dependences, taking place in the assembly of individual building blocks to an  $\mathcal{S}$ -matrix element. In doing so, the PT takes advantage of the observation that longitudinal momenta circulating in triangle or box diagrams (see Fig. 3.4) “pinch” out internal fermion lines thereby generating self-energy-like terms. If these are attributed to the conventional self-energies, both these newly constructed *pinched* self-energies and the remaining triangle- and box-like structures become individually gauge independent. We will not go into the details of the PT and restrict ourselves only to a nice illustration of the principle. The interested reader may find more information and examples in the extensive review on the subject in Ref. [94] or in Refs. [93, 95–100].

As starting point the PT exploits the fact that the  $\mathcal{S}$ -matrix is gauge independent. A typical  $\mathcal{S}$ -matrix element  $\langle f | \mathcal{S} | i \rangle \equiv \mathcal{S}(s, t, \{m_i\})$  with generic initial and final states  $|i\rangle$  and  $\langle f|$ , depending on the Mandelstam variables  $s$  and  $t$  and a set of generic masses  $\{m_i\}$  of the external particles, can be decomposed according to

$$\mathcal{S}(s, t, \{m_i\}) = \mathcal{S}_1(t, \xi_j) + \mathcal{S}_2(t, \{m_i\}, \xi_j) + \mathcal{S}_3(s, t, \{m_i\}, \xi_j) \quad (3.28)$$

into self-energy-like  $\mathcal{S}_1(t, \xi_j)$ , triangle-like  $\mathcal{S}_2(t, \{m_i\}, \xi_j)$  and box-like  $\mathcal{S}_3(s, t, \{m_i\}, \xi_j)$  structures, which individually depend on the gauge fixing parameters  $\xi_j$ . The classification of the various building blocks into the three topologies is illustrated in Fig. 3.4 and proceeds according to their kinematical properties: self-energies depend only on the Mandelstam variable  $t$ , triangles on  $t$  and the masses  $\{m_i\}$  while the boxes show a dependence on all three arguments,  $s$ ,  $t$  and  $\{m_i\}$ .

Taking the gauge independence of the  $\mathcal{S}$ -matrix for granted, it is at hand to rearrange the  $\xi_j$ -dependent pieces of  $\mathcal{S}_1$ ,  $\mathcal{S}_2$  and  $\mathcal{S}_3$  in such a way that the reorganized sub-amplitudes  $\hat{\mathcal{S}}_1(t)$ ,  $\hat{\mathcal{S}}_2(t, \{m_i\})$  and  $\hat{\mathcal{S}}_3(s, t, \{m_i\})$  are individually independent of the gauge fixing parameters  $\xi_j$

$$\mathcal{S}(s, t, \{m_i\}) = \hat{\mathcal{S}}_1(t) + \hat{\mathcal{S}}_2(t, \{m_i\}) + \hat{\mathcal{S}}_3(s, t, \{m_i\}). \quad (3.29)$$

That such a decomposition of  $\mathcal{S}(s, t, \{m_i\})$  is possible, can be seen directly by differentiating Eq. (3.28) w.r.t.  $\xi_j$  and  $s$ . Since  $\mathcal{S}(s, t, \{m_i\})$  does not depend on  $\xi_j$ , the right-hand side vanishes and as  $\mathcal{S}_1$  and  $\mathcal{S}_2$  do not depend on  $s$  we are left with

$$\frac{\partial^2 \mathcal{S}_3(s, t, \{m_i\}, \xi_j)}{\partial \xi_j \partial s} = 0. \quad (3.30)$$

This, however, tells us that  $\mathcal{S}_3$  can be written as a sum of two pieces, one independent of  $\xi_j$  and one independent of  $s$

$$\mathcal{S}_3(s, t, \{m_i\}, \xi_j) = \hat{\mathcal{S}}_3(s, t, \{m_i\}) + h_3(t, \{m_i\}, \xi_j). \quad (3.31)$$

The first piece is the  $\xi_j$ -independent sub-amplitude  $\hat{\mathcal{S}}_3$  we are looking for. The second piece depends on the same parameters as  $\mathcal{S}_2$  and can therefore be added to the triangle sub-amplitude, yielding

$$\tilde{\mathcal{S}}_2(t, \{m_i\}, \xi_j) = \mathcal{S}_2(t, \{m_i\}, \xi_j) + h_3(t, \{m_i\}, \xi_j). \quad (3.32)$$

Inserting this into  $\mathcal{S}$  we are lead to

$$\mathcal{S}(s, t, \{m_i\}) = \mathcal{S}_1(t, \xi_j) + \tilde{\mathcal{S}}_2(t, \{m_i\}, \xi_j) + \hat{\mathcal{S}}_3(s, t, \{m_i\}). \quad (3.33)$$

We can now proceed in the same manner and differentiate Eq. (3.33) w.r.t.  $\{m_i\}$  and  $\xi_j$

$$\frac{\partial^2 \tilde{\mathcal{S}}_2(t, \{m_i\}, \xi_j)}{\partial \xi_j \partial m_j} = 0, \quad m_j \in \{m_i\}, \quad (3.34)$$

which again allows us to decompose  $\tilde{\mathcal{S}}_2$  into two pieces, one independent of  $\xi_j$  and the other independent of  $\{m_i\}$

$$\tilde{\mathcal{S}}_2(s, t, \{m_i\}, \xi_j) = \hat{\mathcal{S}}_2(t, \{m_i\}) + h_2(t, \xi_j). \quad (3.35)$$

Finally, adding  $h_2(t, \xi_j)$  to  $\mathcal{S}_1(t, \xi_j)$ , the resulting function

$$\hat{\mathcal{S}}_1(t) = \mathcal{S}_1(t, \xi_j) + h_2(t, \xi_j) \quad (3.36)$$

has to be independent of  $\xi_j$ , since  $\mathcal{S}(s, t, \{m_i\})$  does not depend on the gauge fixing parameters. Thus we have shown, that  $\mathcal{S}(s, t, \{m_i\})$  can indeed be decomposed into three separately gauge-independent sub-amplitudes with self-energy-, triangle- and box-like kinematic configurations.

The PT is a method to construct these subamplitudes  $\hat{\mathcal{S}}_1(t)$ ,  $\hat{\mathcal{S}}_2(t, \{m_i\})$  and  $\hat{\mathcal{S}}_3(s, t, \{m_i\})$  in a well-defined and unambiguous way using a Feynman diagrammatic approach.

In this thesis, we will make use of the PT in order to formulate gauge-independent self-energies, which we will call *pinched self-energies*. We will come back to this in Sec. 8.5.

**Part II.**

**Gauge-Independent Renormalization  
of the 2HDM**



The existence of a consistent renormalization scheme is a fundamental prerequisite for any perturbative model of elementary particle physics. Without a logically coherent and suitable prescription of treating the divergences, higher-order predictions cannot be made or become meaningless.

For this reason, the development of an appropriate renormalization scheme for the SM has attracted much attention, especially during the 1980s and many authors have contributed to the endeavour of constructing the optimal scheme, e.g. [77, 78, 80, 101, 102] to mention only a few. Also in the case of the MSSM, an intense activity [103–105] on the subject was stimulated, in particular in the course of the 1990s. For both models, the SM and the MSSM, a variety of standard renormalization schemes have emerged, at least at one-loop order, which are nowadays frequently applied.

In the case of 2HDMs, the efforts to establish a complete renormalization scheme are much more scarce. We know of three dedicated studies on the subject, which, however, either do not strive for completeness [38, 39] or are plagued with gauge dependences [40]<sup>1</sup>. On these grounds we deem it important to approach this issue once more and to investigate it in depth. In the development of an appropriate renormalization scheme for the 2HDM we are guided by three major principles. First, we pursue the goal of renormalizing as many parameters as possible in such a way, that they can be interpreted as physical quantities. For this to be the case, the renormalized parameters must not depend on unphysical scales or parameters, e.g. on the renormalization scale or on gauge-fixing parameters. The latter is equivalent to saying that we aim for a renormalization scheme leading to genuinely *gauge-independent* expressions for  $\mathcal{S}$ -matrix elements and thus physical observables.

Furthermore, we strive for a *process-independent* scheme, i.e. a scheme leading to renormalized parameters, that do not depend on a specific process. Such a process dependence is unfavourable, as it introduces a non-universality into the renormalized parameters.

Finally, a renormalization scheme can only be regarded as reasonable, if it leads to *numerically stable* results for physical observables and does not yield artificially huge radiative corrections.

Since adequate renormalization schemes have been elaborated for all parameters already

---

<sup>1</sup>Recently, after the publication of our own results, to be presented in this thesis, the subject was addressed in Ref. [41].

present in the SM, we will especially focus on those parameters, that are specific to the 2HDM, viz. the angles  $\alpha$  and  $\beta$  and the soft- $Z_2$ -breaking scale  $m_{12}$  (cf. Sec. 5.3).

For the development and examination of different renormalization schemes, we will proceed according to following outline:

The first chapter of this part (5) serves the purpose of familiarizing the reader with the subject of 2HDMs and of setting up our notation. We will briefly touch all sectors of the 2HDM which will be important in the subsequent chapters. Furthermore, we will specify the set of parameters that will be considered as independent throughout this part of the thesis and determine the physical mass eigenstates of the scalar sector.

In Ch. 6, we will enter the subject of renormalization. We will introduce counterterms for the chosen set of independent parameters, formulate the OS renormalization conditions for the SM parameters and summarize previous suggestions to fix the three 2HDM-specific parameters. Moreover, we will discuss subtleties arising in the case of mixing fields, which is important for a proper renormalization of the 2HDM scalar sector. Particular emphasis will be laid on the treatment of the tadpoles, since this subject will turn out to be crucial for all ensuing considerations. We will propose two different tadpole schemes, which will be treated in juxtaposition with each other during the whole course of part II.

The first of the two tadpole schemes, dubbed *scheme I*, will be dealt with in Ch. 7. We will first derive expressions for the counterterms of all SM parameters within the framework of scheme I. Afterwards we will turn to a renormalization of the angles  $\alpha$  and  $\beta$  and present the process-independent scheme proposed in Ref. [40]. As we will demonstrate, this scheme is inherently gauge dependent which calls for an alternative renormalization procedure.

Ch. 8 will focus on the second tadpole scheme, referred to as *scheme II*. To highlight its significance, we will first discuss the subject of gauge dependences in counterterms, which are immanent in scheme I but absent in scheme II. Subsequently, we will carefully derive the proper implementation of tadpole scheme II into the 2HDM, deduce expressions for the OS counterterms of the SM parameters and illustrate the emergence of additional tadpole diagrams due to parameter shifts, which have to be taken into account in scheme II. Finally, we will demonstrate how the pinch technique can be applied in the framework of scheme II in order to construct process- and gauge-independent angular counterterms.

Despite the preference for a process-independent scheme, pointed out above, we will investigate in Ch. 9 the definition of the angular counterterms in terms of the two decay processes  $H \rightarrow \tau\tau$  and  $A_0 \rightarrow \tau\tau$ . The resulting scheme is manifestly gauge independent in both tadpole schemes and therefore deserves a closer examination. We will also briefly touch the  $\overline{\text{MS}}$  definition of the angles  $\alpha$  and  $\beta$ .

The last 2HDM-specific parameter  $m_{12}$  will be treated in Ch. 10. We will present two different renormalization schemes for this parameter: one based on  $\overline{\text{MS}}$  conditions, the other depending on the process  $H \rightarrow A_0 A_0$ . Both schemes yield gauge-independent results in tadpole scheme I and II.

Ch. 11 provides a summary of all options of renormalizing the 2HDM parameters discussed so far.

A complete investigation of the different schemes also requires a dedicated study of numerical stability. For this purpose, we will choose in Ch. 12 three example processes, that will serve us as test cases in the numerical analysis. We will first specify all utilized tools and the input parameters entering the numerical evaluation. Afterwards, we will examine the three example processes individually in the framework of all discussed renormalization schemes and scrutinize their numerical stability.

Finally, in Ch. 13 we will summarize all gained insights and conclude part II with a recommendation on the optimal choice for renormalizing the 2HDM.

---

Introduction to the 2HDM

---

There are several possible realizations of 2HDMs. All of them share the property of augmenting the scalar sector of the SM by an additional scalar  $SU(2)$  doublet, while leaving the remaining sectors unchanged. Different realizations can be distinguished by various discrete symmetries their scalar and Yukawa sectors respect or violate. In this thesis, we will concentrate on one specific version of a 2HDM, the *CP-conserving,  $Z_2$ -symmetric* 2HDM, which will be introduced below and which will henceforth be referred to as *the 2HDM*.

For the purpose of acquainting the reader with the 2HDM and to set up our notation we will dedicate this chapter to an introduction to the 2HDM and its various sectors. In doing so, we will concentrate on the electroweak (EW) part and neglect the QCD component, which remains unchanged with respect to the SM.

First, in Sec. 5.1 we will state the full EW 2HDM Lagrangian, and subsequently consider the individual sectors separately. We start with the scalar potential in Sec. 5.2 and discuss its parameters in more detail in Sec. 5.3. Afterwards, we briefly introduce the Yukawa sector in Sec. 5.4 and finally touch the gauge fixing part in Sec. 5.5.

### 5.1. The Lagrangian of the 2HDM

The particle content of the 2HDM coincides with the one of the SM, apart from the fact that its scalar sector comprises two complex scalar  $SU(2)_L$  doublets  $\Phi_1$  and  $\Phi_2$ , given by

$$\Phi_1 = \begin{pmatrix} \phi_1^+ \\ \frac{\tilde{\rho}_1 + i\eta_1}{\sqrt{2}} \end{pmatrix}, \quad \Phi_2 = \begin{pmatrix} \phi_2^+ \\ \frac{\tilde{\rho}_2 + i\eta_2}{\sqrt{2}} \end{pmatrix}, \quad (5.1)$$

instead of only one. Like in the SM, each of the two doublets contains a complex charged component  $\phi_i^+$  as well as a neutral component, which in turn is composed of a real CP-odd field  $\eta_i$  and a real CP-even field  $\tilde{\rho}_i$ ,  $i = 1, 2$ . Since these doublets transform trivially under  $SU(3)_C$ , the addition of the second doublet does not have any influence on the QCD-sector, which is hence identical to the one of the SM. In the following we will therefore concentrate

on the EW part of the 2HDM Lagrangian, denoted by  $\mathcal{L}_{\text{EW}}$

$$\begin{aligned} \mathcal{L}_{\text{EW}} = & \sum_{\psi} i\bar{\psi}\not{D}\psi - \frac{1}{4} \sum_{a=1}^3 W_{\mu\nu}^a W_a^{\mu\nu} - \frac{1}{4} B_{\mu\nu} B^{\mu\nu} + \sum_{i=1,2} (D_{\mu}\Phi_i)^{\dagger} (D^{\mu}\Phi_i) \\ & + \mathcal{L}_{\text{gf}}(\Phi_1, \Phi_2, W_{\mu}^a, B_{\mu}) + \mathcal{L}_{\text{ghost}} \\ & + \mathcal{L}_{\text{Yuk}}(\Phi_1, \Phi_2, \{\psi\}) - V(\Phi_1, \Phi_2). \end{aligned} \quad (5.2)$$

The first line comprises the kinetic term for the fermions, where the sum runs over all species present in the SM, the kinetic terms for the  $SU(2)$  and the  $U(1)$  gauge bosons  $W_{\mu}^a$  and  $B_{\mu}$  with field strength tensors  $W_{\mu\nu}^a$  and  $B_{\mu\nu}$  and the kinetic term for the two scalar  $SU(2)$  doublets. These terms are unchanged with respect to the SM, except for the last one, which can, however, be obtained by a straight-forward extension. Since we restrict ourselves to the electroweak part of the Lagrangian, the covariant derivative  $D_{\mu}$  is given by

$$D_{\mu} = \partial_{\mu} + i\frac{g_2}{2} \sum_{a=1}^3 W_{\mu}^a \tau_a + i\frac{g_1}{2} B_{\mu}, \quad (5.3)$$

where  $g_2$  and  $g_1$  denote the EW gauge couplings associated with  $SU(2)_L$  and  $U(1)_Y$ , respectively, and  $\tau_a$  represent the Pauli matrices.

The second line is composed of the gauge fixing Lagrangian  $\mathcal{L}_{\text{gf}}$  and the corresponding Lagrangian for the unphysical Faddeev-Popov ghosts  $\mathcal{L}_{\text{ghost}}$ . They are defined in an identical manner as the analogous terms in the SM and will be detailed below in Sec. 5.5 after the rotation to the mass basis.

Finally, the third line contains the Yukawa Lagrangian, which describes the interactions between the fermions and the scalar doublets, and the scalar potential  $V(\Phi_1, \Phi_2)$ . In their most general form, these two terms can contain all possible operators up to dimension four which are consistent with Lorentz and gauge invariance. Often, however, additional symmetries are imposed on the scalar potential as well as on the Yukawa Lagrangian in order to evade experimental constraints, e.g. on CP-violation and on FCNC. This will be discussed more thoroughly in the subsequent sections.

Having introduced the 2HDM Lagrangian, we will now discuss the individual terms appearing in  $\mathcal{L}_{\text{EW}}$  separately and in more depth.

## 5.2. The Scalar Potential

We start our discussion of the individual terms in  $\mathcal{L}_{\text{EW}}$  with its most essential part: the scalar potential  $V(\Phi_1, \Phi_2)$ . With no further symmetries other than gauge invariance as well as renormalizability imposed, it comprises 14 independent real parameters. Three of those can be eliminated by a basis transformation so that one is left with a total of 11 degrees of freedom [18].

In this general form the potential of a 2HDM allows for both direct and spontaneous CP violation and shows a very rich vacuum structure. Unlike the SM, 2HDMs can feature different coexisting vacua. Besides they can exhibit so-called inert vacua, where only one of the scalars couples to gauge bosons, as well as vacua breaking the electromagnetic symmetry  $U(1)_{\text{em}}$ . The latter ones have to be excluded from the space of allowed vacua, since  $U(1)_{\text{em}}$  must remain unbroken.

Still, the variety of possible vacua remains enormous. Moreover, without any further restrictions, 2HDMs generically lead to FCNC, which are severely constrained by experimental data. Due to this and since the main purpose of this part of the thesis is to discuss the issue of gauge independence and renormalization, we will restrict ourselves to a CP-conserving 2HDM and in addition impose a  $Z_2$ -symmetry on the scalar potential. This  $Z_2$ -symmetry, if extended to

the Yukawa sector, prevents the occurrence of FCNC. A thorough overview of more general realizations of a 2HDM allowing for FCNC and CP-violation, which is an interesting topic by itself, can be found in [18].

With the foregoing additional constraints, the most general scalar potential is given by [18, 40, 106]

$$\begin{aligned} V(\Phi_1, \Phi_2) = & m_{11}^2 \Phi_1^\dagger \Phi_1 + m_{22}^2 \Phi_2^\dagger \Phi_2 - m_{12}^2 (\Phi_1^\dagger \Phi_2 + \Phi_2^\dagger \Phi_1) \\ & + \frac{\lambda_1}{2} (\Phi_1^\dagger \Phi_1)^2 + \frac{\lambda_2}{2} (\Phi_2^\dagger \Phi_2)^2 + \lambda_3 \Phi_1^\dagger \Phi_1 \Phi_2^\dagger \Phi_2 + \lambda_4 \Phi_1^\dagger \Phi_2 \Phi_2^\dagger \Phi_1 \\ & + \frac{\lambda_5}{2} ((\Phi_1^\dagger \Phi_2)^2 + (\Phi_2^\dagger \Phi_1)^2). \end{aligned} \quad (5.4)$$

It contains eight real parameters, three of which,  $m_{11}$ ,  $m_{22}$  and  $m_{12}$ , have the dimension of a mass, whereas  $\lambda_1 - \lambda_5$  are dimensionless. Strictly speaking, the parameter  $m_{12}$  softly breaks the  $Z_2$ -symmetry. However, it does not lead to FCNCs at tree level and generates finite Higgs-mediated FCNCs starting only from one-loop order on. Furthermore, it is of phenomenological relevance, wherefore it is usually kept in the  $Z_2$ -symmetric potential. We will henceforth refer to the CP-conserving 2HDM with softly broken  $Z_2$ -symmetry as *the 2HDM*.

The exact form of the potential is crucial for the 2HDM vacuum structure since the following minimum conditions have to be fulfilled

$$\left. \frac{\partial V(\Phi_1, \Phi_2)}{\partial \Phi_1} \right|_{\Phi_1=\langle \Phi_1 \rangle, \Phi_2=\langle \Phi_2 \rangle} = 0 = \left. \frac{\partial V(\Phi_1, \Phi_2)}{\partial \Phi_2} \right|_{\Phi_1=\langle \Phi_1 \rangle, \Phi_2=\langle \Phi_2 \rangle}, \quad (5.5)$$

for a certain field configuration to be the correct vacuum state. Here we have introduced the vevs  $\langle \Phi_i \rangle$  of the two doublets. With our choice of the scalar potential to respect CP-invariance and requiring charge conservation, the vevs can be parametrized as

$$\langle \Phi_1 \rangle = \begin{pmatrix} 0 \\ \frac{v_1}{\sqrt{2}} \end{pmatrix}, \quad \langle \Phi_2 \rangle = \begin{pmatrix} 0 \\ \frac{v_2}{\sqrt{2}} \end{pmatrix}. \quad (5.6)$$

This allows us to expand the doublets, spelled out in Eq. (5.1), around their vevs, which yields

$$\Phi_1 = \begin{pmatrix} \phi_1^+ \\ \frac{\rho_1 + i\eta_1 + v_1}{\sqrt{2}} \end{pmatrix}, \quad \Phi_2 = \begin{pmatrix} \phi_2^+ \\ \frac{\rho_2 + i\eta_2 + v_2}{\sqrt{2}} \end{pmatrix}. \quad (5.7)$$

Plugging in this representation into the minimization equations Eq. (5.5) leads to the tadpole conditions, which have to be fulfilled by the vevs and the parameters of the potential

$$T_1^0 \equiv -m_{12}^2 v_2 + m_{11}^2 v_1 + \frac{1}{2} \lambda_1 v_1^3 + \frac{1}{2} \lambda_{345} v_1 v_2^2 = 0, \quad (5.8)$$

$$T_2^0 \equiv -m_{12}^2 v_1 + m_{22}^2 v_2 + \frac{1}{2} \lambda_2 v_2^3 + \frac{1}{2} \lambda_{345} v_1^2 v_2 = 0. \quad (5.9)$$

Here we have introduced the abbreviation  $\lambda_{345} = \lambda_3 + \lambda_4 + \lambda_5$ . Furthermore we have defined the tadpole parameters  $T_1^0$  and  $T_2^0$ , which are bound to vanish at tree level. Since they will play an important role in the renormalization process, we still have to keep them explicit in all relations and set them to zero only after the introduction of counterterms. Defining the matrix

$$T_\varphi^0 \equiv \begin{pmatrix} \frac{T_1^0}{v_1} & 0 \\ 0 & \frac{T_2^0}{v_2} \end{pmatrix} \quad (5.10)$$

we can cast the potential into the following form [38]

$$\begin{aligned}
V = & (\phi_1^- \quad \phi_2^-) \mathcal{M}_{\phi^+} \begin{pmatrix} \phi_1^+ \\ \phi_2^+ \end{pmatrix} + \frac{1}{2} (\eta_1 \quad \eta_2) \mathcal{M}_\eta \begin{pmatrix} \eta_1 \\ \eta_2 \end{pmatrix} + \frac{1}{2} (\rho_1 \quad \rho_2) \mathcal{M}_\rho \begin{pmatrix} \rho_1 \\ \rho_2 \end{pmatrix} \\
& + (\phi_1^- \quad \phi_2^-) T_\varphi^0 \begin{pmatrix} \phi_1^+ \\ \phi_2^+ \end{pmatrix} + \frac{1}{2} (\eta_1 \quad \eta_2) T_\varphi^0 \begin{pmatrix} \eta_1 \\ \eta_2 \end{pmatrix} + \frac{1}{2} (\rho_1 \quad \rho_2) T_\varphi^0 \begin{pmatrix} \rho_1 \\ \rho_2 \end{pmatrix} \\
& + T_1^0 \rho_1 + T_2^0 \rho_2 + \text{trilinear and quadrilinear terms.}
\end{aligned} \tag{5.11}$$

In this representation we have grouped the particles of identical quantum numbers into vectors and identified the terms bilinear in the fields with the tree-level mass matrices  $\mathcal{M}_{\phi^\pm}$ ,  $\mathcal{M}_\eta$  and  $\mathcal{M}_\rho$  for the charged, CP-odd and CP-even scalars in the gauge basis. Note that in defining the mass matrices we have separated tadpole terms, summarized in the matrix  $T_\varphi^0$ . Hence, the mass matrices are defined without tadpole contributions. As a consequence, three equivalent bilinear tadpole terms appear, one for each of the pairs of particles of identical quantum numbers. Explicitly, the mass matrices derived from Eq. (5.4) are given by

$$\mathcal{M}_{\phi^\pm} = \left( m_{12}^2 - \frac{1}{2}(\lambda_4 + \lambda_5)v_1v_2 \right) \begin{pmatrix} \frac{v_2}{v_1} & -1 \\ -1 & \frac{v_1}{v_2} \end{pmatrix}, \tag{5.12}$$

$$\mathcal{M}_\eta = (m_{12}^2 - \lambda_5 v_1 v_2) \begin{pmatrix} \frac{v_2}{v_1} & -1 \\ -1 & \frac{v_1}{v_2} \end{pmatrix}, \tag{5.13}$$

$$\mathcal{M}_\rho = \begin{pmatrix} m_{12}^2 \frac{v_2}{v_1} + \lambda_1 v_1^2 & -m_{12}^2 + \lambda_{345} v_1 v_2 \\ -m_{12}^2 + \lambda_{345} v_1 v_2 & m_{12}^2 \frac{v_1}{v_2} + \lambda_2 v_2^2 \end{pmatrix}. \tag{5.14}$$

The transformation from the gauge eigenstates  $\phi_i^\pm$ ,  $\eta_i$  and  $\rho_i$  to the physical mass eigenstates is performed with the help of orthogonal matrices

$$R(\theta) = \begin{pmatrix} c_\theta & -s_\theta \\ s_\theta & c_\theta \end{pmatrix}, \tag{5.15}$$

which diagonalize the mass matrices. Here the short-hand notation  $c_\theta = \cos(\theta)$  and  $s_\theta = \sin(\theta)$  has been applied and  $\theta$  stands for a generic mixing angle. It is obvious from the expressions in Eqs. 5.12 and 5.13 that the charged and the CP-odd mass matrices are diagonalized by the same mixing angle, which is conventionally called  $\beta$ . The mixing angle of the CP-even scalars is usually denoted as  $\alpha$ . By virtue of this definition, we have

$$R(\beta)^T \mathcal{M}_{\phi^\pm} R(\beta) = \begin{pmatrix} 0 & 0 \\ 0 & m_{H^\pm}^2 \end{pmatrix} \equiv \mathcal{D}_{\phi^\pm}, \tag{5.16}$$

$$R(\beta)^T \mathcal{M}_\eta R(\beta) = \begin{pmatrix} 0 & 0 \\ 0 & m_{A_0}^2 \end{pmatrix} \equiv \mathcal{D}_\eta, \tag{5.17}$$

$$R(\alpha)^T \mathcal{M}_\rho R(\alpha) = \begin{pmatrix} m_H^2 & 0 \\ 0 & m_h^2 \end{pmatrix} \equiv \mathcal{D}_\rho. \tag{5.18}$$

The eigenvalues appearing here are to be identified with the masses of the corresponding mass eigenstates

$$S_{\phi^\pm} \equiv \begin{pmatrix} G^\pm \\ H^\pm \end{pmatrix} = R^T(\beta) \begin{pmatrix} \phi_1^\pm \\ \phi_2^\pm \end{pmatrix}, \tag{5.19}$$

$$S_\eta \equiv \begin{pmatrix} G_0 \\ A_0 \end{pmatrix} = R^T(\beta) \begin{pmatrix} \eta_1 \\ \eta_2 \end{pmatrix}, \tag{5.20}$$

$$S_\rho \equiv \begin{pmatrix} H \\ h \end{pmatrix} = R^T(\alpha) \begin{pmatrix} \rho_1 \\ \rho_2 \end{pmatrix}. \tag{5.21}$$

As required by the Higgs mechanism, the mass eigenstates comprise the three would-be Goldstone bosons  $G_0$ ,  $G^+$  and  $G^-$ , which provide the three longitudinal degrees of freedom for the  $Z$ ,  $W^+$  and  $W^-$  bosons. The five remaining fields combine to form five physical Higgs bosons: two CP-even scalars,  $h$  and  $H$ , where  $h$  is defined as being the lighter of both, one CP-odd field  $A_0$  and two charged ones,  $H^+$  and  $H^-$ .

Later it will prove beneficial to also transfer the tadpole parameters  $T_1^0$  and  $T_2^0$  to the mass basis

$$\begin{pmatrix} T_H^0 \\ T_h^0 \end{pmatrix} = R(\alpha)^T \begin{pmatrix} T_1^0 \\ T_2^0 \end{pmatrix}. \quad (5.22)$$

Furthermore, after the rotation to the mass basis, the bilinear tadpole terms of Eq. (5.11) read

$$\begin{aligned} V \supset & (G^- \quad H^-) \begin{pmatrix} T_{G^+G^+}^0 & T_{G^+H^+}^0 \\ T_{H^+G^+}^0 & T_{H^+H^+}^0 \end{pmatrix} \begin{pmatrix} G^+ \\ H^+ \end{pmatrix} + \frac{1}{2} (G_0 \quad A_0) \begin{pmatrix} T_{G_0G_0}^0 & T_{G_0A_0}^0 \\ T_{A_0G_0}^0 & T_{A_0A_0}^0 \end{pmatrix} \begin{pmatrix} G_0 \\ A_0 \end{pmatrix} \\ & + \frac{1}{2} (H \quad h) \begin{pmatrix} T_{HH}^0 & T_{Hh}^0 \\ T_{hH}^0 & T_{hh}^0 \end{pmatrix} \begin{pmatrix} H \\ h \end{pmatrix}, \end{aligned} \quad (5.23)$$

with

$$\begin{pmatrix} T_{G^+G^+}^0 & T_{G^+H^+}^0 \\ T_{H^+G^+}^0 & T_{H^+H^+}^0 \end{pmatrix} = \begin{pmatrix} T_{G_0G_0}^0 & T_{G_0A_0}^0 \\ T_{A_0G_0}^0 & T_{A_0A_0}^0 \end{pmatrix} = R^T(\beta) T_\varphi^0 R(\beta), \quad (5.24)$$

$$(5.25)$$

$$\begin{pmatrix} T_{HH}^0 & T_{Hh}^0 \\ T_{hH}^0 & T_{hh}^0 \end{pmatrix} = R^T(\alpha) T_\varphi^0 R(\alpha).$$

### 5.3. Independent Parameters of the Scalar Potential

In its original form, given in Eq. (5.4), the scalar potential of the 2HDM incorporates the eight real parameters  $m_{11}^2$ ,  $m_{22}^2$ ,  $m_{12}^2$  and  $\lambda_1 - \lambda_5$  and the two vevs  $v_1$  and  $v_2$ . Using the tadpole equations Eqs. 5.8 and 5.9 two of these,  $m_{11}^2$  and  $m_{22}^2$ , can be traded for the tadpole parameters  $T_1^0$  and  $T_2^0$ .

Yet, often it is more convenient to use another set of parameters, the elements of which can more directly be related to physical observables. Furthermore it turns out that in defining this new set of independent parameters, it is sensible to treat the gauge sector and the scalar sector simultaneously. This is due to the fact that the masses of the gauge bosons

$$M_W^2 = \frac{g_2^2(v_1^2 + v_2^2)}{4} = \frac{g_2^2 v^2}{4}, \quad (5.26)$$

$$M_Z^2 = \frac{(g_1^2 + g_2^2)(v_1^2 + v_2^2)}{4} = \frac{M_W^2}{c_W^2}, \quad (5.27)$$

the electric charge

$$e = g_2 s_W \quad (5.28)$$

and the vev

$$v = \sqrt{v_1^2 + v_2^2} \quad (5.29)$$

cannot at the same time be treated as independent parameters. Here  $s_W$  and  $c_W$  denote the sine and cosine of the Weinberg angle  $\theta_W$ , defined as

$$c_W \equiv \cos(\theta_W) = \frac{M_W}{M_Z}. \quad (5.30)$$

Including the two gauge couplings  $g_2$  and  $g_1$ , the set of independent parameters in the original basis, denoted as set 1, is given by

$$\boxed{\text{set 1} = \{T_1^0, T_2^0, m_{12}^2, \lambda_1, \lambda_2, \lambda_3, \lambda_4, \lambda_5, v_1, v_2, g_1, g_2\}}. \quad (5.31)$$

An obvious choice for the parameters of the new set are the masses of the physical Higgs bosons and of the gauge bosons as well as the electric charge. All of these are physical observables. For reasons which will become clear in Sec. 6, where renormalization is discussed, it is also advantageous to choose the tadpole parameters  $T_H^0$  and  $T_h^0$  in the mass basis as elements of the new set. Furthermore we can pick the two rotation angles  $\alpha$  and  $\beta$  as independent parameters. As last parameter we choose  $m_{12}^2$ . With this choice the new set of parameters, set 2, is given by

$$\boxed{\text{set 2} = \{T_H^0, T_h^0, m_{12}^2, M_H^2, M_h^2, M_{A_0}^2, M_{H^\pm}^2, M_W^2, M_Z^2, e, \alpha, \beta\}}. \quad (5.32)$$

The relations between the parameters of the two sets can directly be deduced from the potential and the definitions in Eqs. 5.16 - 5.18. For  $\lambda_1 - \lambda_5$  we find the relations [106]

$$\lambda_1 = \frac{1}{v^2 c_\beta^2} (s_\alpha^2 m_h^2 + c_\alpha^2 m_H^2 - t_\beta m_{12}^2), \quad (5.33)$$

$$\lambda_2 = \frac{1}{v^2 s_\beta^2} \left( c_\alpha^2 m_h^2 + s_\alpha^2 m_H^2 - \frac{m_{12}^2}{t_\beta} \right), \quad (5.34)$$

$$\lambda_3 = 2 \frac{m_{H^\pm}^2}{v^2} + \frac{1}{v^2} \frac{s_{2\alpha}}{s_{2\beta}} (m_H^2 - m_h^2) - \frac{2m_{12}^2}{v^2 s_{2\beta}}, \quad (5.35)$$

$$\lambda_4 = \frac{m_{A_0}^2 - 2m_{H^\pm}^2}{v^2} + \frac{2m_{12}^2}{v^2 s_{2\beta}}, \quad (5.36)$$

$$\lambda_5 = -\frac{m_{A_0}^2}{v^2} + \frac{2m_{12}^2}{v^2 s_{2\beta}}, \quad (5.37)$$

where we introduce the notation  $t_\beta = \tan \beta$ . Likewise, the angles  $\alpha$  and  $\beta$  can be expressed in terms of set 1 parameters as

$$\tan(\beta) = \frac{v_2}{v_1}, \quad (5.38)$$

$$\tan(2\alpha) = \frac{s_{2\beta} (\lambda_{345} v^2 s_{2\beta} - 2m_{12}^2)}{c_\beta^2 (\lambda_1 v^2 s_{2\beta} - 2m_{12}^2) - s_\beta^2 (\lambda_2 v^2 s_{2\beta} - 2m_{12}^2)}. \quad (5.39)$$

## 5.4. The Yukawa Sector

The most general Yukawa Lagrangian  $\mathcal{L}_{\text{Yuk}}$  for a 2HDM is given by [107, 108]

$$\begin{aligned} \mathcal{L}_{\text{Yuk}} = & - (\bar{Q}_L (\mathcal{Y}_1^D \Phi_1 + \mathcal{Y}_2^D \Phi_2) D_R + \bar{Q}_L (\mathcal{Y}_1^U \bar{\Phi}_1 + \mathcal{Y}_2^U \bar{\Phi}_2) U_R \\ & + \bar{L}_L (\mathcal{Y}_1^E \Phi_1 + \mathcal{Y}_2^E \Phi_2) E_R) + h.c. \end{aligned} \quad (5.40)$$

In the compact notation chosen here, the Yukawa couplings  $\mathcal{Y}_i^J$ ,  $J \in \{D, U, E\}$ , are complex  $3 \times 3$  matrices in flavor space. Furthermore, the left-handed fermions have been grouped

into  $SU(2)_L$  doublets, which are at the same time triplets in flavor space. For the example of the left-handed quark fields, summarized in  $Q_L$ , this amounts to  $(Q_L)_i = (u_{L,i}, d_{L,i})^T$ , where  $i \in \{1, 2, 3\}$  denotes the generation, with the identification  $\{u_1, u_2, u_3\} = \{u, d, t\}$  and  $\{d_1, d_2, d_3\} = \{d, s, b\}$ . Analogous definitions are made for the leptons. The right-handed components are singlets under  $SU(2)$  and triplets in flavor space. We have also introduced the conjugate scalar doublets, defined as  $(\bar{\Phi}_{1/2})_i = \epsilon_{ji} (\Phi_{1/2})_j^*$ , where  $\epsilon_{ij}$  represents the totally anti-symmetric tensor in two dimensions.

Expanding the two scalar doublets around their vevs (cf. Eq. (5.7)) gives rise to an interaction term between two fermions and one scalar and a mass term for the fermions. Generically, the thus generated mass matrix for the fermions of type  $J \in \{D, U, E\}$  has the following form

$$\mathcal{M}^J = (\mathcal{Y}_1^J) \frac{v_1}{\sqrt{2}} + (\mathcal{Y}_2^J) \frac{v_2}{\sqrt{2}}. \quad (5.41)$$

From this expression one can directly see that a diagonalization of the mass matrix does not in general also lead to a diagonalization of the interaction terms, since the two Yukawa matrices  $\mathcal{Y}_1$  and  $\mathcal{Y}_2$  need not be simultaneously diagonalizable. This leads to the occurrence of FCNC. Due to the fact that there are severe constraints on FCNC from experiment, their appearance has to be prohibited by the introduction of suitable discrete symmetries or at least be strongly suppressed.

An obvious possibility to avoid FCNC is to allow all fermions with identical quantum numbers to couple only to one of the two doublets. For the quark sector, there are essentially two options to accomplish this: In the 2HDM of *type I*, all quarks couple to the same doublet, chosen to be  $\Phi_2$  by convention. This is guaranteed by imposing a  $Z_2$  symmetry on the Lagrangian, demanding invariance under  $\Phi_1 \rightarrow -\Phi_1$ . By contrast, in the 2HDM of *type II*, the up-type quarks couple to  $\Phi_2$ , whereas the down-type quarks couple to  $\Phi_1$ . This, in turn, is a consequence of an invariance under  $\Phi_1 \rightarrow -\Phi_1$ ,  $d_{R,i} \rightarrow -d_{R,i}$ .<sup>1</sup>

For both types of models, the leptons are assumed to couple to the same doublet as the down-type quarks. However, there is no theoretical argument against a different assignment of the lepton couplings. Starting from the type I 2HDM but coupling the leptons to  $\Phi_2$  instead of  $\Phi_1$  leads to the *lepton-specific* (LS) model. The fourth possibility, taking the quark couplings of the type II but coupling the leptons to  $\Phi_1$ , yields the *flipped* (F) model. Like for the quarks, the couplings of the leptons can be enforced by imposing the corresponding  $Z_2$  symmetry on the Lagrangian [18].

## 5.5. The Gauge Fixing and the Ghost Sector

As explained in Sec. 3.3, the unphysical degrees of freedom inherent in the gauge field four-vectors force us to impose a gauge condition if we want to quantize a gauge theory. This can be achieved in a consistent manner by a procedure called *gauge fixing*, which is due to L.D. Faddeev and V.N. Popov [92].

During the course of this procedure, additional terms are introduced into the Lagrangian, the gauge-fixing and the ghost Lagrangian,  $\mathcal{L}_{\text{gf}}$  and  $\mathcal{L}_{\text{ghost}}$ . Their exact form depends on the gauge condition imposed on the theory. In this thesis, we will adhere to a class of gauges called the linear  $R_\xi$  gauges, which has proven to be convenient for higher-order calculations and is frequently used. For the sake of completeness, we briefly state the resulting terms, without giving a detailed derivation. Details can be found in any textbook on QFT and gauge

<sup>1</sup>Note that the Higgs sector of the MSSM constitutes a type II 2HDM.

theories, e.g. in Refs. [58, 59, 109]. Following the notation used in [77], we define

$$\mathcal{F}^\gamma = \frac{1}{\sqrt{\xi_A}} (\partial_\mu A^\mu), \quad (5.42)$$

$$\mathcal{F}^Z = \frac{1}{\sqrt{\xi_Z}} (\partial_\mu Z^\mu - \xi_Z M_Z G_0), \quad (5.43)$$

$$\mathcal{F}^\pm = \frac{1}{\sqrt{\xi_W}} (\partial_\mu W^{\pm\mu} \mp i\xi_W M_W G^\pm), \quad (5.44)$$

which allows us to write down a compact expression for  $\mathcal{L}_{\text{gf}}$  [38, 77]

$$\mathcal{L}_{\text{gf}} = -\frac{1}{2} [(\mathcal{F}^\gamma)^2 + (\mathcal{F}^Z)^2 + 2\mathcal{F}^+ \mathcal{F}^-]. \quad (5.45)$$

The parameters  $\xi_A$ ,  $\xi_Z$  and  $\xi_W$  appearing here are the so-called gauge fixing parameters. They are unphysical, wherefore a physical quantity must not depend on them.

Apart from these gauge-fixing terms, the Faddeev-Popov procedure gives rise to terms containing *ghost fields*. As anti-commuting scalar fields, these ghosts violate the spin-statistics theorem and hence have to be considered as unphysical degrees of freedom, which can only appear inside loops but never as external particles. According to the prescription by Faddeev and Popov, the corresponding term in the Lagrangian,  $\mathcal{L}_{\text{ghost}}$ , can be derived as [77]

$$\mathcal{L}_{\text{ghost}} = \bar{u}^j(x) \frac{\delta \mathcal{F}^j}{\delta \vartheta^\beta(x)} u^\beta(x), \quad j = \{\gamma, Z, \pm\}. \quad (5.46)$$

Here  $\bar{u}^j$ ,  $u^j$  represent the Faddeev-Popov ghosts and  $\frac{\delta \mathcal{F}^j}{\delta \vartheta^\beta(x)}$  stands for the variation of  $\mathcal{F}^j$  under an infinitesimal gauge transformation with parameter  $\vartheta(x)$ .

It should be noted, that there are other possibilities to perform the gauge-fixing, leading to different forms of the gauge-fixing and ghost terms [110, 111]. However, for our purposes the linear gauge-fixing proposed here is sufficient and convenient.

With this, we conclude our discussion of the individual terms in  $\mathcal{L}_{\text{ew}}$ . In the subsequent chapter, we enter the central subject of this part of the thesis: the development of a gauge-independent renormalization scheme for the 2HDM.

---

## General Remarks on the Renormalization of the 2HDM

---

In the current chapter, we will set the scene for the endeavour of developing a consistent, suitable renormalization scheme for the 2HDM. We will introduce all necessary counterterms and discuss renormalization conditions to fix them on a general footing. Furthermore, we will detail certain subtleties and important issues, which arise in the renormalization procedure. First, in Sec. 6.1, we will discuss different approaches to the renormalization of mixing fields and specify the choice we will adhere to throughout part II. Afterwards, in 6.2, we will introduce all counterterms required for our purposes in a very generic manner. In doing so, we will dedicate a distinct section (Sec. 6.3) to the subject of tadpole (non-)renormalization. Two tadpole schemes will be presented: The first approach, dubbed scheme I, introduces tadpole counterterms to cancel all higher-order tadpole contributions, order by order in perturbation theory. In contrast, the second approach, scheme II, will get along without tadpole counterterms and instead rely on shifts in the vevs. Since the effect of the tadpole treatment on the renormalization program and on issues of gauge dependence will turn out crucial, the two schemes will be treated separately throughout the rest of Part II.

The subsequent sections will consider OS renormalization conditions for the scalar sector of the 2HDM (Sec. 6.4) as well as for the gauge and fermion sector ( Sec. 6.5).

We will then canvass the subject of mixing angle renormalization in Sec. 6.6, where we summarize different possibilities and give an overview over previous research on the topic. Finally, in Sec. 6.7 we will briefly discuss viable renormalization conditions for the last parameter to be renormalized,  $m_{12}^2$ .

### 6.1. Renormalization of Mixing Fields

Whenever a model contains fields with identical quantum numbers, the renormalization procedure is complicated by the fact that the mixing between these has to be taken into account. The scalar sector of the 2HDM contains three pairs of particles with identical quantum numbers. As shown in the previous chapter, a diagonalization of the corresponding mass matrices leads to the correct tree-level mass eigenstates, which do not mix and therefore exhibit a diagonal propagator in the lowest order of perturbation theory. However, in higher orders quantum corrections reintroduce a mixing between the members of each of the pairs. Consequently, the renormalization procedure has to account for this mixing, which calls for the introduction of matrix valued mass counterterms and WFRCs. All counterterms and WFRCs

appearing in this section are understood to be of one-loop order. For convenience, however, we consistently omit the superscript (1).

There are several different possibilities to introduce these counterterms, which can be discriminated by the number of independent parameters they impose and by the definition of the rotation matrices  $R(\theta)$  ( $\theta = \alpha, \beta$ ).

Especially the latter point is a potential source of confusion since different authors use different definitions of the rotation matrix  $R(\theta)$ . The first option is to define  $R(\theta)$  as the matrix which diagonalizes the *bare* tree-level mass matrix  $\mathcal{M}_b$

$$\begin{aligned} R^T(\theta_b)\mathcal{M}_bR(\theta_b) &= \mathcal{D}_b \\ \Rightarrow R^T(\theta_b)(\mathcal{M}_r + \delta\mathcal{M})R(\theta_b) &= \mathcal{D}_r + \delta\mathcal{D}. \end{aligned} \quad (6.1)$$

Here and in the following  $\mathcal{M}$ ,  $\mathcal{D}$  and  $R(\theta)$  generically stand for one of the three mass and rotation matrices introduced in Eqs. 5.16 - 5.18. In order not to overload the notation, we will consistently omit the indices specifying the respective pair of scalars and leave the angle  $\theta$  implicit.

Alternatively,  $R(\theta)$  can be defined to diagonalize the *renormalized* tree-level mass matrix  $\mathcal{M}_r$ ,

$$\begin{aligned} R^T(\theta_r)\mathcal{M}_rR(\theta_r) &= \mathcal{D}_r \\ \Rightarrow R^T(\theta_r)\mathcal{M}_bR(\theta_r) &= R^T(\theta_r)(\mathcal{M}_r + \delta\mathcal{M})R(\theta_r) \\ &= \mathcal{D}_r + R^T(\theta_r)\delta\mathcal{M}R(\theta_r). \end{aligned} \quad (6.2)$$

These two approaches differ in two important consequences: First, the approach in Eq. (6.1) does not lead to off-diagonal mass counterterms as the matrix  $\delta\mathcal{D}$  is diagonal by definition. In contrast to that, the term  $R^T(\theta_r)\delta\mathcal{M}R(\theta_r)$  in Eq. (6.2) is not diagonal in general. The second difference concerns the rotation angles: The angle  $\theta_b$  in Eq. (6.1) is to be regarded as the *bare* rotation angle, which as a consequence has to receive a counterterm. As opposed to that,  $\theta_r$  in Eq. (6.2) is defined entirely in terms of *renormalized* parameters and therefore is to be considered as *renormalized* quantity, which does not receive a counterterm. Both schemes have been applied to the 2HDM in the literature. Examples for the first approach can be found in [38, 40, 112], whereas the second scheme was used in [39].

In the second approach one has to carefully distinguish between the *rotation* angles  $\alpha_{\text{rot}}$  and  $\beta_{\text{rot}}$ , entering the Lagrangian and the Feynman rules via the rotation matrices that diagonalize the CP-even or the CP-odd and the charged scalar mass matrices, and the *parametric* angles  $\alpha_p$  and  $\beta_p$ , entering via the relations Eqs. 5.38 and 5.39. Since the latter are part of the set of independent parameters we chose, they always have to receive a counterterm. However, the first ones are not renormalized, if we proceed according to Eq. (6.2). Due to this complication, we will work with the first definition of  $R(\theta)$  in the following, i.e. we will introduce counterterms for the rotation matrices and treat the parametric and the rotation angles on an equal footing. We will hence not distinguish between  $\alpha_{\text{rot}}$ ,  $\beta_{\text{rot}}$  and  $\alpha_p$ ,  $\beta_p$ , except in a few exceptional cases.

Next we turn to the subject of field renormalization. Various options are available for the introduction of WFRCs, differing in the numbers of independent parameters. The minimal choice is to introduce two independent parameters, one for each doublet

$$\Phi_i \rightarrow Z_{\Phi_i}^{1/2}\Phi_i, \quad i = 1, 2, \quad (6.3)$$

leading to the following matrices of WFRCs

$$\begin{aligned} \begin{pmatrix} \varphi_1 \\ \varphi_2 \end{pmatrix}_b &= Z_\varphi^{1/2} \begin{pmatrix} \varphi_1 \\ \varphi_2 \end{pmatrix}_r \equiv \begin{pmatrix} Z_{\Phi_1}^{1/2} & 0 \\ 0 & Z_{\Phi_2}^{1/2} \end{pmatrix} \begin{pmatrix} \varphi_1 \\ \varphi_2 \end{pmatrix}_r \\ &= \begin{pmatrix} 1 + \frac{1}{2}\delta Z_{\Phi_1} & 0 \\ 0 & 1 + \frac{1}{2}\delta Z_{\Phi_2} \end{pmatrix} \begin{pmatrix} \varphi_1 \\ \varphi_2 \end{pmatrix}_r, \end{aligned} \quad (6.4)$$

where  $\varphi_i = \phi_i^\pm, \rho_i, \eta_i$ . Here  $Z_\varphi^{1/2}$  is defined as the matrix of WFRCs for the pair of scalars under consideration in the gauge basis. Due to gauge invariance, this choice is sufficient in order to render all Green's functions of the theory finite [113]. However, it is not possible to define a complete OS scheme, where all scalars obey the conditions to be defined below in section 6.1. As a consequence, this minimal scheme requires the introduction of finite wave function correction factors when processes with external scalars are considered [46, 91, 114]. To circumvent the necessity of such factors, one can directly start from a non-minimal set of WFRCs. The most general possibility is to introduce four independent constants for each of the three pairs of particles

$$\begin{aligned} \begin{pmatrix} \varphi_1 \\ \varphi_2 \end{pmatrix}_b &= Z_\varphi^{1/2} \begin{pmatrix} \varphi_1 \\ \varphi_2 \end{pmatrix}_r = \begin{pmatrix} Z_{\varphi_1\varphi_1}^{1/2} & Z_{\varphi_1\varphi_2}^{1/2} \\ Z_{\varphi_2\varphi_1}^{1/2} & Z_{\varphi_2\varphi_2}^{1/2} \end{pmatrix} \begin{pmatrix} \varphi_1 \\ \varphi_2 \end{pmatrix}_r \\ &= \begin{pmatrix} 1 + \frac{1}{2}\delta Z_{\varphi_1\varphi_1} & \frac{1}{2}\delta Z_{\varphi_1\varphi_2} \\ \frac{1}{2}\delta Z_{\varphi_2\varphi_1} & 1 + \frac{1}{2}\delta Z_{\varphi_2\varphi_2} \end{pmatrix} \begin{pmatrix} \varphi_1 \\ \varphi_2 \end{pmatrix}_r. \end{aligned} \quad (6.5)$$

While the introduction of the WFRCs is often presented in the gauge basis, actual calculations are most conveniently performed in the mass basis. The transformation of the matrices  $Z_\varphi^{1/2}$  to the mass basis, necessary for this purpose, is accomplished with the rotation matrix  $R(\theta)$ . Again, attention has to be paid to the proper definition of  $R(\theta)$ .  $R(\theta_b)$  from Eq. (6.1) diagonalizes the *bare* mass matrix and thus connects the *bare* gauge eigenstates with the *bare* mass eigenstates. On the contrary,  $R(\theta_r)$  from Eq. (6.2) transforms the *renormalized* gauge eigenstates to the *renormalized* mass eigenstates. If  $R(\theta)$  is defined in the second way, i.e. as the matrix that diagonalizes the *renormalized* tree-level mass matrix, the relation between  $Z_\varphi^{1/2}$  in the gauge basis and its counterpart  $Z_S^{1/2}$  in the mass basis is simply

$$Z_S^{1/2} = R^T(\theta_r) Z_\varphi^{1/2} R(\theta_r). \quad (6.6)$$

This can directly be derived from the corresponding mass term in the Lagrangian

$$\begin{aligned} \mathcal{L} &\supset \begin{pmatrix} \varphi_1 \\ \varphi_2 \end{pmatrix}_b^\dagger \mathcal{M}_b \begin{pmatrix} \varphi_1 \\ \varphi_2 \end{pmatrix}_b \\ &= \begin{pmatrix} \varphi_1 \\ \varphi_2 \end{pmatrix}_r^\dagger Z_\varphi^{1/2\dagger} (\mathcal{M}_r + \delta\mathcal{M}) Z_\varphi^{1/2} \begin{pmatrix} \varphi_1 \\ \varphi_2 \end{pmatrix}_r \\ &= \begin{pmatrix} \varphi_1 \\ \varphi_2 \end{pmatrix}_r^\dagger R(\theta_r) R^T(\theta_r) Z_\varphi^{1/2\dagger} R(\theta_r) R^T(\theta_r) (\mathcal{M}_r + \delta\mathcal{M}) R(\theta_r) R^T(\theta_r) Z_\varphi^{1/2} R(\theta_r) R^T(\theta_r) \begin{pmatrix} \varphi_1 \\ \varphi_2 \end{pmatrix}_r \\ &= \begin{pmatrix} S_1 \\ S_2 \end{pmatrix}_r^\dagger \underbrace{R^T(\theta_r) Z_\varphi^{1/2\dagger} R(\theta_r)}_{Z_S^{1/2\dagger}} (\mathcal{D}_r + R^T(\theta_r) \delta\mathcal{M} R(\theta_r)) \underbrace{R^T(\theta_r) Z_\varphi^{1/2} R(\theta_r)}_{Z_S^{1/2}} \begin{pmatrix} S_1 \\ S_2 \end{pmatrix}_r, \end{aligned} \quad (6.7)$$

where we have used the relation  $(S_1, S_2)_r^T = R^T(\theta_r) (\varphi_1, \varphi_2)_r^T$ , with

$$(S_1, S_2) \in \{(H, h), (G_0, A_0), (G^\pm, H^\pm)\}.$$

$Z_S^{1/2}$  is to be understood as the matrix corresponding to the pair of particles under consideration.

If, on the other hand,  $R(\theta)$  is defined according to Eq. (6.1), more care has to be taken to arrive at the correct definition of  $Z_S^{1/2}$ . Starting again from the mass term in the Lagrangian,

we find

$$\begin{aligned}
\mathcal{L} &\supset \begin{pmatrix} \varphi_1 \\ \varphi_2 \end{pmatrix}_b^\dagger \mathcal{M}_b \begin{pmatrix} \varphi_1 \\ \varphi_2 \end{pmatrix}_b \\
&= \begin{pmatrix} \varphi_1 \\ \varphi_2 \end{pmatrix}_b^\dagger R(\theta_b) R^T(\theta_b) \mathcal{M}_b R(\theta_b) R^T(\theta_b) \begin{pmatrix} \varphi_1 \\ \varphi_2 \end{pmatrix}_b \\
&= \begin{pmatrix} S_1 \\ S_2 \end{pmatrix}_b^\dagger (\mathcal{D}_b) \begin{pmatrix} S_1 \\ S_2 \end{pmatrix}_b \\
&= \begin{pmatrix} S_1 \\ S_2 \end{pmatrix}_r^\dagger Z_S^{1/2\dagger} (\mathcal{D}_r + \delta\mathcal{D}) Z_S^{1/2} \begin{pmatrix} S_1 \\ S_2 \end{pmatrix}_r.
\end{aligned} \tag{6.8}$$

The matrix  $Z_S^{1/2}$  can now be connected to  $Z_\varphi^{1/2}$  in the gauge basis as follows

$$\begin{aligned}
Z_S^{1/2} \begin{pmatrix} S_1 \\ S_2 \end{pmatrix}_r &= \begin{pmatrix} S_1 \\ S_2 \end{pmatrix}_b = R^T(\theta_b) \begin{pmatrix} \varphi_1 \\ \varphi_2 \end{pmatrix}_b = R^T(\theta_b) Z_\varphi^{1/2} \begin{pmatrix} \varphi_1 \\ \varphi_2 \end{pmatrix}_r \\
&= R^T(\theta_b) Z_\varphi^{1/2} R(\theta_r) R^T(\theta_r) \begin{pmatrix} \varphi_1 \\ \varphi_2 \end{pmatrix}_r \\
&= R^T(\theta_b) Z_\varphi^{1/2} R(\theta_r) \begin{pmatrix} S_1 \\ S_2 \end{pmatrix}_r.
\end{aligned} \tag{6.9}$$

From this, the relation between  $Z_S^{1/2}$  and  $Z_\varphi^{1/2}$  can directly be read off

$$Z_S^{1/2} = R^T(\theta_b) Z_\varphi^{1/2} R(\theta_r) = R^T(\theta_r + \delta\theta) Z_\varphi^{1/2} R(\theta_r) = R^T(\delta\theta) R^T(\theta_r) Z_\varphi^{1/2} R(\theta_r), \tag{6.10}$$

where the last equality follows directly from the angle sum identities for sine and cosine. Note in particular, that with this definition of  $R^T(\theta)$ , the angular counterterms find their way into the WFRCs. This fact has to be considered explicitly, if the WFRCs are not introduced in their most general form. If, however, the WFRCs in the gauge basis comprise four independent elements, this relation is no longer crucial, since in this case the four independent constants can be adjusted to fulfill any renormalization condition, independent of angular counterterms.

In the subsequent chapters, we will omit the indices  $r$  and  $b$  and state them explicitly only, where necessary. Whether a quantity is bare or renormalized should be clear from the context. Furthermore, we will throughout use a rotation matrix  $R^T(\theta)$  defined according to Eq. (6.1) and hence WFRCs in the sense of Eq. (6.10). In most cases, the entrance of the angular counterterms into the WFRCs will not be relevant, since we assume them to comprise four independent elements in the gauge basis. However, in Sec. 7.4 we drop this assumption and make use of the relation in Eq. (6.10), in order to derive expressions for  $\delta\alpha$  and  $\delta\beta$ .

## 6.2. Introduction of Counterterms

Following the procedure sketched in Sec. 3.1.2 in order to renormalize the 2HDM, we have to introduce counterterms for all parameters of the set chosen in Eq. (5.32) as well as wave function renormalization constants for the fields of the model. Again, all counterterms and WFRCs introduced in this section are to be understood as being of one-loop order.

For the gauge sector, this prescription leads to the following set of counterterms

$$M_W^2 \rightarrow M_W^2 + \delta M_W^2, \tag{6.11}$$

$$M_Z^2 \rightarrow M_Z^2 + \delta M_Z^2, \tag{6.12}$$

$$e \rightarrow (1 + \delta Z_e) e \tag{6.13}$$

and wave function renormalization constants

$$W^\pm \rightarrow \left(1 + \frac{1}{2}\delta Z_W\right) W^\pm \quad (6.14)$$

$$\begin{pmatrix} Z \\ \gamma \end{pmatrix} \rightarrow \begin{pmatrix} 1 + \frac{1}{2}\delta Z_{ZZ} & \frac{1}{2}\delta Z_{Z\gamma} \\ \frac{1}{2}\delta Z_{\gamma Z} & 1 + \frac{1}{2}\delta Z_{\gamma\gamma} \end{pmatrix} \begin{pmatrix} Z \\ \gamma \end{pmatrix}. \quad (6.15)$$

For convenience we also introduce the abbreviation

$$\delta g_2 = \delta \left( \frac{e}{s_W} \right) = \left( \delta Z_e + \frac{1}{2} \frac{1}{M_Z^2 - M_W^2} (\delta M_W^2 - c_W^2 \delta M_Z^2) \right), \quad (6.16)$$

for the counterterm of the gauge coupling  $g_2$ , which is a dependent parameter in our scheme. In the Higgs sector our choice of the set of independent parameters gives rise to the subsequent renormalization constants

$$m_h^2 \rightarrow m_h^2 + \delta m_h^2, \quad (6.17)$$

$$m_H^2 \rightarrow m_H^2 + \delta m_H^2, \quad (6.18)$$

$$m_{A_0}^2 \rightarrow m_{A_0}^2 + \delta m_{A_0}^2, \quad (6.19)$$

$$m_{H^\pm}^2 \rightarrow m_{H^\pm}^2 + \delta m_{H^\pm}^2, \quad (6.20)$$

$$\alpha \rightarrow \alpha + \delta\alpha, \quad (6.21)$$

$$\beta \rightarrow \beta + \delta\beta, \quad (6.22)$$

$$m_{12}^2 \rightarrow m_{12}^2 + \delta m_{12}^2. \quad (6.23)$$

As outlined in the previous section, we have to introduce matrix valued WFRCs for the scalar fields, which acquire the following form in the mass basis

$$\begin{pmatrix} H \\ h \end{pmatrix} \rightarrow \begin{pmatrix} 1 + \frac{1}{2}\delta Z_{HH} & \frac{1}{2}\delta Z_{Hh} \\ \frac{1}{2}\delta Z_{hH} & 1 + \frac{1}{2}\delta Z_{hh} \end{pmatrix} \begin{pmatrix} H \\ h \end{pmatrix}, \quad (6.24)$$

$$\begin{pmatrix} G_0 \\ A_0 \end{pmatrix} \rightarrow \begin{pmatrix} 1 + \frac{1}{2}\delta Z_{G_0 G_0} & \frac{1}{2}\delta Z_{G_0 A_0} \\ \frac{1}{2}\delta Z_{A_0 G_0} & 1 + \frac{1}{2}\delta Z_{A_0 A_0} \end{pmatrix} \begin{pmatrix} G_0 \\ A_0 \end{pmatrix}, \quad (6.25)$$

$$\begin{pmatrix} G^\pm \\ H^\pm \end{pmatrix} \rightarrow \begin{pmatrix} 1 + \frac{1}{2}\delta Z_{G^\pm G^\pm} & \frac{1}{2}\delta Z_{G^\pm H^\pm} \\ \frac{1}{2}\delta Z_{H^\pm G^\pm} & 1 + \frac{1}{2}\delta Z_{H^\pm H^\pm} \end{pmatrix} \begin{pmatrix} G^\pm \\ H^\pm \end{pmatrix}. \quad (6.26)$$

A complete renormalization of the 2HDM would, of course, also require the introduction of counterterms for the strong and the Yukawa sector. However, since these counterterms will not enter our calculation in the following, we refrain from introducing them here. They are identical to the ones of the SM and therefore can directly be taken over from e.g. Ref. [77]. The only renormalization constants of the fermion sector, that will be needed below, are the mass counterterms and WFRCs for the  $\tau$  lepton, which we introduce as

$$m_\tau \rightarrow m_\tau + \delta m_\tau, \quad (6.27)$$

$$\Psi_\tau^L \rightarrow \left(1 + \frac{\delta Z_\tau^L}{2}\right) \Psi_\tau^L, \quad \Psi_\tau^R \rightarrow \left(1 + \frac{\delta Z_\tau^R}{2}\right) \Psi_\tau^R, \quad (6.28)$$

$L$  and  $R$  denoting the left- and the right-handed components of the spinor  $\Psi_\tau$ .

Finally, also the tadpole parameters  $T_1^0$  and  $T_2^0$  introduced in Sec. 5.1 can be assigned counterterms, which are supposed to cancel the higher-order tadpole contributions. Yet, the introduction of such counterterms is not obligatory and in fact we will find that it can sometimes be advisable not to renormalize the tadpole parameters. Due to the importance of this point, different possibilities of treating tadpoles will be covered separately in the next section.

### 6.3. Treatment of the Tadpoles

Radiative corrections give rise to additional contributions linear in the Higgs fields, which are diagrammatically represented by tadpole diagrams. Since these tadpole contributions violate the minimum conditions Eqs. 5.8 and 5.9 in higher orders, they have to be cancelled by the introduction of appropriate counterterms or shifts.

There are essentially two possibilities to treat the tadpole contributions [115, 116]. We will study both possibilities and their implications for the renormalization program in detail in Secs. 7 and 8.

The first possibility, which we call tadpole scheme I, is to introduce counterterms for the tadpole parameters

$$T_1^0 \rightarrow T_1^0 + \delta T_1 = 0 + \delta T_1, \quad (6.29)$$

$$T_2^0 \rightarrow T_2^0 + \delta T_2 = 0 + \delta T_2 \quad (6.30)$$

and to require these to cancel the tadpole diagrams, order by order in the perturbative expansion. To one-loop order the corresponding renormalization conditions can pictorially be

**Figure 6.1.:** Pictorial representation of the tadpole conditions in scheme I. The empty circle stands for generic one-loop contributions to the tadpole, while the crossed circle denotes the tadpole counterterm with  $i = 1, 2$ .

represented as shown in Fig. 6.1, leading to the following definition of the tadpole counterterms

$$\delta^{(1)} T_i = T_i^{(1)}, \quad i=1,2. \quad (6.31)$$

The clear advantage of this procedure, which is advocated e.g. in Refs. [58, 59, 77, 80], is the fact that all tadpole diagrams are cancelled by their respective counterterm and therefore need not be taken into account. Yet there is a price to be paid for this simplification of the calculation: By the introduction of the tadpole counterterms, part of the gauge dependence, formerly absorbed by the tadpole diagrams, is shifted into counterterms for physical parameters, like masses and mixing angles. As a result, these previously gauge-independent counterterms obtain an explicit dependence on the gauge fixing parameters. It is, however, important to note that this does not automatically imply a gauge dependence of the physical parameters themselves. For instance the pole mass, i.e. the location of the (complex) pole of the propagator of a physical particle, remains a gauge-independent quantity, even though the corresponding mass counterterm might explicitly depend on the gauge fixing parameters. This is shown and discussed by Gambino et al. in Ref. [88] and we will come back to this point in Sec. 8.1.

The second possibility, applied to the SM e.g. in Refs. [97, 101, 102, 117, 118], is not to introduce counterterms for the tadpole parameters but rather cancel the tadpole diagrams by shifts in the vevs  $v_i$ . We will refer to this scheme as tadpole scheme II. Instead of the conditions shown in Fig. 6.1, one now has to demand a cancellation of the shifted “tree-level” tadpoles  $T_i^0(v_j^{(0)} + \Delta v_j)$ ,  $i, j \in 1, 2$ , (i.e. the coefficient of the Lagrangian terms linear in the scalar fields, evaluated at the shifted vevs  $v_j^{(0)} + \Delta v_j$ ,  $v_j^{(0)}$  denoting the tree-level vev) and the

$$iT_i^{(1)} - iT_i^0(v_j^{(0)} + \Delta^{(1)}v_j)$$

$$+ \quad = \quad 0$$

**Figure 6.2.:** Pictorial representation of the tadpole conditions in scheme II. The empty circle stands for generic one-loop contributions to the tadpole, while the cross denotes the shifted “tree-level” tadpole  $T_i^0$ ,  $i=1,2$ .

tadpole diagrams up to the desired loop-order. At one-loop level for example, the equation illustrated in Fig. 6.2 has to be fulfilled. As a consequence of this condition, the vevs receive a shift  $\Delta v_i^{(n+1)}$  when going from the  $n$ th to the  $n+1$ st loop level

$$v_i^{(n+1)} = v_i^{(n)} + \Delta v_i^{(n+1)}. \quad (6.32)$$

Expressed in terms of the tree-level vev  $v_i^{(0)}$ , we find for  $v_i^{(n+1)}$

$$v_i^{(n+1)} = v_i^{(0)} + \sum_{j=1}^{n+1} \Delta v_i^{(j)} \equiv v_i^{(0)} + \Delta^{(n+1)}v_i. \quad (6.33)$$

This shift per definition guarantees a cancellation of the (shifted) tree-level and the higher-order tadpoles. Hence, at first sight one might erroneously conclude that, due to this cancellation, also in scheme II no tadpole diagrams have to be taken into account. However, when equation Eq. (6.32) is inserted into the Feynman rules for vertices with scalars and into the relations between the particle masses and the vevs, the shifts  $\Delta v_i^{(n)}$  “restore” these tadpole diagrams. That is they lead to additional higher-order terms both in the Feynman rules and in the expressions for the masses, which exactly correspond to the cancelled tadpole diagrams. As a consequence, tadpoles have to be attached to every vertex, where this is possible (i.e. allowed by the Feynman rules). Note that this “reappearance” of the tadpoles is a result of the fact, that we keep expanding around the tree-level vevs  $v_i^{(0)}$  in tadpole scheme II. For the SM this scheme has been worked out in detail in Ref. [102]. In Ch. 8 we will derive the same for the more general case of the 2HDM and study its implications. Since we will only consider corrections of one-loop order, we will omit all indices in the following.  $v_i$  is always to be understood as the tree-level vev, while  $\Delta v_i$  will henceforth denote the shift of one-loop order.<sup>1</sup>

Yet, we will start our investigation of the different renormalization schemes for the 2HDM within the framework of tadpole scheme I, i.e. work with tadpole counterterms introduced according to Eqs. 6.29 and 6.30. As we have seen in Sec. 5.2, tadpole terms also appear in the bilinear parts of the scalar potential. In scheme I, these will also receive counterterms

$$\begin{pmatrix} \frac{T_1^0}{v_1} & 0 \\ 0 & \frac{T_2^0}{v_2} \end{pmatrix} \rightarrow \begin{pmatrix} \frac{\delta T_1}{v_1} & 0 \\ 0 & \frac{\delta T_2}{v_2} \end{pmatrix} \equiv \delta T_\varphi. \quad (6.34)$$

<sup>1</sup>Note that the shifts  $\Delta v_i$  are UV-divergent. In order to distinguish them from ordinary counterterms we will, however, denote them with capital  $\Delta$  instead of small  $\delta$ . Furthermore, note that tadpole scheme II is in practice equivalent to not introducing any tadpole counterterms or vev shifts at all and simply taking into account all tadpole diagrams. This will become apparent in sections 8.2-8.4. Nevertheless, the detour over the vev shifts is necessary in order to explicitly demonstrate that the necessary condition  $\langle \Phi_i \rangle = 0$  is fulfilled to all orders.

After a rotation to the mass basis we get

$$\delta T_S \equiv R^T(\theta)\delta T_\varphi R(\theta) = \begin{pmatrix} \delta T_{S_1 S_1} & \delta T_{S_1 S_2} \\ \delta T_{S_2 S_1} & \delta T_{S_2 S_2} \end{pmatrix}, \quad (6.35)$$

with

$$\delta T_{S_1 S_1} = c_\theta^2 \frac{\delta T_1}{v_1} + s_\theta^2 \frac{\delta T_2}{v_2}, \quad (6.36)$$

$$\delta T_{S_2 S_2} = s_\theta^2 \frac{\delta T_1}{v_1} + c_\theta^2 \frac{\delta T_2}{v_2}, \quad (6.37)$$

$$\delta T_{S_1 S_2} = c_\theta s_\theta \left( \frac{\delta T_2}{v_2} - \frac{\delta T_1}{v_1} \right) = \delta T_{S_2 S_1}, \quad (6.38)$$

and

$$\theta = \begin{cases} \alpha & \text{for } (S_1, S_2) = (H, h) \\ \beta & \text{for } (S_1, S_2) \in \{(G_0, A_0), (G^\pm, H^\pm)\} \end{cases}. \quad (6.39)$$

Let us conclude with the remark that the two approaches proposed in this section constitute two contrary roads that can be taken. They will lead to very different consequences for the renormalization procedure, especially concerning the subject of gauge dependence. Therefore, we will take both roads in turn and investigate their implications.

## 6.4. On-Shell Renormalization of the Scalar Masses and Fields

We have now introduced all counterterms required for a renormalization of the 2HDM. The next step is to formulate renormalization conditions to fix these parameters, or in other words, to choose a renormalization scheme. Our goal is to define as many parameters as possible via physical conditions such that a direct relation between the parameters and a physical observable can be established. For the mass parameters, such physical conditions come in terms of the OS conditions (cf. Subs. 3.1.2).

Furthermore it is desirable, to fix the WFRCs in such a way that all fields fulfill proper on-shell conditions, and therefore no additional finite wave function correction factors are needed (cf. Sec. 3.2.1).

Both, the on-shell conditions for the fields and for the mass parameters are closely related to the propagators of the particles under consideration. They are therefore most appropriately formulated simultaneously, which is true to an even greater extent for mixing particles, possessing matrix valued propagators. The on-shell conditions for WFRCs and mass parameters can be condensed into the following three points:

- The renormalized mass parameter  $m$  corresponds to the physical mass of the particle under consideration, i.e. to the pole of its propagator.
- The residue of the pole of the propagator equals  $i$  for particles which are on their mass shell, i.e. whose momenta fulfill  $p^2 = m^2$ .
- Mixing between particles of identical quantum numbers vanishes for particles on their mass shell.

These conditions fix all mass counterterms and WFRCs uniquely. For the SM the resulting renormalization constants have been deduced and discussed in detail e.g. in [59, 77, 80]. Therefore, in deriving the counterterms we will restrict ourselves to the scalar sector of the 2HDM, which goes beyond the SM. Furthermore, we will treat all scalars as stable, i.e. we will neglect their finite widths, which, in the case of CP conserving couplings, leads to real

mass counterterms and WFRs [80]. Strictly speaking, of course, the scalars are unstable and therefore a more rigorous derivation would have to take into account their finite widths and thus the fact, that the poles of their propagators are complex quantities. As a consequence, both the mass counterterms and the WFRs would develop an imaginary part, even in the case of CP-conservation [119–122]. However, in the final results for the decay widths, which we will calculate in this part of the thesis, all imaginary parts, whether they originate from vertex corrections or from the counterterms, drop out. This is due to the fact that all higher-order terms enter only linearly into the amplitude and therefore vanish upon taking the square of the absolute value (cf. Subs. 3.2.2).

The renormalization conditions are most conveniently expressed in terms of the renormalized scalar two-point functions  $\hat{\Gamma}_S$ , where  $S \in \{S_{\phi^\pm}, S_\eta, S_\rho\}$  stands for the pair of mixing scalars under consideration. Using the general notation of Eq. (5.16)- Eq. (5.21) for the mass matrices,  $\hat{\Gamma}_S$  is given in the mass basis by

$$\begin{aligned} \hat{\Gamma}_S(p^2) &= (p^2 \mathbf{1}_{2 \times 2} - \mathcal{D}_S + \hat{\Sigma}_S(p^2)) \\ &= \begin{pmatrix} p^2 - m_{S_1}^2 - \delta m_{S_1}^2 & 0 \\ 0 & p^2 - m_{S_2}^2 - \delta m_{S_2}^2 \end{pmatrix} + \begin{pmatrix} \hat{\Sigma}_{S_1 S_1}(p^2) & \hat{\Sigma}_{S_1 S_2}(p^2) \\ \hat{\Sigma}_{S_2 S_1}(p^2) & \hat{\Sigma}_{S_2 S_2}(p^2) \end{pmatrix}. \end{aligned} \quad (6.40)$$

$\hat{\Sigma}_{S_i S_j}(p^2)$  denotes the renormalized self-energy, i.e. the sum of all one particle irreducible (1PI) diagrams, including counterterms, contributing to the transition  $S_i \rightarrow S_j$ ,  $i, j \in \{1, 2\}$  for the respective pair of particles. Its explicit form depends on the treatment of the tadpoles and will therefore be stated later, when we present the two tadpoles schemes separately.

$\hat{\Gamma}_S$  is related to the corresponding propagator matrix  $\hat{G}_S(p^2)$  by:

$$\hat{G}_S(p^2) = i \hat{\Gamma}_S^{-1}(p^2) = \frac{i}{\underbrace{\hat{\Gamma}_{S_1 S_1}(p^2) \hat{\Gamma}_{S_2 S_2}(p^2) - \hat{\Gamma}_{S_1 S_2}(p^2) \hat{\Gamma}_{S_2 S_1}(p^2)}_{=\det \hat{\Gamma}_S(p^2)}} \begin{pmatrix} \hat{\Gamma}_{S_2 S_2}(p^2) & -\hat{\Gamma}_{S_2 S_1}(p^2) \\ -\hat{\Gamma}_{S_1 S_2}(p^2) & \hat{\Gamma}_{S_1 S_1}(p^2) \end{pmatrix}.$$

As can be inferred from this, the requirement for the propagator to have a pole at the physical mass translates into the following condition

$$\det \hat{\Gamma}_S(p^2) \Big|_{p^2=m_{S_1}^2} = 0 = \det \hat{\Gamma}_S(p^2) \Big|_{p^2=m_{S_2}^2}. \quad (6.41)$$

Demanding at the same time the mixing between  $S_1$  and  $S_2$  to vanish on-shell, i.e.

$$\hat{\Gamma}_{S_1 S_2}(p^2) \Big|_{p^2=m_{S_1}^2} = 0, \quad (6.42)$$

$$\hat{\Gamma}_{S_1 S_2}(p^2) \Big|_{p^2=m_{S_2}^2} = 0, \quad (6.43)$$

this reduces to the conditions

$$\hat{\Gamma}_{S_1 S_1}(p^2) \Big|_{p^2=m_{S_1}^2} = 0, \quad (6.44)$$

$$\hat{\Gamma}_{S_2 S_2}(p^2) \Big|_{p^2=m_{S_2}^2} = 0. \quad (6.45)$$

Note that we need to impose Eqs. 6.42 and 6.43 only on one of the off-diagonal elements, since CP-invariance guarantees that  $\hat{\Gamma}_{S_1 S_2}(p^2) = \hat{\Gamma}_{S_2 S_1}(p^2)$ . Finally, the requirement for the propagators of on-shell particles to be properly normalized yields

$$\frac{\partial \hat{\Gamma}_{S_1 S_1}(p^2)}{\partial p^2} \Big|_{p^2=m_{S_1}^2} = 1, \quad (6.46)$$

$$\frac{\partial \hat{\Gamma}_{S_2 S_2}(p^2)}{\partial p^2} \Big|_{p^2=m_{S_2}^2} = 1. \quad (6.47)$$

From the six equations Eqs. 6.42 - 6.47 we can deduce the six renormalization constants  $\delta m_{S_1}^2$ ,  $\delta m_{S_2}^2$ ,  $\delta Z_{S_1 S_1}$ ,  $\delta Z_{S_2 S_2}$ ,  $\delta Z_{S_1 S_2}$  and  $\delta Z_{S_2 S_1}$ , which appear in  $\hat{\Sigma}_S$  (cf. sections 7.1 and 8.3) for each of the three pairs  $(S_1, S_2)$ . Note that all equations can only be fulfilled simultaneously, if a sufficient amount of independent WFRCs are introduced. In the minimal scheme outlined in Sec. 6.1, where we have only two independent WFRCs for all three pairs of particles, a complete OS renormalization is not possible.

## 6.5. On-Shell Renormalization of the Gauge and Fermion Sector

Also the renormalization constants of the gauge and the fermion sector,  $\delta M_W^2$ ,  $\delta M_Z^2$ ,  $\delta e$ ,  $\delta m_\tau$  and the WFRCs of the gauge bosons and fermions, can be defined by on-shell conditions. Since this proceeds exactly as in the SM, we will resign from a detailed derivation and refer the reader to the literature [59, 77, 80].

The results will again depend on the treatment of the tadpoles and will therefore be stated in the corresponding sections 7.2 and 7.3 (scheme I) or 8.3 (scheme II).

One remark is in order, concerning the renormalization of the gauge fixing Lagrangian  $\mathcal{L}_{\text{gf}}$ . As has been shown in [78, 123] and emphasized in [38] in linear  $R_\xi$  gauge it is not necessary to renormalize  $\mathcal{L}_{\text{gf}}$ . Rather,  $\mathcal{L}_{\text{gf}}$  can be regarded as fixing the gauge of the *renormalized* Lagrangian, not the bare one, and therefore to be defined in terms of already *renormalized* fields and parameters. Consequently, we need not introduce renormalization constants for the gauge fixing parameters and no WFRCs appear in  $\mathcal{L}_{\text{gf}}$ .

## 6.6. Renormalization of $\alpha$ and $\beta$

It has been known for a while that the renormalization of mixing angles has to be treated with care. If performed naively, the renormalization procedure is prone to lead to gauge-dependent expressions for amplitudes and thus physical observables. This is, however, not acceptable as one of the most important criteria for a good renormalization scheme is its capability of producing gauge-independent results for physical quantities. Apart from gauge independence, also numerical stability of physical results is a requested feature a good renormalization scheme for the mixing angles should exhibit. Furthermore, it is preferable to renormalize the angles in such a way, that they themselves can be regarded as physical parameters. For this to be the case, the renormalized angles should, aside from being independent of gauge-fixing parameters, be fixed by universal, i.e. process-independent renormalization conditions.

The issue of gauge dependence entering through the renormalization of mixing particles has been studied in detail for the case of the CKM matrix [124–129] and for the mixing of scalars in the MSSM [127, 130–132].

After it was pointed out in Ref. [124] that the on-shell renormalization of the CKM matrix proposed in Ref. [77, 133] leads to gauge-dependent amplitudes, numerous alternative definitions for the counterterms of the quark mixing matrix were suggested. Among these are schemes based  $\overline{\text{MS}}$  conditions [128], process-dependent schemes [126] as well as more elaborate schemes. The latter make use of Ward Takahashi Identities [124] and BRST<sup>2</sup> invariance [129] to guarantee gauge invariance or apply a two-step procedure [136, 137] to accomplish all desired properties of the renormalized CKM matrix.

In addition to these, Yamada has proposed in Ref. [127] a scheme based on the pinch technique

<sup>2</sup>The concept of BRST invariance, named so after Becchi, Rouet, Stora, Tyutin, constitutes an extension of the conventional gauge invariance to gauge fields. After gauge fixing, the Lagrangian is no longer invariant under gauge transformations, however, by the inclusion of gauge fields in the transformation, a new symmetry, the BRST symmetry, can be established. [134, 135]

(PT) to construct counterterms for the quark mixing angles leading to gauge-independent amplitudes. He has shown that, if instead of the conventional self-energies, used in Ref. [77,133], the pinched self-energies are utilized to define the angular counterterms, gauge independence of physical quantities is guaranteed. Furthermore, he has extended this renormalization prescriptions to the case of general fermion or scalar sectors and illustrated the procedure using the example of the MSSM squark sector.

In a subsequent publication together with Espinosa [131] he addressed the mixing of scalars in the MSSM and in particular examined the case of the CP-even Higgs bosons. Again, the pinch technique was invoked to construct a gauge-independent renormalization scheme for the mixing angles, i.e. a scheme leading to gauge-independent physical quantities.

Similar results have been obtained by the authors of Ref. [132], although their approach, based on an investigation of the singularity structure of one-loop scattering amplitudes, differs from the one chosen by Yamada and Espinosa.

In addition to these examinations, different schemes for the angular parameter  $\tan(\beta)$  of the MSSM and the resulting gauge dependence have been investigated in Refs. [115, 116, 138]. Freitas et al. have found in Ref. [138], that there exists no scheme for  $\tan(\beta)$  in the MSSM, such that all requirements mentioned above, i.e. gauge independence, process independence and numerical stability are simultaneously fulfilled.

Such dedicated studies on the renormalization of the scalar mixing angles are missing for the case of the 2HDM<sup>3</sup>. For this reason, we will present different renormalization schemes for  $\alpha$  and  $\beta$  in the following sections and examine their capability to accomplish the demanded prerequisites.

First, we will investigate a process-independent definition in the framework of tadpole scheme I (Sec. 7.4) and afterwards in scheme II (Sec. 8.5). Then we will turn to a process-dependent renormalization of the angular counterterms (Ch. 9), treating both tadpole schemes simultaneously and finally have a glance at an  $\overline{\text{MS}}$  definition (Sec. 9.5).

## 6.7. Renormalization of $m_{12}^2$

The last 2HDM parameter that needs to be renormalized is  $m_{12}^2$ . Since this parameter only appears in trilinear and quadrilinear Higgs couplings,  $\delta m_{12}^2$  has to be defined in terms of a multi-Higgs vertex.

One possibility is to determine  $m_{12}^2$  as an  $\overline{\text{MS}}$  parameter, i.e. require  $\delta m_{12}^2$  to cancel the remaining terms proportional to the  $\overline{\text{MS}}$ -divergence  $\Delta_{\overline{\text{MS}}}$  in an amplitude containing a trilinear (or quadrilinear) Higgs vertex.

Another possibility is to include also finite terms into  $\delta m_{12}^2$ . These can be determined, for example, by demanding an appropriate loop-corrected decay width to equal the tree-level one. Ideally,  $\delta m_{12}^2$  should be fixed such that the loop-corrected observable equals an experimental measurement. However, lacking any measurement for a suitable observable, requiring the equality with the tree-level result is the best that can be done at the moment. Still, kinematics restricts the applicability of this method to a limited part of the 2HDM parameter space, as will be detailed below (cf. Sec. 10.2).

Upon writing this, the renormalization of  $m_{12}^2$  has hardly attracted interest in the literature. To our knowledge, only Ref. [40], where  $m_{12}^2$  is defined by an  $\overline{\text{MS}}$  condition, has dealt with this subject.

In this thesis, we will examine two renormalization schemes for the parameter  $m_{12}$ . First, in Sec. 10.1, we will investigate an  $\overline{\text{MS}}$ -like renormalization for  $m_{12}^2$  within both tadpole frameworks. Afterwards, in Sec. 10.2, we will consider a process-dependent definition.

<sup>3</sup>While writing this thesis a publication by Denner et al. [41] appeared proposing an  $\overline{\text{MS}}$  scheme for  $\alpha$  and  $\beta$ .



---

Renormalization in Tadpole Scheme I

---

Due to its convenience, the treatment of the tadpoles along the lines of tadpole scheme I nowadays has become the standard treatment. It is conventionally applied in the SM [58, 59, 77, 80], in supersymmetric extensions [103, 104] as well as in the 2HDM [38–40]. Therefore, we will use scheme I as starting point for our investigation of the two tadpole schemes and their consequences on the renormalization of the other parameters and fields.

We will first state explicit expressions for the OS mass and charge counterterms as well as for the WFRs of the scalar ( Sec. 7.1), the gauge ( Sec. 7.2) and the fermion sector ( Sec. 7.3), determined in the framework of scheme I.

Subsequently, we will present a process-independent renormalization scheme for the angular counterterms ( Sec. 7.4). This scheme will turn out to yield gauge-dependent expressions for amplitudes and thus physical observables, which will prompt us to switch to tadpole scheme II.

### 7.1. On-Shell Renormalization of the Scalar Sector in Tadpole Scheme I

We start with a derivation of the counterterms for the scalar sector of the 2HDM. The corresponding OS renormalization conditions for the masses and fields have already been introduced in Sec. 6.4. After having specified the treatment of the tadpoles, we are now in a position to derive concrete expression for the respective counterterms. For this purpose, we need the renormalized two-point function in the tadpole scheme I, which is given in the mass basis by

$$\begin{aligned}
 \hat{\Gamma}_S((p^2)) &= Z_S^{1/2\dagger} (p^2 \mathbb{1}_{2 \times 2} - (\mathcal{D} + \delta\mathcal{D})_S - \delta T_S + \Sigma_S(p^2)) Z_S^{1/2} \\
 &= \begin{pmatrix} 1 + \frac{1}{2}\delta Z_{S_1 S_1} & \frac{1}{2}\delta Z_{S_1 S_2} \\ \frac{1}{2}\delta Z_{S_2 S_1} & 1 + \frac{1}{2}\delta Z_{S_2 S_2} \end{pmatrix}^\dagger \left[ \begin{pmatrix} p^2 - m_{S_1}^2 - \delta m_{S_1}^2 & 0 \\ 0 & p^2 - m_{S_2}^2 - \delta m_{S_2}^2 \end{pmatrix} \right. \\
 &\quad \left. - \begin{pmatrix} \delta T_{S_1 S_1} & \delta T_{S_1 S_2} \\ \delta T_{S_2 S_1} & \delta T_{S_2 S_2} \end{pmatrix} + \begin{pmatrix} \Sigma_{S_1 S_1}(p^2) & \Sigma_{S_1 S_2}(p^2) \\ \Sigma_{S_2 S_1}(p^2) & \Sigma_{S_2 S_2}(p^2) \end{pmatrix} \right] \begin{pmatrix} 1 + \frac{1}{2}\delta Z_{S_1 S_1} & \frac{1}{2}\delta Z_{S_1 S_2} \\ \frac{1}{2}\delta Z_{S_2 S_1} & 1 + \frac{1}{2}\delta Z_{S_2 S_2} \end{pmatrix}^\dagger.
 \end{aligned} \tag{7.1}$$

Here we use the generic notation introduced in Eqs. 5.16 - 5.21 for mass matrices and  $S \in \{S_{\phi^\pm}, S_\eta, S_\rho\}$ . Due to the prescription for the tadpoles we use in this section, tadpole diagrams

are not considered to be part of  $\Sigma_{S_i S_j}(p^2)$ , the unrenormalized scalar self-energy. Furthermore note the appearance of the matrix  $\delta T_S$  defined in Eq. (6.35), which results from our definition of  $\mathcal{M}_\varphi$ ,  $\varphi \in \{\phi^\pm, \eta, \rho\}$ , in Sec. 5.2 and the treatment of the tadpoles. Expanding Eq. (7.1) to one-loop order, the elements of  $\hat{\Gamma}_S$  take the following form

$$\hat{\Gamma}_{S_i S_i}(p^2) = (p^2 - m_{S_i}^2) - \delta m_{S_i}^2 + \delta Z_{S_i S_i}(p^2 - m_{S_i}^2) + \Sigma_{S_i S_j}(p^2) - \delta T_{S_i S_i}, \quad (7.2)$$

$$\hat{\Gamma}_{S_i S_j}(p^2) = \frac{1}{2} \delta Z_{S_j S_i}(p^2 - m_{S_j}^2) + (p^2 - m_{S_i}^2) \frac{1}{2} \delta Z_{S_i S_j} + \Sigma_{S_i S_j}(p^2) - \delta T_{S_i S_j}, \quad i \neq j. \quad (7.3)$$

Plugging Eqs. 7.2 and 7.3 into Eqs. 6.42 - 6.47 and solving for the renormalization constants, we find for the mass counterterms

$$\delta m_h^2 = \text{Re}(\Sigma_{hh}(m_h^2) - \delta T_{hh}), \quad (7.4)$$

$$\delta m_H^2 = \text{Re}(\Sigma_{HH}(m_H^2) - \delta T_{HH}), \quad (7.5)$$

$$\delta m_{A_0}^2 = \text{Re}(\Sigma_{A_0 A_0}(m_{A_0}^2) - \delta T_{A_0 A_0}), \quad (7.6)$$

$$\delta m_{H^\pm}^2 = \widetilde{\text{Re}}(\Sigma_{H^\pm H^\pm}(m_{H^\pm}^2) - \delta T_{H^\pm H^\pm}), \quad (7.7)$$

for the diagonal WFRCS

$$\begin{aligned} \delta Z_{hh} &= -\text{Re} \left( \frac{\partial \Sigma_{hh}(p^2)}{\partial p^2} \right) \Big|_{p^2=m_h^2}, & \delta Z_{HH} &= -\text{Re} \left( \frac{\partial \Sigma_{HH}(p^2)}{\partial p^2} \right) \Big|_{p^2=m_H^2}, \\ \delta Z_{A_0 A_0} &= -\text{Re} \left( \frac{\partial \Sigma_{A_0 A_0}(p^2)}{\partial p^2} \right) \Big|_{p^2=m_{A_0}^2}, & \delta Z_{G_0 G_0} &= -\text{Re} \left( \frac{\partial \Sigma_{G_0 G_0}(p^2)}{\partial p^2} \right) \Big|_{p^2=0}, \\ \delta Z_{H^\pm H^\pm} &= -\widetilde{\text{Re}} \left( \frac{\partial \Sigma_{H^\pm H^\pm}(p^2)}{\partial p^2} \right) \Big|_{p^2=m_{H^\pm}^2}, & \delta Z_{G^\pm G^\pm} &= -\widetilde{\text{Re}} \left( \frac{\partial \Sigma_{G^\pm G^\pm}(p^2)}{\partial p^2} \right) \Big|_{p^2=0} \end{aligned} \quad (7.8)$$

and for the off-diagonal WFRCS

$$\begin{aligned} \delta Z_{hH} &= -\frac{2\text{Re}(\Sigma_{Hh}(m_H^2) - \delta T_{Hh})}{m_H^2 - m_h^2}, & \delta Z_{Hh} &= \frac{2\text{Re}(\Sigma_{Hh}(m_h^2) - \delta T_{Hh})}{m_H^2 - m_h^2}, \\ \delta Z_{G_0 A_0} &= -\frac{2\text{Re}(\Sigma_{G_0 A_0}(m_{A_0}^2) - \delta T_{G_0 A_0})}{m_{A_0}^2}, & \delta Z_{A_0 G_0} &= \frac{2\text{Re}(\Sigma_{G_0 A_0}(0) - \delta T_{G_0 A_0})}{m_{A_0}^2}, \\ \delta Z_{G^\pm H^\pm} &= -\frac{2\widetilde{\text{Re}}(\Sigma_{G^\pm H^\pm}(m_{H^\pm}^2) - \delta T_{G^\pm H^\pm})}{m_{H^\pm}^2}, & \delta Z_{H^\pm G^\pm} &= \frac{2\widetilde{\text{Re}}(\Sigma_{G^\pm H^\pm}(0) - \delta T_{G^\pm H^\pm})}{m_{H^\pm}^2}, \end{aligned} \quad (7.9)$$

where we have used  $\Sigma_{S_i S_j} = \Sigma_{S_j S_i}$  and  $\delta T_{S_i S_j} = \delta T_{S_j S_i}$  for  $i, j = 1, 2$ . One comment is in order concerning the prescription to take the real parts  $\text{Re}()$  in defining the counterterms in Eqs. 7.4 - 7.9. This prescription is necessary since we treat all scalars as stable particles, i.e. neglect the absorptive parts of their self-energies, as mentioned at the beginning of Sec. 6.4. Aoki et al. have shown in Ref. [80] that for CP-conserving couplings this approximation leads to strictly real counterterms. Of course, with strictly real renormalization constants we can fulfill the OS conditions in Eqs. 6.42 - 6.47 only for the real parts of  $\hat{\Gamma}_S$ . However, the additional imaginary parts of the renormalization constants, which a more rigorous treatment of the absorptive parts would yield, do not contribute to our final result. This is because all imaginary parts drop out when building the squared amplitude at strict one-loop order (cf. Subs. 3.2.2), as required for the calculation of decay widths or cross-sections. Therefore, for our purposes it is sufficient to fulfill the OS conditions only for the real parts of Eq. (6.42) to Eq. (6.47). Furthermore, we have introduced the symbol  $\widetilde{\text{Re}}()$ , which takes the real parts of loop functions but keeps imaginary parts entering through complex couplings, caused e.g. by a complex CKM matrix. Its purpose is to discard only the unwanted absorptive parts and keep effects of CP-violation. Strictly speaking, we do not necessitate this prescription since

the CKM-matrix elements, the only potentially complex parameters in our model, enter in Eqs. 7.4 - 7.9 only as squares of the absolute values. Moreover, in the numerical evaluation we will consider the CKM matrix to be real, anyways. We still keep the notation  $\widetilde{\text{Re}}()$ , in order to stay in line with the usual conventions [59, 77].

## 7.2. On-Shell Renormalization of the Gauge Sector in Tadpole Scheme I

Next, we want to specify the counterterms of the gauge sector. The masses  $M_W^2$ ,  $M_Z^2$  and the WFRs of the gauge bosons are renormalized in the same way as in the SM. Since the corresponding OS conditions are well-known and can be found e.g. in [59, 77, 80], we only state the results for the counterterms

$$\delta M_W^2 = \widetilde{\text{Re}} \left( \Sigma_{WW}^T(M_W^2) \right), \quad (7.10)$$

$$\delta M_Z^2 = \text{Re} \left( \Sigma_{ZZ}^T(M_Z^2) \right), \quad (7.11)$$

$$\delta Z_{WW} = - \widetilde{\text{Re}} \left( \frac{\partial \Sigma_{WW}^T(p^2)}{\partial p^2} \right) \Big|_{p^2=M_W^2}, \quad (7.12)$$

$$\delta Z_{ZZ} = - \text{Re} \left( \frac{\partial \Sigma_{ZZ}^T(p^2)}{\partial p^2} \right) \Big|_{p^2=M_Z^2}, \quad (7.13)$$

$$\delta Z_{AA} = - \text{Re} \left( \frac{\partial \Sigma_{AA}^T(p^2)}{\partial p^2} \right) \Big|_{p^2=0}, \quad (7.14)$$

$$\delta Z_{ZA} = 2 \text{Re} \left( \frac{\Sigma_{ZA}^T(0)}{M_Z^2} \right), \quad (7.15)$$

$$\delta Z_{AZ} = -2 \text{Re} \left( \frac{\Sigma_{AZ}^T(M_Z^2)}{M_Z^2} \right). \quad (7.16)$$

In these expression  $\Sigma_{V_i V_j}^T(p^2)$ , with  $V_i, V_j \in \{W^\pm, Z, \gamma\}$ , denotes the transverse part of the  $V_i$ - $V_j$  self-energy. For later convenience, we also state the full expression for  $\hat{\Gamma}_{V_i V_j}(p^2)$ , the renormalized two-point function of the gauge bosons  $V_i$  and  $V_j$  in general  $R_\xi$  gauge, from which the above renormalization constants can be derived

$$\begin{aligned} \hat{\Gamma}_{V_i V_j}(p^2) = & - \left( g^{\mu\nu} - \frac{p^\mu p^\nu}{p^2} \right) (p^2 - M_{V_i}^2) \delta_{ij} - \frac{p^\mu p^\nu}{p^2} \frac{1}{\xi_{V_i}} (p^2 - \xi_{V_i} M_{V_i}^2) \delta_{ij}, \\ & - \left( g^{\mu\nu} - \frac{p^\mu p^\nu}{p^2} \right) \hat{\Sigma}_{V_i V_j}^T(p^2) - \frac{p^\mu p^\nu}{p^2} \hat{\Sigma}_{V_i V_j}^L(p^2). \end{aligned} \quad (7.17)$$

The renormalized transverse and longitudinal self-energies appearing here are given by

$$\hat{\Sigma}_{V_i V_j}^T(p^2) = \frac{\delta Z_{V_j V_i}}{2} (p^2 - M_{V_j}^2) + (p^2 - M_{V_i}^2) \frac{\delta Z_{V_i V_j}}{2} - \delta M_{V_i}^2 \delta_{ij} + \Sigma_{V_i V_j}^T(p^2), \quad (7.18)$$

$$\hat{\Sigma}_{V_i V_j}^L(p^2) = - \frac{\delta Z_{V_j V_i}}{2} M_{V_j}^2 - M_{V_i}^2 \frac{\delta Z_{V_i V_j}}{2} - \delta M_{V_i}^2 \delta_{ij} + \Sigma_{V_i V_j}^L(p^2). \quad (7.19)$$

Also the renormalization of the electric charge  $e$ , defined in the Thomson limit, can be performed like in the SM [59, 77, 80]

$$\delta Z_e^{\alpha(0)} = \frac{1}{2} \frac{\delta \Sigma_{AA}^T(p^2)}{\partial p^2} \Big|_{p^2=0} + \frac{s_W}{c_W} \frac{\Sigma_{AZ}^T(0)}{M_Z^2}, \quad (7.20)$$

where  $s_W$  and  $c_W$  denote the sine and cosine of the Weinberg angle  $\theta_W$  (cf. Eq. (5.30))<sup>1</sup>. However, since the counterterm defined according to Eq. (7.20) shows a strong dependence on the masses of light fermions, it is advantageous to modify the renormalization conditions and fix the electric charge at the electroweak scale

$$\delta Z_e^{\alpha(M_Z^2)} = \delta Z_e^{\alpha(0)} - \frac{1}{2} \left( \frac{\partial \Sigma_{AA}^{T,\text{light}}(p^2)}{\partial p^2} \Big|_{p^2=0} - \frac{\Sigma_{AA}^{T,\text{light}}(M_Z^2)}{M_Z^2} \right). \quad (7.21)$$

<sup>1</sup>Note, that the sign of the second term in Eq. (7.20) is opposite to the one in [77], which is due to a different definition of the covariant derivative (cf. Eq. (5.3)).

The superscript *light* indicates that only the contributions of light fermions, i.e. of all leptons and quarks apart from the top, are taken into account in the respective self-energies. After this subtraction the problematic logarithms depending on the light fermion masses, which appear in  $\delta Z_e^{\alpha(0)}$ , no longer contribute [77, 91]. They have been resummed into  $\alpha_{\text{em}} = e^2/4\pi$  according to

$$\alpha_{\text{em}} = \alpha_{\text{em}}(0) \rightarrow \alpha_{\text{em}}(M_Z^2) = \frac{\alpha_{\text{em}}}{1 - \Delta\alpha}, \quad (7.22)$$

with  $\Delta\alpha = \Delta\alpha_{\text{lept}} + \Delta\alpha_{\text{had}}^{(5)}$ .  $\Delta\alpha_{\text{lept}}$  contains the contributions of the leptons and has been calculated up to three-loop order in [139], whereas  $\Delta\alpha_{\text{had}}^{(5)}$  comprises contributions from the light quarks and has been determined in Refs. [140, 141]. Renormalizing the electric charge at the electroweak scale, we have to adopt  $\alpha(M_Z^2)$  as input parameter.

### 7.3. On-Shell Renormalization of the Fermion Sector in Tadpole Scheme I

Also the renormalization of the fermion sector proceeds exactly like in the SM. For this reason we refer the reader again to Refs. [59, 77, 80] and only state the renormalization constants for the  $\tau$  leptons, which we introduced in Eqs. 6.27 and 6.28, for later use.

In the OS scheme, these constants are fixed in terms of the renormalized fermionic two-point function. For generic fermions  $f_i$  and  $f_j$ , the latter one is given by

$$\begin{aligned} \hat{\Gamma}_{f_i f_j}(p) = & (\not{p} - m_{f_i})\delta_{ij} + \not{p}\omega_- \hat{\Sigma}_{f_i f_j}^L(p^2) + \not{p}\omega_+ \hat{\Sigma}_{f_i f_j}^R(p^2) \\ & + m_{f_i}\omega_- \hat{\Sigma}_{f_i f_j}^{S,l}(p^2) + m_{f_j}\omega_+ \hat{\Sigma}_{f_i f_j}^{S,r}(p^2), \end{aligned} \quad (7.23)$$

where the renormalized self-energy has been split into its left-handed, right-handed and scalar constituents and  $\omega_-/\omega_+$  stand for the projectors onto left/right-handed spinor components, respectively. Below, we will only need the diagonal elements of the self-energies, which are given by

$$\hat{\Sigma}_{f_i f_i}^L(p^2) = \delta Z_{f_i f_i}^L + \Sigma_{f_i f_i}^L(p^2), \quad (7.24)$$

$$\hat{\Sigma}_{f_i f_i}^R(p^2) = \delta Z_{f_i f_i}^R + \Sigma_{f_i f_i}^R(p^2), \quad (7.25)$$

$$\hat{\Sigma}_{f_i f_i}^{S,l}(p^2) = -\frac{\delta m_{f_i}}{m_{f_i}} - \frac{1}{2}\delta(Z_{f_i f_i}^L + Z_{f_i f_i}^R) + \Sigma_{f_i f_i}^{S,l}(p^2), \quad (7.26)$$

$$\hat{\Sigma}_{f_i f_i}^{S,r}(p^2) = -\frac{\delta m_{f_i}}{m_{f_i}} - \frac{1}{2}\delta(Z_{f_i f_i}^L + Z_{f_i f_i}^R) + \Sigma_{f_i f_i}^{S,r}(p^2). \quad (7.27)$$

With these, the renormalization constants for the  $\tau$  lepton can be expressed as

$$\delta m_\tau = \frac{m_\tau}{2} \widetilde{\text{Re}} \left( \Sigma_{\tau\tau}^L(m_\tau^2) + \Sigma_{\tau\tau}^R(m_\tau^2) + \Sigma_{\tau\tau}^{S,l}(m_\tau^2) + \Sigma_{\tau\tau}^{S,r}(m_\tau^2) \right), \quad (7.28)$$

$$\delta Z_\tau^L = -\widetilde{\text{Re}}(\Sigma_{\tau\tau}^L(m_\tau^2)) - m_\tau^2 \widetilde{\text{Re}} \left( \frac{\partial \Sigma_{\tau\tau}^T(p^2)}{\partial p^2} + \frac{\partial \Sigma_{\tau\tau}^R(p^2)}{\partial p^2} + \frac{\partial \Sigma_{\tau\tau}^{S,l}}{\partial p^2} + \frac{\partial \Sigma_{\tau\tau}^{S,r}}{\partial p^2} \right) \Bigg|_{p^2=m_\tau^2}, \quad (7.29)$$

$$\delta Z_\tau^R = -\widetilde{\text{Re}}(\Sigma_{\tau\tau}^R(m_\tau^2)) - m_\tau^2 \widetilde{\text{Re}} \left( \frac{\partial \Sigma_{\tau\tau}^T(p^2)}{\partial p^2} + \frac{\partial \Sigma_{\tau\tau}^R(p^2)}{\partial p^2} + \frac{\partial \Sigma_{\tau\tau}^{S,l}}{\partial p^2} + \frac{\partial \Sigma_{\tau\tau}^{S,r}}{\partial p^2} \right) \Bigg|_{p^2=m_\tau^2}. \quad (7.30)$$

### 7.4. A Process-Independent Definition of $\alpha$ and $\beta$ and its Gauge Dependence

After having defined the OS counterterms for all masses and  $e$  as well as the WFRCs, we next turn to the renormalization of  $\alpha$  and  $\beta$ . Since one of the criteria for a good renormalization

scheme for the angles is universality, we start our investigation with a process-independent scheme, proposed by Kanemura, Okada, Senaha, and Yuan in Ref. [40] and studied further in Ref. [112]. We will refer to their scheme as *KOSY scheme*. The scheme will turn out to lead to gauge-dependent amplitudes, and thus physical observables, and therefore not to be appropriate. Yet it will give us valuable insight into the origin of this gauge dependence and allow us to pave the way for a gauge-independent scheme.

#### 7.4.1. $\alpha$ and $\beta$ in the KOSY Scheme

Kanemura et al. use the relation between the WFRM matrices in the gauge and in the mass basis, stated in Eq. (6.10), as starting point to define counterterms for  $\alpha$  and  $\beta$ . They introduce three symmetric  $2 \times 2$  matrices  $Z_\varphi^{1/2}$  in the gauge basis, one for each of the three pairs of scalars with identical quantum numbers. Then, employing the fact that  $R^T(\theta_r)Z_\varphi^{1/2}R(\theta_r)$  is symmetric if this is the case for  $Z_\varphi^{1/2}$ , they establish the following relation between the angular counterterms and the WFRMs in the mass basis

$$\begin{aligned} Z_S^{1/2} &= R(\delta\theta)^T \begin{pmatrix} 1 + \frac{1}{2}\delta Z_{S_1 S_1} & \delta C_{S_1 S_2} \\ \delta C_{S_1 S_2} & 1 + \frac{1}{2}\delta Z_{S_2 S_2} \end{pmatrix} \\ &= \begin{pmatrix} 1 + \frac{1}{2}\delta Z_{S_1 S_1} & \delta C_{S_1 S_2} + \delta\theta \\ \delta C_{S_1 S_2} - \delta\theta & 1 + \frac{1}{2}\delta Z_{S_2 S_2} \end{pmatrix} + \mathcal{O}(\delta^2). \end{aligned} \quad (7.31)$$

Here  $\mathcal{O}(\delta^2)$  denotes terms of quadratic or higher order in the counterterms and the  $\delta C_{S_1 S_2}$  are real constants, parametrizing the off-diagonal matrix elements. We can directly read off

$$\frac{1}{2}\delta Z_{S_1 S_2} = \delta C_{S_1 S_2} + \delta\theta, \quad (7.32)$$

$$\frac{1}{2}\delta Z_{S_2 S_1} = \delta C_{S_1 S_2} - \delta\theta, \quad (7.33)$$

$$\Rightarrow \delta\theta = \frac{\delta Z_{S_1 S_2} - \delta Z_{S_2 S_1}}{4}. \quad (7.34)$$

Inserting the expressions for the OS WFRMs in the mass basis (cf. Eq. (7.9)), we arrive at

$$\delta\alpha^K = \frac{\delta Z_{Hh} - \delta Z_{hH}}{4} = \frac{\text{Re} [\Sigma_{Hh}(m_h^2) + \Sigma_{Hh}(m_H^2) - 2\delta T_{Hh}]}{2(m_H^2 - m_h^2)}, \quad (7.35)$$

$$\delta\beta_o^K = \frac{\delta Z_{G_0 A_0} - \delta Z_{A_0 G_0}}{4} = -\frac{\text{Re} [\Sigma_{G_0 A_0}(m_{A_0}^2) + \Sigma_{G_0 A_0}(0) - 2\delta T_{G_0 A_0}]}{2m_{A_0}^2}, \quad (7.36)$$

$$\delta\beta_c^K = \frac{\delta Z_{G^\pm H^\pm} - \delta Z_{H^\pm G^\pm}}{4} = -\frac{\text{Re} [\Sigma_{G^\pm H^\pm}(m_{H^\pm}^2) + \Sigma_{G^\pm H^\pm}(0) - 2\delta T_{G^\pm H^\pm}]}{2m_{H^\pm}^2}. \quad (7.37)$$

Note that this method leads to two different counterterms for the mixing angles of the CP-odd and the charged scalars. This is not surprising since in higher orders, the mass matrices of the two pairs of particles receive disparate radiative corrections. Keeping the rotation angles fixed at the tree-level values the counterterms for the charged and the CP-odd versions of  $\beta$  differ if one demands all particles to be renormalized on-shell.

However, this holds only for the finite parts of  $\delta\beta_o^K$  and  $\delta\beta_c^K$ . The divergences contained in these two counterterms are still identical. Hence, if one is interested only in cancelling the divergences of higher-order Greens functions, it is possible to pick one of the two versions of  $\delta\beta^K$ , as the authors of [40] suggest. Then, of course, only either the CP-odd or the charged scalars can be renormalized properly on-shell, depending on the choice of  $\delta\beta^K$ . For the other scalar pair, finite wave function correction factors are required if one of its members appears as external particle in a process.

All processes that we will consider in this part of the thesis feature only either of the scalars in question as external particle, such that we can always choose  $\delta\beta^K$  accordingly and never need to deal with finite wave function correction factors. Without mentioning, we will assume  $\delta\beta^K$  always to be chosen appropriately.

### 7.4.2. The Origin of the Gauge Dependence

Although the derivation of the angular counterterms in the last section seems well motivated and is process-independent, the KOSY scheme is unfavorable since it leads to gauge-dependent amplitudes. To investigate the origin of this gauge dependence, we start from the explicit expressions for the angular counterterms. A straightforward calculation and a subsequent extraction of terms containing gauge fixing parameters yields the following  $\xi$ -dependent parts of  $\delta\alpha^K$  and  $\delta\beta^K$ <sup>2</sup>

$$\begin{aligned} \delta\alpha^K|_\xi &= \frac{m_{12}^2 c_{\beta-\alpha} s_{\beta-\alpha}}{8\pi^2 v^2 s_{2\beta} (m_H^2 - m_h^2)} (2A_0(\xi_W M_W^2) + A_0(\xi_Z M_Z^2)) \\ &+ \frac{g_2^2 c_{\beta-\alpha} s_{\beta-\alpha}}{256\pi^2 M_W^2} [2M_{A_0}^2 (B_0(m_h^2, m_{A_0}^2, \xi_Z M_Z^2) - B_0(m_H^2, m_{A_0}^2, \xi_Z M_Z^2)) \\ &+ 4M_{H^\pm}^2 (B_0(m_h^2, m_{H^\pm}^2, \xi_W M_W^2) - B_0(m_H^2, m_{H^\pm}^2, \xi_W M_W^2)) \\ &+ M_H^2 (2B_0(m_H^2, m_{A_0}^2, \xi_Z M_Z^2) + 4B_0(m_H^2, m_{H^\pm}^2, \xi_W M_W^2) \\ &\quad - 2B_0(m_H^2, \xi_W M_W^2, \xi_W M_W^2) - B_0(m_H^2, \xi_Z M_Z^2, \xi_Z M_Z^2)) \\ &- M_h^2 (2B_0(m_h^2, m_{A_0}^2, \xi_Z M_Z^2) + 4B_0(m_h^2, m_{H^\pm}^2, \xi_W M_W^2) \\ &\quad - 2B_0(m_h^2, \xi_W M_W^2, \xi_W M_W^2) - B_0(m_h^2, \xi_Z M_Z^2, \xi_Z M_Z^2))] , \end{aligned} \quad (7.38)$$

$$\begin{aligned} \delta\beta_c^K|_\xi &= \frac{g_2^2 c_{\beta-\alpha} s_{\beta-\alpha}}{128\pi^2 M_W^2} [M_h^2 (B_0(0, m_h^2, \xi_W M_W^2) - B_0(m_{H^\pm}^2, m_h^2, \xi_W M_W^2)) \\ &+ M_{H^\pm}^2 (B_0(m_{H^\pm}^2, m_h^2, \xi_W M_W^2) - B_0(m_{H^\pm}^2, m_H^2, \xi_W M_W^2)) \\ &+ M_H^2 (B_0(m_{H^\pm}^2, m_h^2, \xi_W M_W^2) - B_0(0, m_H^2, \xi_W M_W^2))] . \end{aligned} \quad (7.39)$$

Similar expressions hold for  $\delta\beta_o$ . Here  $A_0$  and  $B_0$  denote the scalar one- and two-point functions [142] in the convention stated in App. D.1. In order for the final amplitude to be gauge independent, the gauge-dependent terms entering via  $\delta\alpha^K$  and  $\delta\beta^K$  have to cancel with gauge-dependent terms in the remaining amplitude. However, a closer investigation shows that this cancellation occurs only for the first line in Eq. (7.38), i.e. for the gauge-dependent  $A_0$  functions in  $\delta\alpha^K$ . The gauge-dependent  $B_0$  functions, both in  $\delta\alpha^K$  and  $\delta\beta^K$ , are left uncanceled and lead to a gauge dependence of the full amplitude.

Let us exemplify this point by means of the amplitude for the decay  $H^+ \rightarrow W^+ h$ . Defining the *remaining amplitude*  $\mathcal{A}_{H^+ \rightarrow W^+ h}^{\text{rem}}$  as

$$\mathcal{A}_{H^+ \rightarrow W^+ h}^{\text{rem}} \equiv \mathcal{A}_{H^+ \rightarrow W^+ h}^{\mathcal{O}(1\text{-loop})} \Big|_{\delta\beta=\alpha=0} , \quad (7.40)$$

i.e. as the amplitude calculated up to one-loop order with the contribution of the angular counterterms set to zero, we find the following terms depending on  $\xi$

$$\mathcal{A}_{H^+ \rightarrow W^+ h}^{\text{rem}}|_\xi = \frac{g m_{12}^2 c_{\beta-\alpha} s_{\beta-\alpha}^2 p_1 \cdot \epsilon_3^*}{8\pi^2 v^2 s_{2\beta} (m_H^2 - m_h^2)} (2A_0(\xi_W M_W^2) + A_0(\xi_Z M_Z^2)) . \quad (7.41)$$

<sup>2</sup> Note that it is not possible to define the gauge-dependent parts of  $\delta\alpha^K$  and  $\delta\beta^K$  uniquely in a straightforward way, as explained below and in App. C.2. For the argumentation in this section, however, we do not need a unique definition of the truly gauge-dependent parts and the arbitrary choice of representing the terms containing gauge fixing parameters made here is sufficient.

Here  $\epsilon_3^*$  denotes the polarization vector of the outgoing  $W^+$  boson and  $p_1$  the momentum of the incoming  $H^+$ . On the other hand, the contribution of  $\delta\alpha^K$  and  $\delta\beta^K$  to the amplitude, designated as  $\mathcal{A}_{H^+\rightarrow W^+h}^{\delta\alpha,\delta\beta}$ , exhibits the following  $\xi$ -dependent part

$$\begin{aligned} \mathcal{A}_{H^+\rightarrow W^+h}^{\delta\alpha^K,\delta\beta^K} \Big|_{\xi} &= -gp_1 \cdot \epsilon_3^* (s_{\beta-\alpha}(\delta\alpha^K - \delta\beta_c^K)) \Big|_{\xi} \\ &= -\frac{gm_{12}^2 c_{\beta-\alpha} s_{\beta-\alpha}^2 p_1 \cdot \epsilon_3^*}{8\pi^2 v^2 s_{2\beta} (m_H^2 - m_h^2)} (2A_0(\xi_W M_W^2) + A_0(\xi_Z M_Z^2)) + B_0 \text{ terms.} \end{aligned} \quad (7.42)$$

Obviously, adding the two expressions, the  $A_0$  terms cancel, but we are left with a gauge-dependent result due to the appearance of gauge-dependent  $B_0$  functions in  $\delta\alpha^K$  and  $\delta\beta_c^K$ . Similar observations can be made for the amplitudes of other processes.

In the following, we will denote a scheme as *gauge-dependent scheme* if it leads to gauge-dependent amplitudes and as *gauge-independent scheme* otherwise.

Eventually, this gauge dependence means that the angles  $\alpha$  and  $\beta$ , which are extracted from an observable in the framework of the KOSY scheme, depend on the chosen gauge. They can hence not directly be interpreted as physical quantities. In order to arrive at physically meaningful values for the angles, the relation between the angles in the KOSY scheme and the angles in some other, gauge-independent scheme need to be known. Furthermore, the chosen gauge always has to be specified when extracting  $\alpha$  and  $\beta$  from experimental data [138, 143]. Likewise, the expressions for decay widths or cross sections, calculated in the context of the KOSY scheme for an arbitrary set of input parameters, depend on the gauge fixing parameters. Two conclusions can be drawn from the observations of this section:

1. The KOSY scheme leads to gauge-dependent expressions for amplitudes and therefore also gauge-dependent cross sections and decay widths.
2. Striving for gauge-independent and UV-finite amplitudes, it is impossible to define a gauge-independent counterterm for  $\alpha$ . The gauge-dependent and UV-divergent  $A_0$  functions in  $\delta\alpha^K$  are required to cancel those appearing in the remaining amplitude.

While the first point makes a statement about the KOSY scheme only, the second item is more general and holds for any scheme relying on the renormalization conditions introduced in sections 7.1 to 7.3.

The fact that  $\delta\alpha^K$  cannot be defined in a gauge-independent way is to be traced back to our treatment of the tadpoles in this section. We will see in the following chapter, that this gauge dependence vanishes in a natural manner when switching to tadpole scheme II.

Before closing this section, let us briefly comment on the proposal brought forward by Kanemura et al. in a subsequent publication [112] to cure the gauge dependence, introduced by their definition of  $\delta\beta_{o/c}^K$ . Instead of starting from symmetric WFRC matrices in the gauge basis (cf. Eq. (7.31)) as in their original publication, they now suggest to introduce two independent off-diagonal renormalization constants  $\delta C_{S_1 S_2}$  and  $\delta C_{S_2 S_1}$ . This additional degree of freedom allows them to define  $\delta\beta_{o/c}^K$  as the gauge-independent part of Eq. (7.36) or Eq. (7.37), respectively. However, the authors do not specify how to extract the gauge-independent parts of these expressions. Indeed, it is far from obvious how this extraction can be accomplished in a unique way. The representation of  $\delta\beta$  in Eq. (7.39) in terms of Passarino-Veltman functions is an arbitrary choice and any other equivalent representation of the loop-integrals can lead to other gauge-dependent parts (see App. C.2). Hence, the terms given in Eq. (7.39) cannot be regarded as the unique, truly gauge-dependent part of  $\delta\beta$ . In order to unambiguously extract the gauge dependence contained in an expression, a special technique like the pinch technique introduced in Sec. 3.3 is needed, which in turn requires the application of tadpole scheme II. Furthermore, Kanemura et al. do not comment on the case of  $\delta\alpha^K$ , where the situation is complicated by the fact that part of the gauge-dependent terms have to be kept

in  $\delta\alpha^K$  to obtain a gauge-independent amplitude. Therefore, it remains unclear how a gauge-independent result can be achieved in the KOSY scheme in an unambiguous way. In the following, we will show that the issue of this ambiguity can be resolved by treating the tadpoles according to scheme II.

---

## Renormalization in Tadpole Scheme II

---

The current chapter is dedicated to the introduction, illustration and investigation of tadpole scheme II. Although it is not as popular as scheme I, there are various publications based on tadpole scheme II, especially in the context of the SM [97, 101, 102, 117, 143, 144] but also for BSM studies [118, 145].

In order to motivate the usage of this scheme, we will start in Sec. 8.1 with a general discussion on the subject of gauge dependence of counterterms. This will provide us with a deeper understanding of the entanglement of tadpole (non-)renormalization and gauge dependence and strongly encourage the application of scheme II. For this purpose, we will illustrate in Sec. 8.2 in great detail how to properly implement this scheme in the framework of the 2HDM. We will investigate its consequences for mass and charge counterterms and WFRCs as well as for the couplings in Secs. 8.3 and 8.4, respectively. Afterwards, in Sec. 8.5, we will turn to the renormalization of the mixing angles  $\alpha$  and  $\beta$  and demonstrate how the problematic gauge-dependent terms encountered in the KOSY scheme can be avoided if tadpole scheme II is employed.

### 8.1. Tadpole Renormalization as the Origin of Gauge Dependence

Before we dedicate ourselves to tadpole scheme II and derive all required counterterms in this framework, we first want to discuss the matter of gauge dependence of counterterms. We will keep the discussion generic and focus in particular on the differences arising in the two tadpole schemes. This will allow us to draw important conclusions on viable renormalization conditions within the two schemes.

When analyzing the gauge dependence of counterterms, one has to distinguish two different types of counterterms [88, 129]. The first group, which we will refer to as the group of *unphysical* counterterms, comprises WFRCs, tadpole counterterms and counterterms for gauge fixing parameters<sup>1</sup>. These counterterms cannot be defined in terms of physical observables like cross sections or decay rates. As a consequence, they will in general exhibit a dependence on the gauge fixing parameters.

---

<sup>1</sup>Note that we did not introduce counterterms for the gauge fixing parameters.

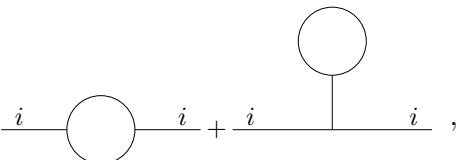
The second group is composed of counterterms for *physical* parameters, i.e. for the parameters of the classical gauge-invariant Lagrangian, like masses, gauge couplings and mixing angles. For brevity, we will denote these as *physical* counterterms in the following, although, strictly speaking, a counterterm cannot be physical. Unlike the counterterms of the first group, the physical counterterms can be fixed by renormalization conditions formulated in terms of physical quantities. Such renormalization conditions guarantee the gauge independence of the *renormalized* parameters [88]. However, in contrast to the parameters themselves their counterterms can still depend on the gauge fixing parameters. Although this point might seem contradictory at first glance, it can be explained by the interplay between the renormalization of physical parameters and tadpole renormalization.

The most prominent example where this interplay becomes obvious is the renormalization of mass parameters. Certainly, the determination of a mass parameter  $m_i$  as the (complex) pole of the propagator of a particle is a physical definition and it has been shown by many authors that the thus defined pole mass is indeed gauge independent<sup>2</sup> [88, 146, 147]. Yet, the corresponding counterterm, defined according to the OS conditions as

$$\delta m_i = \Sigma_{ii}(m_i^2), \quad (8.1)$$

is independent of the gauge fixing parameters only if tadpole diagrams are taken into account in the self-energy  $\Sigma_{ii}$  (see Eq. (8.2)) [88, 97, 102, 117, 118, 143]. In order to distinguish between the self-energy without and with tadpole diagrams, we will denote the latter one as  $\tilde{\Sigma}_{ii}$  and call  $\Sigma_{ii}$  the *conventional* and  $\tilde{\Sigma}_{ii}$  the *tadpole self-energy*. Schematically we have

$$\begin{aligned} \delta m_i^{2,I} &= \Sigma_{ii}(m_i^2) \rightarrow \text{gauge-dependent}, \\ \delta m_i^{2,II} &= \tilde{\Sigma}_{ii}(m_i^2) \rightarrow \text{gauge-independent}, \end{aligned}$$

$$\text{with } i\tilde{\Sigma}_{ii} = \text{---} \bigcirc \text{---} + \text{---} \bigcirc \text{---} \quad (8.2)$$


where the empty circles represent generic corrections to the propagator or the tadpole. Thus, gauge-independent mass counterterms can only be obtained if the tadpole diagrams are not cancelled by tadpole counterterms but explicitly taken into account. In other words, gauge-independent OS mass counterterms are possible only if tadpole scheme II is applied. The same holds for all other physical parameters and in particular also for mixing angles [88].

The reason for this different behaviour of the counterterms in tadpole scheme I and II lies in the different definition of the vevs. In scheme I the bare vevs are defined as the minima of the *loop-corrected* effective potential and are therefore gauge dependent [116]. This gauge dependence is propagated into all other bare parameters which depend on the vevs. In order for the renormalized physical parameters to be independent of the gauge fixing, the gauge-dependent terms in the bare parameters have to be absorbed into the counterterms. Note that these gauge-dependent terms are always entirely composed of  $A_0$  functions<sup>3</sup>.

On the contrary, in scheme II the bare vevs are defined as minima of the *tree-level* potential. Hence, they can be expressed uniquely in terms of parameters of the tree-level potential and are manifestly gauge independent. The same is true for the bare parameters defined in terms of the vevs and thus also for their counterterms.

<sup>2</sup>For unstable particles the imaginary part of the pole has to be taken into account beyond one-loop order [88, 119–122] to obtain a gauge-independent pole mass.

<sup>3</sup>This can easily be seen from the fact that the only difference between the schemes I and II arises from the treatment of tadpole terms, i.e.  $A_0$  functions. The gauge dependence of terms in scheme I, which are gauge independent in scheme II, can hence only be given by  $A_0$  functions.

These observations immediately raise the question which implications this different behaviour of physical counterterms has for a suitable renormalization scheme.

First, it is important to note that also in scheme II the physical counterterms are not guaranteed to come out gauge independent if they are determined in an arbitrary renormalization scheme. In case that unphysical renormalization conditions are applied, nothing prevents the counterterms from becoming gauge dependent. However, striving for gauge-independent expressions for physical observables, this gauge dependence must be avoided. In tadpole scheme II, all physical counterterms have to be defined in a manner that ensures them to be *gauge independent*. Otherwise, their gauge dependence will be propagated into the  $\mathcal{S}$ -matrix and spoil its gauge independence. One possibility to guarantee gauge independence of the physical counterterms and thus of the  $\mathcal{S}$ -matrix is to fix these counterterms by renormalization conditions relying on physical observables. In scheme II, such a definition automatically leads to gauge-independent counterterms.

This is to be compared to the situation in scheme I. There, the physical counterterms are required to include *gauge-dependent* terms to cancel remaining gauge dependences in the rest amplitude (cf. Subs. 7.4.2). As we have seen in the previous section, unphysical conditions can lead to a counterterm which contains, in addition to the required gauge-dependent terms given by  $A_0$  functions, further gauge-dependent parts, which remain uncancelled. Again, the fail-safe way to ensure gauge independence of the final results for physical observables is to resort to physical conditions to fix the physical counterterms. Such prescriptions guarantee the counterterms to contain exactly those gauge-dependent  $A_0$  functions needed to preserve the gauge independence of the  $\mathcal{S}$ -matrix.

Hence, in both tadpole schemes gauge-independent amplitudes can be obtained by fixing all physical parameters in terms of physical renormalization conditions. In tadpole scheme II the resulting counterterms are gauge-independent, whereas in scheme I they contain exactly those gauge dependent terms necessary to cancel gauge dependences present in the remaining amplitude.

Yet, in some cases, like in the case of mixing angles, we might wish to start from a renormalization condition not relying on a particular physical observable in order to maintain a universal definition of the respective parameters. At this point, tadpole scheme II demonstrates its advantages: In scheme II we “only” have to ensure the gauge independence of all physical counterterms. Therefore, we are free to start from any renormalization conditions as long as we are given a technique to extract the truly gauge-independent parts of the resulting expressions for the counterterms. The *pinch technique*, introduced in Sec. 3.3, constitutes precisely such a technique.

A similar procedure is not possible in tadpole scheme I, which is due to the fact that the application of the PT requires a treatment of the tadpoles according to scheme II. Furthermore, even if there was a method in scheme I to extract the truly gauge-independent part of a counterterm, like e.g. the angular counterterms, this would still not solve the problem. This is because gauge-dependent physical counterterms are mandatory in scheme I to obtain a gauge-independent amplitude. We know of no procedure to dismiss all unwanted gauge-dependent terms, like those containing the  $B_0$  functions in Eq. (7.38) and Eq. (7.39), but retain the necessary terms, like the those comprising the  $A_0$  functions in the same equations. Trying to accomplish this by hand, we would be faced with the ambiguity of how to define the proper gauge-independent parts of the  $B_0$  functions, alluded to in the footnote on page 66 and illustrated in App. C.2.

Hence, in order to attain gauge-independent amplitudes in scheme I in a well-defined manner, all physical counterterms have to be defined by physical renormalization conditions. This, though feasible, constitutes a loss of generality in the case of parameters that are not connected to a single observable only, e.g. in the case of  $\alpha$  and  $\beta$ . Defining these parameters in terms of a physical quantity leads to an undesirable process dependence of the parameters

and complicated expressions for the counterterms.

For the sake of completeness, let us note that there is a third customarily-chosen option for the renormalization of physical parameters, which is given by the  $\overline{\text{MS}}$  scheme. This scheme, however, also exhibits certain drawbacks. First, parameters defined by  $\overline{\text{MS}}$  conditions cannot directly be interpreted as physical quantities, as can be seen e.g. from the fact that they depend on the renormalization scale  $\mu_r$ . Moreover, in the context of tadpole scheme I, the  $\overline{\text{MS}}$  scheme can lead to gauge-dependent  $\mathcal{S}$ -matrix elements, for example if applied in order to fix the counterterms for the angle  $\alpha$ .<sup>4</sup> We will come back to this issue in Sec. 9.5. Finally, in the particular case of the mixing angles in the 2HDM,  $\overline{\text{MS}}$  schemes are found to yield numerically large radiative corrections, if at the same time OS conditions for masses and fields are kept [148]. This will be commented on in Sec. 9.5. In summary, we can draw the following conclusions concerning the applicability of various renormalization schemes within the the two tadpole frameworks:

- In both tadpole schemes, gauge-independent results can be obtained by defining all physical counterterms in terms of observables. This, however, leads to an undesirable *process dependence* for parameters like e.g. the mixing angles.
- In tadpole scheme II,  $\overline{\text{MS}}$  conditions can be applied to attain process-independent parameters and gauge-independent physical observables. However, in tadpole scheme I,  $\overline{\text{MS}}$  renormalized parameters can result in an artificial gauge dependence of  $\mathcal{S}$ -matrix elements. Furthermore, in the case of the 2HDM mixing angles,  $\overline{\text{MS}}$ -like schemes can suffer from *numerical instabilities* [148].
- In tadpole scheme II, a third possibility opens up: The fact that physical counterterms are necessarily gauge independent together with the virtues of the PT allows for a process-independent, non- $\overline{\text{MS}}$  definition of these counterterms. For scheme I, a similar procedure is not available.

Another conclusion, which can directly be drawn, is that in tadpole scheme II, all gauge-dependent terms entering the  $\mathcal{S}$ -matrix through loop-corrections have to be cancelled by the counterterms of unphysical parameters, i.e. by WFRCs in our case. This is to be inferred from the gauge independence of  $\mathcal{S}$ -matrix elements on the one hand and of the physical counterterms on the other (cf. [88, 124]). Hence, in scheme II, the matter of gauge dependence is completely decoupled from the renormalization of physical parameters and we need not worry about intricate cancellations of gauge fixing parameter dependent terms among various counterterms and virtual corrections.

These observations clearly advocate the usage of tadpole scheme II. For this reason, we will dedicate the subsequent section to a detailed derivation of its implementation in the framework of the 2HDM.

As a final remark, note that a mixture of the different renormalization conditions proposed above is possible. We will, for instance, always apply OS conditions, i.e. physical conditions, for all mass parameters and gauge couplings while varying the schemes for  $\alpha$ ,  $\beta$  and  $m_{12}^2$ .

## 8.2. Implementation of Tadpole Scheme II in the Framework of the 2HDM

After having motivated the utilization of tadpole scheme II, we will now study in detail its application to the 2HDM and derive the corresponding implications. The altered treatment

<sup>4</sup>This is well-known also from electroweak SM calculations, where  $\overline{\text{MS}}$  conditions, if applied e.g. to quark mass parameters, are found to result in gauge-dependent  $\overline{\text{MS}}$  masses within tadpole scheme I [117, 143, 144]. While not posing a problem in itself, since  $\overline{\text{MS}}$  masses are not to be regarded as physical, this renders the relation between the physical quantities and the renormalized parameters gauge-dependent and leads to an artificial gauge parameter dependence in  $\mathcal{S}$ -matrix elements [143].

of the tadpoles in scheme II affects the relation between vevs and vev-dependent parameters and couplings as well as the expressions for counterterms and WFRCs. Both consequences will be derived and examined in the following. For the SM these investigation has been performed by Fleischer et al. and we are going follow their derivation presented in Ref. [102] in our generalization of their study to the 2HDM.

Analogously to the case of the SM, we use as our starting point the conditions shown in Fig. 8.1 (cf. Sec. 6.3). These conditions can be expressed either in the gauge basis or in the

$$iT_i^{(1)} - iT_i^0(v_j^{(0)} + \Delta^{(1)}v_j)$$

$$+ \quad = \quad 0$$

**Figure 8.1.:** Pictorial representation of the tadpole conditions in scheme II. The empty circle stands for generic one-loop contributions to the tadpole, while the cross denotes the shifted “tree-level” tadpole  $T_i^0$ ,  $i = 1, 2$ .

mass basis. However, in the gauge basis, they lead to more concise expressions. Therefore we will use the tadpole conditions in the gauge basis in the following paragraph. Furthermore, we start from the original parameter set Eq. (5.31), i.e. we use the parameters  $\lambda_1 \dots \lambda_5$  and  $m_{11}^2, m_{22}^2, m_{12}^2$ , since these, unlike the the masses and angles in set 2 Eq. (5.32), do not depend on  $v_1$  and  $v_2$  and hence are not affected by a shift in the vevs.

At tree level, the tadpole conditions lead to the tadpole equations Eqs. 5.8 and 5.9. The solution of these equations provides us with the tree level values of the vevs  $v_1$  and  $v_2$ .

Including higher orders of the perturbative expansion, the vevs  $v_1$  and  $v_2$  acquire a shift

$$v_1 \rightarrow v_1 + \Delta v_1, \quad (8.3)$$

$$v_2 \rightarrow v_2 + \Delta v_2, \quad (8.4)$$

such that the condition in Fig. 8.1 is fulfilled. At one loop level this condition yields

$$T_1^{(1)} - T_1^0(v_1 + \Delta^{(1)}v_1, v_2 + \Delta^{(1)}v_2) \equiv T_1^{(1)} - T_1^0 - \Delta^{(1)}T_1 = 0, \quad (8.5)$$

$$T_2^{(1)} - T_2^0(v_1 + \Delta^{(1)}v_1, v_2 + \Delta^{(1)}v_2) \equiv T_2^{(1)} - T_2^0 - \Delta^{(1)}T_2 = 0, \quad (8.6)$$

with

$$\Delta^{(1)}T_1 = \left( m_{12}^2 \frac{v_1}{v_2} + \lambda_1 v_1^2 \right) \Delta^{(1)}v_1 + \left( -m_{12}^2 + \lambda_{345} v_1 v_2 \right) \Delta^{(1)}v_2, \quad (8.7)$$

$$\Delta^{(1)}T_2 = \left( -m_{12}^2 + \lambda_{345} v_1 v_2 \right) \Delta^{(1)}v_1 + \left( m_{12}^2 \frac{v_2}{v_1} + \lambda_2 v_2^2 \right) \Delta^{(1)}v_2. \quad (8.8)$$

In the following we will omit the superscripts (1) for the vev shifts, which are always regarded to be of one-loop order. Inserting these expressions for  $\Delta T_1$  and  $\Delta T_2$  and applying the tree-level tadpole conditions, Eqs. 8.5 and 8.6 can be solved for  $\Delta v_1$  and  $\Delta v_2$ , which yields

$$\Delta v_1 = \frac{v_1(m_{12}^2(v_1 T_1^{(1)} + v_2 T_2^{(1)}) - \lambda_{345} T_2^{(1)} v_1 v_2^2 + \lambda_2 T_1^{(1)} v_2^3)}{\lambda_1 m_{12}^2 v_1^4 + \lambda_2 m_{12}^2 v_2^4 + 2\lambda_{345} m_{12}^2 v_1^2 v_2^2 + (\lambda_1 \lambda_2 - \lambda_{345}^2) v_1^3 v_2^3}, \quad (8.9)$$

$$\Delta v_2 = \frac{v_1(m_{12}^2(v_1 T_1^{(1)} + v_2 T_2^{(1)}) - \lambda_{345} T_1^{(1)} v_1^2 v_2 + \lambda_1 T_2^{(1)} v_1^3)}{\lambda_1 m_{12}^2 v_1^4 + \lambda_2 m_{12}^2 v_2^4 + 2\lambda_{345} m_{12}^2 v_1^2 v_2^2 + (\lambda_1 \lambda_2 - \lambda_{345}^2) v_1^3 v_2^3}. \quad (8.10)$$

Having derived these expressions, we can now use the relations Eqs. 5.33 - 5.37 between parameter sets 1 and 2 as well as the connection of Eq. (5.22) between the tadpoles in the

gauge and in the mass basis to formulate  $\Delta v_1$  and  $\Delta v_2$  in terms of physical parameters

$$\Delta v_1 = \frac{T_H^{(1)} c_\alpha}{m_H^2} - \frac{T_h^{(1)} s_\alpha}{m_h^2}, \quad (8.11)$$

$$\Delta v_2 = \frac{T_H^{(1)} s_\alpha}{m_H^2} + \frac{T_h^{(1)} c_\alpha}{m_h^2}, \quad (8.12)$$

where  $T_h^{(1)}$  and  $T_H^{(1)}$  are to be understood as the one-loop tadpole diagrams in the mass basis. The shifts  $\Delta v_1$  and  $\Delta v_2$  are propagated into all parameters of the 2HDM which depend on the vevs, i.e. into all mass parameters, the tadpole parameters  $T_H$  and  $T_h$  as well as  $\alpha_p$  and  $\beta_p$ . In the case of the last two parameters one has to carefully distinguish between the mixing angles  $\alpha_{\text{rot}}$ ,  $\beta_{\text{rot}}$  and the angles  $\alpha_p$ ,  $\beta_p$  in their role as parameters of the scalar potential, defined according to Eq. (5.39) and Eq. (5.38). Only the parametric angles depend on the vevs and receive a shift. The mixing angles  $\alpha_{\text{rot}}$ ,  $\beta_{\text{rot}}$ , on the contrary, are still defined to diagonalize the same tree-level mass matrices  $\mathcal{M}_\rho$  or  $\mathcal{M}_\eta$  and  $\mathcal{M}_{\phi^\pm}$  as in tadpole scheme I and therefore remain unaffected.

Closely following the procedure outlined in Ref. [102], we next have to determine the exact form of the shifts induced by Eqs. 8.3 and 8.4 in the individual vev-dependent parameters of the 2HDM. The shift in  $T_H$  and  $T_h$  is trivial. Rotating Eqs. 8.5 and 8.6 to the mass basis directly leads to

$$\begin{pmatrix} \Delta T_H \\ \Delta T_h \end{pmatrix} \equiv R^T(\alpha) \begin{pmatrix} \Delta T_1 \\ \Delta T_2 \end{pmatrix} = \begin{pmatrix} T_H^{(1)} \\ T_h^{(1)} \end{pmatrix}. \quad (8.13)$$

For the scalar mass parameters, we have to go back to the expressions for the bilinear terms of the Higgs potential, stated in Sec. 5.2. Note that in order to consistently apply the scheme developed in Ref. [102], we also have to take the bilinear tadpole terms (cf. Eq. (5.11)) into account. Thus, e.g. in the case of the CP-even scalars, we have to consider the following mass matrix

$$\widetilde{\mathcal{M}}_\rho = \begin{pmatrix} m_{12}^2 \frac{v_2}{v_1} + \lambda_1 v_1^2 & -m_{12}^2 + \lambda_{345} v_1 v_2 \\ -m_{12}^2 + \lambda_{345} v_1 v_2 & m_{12}^2 \frac{v_1}{v_2} + 3\lambda_2 v_2^2 \end{pmatrix} + \begin{pmatrix} \frac{T_1^0}{v_1} & 0 \\ 0 & \frac{T_2^0}{v_2} \end{pmatrix}. \quad (8.14)$$

Performing the shifts of Eqs. 8.3 and 8.4, while also taking into account those induced in  $T_1^0$  and  $T_2^0$ , we find for the shift in  $\widetilde{\mathcal{M}}_\rho$

$$\Delta \mathcal{M}_\rho = \begin{pmatrix} 3\lambda_1 v_1 \Delta v_1 + \lambda_{345} \Delta v_2 & \lambda_{345} v_2 \Delta v_1 + \lambda_{345} v_1 \Delta v_2 \\ \lambda_{345} v_2 \Delta v_1 + \lambda_{345} v_1 \Delta v_2 & \lambda_{345} v_1 \Delta v_1 + \lambda_2 v_2 \Delta v_2 \end{pmatrix}. \quad (8.15)$$

After having determined these shifts, we can set  $T_1^0$  and  $T_2^0$  to zero and omit the tilde  $\sim$ , which has already been done in Eq. (8.15). The corresponding shifts in  $\mathcal{D}_\rho$ , the CP-even mass matrix in the mass basis, can be obtained from this by a rotation with  $R(\alpha)$ . Replacing  $\Delta v_1$  and  $\Delta v_2$  in the resulting matrix with the explicit expressions in Eq. (8.11) and Eq. (8.12) and finally formulating the result in terms of the physical parameter set, we arrive at

$$\Delta \mathcal{D}_\rho = \begin{pmatrix} \Delta m_H^2 & \Delta m_{Hh}^2 \\ \Delta m_{hH}^2 & \Delta m_h^2 \end{pmatrix}, \quad (8.16)$$

with

$$\Delta m_H^2 = - \frac{s_{\beta-\alpha} \left( (m_h^2 + 2m_H^2) s_{2\alpha} s_{2\beta} - 2m_{12}^2 (3s_{2\alpha} + s_{2\beta}) \right)}{m_h^2 v s_{2\beta}^2} T_h^{(1)} \quad (8.17)$$

$$- 3 \frac{\left( 4m_{12}^2 s_{\alpha+\beta} s_{\beta-\alpha}^2 + m_H^2 (c_{\beta-\alpha} s_{2\alpha} - 2s_{\alpha+\beta}) s_{2\beta} \right)}{m_H^2 v s_{2\beta}^2} T_H^{(1)},$$

$$\Delta m_h^2 = - 3 \frac{\left( 4m_{12}^2 c_{\alpha+\beta} c_{\beta-\alpha}^2 - m_h^2 (2c_{\alpha+\beta} + s_{2\alpha} s_{\beta-\alpha}) s_{2\beta} \right)}{m_h^2 v s_{2\beta}^2} T_h^{(1)} \quad (8.18)$$

$$+ \frac{c_{\beta-\alpha} \left( (2m_h^2 + m_H^2) s_{2\alpha} s_{2\beta} - 2m_{12}^2 (3s_{2\alpha} - s_{2\beta}) \right)}{m_H^2 v s_{2\beta}^2} T_H^{(1)},$$

$$\Delta m_{Hh}^2 = \frac{c_{\beta-\alpha} \left( (2m_h^2 + m_H^2) s_{2\alpha} s_{2\beta} - 2m_{12}^2 (3s_{2\alpha} - s_{2\beta}) \right)}{M_h^2 v s_{2\beta}^2} T_h^{(1)} \quad (8.19)$$

$$- \frac{s_{\beta-\alpha} \left( (m_h^2 + 2m_H^2) s_{2\alpha} s_{2\beta} - 2m_{12}^2 (3s_{2\alpha} + s_{2\beta}) \right)}{M_H^2 v s_{2\beta}^2} T_H^{(1)} = \Delta m_{hH}^2.$$

We can proceed in the same way for the CP-odd and the charged scalars.

Analogous shifts also appear in the mass terms for gauge bosons and fermions, as we illustrate for the case of the  $W$ -boson and the  $\tau$ -lepton. In terms of the vevs  $v_1$  and  $v_2$  their masses are given by

$$M_W^2 = \frac{g_2^2 (v_1^2 + v_2^2)}{4}, \quad (8.20)$$

$$m_\tau = \frac{y_\tau (v_1 (Y_2 c_\alpha - Y_1 s_\alpha) + v_2 (Y_1 c_\alpha + Y_2 s_\alpha))}{\sqrt{2}}, \quad (8.21)$$

where  $y_\tau$  denotes the SM  $\tau$ -Yukawa coupling and  $Y_1$  and  $Y_2$  are combinations of trigonometric functions of  $\alpha$  and  $\beta$  that depend on the 2HDM type under consideration (cf. App. A.2).

Inserting the shifts of Eqs. 8.11 and 8.12 and then translating the result to parameter set 2 leads to

$$\Delta M_W^2 = \frac{M_W e s_{\beta-\alpha}}{m_h^2 s_W} T_h^{(1)} + \frac{M_W e c_{\beta-\alpha}}{m_H^2 s_W} T_H^{(1)}, \quad (8.22)$$

$$\Delta m_\tau = \frac{y_\tau Y_1}{\sqrt{2} m_h^2} T_h^{(1)} + \frac{y_\tau Y_2}{\sqrt{2} m_H^2} T_H^{(1)}. \quad (8.23)$$

For a subsequent interpretation of these mass shifts, it is important to note that they correspond exactly to the contribution of tadpole diagrams to the self-energies of the respective particles. We define

$$\begin{aligned} T_{\phi_i \phi_j} &\equiv -i \left[ \text{tadpole}_h(\phi_i, \phi_j) - \text{tadpole}_H(\phi_i, \phi_j) \right] \quad (8.24) \\ &= -i \left[ (i g_{h\phi_i \phi_j}) \left( \frac{i}{-m_h^2} \right) \left( \frac{T_h^{(1)}}{-i} \right) + (i g_{H\phi_i \phi_j}) \left( \frac{i}{-m_H^2} \right) \left( \frac{T_H^{(1)}}{-i} \right) \right], \end{aligned}$$

with  $\phi_i, \phi_j \in \{h, H\}$ ,

$$\begin{aligned}
T_{WW} &\equiv -i \text{ (diagram with } h \text{ tadpole)} - i \text{ (diagram with } H \text{ tadpole)} \\
&= -i \left[ (ig_{WW h}) \left( \frac{i}{-m_h^2} \right) \left( \frac{T_h^{(1)}}{-i} \right) + (ig_{WW H}) \left( \frac{i}{-m_H^2} \right) \left( \frac{T_H^{(1)}}{-i} \right) \right]
\end{aligned} \tag{8.25}$$

and

$$\begin{aligned}
T_{\tau\tau} &\equiv -i \text{ (diagram with } h \text{ tadpole)} - i \text{ (diagram with } H \text{ tadpole)} \\
&= -i \left[ (ig_{\tau\tau h}) \left( \frac{i}{-m_h^2} \right) \left( \frac{T_h^{(1)}}{-i} \right) + (ig_{\tau\tau H}) \left( \frac{i}{-m_H^2} \right) \left( \frac{T_H^{(1)}}{-i} \right) \right],
\end{aligned} \tag{8.26}$$

where the empty circles denote generic one-loop tadpole contributions and the following 2HDM Higgs couplings have been used

$$g_{HHH} = \frac{3}{vs_{2\beta}^2} (4m_{12}^2 s_{\alpha+\beta} s_{\beta-\alpha}^2 + m_H^2 (c_{\beta-\alpha} s_{2\alpha} - 2s_{\alpha+\beta}) s_{2\beta}), \tag{8.27}$$

$$g_{HHh} = \frac{s_{\beta-\alpha}}{vs_{2\beta}^2} ((m_h^2 + 2m_H^2) s_{2\alpha} s_{2\beta} - 2m_{12}^2 (3s_{2\alpha} + s_{2\beta})), \tag{8.28}$$

$$g_{Hhh} = -\frac{c_{\beta-\alpha}}{vs_{2\beta}^2} ((2m_h^2 + m_H^2) s_{2\alpha} s_{2\beta} - 2m_{12}^2 (3s_{2\alpha} - s_{2\beta})), \tag{8.29}$$

$$g_{hhh} = \frac{3}{vs_{2\beta}^2} (4m_{12}^2 c_{\alpha+\beta} c_{\beta-\alpha}^2 - m_h^2 (2c_{\alpha+\beta} + s_{2\alpha} s_{\beta-\alpha}) s_{2\beta}) \tag{8.30}$$

and

$$g_{hWW} = \frac{M_W e s_{\beta-\alpha}}{s_W}, \quad g_{HWW} = \frac{M_W e c_{\beta-\alpha}}{s_W}, \tag{8.31}$$

$$g_{h\tau\tau} = -\frac{y_\tau Y_1}{\sqrt{2}}, \quad g_{H\tau\tau} = -\frac{y_\tau Y_2}{\sqrt{2}}. \tag{8.32}$$

For simplicity we have furthermore split off the Lorentz structure. With these definitions we can establish the following relations

$$-\Delta m_H^2 = T_{HH}, \tag{8.33}$$

$$-\Delta m_h^2 = T_{hh}, \tag{8.34}$$

$$-\Delta m_{Hh}^2 = T_{Hh}, \tag{8.35}$$

$$-\Delta M_W^2 = -T_{WW}, \tag{8.36}$$

$$-\Delta m_\tau = T_{\tau\tau}. \tag{8.37}$$

Again, equivalent results can be obtained for the other scalars, gauge bosons and fermions. The shifts in the remaining vev-dependent parameters,  $\alpha_p$  and  $\beta_p$ , can directly be derived from their definitions in terms of  $v_1$  and  $v_2$ , as we illustrate in App. A.1. These shifts in the parameters have three important consequences:

1. The shifts in the diagonal elements of the mass matrices appear in the diagonal elements of the corresponding inverse propagators, thus giving an additional contribution to the mass counterterms defined according to the prescriptions of the on-shell scheme. These additional contributions render the mass counterterms gauge-independent [88, 102].

2. The shifts in the off-diagonal elements of the mass matrices appear in the off-diagonal elements of the inverse scalar propagators, thus leading to an additional term in the corresponding off-diagonal WFRCs defined in the on-shell scheme.
3. The shifts induced in the vev-dependent parameters appear in the Feynman rules for scalar vertices and reproduce the tadpole diagrams contributing to the vertex corrections.

We will investigate the third point below. First, however, we will concentrate on the influence of the shifts on the mass and charge counterterms and WFRCs.

### 8.3. Transformation of the On-Shell Counterterms in Tadpole Scheme II

In tadpole scheme II, the elements of the inverse propagator of a generic pair of scalar fields have the form

$$\hat{\Gamma}_{S_i S_i}(p^2) = (p^2 - m_{S_i}^2)(1 + \delta Z_{S_i S_i}) - \Delta m_{S_i}^2 - \delta m_{S_i}^2 + \Sigma_{S_i S_i}(p^2), \quad (8.38)$$

$$\hat{\Gamma}_{S_i S_j}(p^2) = \frac{\delta Z_{S_j S_i}}{2}(p^2 - m_{S_j}^2) + (p^2 - m_{S_i}^2) \frac{\delta Z_{S_i S_j}}{2} - \Delta m_{S_i S_j}^2 + \Sigma_{S_i S_j}(p^2), \quad i \neq j. \quad (8.39)$$

Note that, unlike in Eqs. 7.2 and 7.3, no tadpole counterterms appear here. Instead, the mass shifts  $\Delta m_{S_i}^2$  and  $\Delta m_{S_i S_j}^2$  show up.

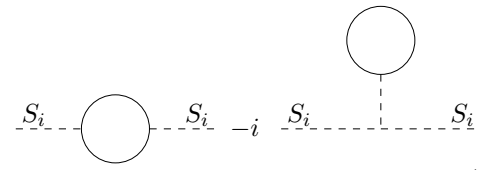
According to the OS renormalization conditions, we have to determine the counterterm  $\delta m_{S_i}^2$  in such way that the parameter  $m_{S_i}$ , appearing in the inverse propagator, corresponds to the pole mass of the particle under consideration. Solving the equation

$$\hat{\Gamma}_{S_i S_i}(p^2) \Big|_{p^2=m_{S_i}^2} = 0, \quad (8.40)$$

resulting from this condition, for  $\delta m_{S_i}^2$  leads to

$$\delta m_{S_i}^2 = -\Delta m_{S_i}^2 + \Sigma_{S_i S_i}(m_{S_i}^2).$$

Afterwards making use of Eqs. 8.33 and 8.34 we get

$$\delta m_{S_i}^2 = T_{S_i S_i} + \Sigma_{S_i S_i}(m_{S_i}^2) \equiv \tilde{\Sigma}_{S_i S_i}(m_{S_i}^2) = -i \text{---} S_i \text{---} \text{---} S_i \text{---} -i \text{---} S_i \text{---} \text{---} S_i \text{---} , \quad (8.41)$$


where the first diagram symbolically stands for all contributions to the conventional self-energy while the second diagram denotes the contributions of tadpole diagrams. The scalar mass counterterms resulting from this definition are gauge independent, as one can verify by explicitly calculating these diagrams in general  $R_\xi$ -gauge [88, 102].

Next, we can define the self-energy  $\tilde{\Sigma}_{S_i S_j}$  in the same manner and use the OS conditions Eqs. 6.42 and 6.43 to solve for  $\delta Z_{S_i S_j}$  and  $\delta Z_{S_j S_i}$

$$\delta Z_{S_i S_j} = -2 \frac{\tilde{\Sigma}_{S_i S_j}(m_{S_j}^2)}{m_{S_j}^2 - m_{S_i}^2}, \quad \delta Z_{S_j S_i} = 2 \frac{\tilde{\Sigma}_{S_i S_j}(m_{S_i}^2)}{m_{S_j}^2 - m_{S_i}^2}. \quad (8.42)$$

Note that the diagonal WFRCs, unlike the off-diagonal ones, do not receive a contribution by tadpole diagrams. Since the tadpoles do not depend on the external momentum, their

contributions drop out when taking the derivative prescribed by Eq. (6.46) and Eq. (6.47). For the gauge bosons we can proceed analogously. The transverse part of the renormalized two-point functions for generic gauge bosons  $V_i$  and  $V_j$  in tadpole scheme II is given by (cf. Eqs. 7.17 and 7.18)

$$\hat{\Gamma}_{V_i V_i}^T(p^2) = -((p^2 - M_{V_i}^2)(1 + \delta Z_{V_i V_i}) - \delta M_{V_i}^2 - \Delta M_{V_i}^2 + \Sigma_{V_i V_i}^T(p^2)), \quad (8.43)$$

$$\hat{\Gamma}_{V_i V_j}^T(p^2) = -\left(\frac{\delta Z_{V_j V_i}}{2}(p^2 - M_{V_j}^2) + (p^2 - M_{V_i}^2)\frac{\delta Z_{V_i V_j}}{2} + \Sigma_{V_i V_j}^T(p^2)\right), \quad (8.44)$$

so that the on-shell conditions lead to

$$\delta M_{V_i}^2 = -\Delta M_{V_i}^2 + \Sigma_{V_i V_i}^T(M_{V_i}^2) \equiv \tilde{\Sigma}_{V_i V_i}^T(M_{V_i}^2) = i \text{ [diagram: wavy line with a loop] } + i \text{ [diagram: wavy line with a tadpole] }, \quad (8.45)$$

As in Eq. (8.41) the diagrams symbolize all possible contributions to the conventional self-energy and the tadpole diagrams. Again, it can be shown that the mass counterterms defined in this way are gauge independent [88, 101]. Like in the scalar case, the diagonal WFRCs are not affected by the shifts. Furthermore, there is no tadpole contribution to the  $A$ - $Z$ -mixing self-energy, wherefore also  $\delta Z_{AZ}$  and  $\delta Z_{ZA}$  remain unchanged as compared to tadpole scheme I.

Finally, as can easily be verified, only the scalar parts of the fermion self-energies are influenced by the change of the tadpole schemes. In scheme II they attain the following form

$$\hat{\Sigma}_{f_i f_i}^{S,l}(p^2) = -\frac{\delta m_{f_i} + \Delta m_{f_i}}{m_{f_i}} - \frac{1}{2}\delta(Z_{f_i f_i}^L + Z_{f_i f_i}^R) + \Sigma_{f_i f_i}^{S,l}(p^2), \quad (8.46)$$

$$\hat{\Sigma}_{f_i f_i}^{S,r}(p^2) = -\frac{\delta m_{f_i} + \Delta m_{f_i}}{m_{f_i}} - \frac{1}{2}\delta(Z_{f_i f_i}^L + Z_{f_i f_i}^R) + \Sigma_{f_i f_i}^{S,r}(p^2), \quad (8.47)$$

which results in altered, gauge-independent fermion mass counterterms

$$\begin{aligned} \delta m_{f_i} &= \frac{m_{f_i}}{2} \widetilde{\text{Re}} \left( \Sigma_{f_i f_i}^L(m_{f_i}^2) + \Sigma_{f_i f_i}^R(m_{f_i}^2) + \Sigma_{f_i f_i}^{S,l}(m_{f_i}^2) - \frac{\Delta m_{f_i}}{m_{f_i}} + \Sigma_{f_i f_i}^{S,r}(m_{f_i}^2) - \frac{\Delta m_{f_i}}{m_{f_i}} \right) \\ &\equiv \frac{m_{f_i}}{2} \widetilde{\text{Re}} \left( \Sigma_{f_i f_i}^L(m_{f_i}^2) + \Sigma_{f_i f_i}^R(m_{f_i}^2) + \tilde{\Sigma}_{f_i f_i}^{S,l}(m_{f_i}^2) + \tilde{\Sigma}_{f_i f_i}^{S,r}(m_{f_i}^2) \right). \end{aligned} \quad (8.48)$$

The last parameter defined via on-shell conditions, the electric charge  $e$ , remains unchanged when switching from tadpole scheme I to scheme II. This can directly be read off the explicit form in Eq. (7.21) noting that neither  $\Sigma_{AZ}$  nor  $\Sigma_{AA}$  receive contributions by tadpole diagrams. Also the dependent counterterm  $\delta g_2$  does not get modified.

To conclude this section, we summarize all counterterms that are altered under a change of schemes

$$\delta m_h^2 = \text{Re}(\tilde{\Sigma}_{hh}(m_h^2)), \quad (8.49) \quad \delta m_{H^\pm}^2 = \widetilde{\text{Re}}(\tilde{\Sigma}_{H^\pm H^\pm}(m_{H^\pm}^2)), \quad (8.52)$$

$$\delta m_H^2 = \text{Re}(\tilde{\Sigma}_{HH}(m_H^2)), \quad (8.50) \quad \delta M_W^2 = \widetilde{\text{Re}}\left(\tilde{\Sigma}_{WW}^T(M_W^2)\right), \quad (8.53)$$

$$\delta m_{A_0}^2 = \text{Re}(\tilde{\Sigma}_{A_0 A_0}(m_{A_0}^2)), \quad (8.51) \quad \delta M_Z^2 = \text{Re}\left(\tilde{\Sigma}_{ZZ}^T(M_Z^2)\right), \quad (8.54)$$

$$\delta m_\tau = \frac{m_\tau}{2} \widetilde{\text{Re}} \left( \Sigma_{\tau\tau}^L(m_\tau^2) + \Sigma_{\tau\tau}^R(m_\tau^2) + \tilde{\Sigma}_{\tau\tau}^{S,l}(m_\tau^2) + \tilde{\Sigma}_{\tau\tau}^{S,r}(m_\tau^2) \right), \quad (8.55)$$



we find

$$\begin{aligned}
\frac{\partial g_{abc}}{\partial v_i} \Delta v_i &= \frac{\partial g_{abc}}{\partial v_h} \sum_{i=1,2} \frac{\partial v_h}{\partial v_i} \Delta v_i + \frac{\partial g_{abc}}{\partial v_H} \sum_{i=1,2} \frac{\partial v_H}{\partial v_i} \Delta v_i \\
&= \frac{\partial g_{abc}}{\partial v_h} \left( -s_\alpha \left( \frac{c_\alpha}{m_H^2} T_H^{(1)} - \frac{s_\alpha}{m_h^2} T_h^{(1)} \right) + c_\alpha \left( \frac{s_\alpha}{m_H^2} T_H^{(1)} + \frac{c_\alpha}{m_h^2} T_h^{(1)} \right) \right) \\
&\quad + \frac{\partial g_{abc}}{\partial v_H} \left( c_\alpha \left( \frac{c_\alpha}{m_H^2} T_H^{(1)} - \frac{s_\alpha}{m_h^2} T_h^{(1)} \right) + s_\alpha \left( \frac{s_\alpha}{m_H^2} T_H^{(1)} + \frac{c_\alpha}{m_h^2} T_h^{(1)} \right) \right) \\
&= \frac{\partial g_{abc}}{\partial v_h} \frac{T_h^{(1)}}{m_h^2} + \frac{\partial g_{abc}}{\partial v_H} \frac{T_H^{(1)}}{m_H^2},
\end{aligned} \tag{8.67}$$

where we have used the expressions for the shifts  $\Delta v_i$  from Eqs. 8.11 and 8.12. This is almost the relation we seek to establish. The only missing ingredient is the following connection between the couplings  $g_{abc}$  and  $g_{abcd}$

$$\frac{\partial g_{abc}}{\partial v_d} = g_{abcd}. \tag{8.68}$$

In the case of  $a, b, c$  denoting three scalar mass eigenstates, the desired relation can directly be read off the Higgs potential. The quartic terms can be parametrized as

$$V_H^{\text{quart}} = \sum_{i,j,k,l} c_{ijkl} (h_i + v_i)(h_j + v_j)(h_k + v_k)(h_l + v_l), \tag{8.69}$$

$$h_{i/j/k/l} \in \{h, H, A_0, G_0, H^\pm, G^\pm\},$$

where some of the  $v_i$  might be zero (in the case of  $h_i$  neither denoting  $h$  nor  $H$ ). From this we get

$$i g_{abc} = -i \frac{\partial V_H^{\text{quart}}}{\partial h_a \partial h_b \partial h_c} \Big|_{h_i=0} = -i \sum_l \sigma_{abcl} c_{abcl} v_l, \tag{8.70}$$

$$i g_{abcd} = -i \frac{\partial V_H^{\text{quart}}}{\partial h_a \partial h_b \partial h_c \partial h_d} \Big|_{h_i=0} = -i \sigma_{abcd} c_{abcd}. \tag{8.71}$$

Here we have introduced combinatorial factors  $\sigma$ , which depend on the number of identical particles in the vertex. Eqs. 8.70 and 8.71 reveal the validity of Eq. (8.68).

Apart from in these purely scalar vertices, tadpole diagrams are also induced in vertices with gauge bosons and scalars. It can be shown in an identical manner that Eq. (8.62) holds also in this case.

This demonstrates that the shifts in the vevs induce shifts in the couplings which exactly reproduce the tadpole diagrams. As a consequence, tadpole diagrams have to be taken into account in every vertex where they can be attached according to the Feynman rules.

Although the investigation of the shifts in the couplings is most conveniently performed with couplings expressed in terms of the parameters of set 1, sometimes one might wish to start from the expressions in terms of set 2 parameters. In this case one has to apply the chain rule since the parameters of set 2 depend on the vevs  $v_1$  and  $v_2$ . Let  $\{\lambda_k\}$  and  $\{p_m\}$  generically denote the parameters of set 1 and set 2, respectively, then the application of the chain rule yields

$$\sum_{i=1,2} \frac{\partial g_{abc}(\{v_j, \lambda_k\})}{\partial v_i} \Delta v_i = \sum_{l,i} \frac{\partial g'_{abc}(\{p_m\})}{\partial p_l} \frac{\partial p_l}{\partial v_i} \Delta v_i = \sum_l \frac{\partial g'_{abc}(\{p_m\})}{\partial p_l} \Delta p_l, \tag{8.72}$$

where  $g'_{abc}(\{p_m\}) = g_{abc}(\{v_j(\{p_m\})\}, \{\lambda_k(\{p_m\})\})$  and the shifts  $\Delta p_l$  are exactly those shifts in the 2HDM parameters we present in Sec. 8.2 ( Eqs. 8.17 - 8.19, 8.22 and 8.23) and

App. A.1 (Eqs. A.1, A.2). Together with the relation in Eq. (8.63) this proves the third statement made at the end of Sec. 8.2, i.e. that the shifts in the parameters, induced by the vev shifts, reproduce the tadpole diagrams attached to scalar vertices.

One word of caution is in order, however, since also in the translation rules from set 1 to set 2 (cf. Eqs. 5.33 - 5.37) additional tadpole terms have to be taken into account in order to determine the shifts correctly. In Eqs. 5.33 - 5.37 these tadpole terms have already been set to zero. The full expressions, including all tadpole terms, are given in App. A.1.

## 8.5. Process-Independent Definition of $\alpha$ and $\beta$ in Tadpole Scheme II

As detailed in Sec. 8.1, the altered treatment of the tadpoles allows and even requires us to fix all counterterms of physical parameters in such a way that they become gauge independent. Consequently, we next have to find a definition for the angular counterterms fulfilling this requirement. One possibility is to start from the same definition of  $\delta\alpha$  and  $\delta\beta$  as in the KOSY scheme, now using the modified WFRCs of Eqs. 8.56 - 8.61, and to keep only the truly gauge independent (g.i.) parts of the resulting counterterms. Formally, this amounts to

$$\delta\alpha = \left. \frac{\delta Z_{Hh} - \delta Z_{hH}}{4} \right|_{\text{g.i.}} = \left. \frac{\text{Re} \left[ \tilde{\Sigma}_{Hh}(m_h^2) + \tilde{\Sigma}_{Hh}(m_H^2) \right]}{2(m_H^2 - m_h^2)} \right|_{\text{g.i.}}, \quad (8.73)$$

$$\delta\beta_o = \left. \frac{\delta Z_{G_0 A_0} - \delta Z_{A_0 G_0}}{4} \right|_{\text{g.i.}} = - \left. \frac{\text{Re} \left[ \tilde{\Sigma}_{G_0 A_0}(m_{A_0}^2) + \tilde{\Sigma}_{G_0 A_0}(0) \right]}{2m_{A_0}^2} \right|_{\text{g.i.}}, \quad (8.74)$$

$$\delta\beta_c = \left. \frac{\delta Z_{G^\pm H^\pm} - \delta Z_{H^\pm G^\pm}}{4} \right|_{\text{g.i.}} = - \left. \frac{\text{Re} \left[ \tilde{\Sigma}_{G^\pm H^\pm}(m_{H^\pm}^2) + \tilde{\Sigma}_{G^\pm H^\pm}(0) \right]}{2m_{H^\pm}^2} \right|_{\text{g.i.}}. \quad (8.75)$$

Note that the definition of  $\delta\alpha$  and  $\delta\beta$  in terms of the WFRCs does not automatically yield gauge-independent results for the angular counterterms. Although the gauge-dependent  $A_0$ -functions appearing in Eqs. 7.38 - 7.39 vanish when switching to tadpole scheme II, the gauge-dependent  $B_0$ -functions remain. This can be ascribed to the fact that the renormalization conditions of the KOSY scheme are not physical. However, due to the altered treatment of the tadpoles, we can now extract the gauge-independent parts of counterterms in a well-defined and unique way by applying the pinch technique. With the help of the PT, we can formulate gauge-independent self-energies and then use these in the expressions Eqs. 8.73 - 8.75 to arrive at gauge-independent angular counterterms.

Espinosa and Yamada have calculated the pinched self-energies for the case of two CP-even Higgs bosons and stated explicit expressions for their results in [131]. Albeit their calculation refers to the case of the MSSM, their findings are valid also in the context of the 2HDM. Espinosa and Yamada express their result for the self-energies in terms of tadpole self-energies calculated in Feynman gauge plus additional gauge-independent terms

$$\Sigma_{Hh}^{\text{pinch}}(p^2) = \tilde{\Sigma}_{Hh}(p^2) \Big|_{\xi=1} + \Sigma_{Hh}^{\text{add}}(p^2) \quad (8.76)$$

where  $\xi$  represents all gauge-fixing parameters introduced in Sec. 5.5 and

$$\begin{aligned} \Sigma_{Hh}^{\text{add}}(p^2) = & \frac{g_2^2 s_{\beta-\alpha} c_{\beta-\alpha}}{32\pi^2 c_W^2} \left( p^2 - \frac{m_H^2 + m_h^2}{2} \right) \left[ (B_0(p^2, M_Z^2, m_{A_0}^2) - B_0(p^2, M_Z^2, M_Z^2)) \right. \\ & \left. + 2c_W^2 (B_0(p^2, M_W^2, m_{H^\pm}^2) - B_0(p^2, M_W^2, M_W^2)) \right]. \end{aligned} \quad (8.77)$$

Inserting this into the definition of  $\delta\alpha$ , we arrive at a gauge-independent OS definition for the mixing angle. By OS we mean in this case, that the momenta entering the self-energies correspond to the masses of the mixing particles, i.e. to  $m_h^2$  and  $m_H^2$ , as required by the KOSY procedure. Alternatively, one can define  $\delta\alpha$  in terms of self-energies evaluated at the momentum  $p_*^2 = \frac{m_h^2 + m_H^2}{2}$ . As can directly be read off Eq. (8.77), for this choice of the external momentum the additional terms vanish and the pinched self-energies correspond to the tadpole self-energies evaluated in Feynman gauge.

In order to define  $\delta\beta_o$  or  $\delta\beta_c$  in a similar way, we need the pinched  $A_0$ - $G_0$ - or  $H^\pm$ - $G^\pm$ -self-energy, respectively. To our knowledge, they are not yet available in the literature, wherefore we derived the relevant terms in two independent calculations from scratch. Our final result is given by

$$\Sigma_{G_0 A_0}^{\text{pinch}}(p^2) = \tilde{\Sigma}_{G_0 A_0}(p^2) \Big|_{\xi=1} + \Sigma_{G_0 A_0}^{\text{add}}(p^2), \quad (8.78)$$

$$\Sigma_{G^\pm H^\pm}^{\text{pinch}}(p^2) = \tilde{\Sigma}_{G^\pm H^\pm}(p^2) \Big|_{\xi=1} + \Sigma_{G^\pm H^\pm}^{\text{add}}(p^2), \quad (8.79)$$

with

$$\Sigma_{G_0 A_0}^{\text{add}}(p^2) = \frac{g_2^2 s_{\beta-\alpha} c_{\beta-\alpha}}{32\pi^2 c_W^2} \left( p^2 - \frac{m_{A_0}^2}{2} \right) \left[ (\text{B}_0(p^2, M_Z^2, m_H^2) - \text{B}_0(p^2, M_Z^2, m_h^2)) \right], \quad (8.80)$$

$$\Sigma_{G^\pm H^\pm}^{\text{add}}(p^2) = \frac{g_2^2 s_{\beta-\alpha} c_{\beta-\alpha}}{16\pi^2} \left( p^2 - \frac{m_{H^\pm}^2}{2} \right) \left[ (\text{B}_0(p^2, M_W^2, m_H^2) - \text{B}_0(p^2, M_W^2, m_h^2)) \right]. \quad (8.81)$$

As in the case of the CP-even scalars, the pinched self-energy can be expressed in terms of the tadpole self-energy in the Feynman gauge plus additional terms that vanish if the external momentum is chosen to be  $p_*^2 = \frac{m_{A_0}^2}{2}$  or  $p_*^2 = \frac{m_{H^\pm}^2}{2}$ , respectively.

In the following we will refer to the scheme using the first choice of the momenta as *pinched on-shell* (p-OS) scheme and to the one selecting the second possibility as *pinched  $p_*$*  (p- $p_*$ ) scheme.

To summarize, we state the expressions for  $\delta\alpha$  and  $\delta\beta$  in the different renormalization schemes

$$\delta\alpha^{\text{p-OS}} = \frac{1}{2(m_H^2 - m_h^2)} \text{Re} \left[ \Sigma_{Hh}^{\text{pinch}}(m_h^2) + \Sigma_{Hh}^{\text{pinch}}(m_H^2) \right], \quad (8.82)$$

$$\delta\beta_o^{\text{p-OS}} = -\frac{1}{2m_{A_0}^2} \text{Re} \left[ \Sigma_{G_0 A_0}^{\text{pinch}}(m_{A_0}^2) + \Sigma_{G_0 A_0}^{\text{pinch}}(0) \right], \quad (8.83)$$

$$\delta\beta_c^{\text{p-OS}} = -\frac{1}{2m_{H^\pm}^2} \text{Re} \left[ \Sigma_{G^\pm H^\pm}^{\text{pinch}}(m_{H^\pm}^2) + \Sigma_{G^\pm H^\pm}^{\text{pinch}}(0) \right], \quad (8.84)$$

$$\delta\alpha^{\text{p-}p_*} = \frac{1}{(m_H^2 - m_h^2)} \text{Re} \left[ \tilde{\Sigma}_{Hh} \left( \frac{m_H^2 + m_h^2}{2} \right) \right]_{\xi=1}, \quad (8.85)$$

$$\delta\beta_o^{\text{p-}p_*} = -\frac{1}{m_{A_0}^2} \text{Re} \left[ \tilde{\Sigma}_{G_0 A_0} \left( \frac{m_{A_0}^2}{2} \right) \right]_{\xi=1}, \quad (8.86)$$

$$\delta\beta_c^{\text{p-}p_*} = -\frac{1}{m_{H^\pm}^2} \text{Re} \left[ \tilde{\Sigma}_{G^\pm H^\pm} \left( \frac{m_{H^\pm}^2}{2} \right) \right]_{\xi=1}. \quad (8.87)$$

Both the p-OS and p- $p_*$  scheme lead to process- and gauge-independent definitions of the angular counterterms and therefore fulfill at least two of the desired criteria for a good renormalization scheme stated in Sec. 6.6. The issue of numerical stability, which constitutes the third criterion, will be discussed in Sec. 12.

One further comment is in order concerning the relation to the KOSY scheme. If we wanted

to establish a relation between the WFRCs in the mass basis and the angular counterterms as in Eq. (7.31), we would have to start from a non-symmetric matrix of WFRCs  $Z_\varphi$  in the gauge basis in order to be able to define  $\delta\alpha$  and  $\delta\beta$  according to Eqs. 8.82 - 8.84 or Eqs. 8.82 - 8.84, respectively. Without the additional degree of freedom resulting from allowing  $Z_\varphi$  to be non-symmetric, we would inevitably be led to a definition as in Eq. (7.34) and we would not be able to define the angular counterterms as the gauge-independent part of this equation. However, it is important to emphasize once again that a similar procedure, i.e. the introduction of a non-symmetric WFRC-matrix in the gauge basis, does not cure the gauge dependence of the KOSY scheme. In tadpole scheme I, we do not have the PT at our disposal and therefore cannot extract the gauge-independent parts in a unique, well-defined way. This was already discussed at the end of Subs. 7.4.2.

Moreover, the additional degree of freedom we have implicitly assumed in deriving Eqs. 8.82 - 8.87 leads to an independence of the off-diagonal WFRCs from the angular counterterms. This in turn implies that the *CP-odd*  $\delta\beta_o$  can be used in processes with *charged* external Higgs bosons and vice versa without the need for finite wave function correction factors. A glance at Eq. (7.32) and Eq. (7.33) confirms this statement: Using an independent constant  $\delta C_{S_2 S_1}$  in Eq. (7.33),  $\delta C_{S_1 S_2}$  and  $\delta C_{S_2 S_1}$  can be adjusted in such a way that the on-shell conditions for the scalars in Eqs. 6.42 and 6.43 are fulfilled, independent of the definition of the angular counterterm.



---

## A Process-Dependent Scheme for $\alpha$ and $\beta$

---

In the previous two sections we have explored renormalization schemes for  $\alpha$  and  $\beta$  not relying on any specific physical process. We saw that these schemes are susceptible to resulting in gauge-dependent physical matrix elements. Furthermore, we observed that, if the tadpole scheme II is applied, the PT can be invoked to erase this gauge dependence. However, to our knowledge in tadpole scheme I no comparable technique is available to accomplish this task. Therefore, it might be worthwhile to abandon the criterion of process independence and examine the definition of  $\delta\alpha$  and  $\delta\beta$  by means of a physical observable. This procedure is guaranteed to lead to gauge-independent final results for physical quantities. Yet, the price to be paid for gauge independence in this case is a loss of a universal definition of the mixing angles  $\alpha$  and  $\beta$ . Furthermore, a process-dependent definition leads to an inflation of the expressions for the angular counterterms.

Process-dependent definitions of the angular counterterms are possible in both tadpole schemes. In scheme I the resulting  $\delta\alpha$  contains exactly those gauge-dependent  $A_0$  functions which are required to achieve gauge independence of amplitudes, whereas  $\delta\beta$  is gauge independent. If the tadpoles are treated according to scheme II, both  $\delta\alpha$  and  $\delta\beta$  are gauge independent.

In this chapter we will first present the general renormalization conditions for a process dependent scheme and determine suitable processes to fix the angular counterterms (Sec. 9.1). Afterwards, we will derive explicit expression for  $\delta\beta$  (Sec. 9.2) and  $\delta\alpha$  (Sec. 9.3) and discuss their gauge dependence in both tadpole schemes (Sec. 9.4).

In the last section (Sec. 9.5), we will briefly discuss  $\overline{\text{MS}}$  definitions of the angular counterterms, which can directly be obtained from the process-dependent expressions.

### 9.1. Process Selection

A process-dependent definition of a counterterm relies on the fact that the 2HDM is renormalizable. Hence, the UV divergences contained in a counterterm must be universal, i.e. the counterterm must be capable of cancelling the remaining UV divergences in every vertex where it contributes. This allows us to pick any suitable process to fix a counterterm and use the thus determined renormalization constant in arbitrary other processes. Ideally, a process-dependent renormalization condition should rely on the measurement of a physical quantity  $\mathcal{B}$ , e.g. a decay width, and require the observable  $\mathcal{B}^{\mathcal{O}(n\text{-loop})}$ , calculated to  $n$ th loop-order, to

equal the measured value

$$\mathcal{B}^{\mathcal{O}(n\text{-loop})} = \mathcal{B}^{\text{measured}}. \quad (9.1)$$

However, lacking any measurement of a suitable observable within the 2HDM so far, we can only demand equality to the tree-level result. Therefore, in this section we will use the renormalization condition

$$\Gamma^{\mathcal{O}(1\text{-loop})} = \Gamma^{\text{tree}}, \quad (9.2)$$

where  $\Gamma$  denotes the width of some appropriately chosen decay process. There are some prerequisites suitable processes should fulfill.

First, in order to fix both  $\delta\alpha$  and  $\delta\beta$ , we need two processes that depend on  $\alpha$  and  $\beta$  in such a way that we can solve for both angular counterterms.

Second, the processes should not contain *inseparable IR divergences*, i.e. IR divergences that cannot be treated independently of the renormalization process. The occurrence of IR divergences, caused by internal photon propagators, necessitates the inclusion of real photon emission contributions. If these so-called real corrections and the virtual QED corrections, taken together, do not constitute a UV-finite subset, the bremsstrahlung corrections will enter the definition of the angular counterterms. As a consequence, these will receive a dependence on experimental phase space cuts, which is considered to be unacceptable [138].

Third, the processes should be kinematically not too restricted since this would limit the applicability of the renormalization scheme to a small area of the 2HDM parameter space.

Finally, it is desirable that the processes are phenomenologically relevant such that there is a chance for them to be measured in the future, provided the 2HDM is realized in nature.

Several processes have been applied in the literature to renormalize the scalar mixing angles in the 2HDM or in the MSSM. In Ref. [149], the process  $H^\pm \rightarrow HW^\pm$  is used to renormalize the combination  $\delta(\beta - \alpha)$ . Yet, the authors restrict themselves to the dominant top quark corrections. Taking into account the full electroweak corrections, we encounter the problem of inseparable IR divergences, explained above. The same is true for the process  $H^\pm \rightarrow \tau^\pm\nu$ , considered in [150] to renormalize  $\tan(\beta)$  in the MSSM. For this reason the authors of [138] propose as an alternative the decay  $A_0 \rightarrow \tau^+\tau^-$ . In the latter process the pure QED corrections constitute a UV-finite subset and can therefore be separated from the renormalization procedure.

Since the process  $A_0 \rightarrow \tau^+\tau^-$  is kinematically non-restrictive and may be phenomenologically viable, we will use it in this chapter to renormalize  $\beta$ . In order to fix  $\delta\alpha$  in a similar manner, we need a second process, for which we choose  $H \rightarrow \tau^+\tau^-$ . This process likewise allows for a separation of the pure QED corrections and shares the other advantages of  $A_0 \rightarrow \tau^+\tau^-$ . Other possible choices are discussed in detail in Ref. [148].

## 9.2. Determination of $\delta\beta$ from $A_0 \rightarrow \tau\tau$

Using the process  $A_0 \rightarrow \tau\tau$  to define  $\delta\beta$ , we require the following renormalization condition to be fulfilled

$$\Gamma_{A_0 \rightarrow \tau\tau}^{\mathcal{O}(1\text{-loop}),\text{weak}} = \Gamma_{A_0 \rightarrow \tau\tau}^{\text{tree}}. \quad (9.3)$$

The superscript *weak* indicates that  $\Gamma_{A_0 \rightarrow \tau\tau}^{\mathcal{O}(1\text{-loop}),\text{weak}}$  is supposed to contain only purely weak corrections while all QED corrections are excluded. In Subs. 3.2.2 we have stated a generic formula for the partial decay width of a scalar  $\phi$ . Plugging in the elements specific to the process under consideration, we arrive at

$$\Gamma_{A_0 \rightarrow \tau\tau}^{\mathcal{O}(1\text{-loop}),\text{weak}} = \frac{1}{16\pi m_{A_0}^3} \lambda(m_{A_0}^2, m_\tau^2, m_\tau^2) \sum_{s_1, s_2} \left| \mathcal{A}_{A_0 \rightarrow \tau\tau}^{\text{weak}} \right|_{\mathcal{O}(1\text{-loop})}^2, \quad (9.4)$$

where the sum runs over all possible spin states of the outgoing fermions. Furthermore we have, following the notation introduced in Subs. 3.2.2

$$\left| \mathcal{A}_{A_0 \rightarrow \tau\tau}^{\text{weak}} \right|_{\mathcal{O}(1\text{-loop})}^2 = \left| \mathcal{A}_{A_0 \rightarrow \tau\tau}^{\text{tree}} \right|^2 + 2\text{Re} \left[ \mathcal{A}_{A_0 \rightarrow \tau\tau}^{\text{tree}*} \left( \mathcal{A}_{A_0 \rightarrow \tau\tau}^{\text{virt}(1)} + \mathcal{A}_{A_0 \rightarrow \tau\tau}^{\text{ct}(1)} \right)^{\text{weak}} \right]. \quad (9.5)$$

$\mathcal{A}_{A_0 \rightarrow \tau\tau}^{\text{virt}(1),\text{weak}}$  comprises all purely weak one-loop corrections contributing to the process under consideration, whereas  $\mathcal{A}_{A_0 \rightarrow \tau\tau}^{\text{ct}(1),\text{weak}}$  denotes the corresponding counterterm amplitude. Due to the fact that we have renormalized all external particles on-shell, we do not have to consider diagrams with external leg corrections in  $\mathcal{A}_{A_0 \rightarrow \tau\tau}^{\text{virt}(1),\text{weak}}$  (cf. Subs. 3.2.1 and 3.2.2). In the following we will omit the superscript (1) with the implicit understanding that we always work to strict one-loop order. Both  $\mathcal{A}_{A_0 \rightarrow \tau\tau}^{\text{virt},\text{weak}}$  and  $\mathcal{A}_{A_0 \rightarrow \tau\tau}^{\text{ct},\text{weak}}$  can be written in a factorized form by extracting the tree-level amplitude, i.e

$$\left( \mathcal{A}_{A_0 \rightarrow \tau\tau}^{\text{virt}} + \mathcal{A}_{A_0 \rightarrow \tau\tau}^{\text{ct}} \right)^{\text{weak}} = \mathcal{A}_{A_0 \rightarrow \tau\tau}^{\text{tree}} \left( \mathcal{F}_{A_0 \rightarrow \tau\tau}^{\text{virt}} + \mathcal{F}_{A_0 \rightarrow \tau\tau}^{\text{ct}} \right)^{\text{weak}}, \quad (9.6)$$

where we introduced the scalar form factors  $\mathcal{F}_{A_0 \rightarrow \tau\tau}^{\text{virt},\text{weak}}$  and  $\mathcal{F}_{A_0 \rightarrow \tau\tau}^{\text{ct},\text{weak}}$ . As a consequence of this factorization, we can pull the form factors out of the spin sum, which allows us to write:

$$\Gamma_{A_0 \rightarrow \tau\tau}^{\mathcal{O}(1\text{-loop}),\text{weak}} = \Gamma_{A_0 \rightarrow \tau\tau}^{\text{tree}} \left( 1 + 2\text{Re} \left( \mathcal{F}_{A_0 \rightarrow \tau\tau}^{\text{virt}} + 2\mathcal{F}_{A_0 \rightarrow \tau\tau}^{\text{ct}} \right)^{\text{weak}} \right). \quad (9.7)$$

Obviously, Eq. (9.3) is fulfilled if

$$\mathcal{F}_{A_0 \rightarrow \tau\tau}^{\text{ct},\text{weak}} = -\mathcal{F}_{A_0 \rightarrow \tau\tau}^{\text{virt},\text{weak}} \quad (9.8)$$

holds. Plugging in the explicit expression for  $\mathcal{F}_{A_0 \rightarrow \tau\tau}^{\text{ct},\text{weak}}$ ,

$$\begin{aligned} \mathcal{F}_{A_0 \rightarrow \tau\tau}^{\text{ct},\text{weak}} = & \frac{\delta g_2}{g_2} + \frac{\delta m_\tau^{\text{weak}}}{m_\tau} - \frac{\delta M_W^2}{2M_W^2} + \frac{1 + Y_3^2}{Y_3} \delta\beta \\ & + \frac{\delta Z_{A_0 A_0}}{2} - \frac{1}{Y_3} \frac{\delta Z_{G_0 A_0}}{2} + \frac{\delta Z_\tau^{L,\text{weak}}}{2} + \frac{\delta Z_\tau^{R,\text{weak}}}{2}, \end{aligned} \quad (9.9)$$

which can be read off the Lagrangian, we can solve for  $\delta\beta$

$$\begin{aligned} \delta\beta = & \frac{-Y_3}{1 + Y_3^2} \left( \mathcal{F}_{A_0 \rightarrow \tau\tau}^{\text{virt},\text{weak}} + \frac{\delta g_2}{g_2} + \frac{\delta m_\tau^{\text{weak}}}{m_\tau} - \frac{\delta M_W^2}{2M_W^2} \right. \\ & \left. + \frac{\delta Z_{A_0 A_0}}{2} - \frac{1}{Y_3} \frac{\delta Z_{G_0 A_0}}{2} + \frac{\delta Z_\tau^{L,\text{weak}}}{2} + \frac{\delta Z_\tau^{R,\text{weak}}}{2} \right). \end{aligned} \quad (9.10)$$

Like  $Y_{1,2}$ , introduced above,  $Y_3$  is a modifier of the Yukawa couplings, depending on the type of 2HDM under consideration (cf. Tab. A.1). Moreover, note that apart from the virtual corrections, only  $\delta m_\tau$  and  $\delta Z_\tau^{L,R}$  are affected by the prescription to omit the pure QED corrections, specifically the photon loop contributing to the  $\tau$ - $\tau$ -self-energy. The omitted QED corrections

$$\frac{\delta m_\tau^{\text{QED}}}{m_\tau} + \frac{\delta Z_\tau^{L,\text{QED}}}{2} + \frac{\delta Z_\tau^{R,\text{QED}}}{2} + \mathcal{F}_{A_0 \rightarrow \tau\tau}^{\text{virt},\text{QED}}$$

form a UV-finite subset and incorporate all IR divergences contained in the amplitude.

### 9.3. Determination of $\delta\alpha$ from $H \rightarrow \tau\tau$

We can proceed in the same way in order to extract  $\delta\alpha$  from the prescription

$$\Gamma_{H \rightarrow \tau\tau}^{\mathcal{O}(1\text{-loop}),\text{weak}} = \Gamma_{H \rightarrow \tau\tau}^{\text{tree}}. \quad (9.11)$$

Since the factorization

$$(\mathcal{A}_{H \rightarrow \tau\tau}^{\text{virt}} + \mathcal{A}_{H \rightarrow \tau\tau}^{\text{ct}})^{\text{weak}} = \mathcal{A}_{H \rightarrow \tau\tau}^{\text{tree}} (\mathcal{F}_{H \rightarrow \tau\tau}^{\text{virt}} + \mathcal{F}_{H \rightarrow \tau\tau}^{\text{ct}})^{\text{weak}} \quad (9.12)$$

also holds for the process  $H \rightarrow \tau\tau$ , the condition in Eq. (9.11) is reduced to

$$\mathcal{F}_{H \rightarrow \tau\tau}^{\text{ct,weak}} = -\mathcal{F}_{H \rightarrow \tau\tau}^{\text{virt,weak}}. \quad (9.13)$$

Like above,  $\mathcal{A}_{H \rightarrow \tau\tau}^{\text{virt,weak}}$  is defined to incorporate all contributing weak one-loop corrections and  $\mathcal{A}_{H \rightarrow \tau\tau}^{\text{ct,weak}}$  denotes the corresponding counterterm amplitude. Again, external leg corrections do not have to be considered in the virtual amplitude due to the determination of all WFRCs according to OS conditions. Inserting the exact expression for  $\mathcal{F}_{H \rightarrow \tau\tau}^{\text{ct,weak}}$

$$\begin{aligned} \mathcal{F}_{H \rightarrow \tau\tau}^{\text{ct,weak}} = & \frac{\delta g_2}{g_2} + \frac{\delta m_\tau^{\text{weak}}}{m_\tau} - \frac{\delta M_W^2}{2M_W^2} + \frac{Y_1}{Y_2} \delta\alpha + Y_3 \delta\beta \\ & + \frac{\delta Z_{HH}}{2} + \frac{Y_1}{Y_2} \frac{\delta Z_{hH}}{2} + \frac{\delta Z_\tau^{L,\text{weak}}}{2} + \frac{\delta Z_\tau^{R,\text{weak}}}{2}, \end{aligned} \quad (9.14)$$

we can solve for  $\delta\alpha$

$$\begin{aligned} \delta\alpha = & -\frac{Y_2}{Y_1} \left( \mathcal{F}_{H \rightarrow \tau\tau}^{\text{virt,weak}} + \frac{\delta g_2}{g_2} + \frac{\delta m_\tau^{\text{weak}}}{m_\tau} - \frac{\delta M_W^2}{2M_W^2} + Y_3 \delta\beta \right. \\ & \left. + \frac{\delta Z_{HH}}{2} + \frac{Y_1}{Y_2} \frac{\delta Z_{hH}}{2} + \frac{\delta Z_\tau^{L,\text{weak}}}{2} + \frac{\delta Z_\tau^{R,\text{weak}}}{2} \right). \end{aligned} \quad (9.15)$$

Again,

$$\frac{\delta m_\tau^{\text{QED}}}{m_\tau} + \frac{\delta Z_\tau^{L,\text{QED}}}{2} + \frac{\delta Z_\tau^{R,\text{QED}}}{2} + \mathcal{F}_{H \rightarrow \tau\tau}^{\text{virt,QED}}$$

constitutes a UV-finite subset and comprises the complete IR-divergence of the amplitude.

### 9.4. Discussion of the Gauge Dependence of $\delta\alpha$ and $\delta\beta$

The expressions derived for the angular counterterms in the previous sections are general, i.e. they hold for both tadpole schemes. However, the individual building blocks depend on the specific scheme choice. As discussed in Sec. 8.3, when switching from tadpole scheme I to scheme II, modifications are induced in  $\delta m_\tau$ ,  $\delta M_W^2$  and all the off-diagonal scalar WFRCs. For the processes under consideration, the form factors for the virtual corrections do not receive a modification under the change of tadpole schemes. This is due to the fact that a vertex of two fermions and two scalars is forbidden by dimensional arguments in any renormalizable theory. Hence, we cannot attach tadpole diagrams to the tree-level vertex of the two investigated processes. In general, however, new topologies comprising tadpole diagrams arise in the virtual corrections when changing the tadpole scheme.

We are now interested in the gauge dependence inherent in the angular counterterms in Eqs. 9.10 and 9.15. As we have seen in Sec. 8.1, in tadpole scheme II any gauge dependence

of an amplitude originating from the virtual corrections is cancelled by the WFRCs (or external leg corrections, if the fields are not renormalized on-shell). This requires all counterterms for physical parameters, including the mixing angles, to be gauge independent. By contrast, in tadpole scheme I the sum of virtual corrections and WFRC contributions exhibits a gauge dependence, which has to be cancelled by gauge-dependent parameter counterterms. Furthermore, the investigations in Subs. 7.4.2 have shown that part of this gauge dependence, which comes in terms of  $A_0$ -functions, has to be cancelled by the angular counterterms. Since a process-dependent definition of  $\delta\alpha$  and  $\delta\beta$  is guaranteed to lead to gauge-independent amplitudes, we expect to find in the angular counterterms for both schemes exactly those gauge dependent terms which are required for this purpose. That is, we anticipate gauge-independent angular counterterms for tadpole scheme II, whereas in scheme I we expect  $\delta\beta$  to be gauge independent but  $\delta\alpha$  to contain the gauge-dependent  $A_0$ -functions we encountered in Subs. 7.4.2. Indeed, a calculation in general  $R_\xi$  gauge and a subsequent extraction of all terms containing a gauge fixing parameter  $\xi \in \{\xi_W, \xi_Z, \xi_A\}$  yields

$$\delta\beta_I^{\text{proc}}|_\xi = \delta\beta_{II}^{\text{proc}}|_\xi = 0, \quad (9.16)$$

$$\delta\alpha_{II}^{\text{proc}}|_\xi = 0, \quad (9.17)$$

$$\delta\alpha_I^{\text{proc}}|_\xi = \frac{m_{12}^2 c_{\beta-\alpha} s_{\beta-\alpha}}{8\pi^2 v^2 s_{2\beta} (m_H^2 - m_h^2)} (2A_0(\xi_W M_W^2) + A_0(\xi_Z M_Z^2)), \quad (9.18)$$

which exactly complies with our expectations.

## 9.5. $\overline{\text{MS}}$ Definition of $\delta\alpha$ and $\delta\beta$

Before closing the chapter, we want to throw a brief glance at an  $\overline{\text{MS}}$  definition of the angular counterterms since such a definition emerges naturally as a byproduct of a process-dependent scheme.

Having determined the expressions for process-dependent angular counterterms,  $\overline{\text{MS}}$  definitions for  $\delta\alpha$  and  $\delta\beta$  can readily be obtained by extracting only those terms in  $\delta\alpha^{\text{proc}}$  and  $\delta\beta^{\text{proc}}$  which are proportional to the  $\overline{\text{MS}}$ -divergence  $\Delta_{\overline{\text{MS}}}$ , defined in Eq. (3.4). This is easily accomplished since the process-dependent counterterms can be expressed in terms of Passarino-Veltman functions, whose dependence on  $\Delta_{\overline{\text{MS}}}$  is well-known and can be found e.g. in [151]. Since the UV-divergences contained in the process-dependent angular counterterms are universal, i.e. do not depend on the particular processes used to fix  $\delta\alpha$  and  $\delta\beta$ , the thus defined  $\overline{\text{MS}}$  counterterms are process-independent.

Formally, the  $\overline{\text{MS}}$  counterterms are given by

$$\delta\alpha_{I/II}^{\overline{\text{MS}}} = \delta\alpha_{I/II}^{\text{proc}}|_{\Delta_{\overline{\text{MS}}}}, \quad (9.19)$$

$$\delta\beta_{I/II}^{\overline{\text{MS}}} = \delta\beta_{I/II}^{\text{proc}}|_{\Delta_{\overline{\text{MS}}}}. \quad (9.20)$$

If tadpole scheme II is applied, the resulting  $\overline{\text{MS}}$  counterterms as well as amplitudes incorporating them are gauge independent. In tadpole scheme I, however, the  $\overline{\text{MS}}$  prescription leads to gauge-dependent amplitudes, as can directly be inferred from Eq. (9.18). Extracting only terms proportional to  $\Delta_{\overline{\text{MS}}}$ , finite, gauge-dependent terms in  $\delta\alpha$ , which are necessary to render the amplitude gauge independent, are omitted.

A further disadvantage of  $\overline{\text{MS}}$  renormalized mixing angles is their renormalization scale dependence, inevitably introduced by the  $\overline{\text{MS}}$  prescription, which prohibits their interpretation as physical quantities.

Finally, as a third drawback, the application of an  $\overline{\text{MS}}$  scheme for the angular counterterms can lead to large corrections [148]. Their occurrence can be traced back to the contributions

of tadpole counterterms (scheme I) or diagrams (scheme II) in the OS WFRCs, which are no longer counterbalanced by equivalent terms in  $\delta\alpha$  and  $\delta\beta$ , if the latter are fixed by  $\overline{\text{MS}}$  conditions<sup>1</sup>. We explicitly verified the appearance of these numerical instabilities, mentioned already in [148].

These reasons advise an  $\overline{\text{MS}}$  definition of the angular counterterms and we will hence not include schemes with  $\overline{\text{MS}}$  renormalized mixing angles in our numerical analysis in Ch. 12.

---

<sup>1</sup>Note that an  $\overline{\text{MS}}$  definition of the angular counterterms was found to be well behaved in [41] for the processes considered by the authors. This is probably due to a suppression of the huge tadpole contributions in their first process, while their second process does not receive contributions from scalar WFRCs. A closer investigation of this issue will be subject of future research.

---

## Different Renormalization Schemes for $m_{12}^2$

---

In order to complete the renormalization program of the 2HDM, we still need to find a definition for  $\delta m_{12}^2$ . Like in the case of the angular counterterms, we will explore and discuss various possibilities, always paying attention to differences arising when switching the tadpole scheme. Since  $m_{12}^2$  only appears in cubic and quartic scalar couplings,  $\delta m_{12}^2$  has to be fixed by a renormalization condition involving a multi-Higgs vertex.

One possibility is to determine  $\delta m_{12}^2$  in a process-dependent way. As discussed in the previous chapter, this amounts to choosing  $\delta m_{12}^2$  in such a manner, that the loop-corrected decay width of a suitably chosen process equals the tree-level one. The clear advantages of applying a process-dependent definition are its physical motivation and the guarantee to achieve gauge-independent results for physical observables. However, in the case of  $m_{12}^2$  process-dependent schemes suffer from tight kinematical restrictions, such that they are applicable only in a limited area of the 2HDM parameter space.

Alternatively,  $m_{12}^2$  can be defined by an  $\overline{\text{MS}}$  prescription, demanding  $\delta m_{12}^2$  to cancel only the terms proportional to  $\Delta_{\overline{\text{MS}}}$  remaining in the amplitude of an arbitrary multi-Higgs process, after all other counterterms have been added. Since these terms are universal, the resulting  $\delta m_{12}^2$  is independent of the particular process chosen and furthermore the renormalization prescription is not subject to kinematic restrictions. Moreover, unlike in the case of the mixing angles, gauge dependence does not pose a problem for the renormalization of  $m_{12}^2$ .

Both options will be discussed below. We begin with a discussion of the  $\overline{\text{MS}}$  scheme in Sec. 10.1 and afterwards address the possibility of a process-dependent definition in Sec. 10.2.

### 10.1. $\overline{\text{MS}}$ Definition of $\delta m_{12}^2$

In order to fix  $\delta m_{12}^2$  according to  $\overline{\text{MS}}$  conditions, we can choose an arbitrary cubic (or quartic) Higgs vertex depending on  $m_{12}^2$  and impose the following requirement

$$\left[ \mathcal{A}_{S_1 S_2 S_3}^{\text{virt}(1)} + \mathcal{A}_{S_1 S_2 S_3}^{\text{ct}(1)} \right]_{\Delta_{\overline{\text{MS}}}} = 0, \quad S_i \in \{H, h, A_0, H^\pm\}. \quad (10.1)$$

$\mathcal{A}_{S_1 S_2 S_3}^{\text{virt}(1)}$  denotes the sum of all virtual one-loop corrections to the vertex under consideration, whereas  $\mathcal{A}_{S_1 S_2 S_3}^{\text{ct}(1)}$  stands for the corresponding counterterm amplitude. Furthermore, the subscript  $\Delta_{\overline{\text{MS}}}$  indicates that only the UV-divergent part of Eq. (10.1) is to be considered

when evaluating the renormalization condition. As in the previous chapter, we will omit the superscript (1) henceforth, leaving the loop order implicit. Since  $\mathcal{A}_{S_1 S_2 S_3}^{\text{ct}}$  contains a term proportional to  $\delta m_{12}^2$ , we can use Eq. (10.1) to fix the last renormalization constant yet undetermined. One major advantage of the  $\overline{\text{MS}}$  scheme is that it allows for a definition of the counterterm at the level of the amplitude, evaluated for an arbitrary momentum configuration. This is due to the fact that  $\overline{\text{MS}}$  definitions only take into account the divergence of an amplitude, which is independent of the kinematics. The resultant benefit is two-fold: On the one hand, the expressions for the counterterms are greatly simplified, on the other hand the scheme is not subject to any kinematic restrictions.

In principle, we are free to choose any convenient trilinear or quadrilinear scalar vertex in condition Eq. (10.1). Since later in this thesis, we will examine the decay  $H \rightarrow hh$ , it is however recommended not to use the corresponding vertex to renormalize  $m_{12}^2$ . Picking any other vertex will provide us with a consistency check for our renormalization scheme.

Choosing e.g. the triple- $h$ -vertex, the counterterm amplitude reads

$$\begin{aligned} \mathcal{A}_{hhh}^{\text{ct}} = & \frac{3\delta Z_{hh}}{2} g_{hhh} + \frac{3\delta Z_{Hh}}{2} g_{Hhh} + M_W C_{M_W}^{hhh} \left( \frac{\delta M_W^2}{2M_W^2} - \frac{\delta g_2}{g_2} \right) \\ & + C_{m_h^2}^{hhh} \delta m_h^2 + C_{m_H^2}^{hhh} \delta m_H^2 + C_{\alpha}^{hhh} \delta \alpha + C_{\beta}^{hhh} \delta \beta + C_{m_{12}^2}^{hhh} \delta m_{12}^2, \end{aligned} \quad (10.2)$$

which together with Eq. (10.1) leads to

$$\begin{aligned} \delta m_{12}^{2, \overline{\text{MS}}} = & \frac{-1}{C_{m_{12}^2}^{hhh}} \left[ \frac{3\delta Z_{hh}}{2} g_{hhh} + \frac{3\delta Z_{Hh}}{2} g_{Hhh} + M_W C_{M_W}^{hhh} \left( \frac{\delta M_W^2}{2M_W^2} - \frac{\delta g_2}{g_2} \right) \right. \\ & \left. + C_{m_h^2}^{hhh} \delta m_h^2 + C_{m_H^2}^{hhh} \delta m_H^2 + C_{\alpha}^{hhh} \delta \alpha + C_{\beta}^{hhh} \delta \beta + \mathcal{A}_{hhh}^{\text{virt}} \right]_{\Delta_{\overline{\text{MS}}}}. \end{aligned} \quad (10.3)$$

The constants  $C_{p_i}^{hhh}$  appearing here can be determined by taking the derivative

$$C_{p_i}^{hhh} = \frac{\partial g_{hhh}}{\partial p_i}. \quad (10.4)$$

Due to their length, we do not explicitly state them here. Moreover, the scalar couplings  $g_{S_i S_j S_k}$ ,  $i, j, k \in h, H$ , can be found in App. A.2.

Both the divergences contained in the virtual corrections  $\mathcal{A}_{hhh}^{\text{virt}}$  and those included in the renormalization constants ( $\delta Z_{Hh}$ ,  $\delta \alpha$  and the mass counterterms) depend on the choice of the tadpole scheme. However, the final result for  $\delta m_{12}^2$  is invariant under a change of the tadpole scheme, since all tadpole-scheme-dependent terms cancel within Eq. (10.3). This is to be expected, bearing in mind that  $m_{12}^2$  is a parameter of the original scalar potential  $V$  in Eq. (5.4) and is as such independent of the vevs (and thus of the tadpoles).

Hence, we conclude that the application of  $\overline{\text{MS}}$  conditions to the parameter  $m_{12}^2$  results in gauge-independent  $\mathcal{S}$ -matrix elements and in a gauge-independent counterterm  $\delta m_{12}^2$  irrespective of the chosen tadpole scheme.

## 10.2. Process-Dependent Definition of $\delta m_{12}^2$

For completeness we shortly also illustrate the second possibility, which consists in a process-dependent renormalization of  $m_{12}^2$ , although its applicability is very limited due to kinematic restrictions. Possible processes to fix  $\delta m_{12}^2$  are decays of a heavy Higgs boson into two lighter ones, i.e.

$$H \rightarrow hh, \quad (10.5)$$

$$H \rightarrow H^+ H^-, \quad (10.6)$$

$$H \rightarrow A_0 A_0, \quad (10.7)$$

$$h \rightarrow A_0 A_0. \quad (10.8)$$

Whether these decays are allowed depends on the mass ratios, which in turn is determined by the chosen parameter point. Since no measurements are available for any of these processes, we will again impose the condition already encountered in the process-dependent scheme for the angular counterterms

$$\Gamma_{S_1 \rightarrow S_2 S_3}^{\mathcal{O}(1\text{-loop})} = \Gamma_{S_1 \rightarrow S_2 S_3}^{\text{tree}}. \quad (10.9)$$

The first decay, Eq. (10.5), represents one of the processes we will study in detail in section 12. Therefore, we refrain from using this process to fix  $\delta m_{12}^2$ . Out of the remaining decays, the one in Eq. (10.7) is least restricted by experimental data and we will hence choose it for a process-dependent definition of  $m_{12}^2$ .

We proceed exactly as in Secs. 9.2 and 9.3, with the exception that this time we do not have to separate IR divergent QED corrections, as no virtual photons appear in a process involving only neutral scalars at one-loop order. With the help of Eqs. 3.22 and 3.25 and due to the fact that the polarization sum is trivial for a purely scalar process, the condition in Eq. (10.9) can be translated to

$$|\mathcal{A}_{H \rightarrow A_0 A_0}|_{\mathcal{O}(1\text{-loop})}^2 = |\mathcal{A}_{H \rightarrow A_0 A_0}^{\text{tree}}|^2 + 2\text{Re} [\mathcal{A}_{H \rightarrow A_0 A_0}^{\text{tree}*} (\mathcal{A}_{H \rightarrow A_0 A_0}^{\text{virt}} + \mathcal{A}_{H \rightarrow A_0 A_0}^{\text{ct}})], \quad (10.10)$$

and further to

$$\mathcal{A}_{H \rightarrow A_0 A_0}^{\text{ct}} = -\mathcal{A}_{H \rightarrow A_0 A_0}^{\text{virt}}. \quad (10.11)$$

$\mathcal{A}_{H \rightarrow A_0 A_0}^{\text{virt}}$  comprises all virtual one-loop corrections contributing to the decay  $H \rightarrow A_0 A_0$  and the corresponding counterterm amplitude  $\mathcal{A}_{H \rightarrow A_0 A_0}^{\text{ct}}$  is given by

$$\begin{aligned} \mathcal{A}_{H \rightarrow A_0 A_0}^{\text{ct}} = & g_{hA_0 A_0} \frac{\delta Z_{hH}}{2} + g_{HA_0 A_0} \left( \delta Z_{A_0 A_0} + \frac{\delta Z_{HH}}{2} \right) + g_{HG_0 A_0} \delta Z_{G_0 A_0} \\ & + M_W C_{M_W}^{HA_0 A_0} \left( \frac{\delta M_W^2}{2M_W^2} - \frac{\delta g_2}{g_2} \right) + C_{m_H^2}^{HA_0 A_0} \delta m_H^2 \\ & + C_{m_{A_0}^2}^{HA_0 A_0} \delta m_{A_0}^2 + C_{\alpha}^{HA_0 A_0} \delta \alpha + C_{\beta}^{HA_0 A_0} \delta \beta + C_{m_{12}^2}^{HA_0 A_0} \delta m_{12}^2, \end{aligned} \quad (10.12)$$

with the coefficients

$$C_{p_i}^{HA_0 A_0} = \frac{\partial g_{HA_0 A_0}}{\partial p_i}. \quad (10.13)$$

All scalar couplings appearing here can be found in App. A.2. Having fixed all the other counterterms, we can solve Eq. (10.11) for  $\delta m_{12}^2$

$$\begin{aligned} \delta m_{12}^{2,\text{proc}} = & \frac{-1}{C_{m_{12}^2}^{HA_0 A_0}} \left( g_{hA_0 A_0} \frac{\delta Z_{hH}}{2} + g_{HA_0 A_0} \left( \delta Z_{A_0 A_0} + \frac{\delta Z_{HH}}{2} \right) + g_{HG_0 A_0} \delta Z_{G_0 A_0} \right. \\ & + M_W C_{M_W}^{HA_0 A_0} \left( \frac{\delta M_W^2}{2M_W^2} - \frac{\delta g_2}{g_2} \right) + C_{m_H^2}^{HA_0 A_0} \delta m_H^2 \\ & \left. + C_{m_{A_0}^2}^{HA_0 A_0} \delta m_{A_0}^2 + C_{\alpha}^{HA_0 A_0} \delta \alpha + C_{\beta}^{HA_0 A_0} \delta \beta + \mathcal{A}_{H \rightarrow A_0 A_0}^{\text{virt}} \right). \end{aligned} \quad (10.14)$$

Like in the  $\overline{\text{MS}}$  scheme,  $\delta m_{12}^{2,\text{proc}}$  is independent of the tadpole scheme choice. This time, though,  $\delta m_{12}^{2,\text{proc}}$  depends on the renormalization scheme selected for the angular counterterms.<sup>1</sup> However, as long as  $\delta \alpha$  and  $\delta \beta$  are determined in the framework of a gauge-independent scheme,  $\delta m_{12}^{2,\text{proc}}$  as well as all amplitudes are gauge independent.

Nevertheless, the adherence to a process-dependent definition is unsatisfactory. Such a definition not only entails a loss of generality but it also limits the applicability of the renormalization scheme to the restricted area of the 2HDM parameter space, where  $m_H \geq 2m_{A_0}$  holds. We will still have a brief glance at the numerical stability of this scheme in Sec. 12.

<sup>1</sup>It also depends on the renormalization of  $e$ , the masses and the fields. However, these are always defined by OS conditions in this thesis.



---

## Overview of the Discussed Renormalization Schemes

---

Before we enter the investigation and discussion of the numerical stability of the possible renormalization schemes, we briefly want to summarize the different options for the angular counterterms and  $\delta m_{12}^2$  in the two tadpole schemes, proposed in the previous chapters.

The angular counterterms have been studied in chapters 7.4, 8.5, and 9, where we found that the choice of a good renormalization scheme is strongly influenced by the selection of the tadpole scheme.

Working in tadpole scheme I, gauge-independent physical observables can only be obtained if  $\delta\beta$  is chosen to be gauge independent whereas  $\delta\alpha$  has to be gauge dependent. To be more precise, the counterterm for  $\alpha$  has to include the gauge-dependent  $A_0$ -functions we derived in Subs. 7.4.2 since otherwise, identical terms with opposite sign appearing in the remaining amplitude are left uncancelled. This renders a process-independent definition of the the angular counterterms difficult in scheme I. We have exemplified this point in Sec. 7.4 by means of the KOSY scheme, proposed in Ref. [40], and we have shown that this process-independent scheme leads to gauge-dependent physical quantities. Furthermore, we argued that it is not possible to eliminate this gauge dependence in a well-defined, unique way, which can be traced back to the arbitrariness of defining the gauge-independent parts of Passarino-Veltman functions. As a consequence, the KOSY scheme is unfavorable. We will still include it in the set of schemes, which we subject to a detailed numerical study in Ch. 12, since the KOSY scheme has proven to show a good numerical behaviour for various processes and therefore serves as a reference point for a numerical comparison.

In Sec. 9.5 we stated that also an  $\overline{\text{MS}}$  definition of the angular counterterms yields gauge-dependent amplitudes in tadpole scheme I. This is due to the fact that the finite gauge-dependent parts of the  $A_0$  functions, necessary in the definition of  $\delta\alpha$ , are not captured in this scheme. Furthermore, we already mentioned the fact that  $\overline{\text{MS}}$  schemes for the angular counterterms can lead to numerically huge corrections, if OS conditions are kept for masses and fields.

Hence, in tadpole scheme I only the process-dependent scheme, detailed in Ch. 9, seems to remain as a viable renormalization scheme.

The situation changes when we switch to tadpoles scheme II. In this scheme both angular counterterms have to be chosen gauge independent in order to attain gauge-independent physical observables. Together with the fact that we have the PT at our disposal in tadpole

scheme II, this allows for a straightforward definition of process- and gauge-independent angular counterterms leading to gauge-independent amplitudes. This was elaborated in Sec. 8.5, where we introduced two process- and gauge-independent definitions of  $\delta\alpha$  and  $\delta\beta$  and denoted the resulting schemes as p-OS and p- $p_*$  scheme. Both come in two versions, depending on whether  $\delta\beta$  is defined by means of the charged or the CP-odd scalar self-energy.

Alternatively, also in tadpole scheme II, we can define process-dependent angular counterterms as proposed in Ch. 9.

Finally, due to their gauge independence,  $\delta\alpha$  and  $\delta\beta$  can be determined by  $\overline{\text{MS}}$  conditions. However, like in tadpole scheme I, the  $\overline{\text{MS}}$  scheme can lead to numerically unstable results caused by uncancelled tadpole terms.

As far as the parameter  $m_{12}^2$  is concerned, we encountered entirely different circumstances. Since  $m_{12}^2$  is a parameter of the original scalar potential and as such independent of the vevs,  $\delta m_{12}^2$  is invariant under a change of the tadpole scheme. In both tadpole schemes,  $\delta m_{12}^2$  can be determined by  $\overline{\text{MS}}$  conditions, resulting in a gauge-independent renormalization scheme and a gauge-independent counterterm  $\delta m_{12}^2$ .

Alternatively, in both tadpole schemes a process-dependent definition of  $\delta m_{12}^2$  is possible in principle. However, the resulting renormalization schemes are subject to severe kinematic constraints, which limits their applicability to only a small part of the 2HDM parameter space.

---

Investigation of Numerical Stability

---

We have now several viable options at our disposal to renormalize the parameters of the 2HDM. As a next step, we want to test their performance as far as numerical stability is concerned. To that end we investigate the three different decay processes

$$H^\pm \rightarrow W^\pm h$$

$$H \rightarrow ZZ$$

$$H \rightarrow hh.$$

These processes cover three distinct classes of tree-level vertices, i.e. scalar-vector-vector, scalar-scalar-vector and scalar-scalar-scalar vertices, and therefore represent a good set of test cases to study our renormalization schemes. The decays  $H^\pm \rightarrow W^\pm h$  and  $H \rightarrow ZZ$  are suitable to examine different renormalization schemes for the angles  $\alpha$  and  $\beta$ . In the vertex  $H^\pm$ - $W^\pm$ - $h$ , both angles appear as actual mixing angles, entering the vertex Feynman rules by means of the rotation matrices. On the contrary in the vertex  $H$ - $Z$ - $Z$ ,  $\beta$  occurs in its role as ratio of the vevs  $v_1$  and  $v_2$ . The last vertex,  $H$ - $h$ - $h$ , contains  $\alpha$  both in its role as mixing angle and as parameter of the potential and furthermore depends on  $m_{12}^2$ . Hence, the corresponding decay is appropriate to deepen the study of schemes for the angular counterterms and to investigate different schemes for  $\delta m_{12}^2$ .

Numerical stability is the last of the three criteria (gauge independence, process independence, numerical stability) a good renormalization scheme should fulfill. Thus, this study will allow us to answer the question whether there is a renormalization scheme for the 2HDM that satisfies all three criteria.

To set the scene, we will first briefly introduce the employed software and utilized tools in Sec. 12.1 and specify all sets of input parameters, adopted in our study, in Sec. 12.2.

Afterwards we will successively examine the three test processes and study the various renormalization schemes on their basis. Sec. 12.3 deals with the decay  $H^\pm \rightarrow W^\pm h$ , while Sec. 12.4 is dedicated to the process  $H \rightarrow ZZ$ . The last section (12.5), finally will be concerned with the purely scalar process  $H \rightarrow hh$  and analyze different renormalization schemes for  $m_{12}^2$ .

The results shown in this chapter have been published in Refs. [42] and [43].

### 12.1. Tools and Software

In order to perform the numerical analysis, we developed a Fortran program, which calculates the decay widths of the three example processes studied in this thesis. The program is based

on the code `CalcGamma` developed for and introduced in Ref. [148], which computes the widths for the two processes  $H^\pm \rightarrow W^\pm h$  in the KOSY scheme (and other schemes, which are not relevant in the following). Our code extends `CalcGamma` by the additional processes  $H \rightarrow ZZ$  and  $H \rightarrow hh$  as well as by further renormalization schemes for the angular counterterms (p-OS, p- $p_*$ , the  $\overline{\text{MS}}$  and process-dependent scheme) and by all renormalization schemes for  $\delta m_{12}^2$  we discussed in the previous chapters.

All amplitudes, self-energies and tadpole contributions implemented in our program were calculated with the `Mathematica` packages `FeynArts 3.7` [152] and `FormCalc 8.1` [153]. `FeynArts 3.7` was employed to generate the Feynman diagrams and corresponding amplitudes, making use of a model file for the 2HDM which is provided by the package. Subsequently, `FormCalc 8.1` was utilized to evaluate fermion traces, contract Lorentz and spinor indices and perform the tensor reduction. The result, given in terms of Passarino-Veltman functions, was then exported as Fortran code and implemented into our program.

For the computation of the decay widths, our program assembles all contributing pieces for the desired tadpole and renormalization scheme. The evaluation of the Passarino-Veltman functions is performed by linking the Fortran library `LoopTools 2.9` [154].

## 12.2. Input Parameter Sets

As last ingredient for the numerical analysis, we still need to specify the values of all input parameters entering our calculation. These will be quoted in the following.

The SM parameters comprise the masses of all SM particles, the electric charge  $e$ , or correspondingly  $\alpha_{\text{em}}$ , and the CKM matrix elements. According to our renormalization condition for the electric charge (cf. Eq. (7.21)), we have to use  $\alpha_{\text{em}}$  at the electroweak scale as input, which is given by [54]

$$\alpha_{\text{em}}(M_Z^2) = \frac{1}{128.962}. \quad (12.1)$$

Since we do not take into account CP-violation, we consider the CKM matrix to be real, using the values recommended in Ref. [54] for its elements

$$V_{\text{CKM}} = \begin{pmatrix} V_{ud} & V_{us} & V_{ub} \\ V_{cd} & V_{cs} & V_{cb} \\ V_{td} & V_{ts} & V_{tb} \end{pmatrix} = \begin{pmatrix} 0.97427 & 0.22536 & 0.00355 \\ -0.22522 & 0.97343 & 0.0414 \\ 0.00886 & -0.0405 & 0.99914 \end{pmatrix}. \quad (12.2)$$

The masses of the SM particles are set to the values recommended by the Particle Data Group [54] and the Higgs cross Section Working Group (HXS WG) [155, 156]. In the case of the Higgs mass, we use the value quoted by the ATLAS and CMS groups [51]. All SM mass values entering our calculation are summarized in Tab. 12.1. Note that the influence of the light quark masses on our results is negligible. They are chosen in accordance with the HXS WG.

Furthermore, we fix the detector sensitivity  $\Delta E$ , which is needed in the real corrections to the decays  $H^\pm \rightarrow W^\pm h$  and whose impact on our analysis was also shown to be insignificant [148], at a value of

$$\Delta E = 10 \text{ GeV}. \quad (12.3)$$

Apart from the SM parameters, we also have to specify the 2HDM specific parameters, which we have chosen in Eq. (5.32) as independent input parameters. As a reminder, these are given by the masses of the (non-SM) Higgs bosons, the mixing angles and  $m_{12}^2$

$$m_H, m_{A_0}, m_{H^\pm}, \alpha, \beta, m_{12}^2. \quad (12.4)$$

parameter	value	
$M_W$	80.385 GeV	[54, 156]
$M_Z$	91.1876 GeV	[54, 156]
$m_e$	510.998928 keV	[54, 156]
$m_\mu$	105.6583715 MeV	[54, 156]
$m_\tau$	1.77682 GeV	[54, 156]
$m_u$	100 MeV	[157]
$m_d$	100 MeV	[157]
$m_s$	100 MeV	[157]
$m_t$	172.5 GeV	[155, 156]
$m_c$	1.51 GeV	[156]
$m_b$	4.92 GeV	[156]
$m_h$	125.09 GeV	[51]

**Table 12.1.:** Input values for the SM parameters used in our numerical analysis.

In our analysis, the SM-like Higgs boson will always be the lighter CP-even Higgs boson  $h$ . However, in principle also the heavier one could play the role of the 125-GeV SM-like Higgs boson. In this case, the parameter list in Eq. (12.4) would include  $m_h$  instead of  $m_H$ .

The parameters of the 2HDM cannot be chosen freely, but have to fulfill certain theoretical and experimental constraints. In order to generate sets of input parameters complying with these, we employed the program **ScannerS** [158, 159]. This tool performs a scan over the 2HDM parameter space and checks for each point whether it is consistent with all requirements. From the theoretical side, **ScannerS** guarantees that for each allowed parameter point the chosen CP-conserving minimum is the global one [160], the scalar potential is bounded from below [18] and tree-level unitarity is not violated [161, 162].

Furthermore the program ensures consistency with the electroweak precision observables [163–169] and takes into account constraints originating from  $B$  physics observables [170–172] as well as from the measurement of  $R_b \equiv \Gamma(Z \rightarrow b\bar{b})/\Gamma(Z \rightarrow \text{hadrons})$  [173–176]. The latter primarily affect the mass of the charged Higgs boson, which was chosen according to the current limit  $m_{H^\pm} \geq 480$  GeV for a type II 2HDM in our scans [177].

All LEP bounds [178] and the LHC bounds in Refs. [179, 180]<sup>1</sup> are considered. In order to test consistency with Higgs data, **ScannerS** is interfaced with **SusHi** [182], which calculates Higgs production cross sections in gluon and b-quark fusion at NNLO QCD and with **HDECAY** [183, 184], which computes the 2HDM Higgs decays. The remaining Higgs production cross sections are taken at NLO as given in Ref. [185]. Electroweak corrections are consistently omitted in all production cross sections and decay widths, since they are not available for the 2HDM. Afterwards, the program packages **HiggsBounds** [186–188] and **HiggsSignals** [189] are linked to check agreement with experimental 95% C.L. Higgs exclusion limits and the observed Higgs signals. Further details can be found in Ref. [159].

With the help of **ScannerS** three sets of 2HDM parameter points were generated<sup>2</sup>, compliant with all constraints mentioned above, each of which corresponds to a specific 2HDM scenario. In addition, the kinematic constraints summarized in Tab. 12.2 were imposed on the individual scans and the conventions  $0 \leq \beta \leq \frac{\pi}{2}$  and  $-\frac{\pi}{2} \leq \alpha \leq \frac{\pi}{2}$  were used throughout. The kinematic restrictions in Scan I are chosen to allow for the decays  $H^\pm \rightarrow W^\pm h$ ,  $H \rightarrow ZZ$  and  $H \rightarrow hh$ . Scan II was devised for an investigation of the decoupling regime (cf. Sec. 12.5), whereas

<sup>1</sup>Later results as published e.g. in [181] have not yet been included.

<sup>2</sup>We gratefully thank Marco Sampaio for providing us with these parameters sets.

Scan I	$m_{H^\pm} > M_W + m_h$ $m_H > 2m_h$
Scan II	$m_H > 2m_h$ $m_H^2 \approx m_{A_0}^2 \approx m_{H^\pm}^2 \approx \frac{m_{12}^2}{s_\beta c_\beta}$
Scan III	$m_H > 2m_h$ $m_H > 2m_{A_0}$

**Table 12.2.:** Additional kinematic constraints for the parameter scans, providing the input parameters for the numerical analysis.

Scan III enables us to study the process-dependent renormalization scheme for  $m_{12}^2$ . For selected scenarios of these scans, further points were produced by keeping all parameters fixed apart from one of the non-SM Higgs boson masses, which was varied in both directions as far as possible without violating any of the conditions implemented in `ScannerS` or of the additionally imposed constraints.

In Tab. 12.3, we summarize the 2HDM specific input values for the scenarios, which will be studied in the subsequent numerical analysis.

	$m_H$ [GeV]	$m_{A_0}$ [GeV]	$m_{H^\pm}$ [GeV]	$m_{12}^2$ [GeV <sup>2</sup> ]	$t_\beta$	$\alpha$	Scan
Scenario 1a	742.84	700.13	[654. . . 804]	$2.076 \cdot 10^5$	1.46	-0.57	I
Scenario 1b	742.84	[700. . . 867]	700.35	$2.076 \cdot 10^5$	1.46	-0.57	I
Scenario 2	[690. . . 809]	705.44	659.16	$2.045 \cdot 10^5$	1.24	-0.61	I
Scenario 3	[600. . . 762]	731.16	711.55	$1.010 \cdot 10^5$	1.10	-0.73	I

**Table 12.3.:** 2HDM specific input parameters for specific scenarios studied in the following sections. All parameter points fulfill the constraints imposed by `ScannerS` as described in the text. Furthermore, additional kinematic constraints are imposed according to those of Scan I.

### 12.3. Numerical Analysis of the Decay $H^\pm \rightarrow W^\pm h$

We start our numerical analysis with the investigation of various renormalization schemes in the decay  $H^\pm \rightarrow W^\pm h$ . The decay width  $\Gamma_{H^\pm \rightarrow W^\pm h}^{O(1\text{-loop})}$  comprises terms proportional to  $\delta\alpha$  and  $\delta\beta$ , however does not depend on  $\delta m_{12}^2$ . We can hence use this process to examine different schemes for the angular counterterms. To be specific, we explore the KOSY scheme, the pinched schemes (p-OS and p- $p_*$ ) as well as the process-dependent scheme presented in Ch. 9. For the pinched schemes we consider both versions of  $\delta\beta$ ,  $\delta\beta_o$  and  $\delta\beta_c$ , which is possible without violating the on-shell conditions for the scalars (cf. Sec. 8.5). In contrast, for the KOSY scheme, we have to restrict ourselves to the charged version if we do not want to include finite wave function correction factors. We use the following abbreviations for the respective schemes

$$\begin{aligned}
\text{KOSY}^{c,o} & : \text{ gauge-dependent KOSY scheme presented in section 7.4, using } \delta\beta_{c,o} \\
\text{p-OS}^{c,o} & : \text{ pinched OS-scheme scheme presented in section 8.5, using } \delta\beta_{c,o} \\
\text{p-}p_*^{c,o} & : \text{ pinched } p_*\text{-scheme scheme presented in section 8.5, using } \delta\beta_{c,o} \\
\text{proc} & : \text{ process-dependent scheme presented in Sec. 9.}
\end{aligned} \tag{12.5}$$

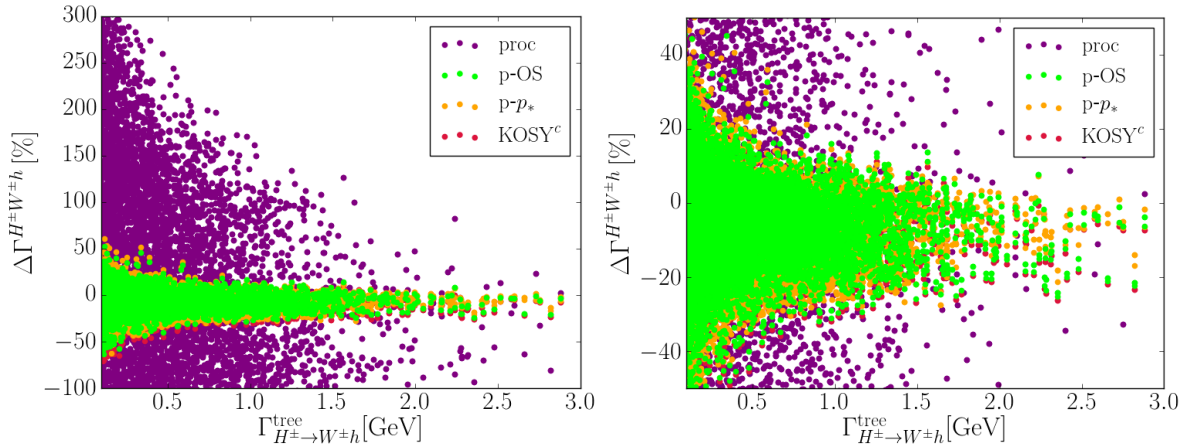


**Figure 12.1.:** Scatter plots for the process  $H^\pm \rightarrow W^\pm h$ , showing the relative one-loop corrections  $\Delta\Gamma^{H^\pm W^\pm h}$  as a function of the tree-level decay width for the parameter points of Scan I. We have cut the plots at  $\Gamma_{H^\pm \rightarrow W^\pm h}^{\text{tree}} = 0.1$  GeV and constrained the range for  $\Delta\Gamma^{H^\pm W^\pm h}$  to  $-100\% - +300\%$  (see the discussion in the text). In the right plot we have zoomed into the central region. Similar plots have been shown in our publication [42].

Let us recall the fact that out of these, the KOSY scheme is based on tadpole scheme I, whereas the pinched schemes require tadpole scheme II. The process-dependent scheme can be applied within both frameworks and leads to a final result for the decay width which is independent of the way the tadpoles are treated.

In order to estimate the numerical stability of the individual schemes, we define the quantity

$$\Delta\Gamma^{H^\pm W^\pm h} = \frac{\Gamma_{H^\pm \rightarrow W^\pm h}^{\mathcal{O}(1\text{-loop})} - \Gamma_{H^\pm \rightarrow W^\pm h}^{\text{tree}}}{\Gamma_{H^\pm \rightarrow W^\pm h}^{\text{tree}}}, \quad (12.6)$$

which constitutes a measure for the size of the  $\mathcal{O}(1\text{-loop})$ -corrections relative to the tree-level result. To gain an overview of the typical behaviour of the renormalization schemes, we first consider the scatter plot in Fig. 12.1, including the parameter points of Scan I. It shows the relative one-loop corrections, quantified by  $\Delta\Gamma^{H^\pm W^\pm h}$ , as a function of the tree-level decay width  $\Gamma_{H^\pm \rightarrow W^\pm h}^{\text{tree}}$  for the four schemes listed in Eq. (12.5). Here no distinction is made between the different versions of  $\delta\beta$  in the pinched schemes.

As the plot on the left-hand side demonstrates, the process-dependent scheme leads to pathologically huge relative one-loop corrections, which can be up to two orders of magnitude larger than the corresponding corrections in the other schemes in many scenarios. This behaviour is caused by the electroweak radiative corrections to the decays  $A_0 \rightarrow \tau\tau$  and  $H \rightarrow \tau\tau$ , included in the angular counterterms of the process-dependent scheme.

A closer look at the one-loop amplitude  $\mathcal{A}_{H^\pm \rightarrow W^\pm h}^{\mathcal{O}(1\text{-loop})}$  of the decay  $H^\pm \rightarrow W^\pm h$  (cf. App. B.1) reveals an overall proportionality of the radiative corrections to  $c_{\beta-\alpha}$ , which is driven to small values by LHC Higgs data. However, the angular counterterms (and the off-diagonal WFRCS) enter with a prefactor  $s_{\beta-\alpha}$ , which for the same reason attains values close to one. Therefore, the contributions of the angular counterterms are enhanced by a factor  $s_{\beta-\alpha}/c_{\beta-\alpha}$  relative to the other terms in  $\mathcal{A}_{H^\pm \rightarrow W^\pm h}^{\mathcal{O}(1\text{-loop})}$ . While in the pinched and in the KOSY schemes the finite parts of the angular counterterms partly cancel those in the off-diagonal WFRCS, the process-dependent scheme introduces additional finite terms. Due to the enhancement factor, the impact of these additional terms on the final result is huge, wherefore the process-dependent scheme is not suitable for the renormalization of the decay  $H^\pm \rightarrow W^\pm h$ .

In contrast to those of the process-dependent scheme, the relative corrections in the other schemes typically range between  $-40\%$  and  $+40\%$  and are of comparable size in all three schemes. This can be seen in the plot on the right in Fig. 12.1, which zooms into the central

region of the left plot. It should be noted that all points at the far left of each plot correspond to scenarios with values of  $c_{\beta-\alpha}$  close to zero, for which the tree-level coupling  $g_{H^\pm W^\pm h}$  and hence the tree-level decay width disappears. For these points the relative corrections can go below  $-40\%$  or beyond  $+40\%$ , due to the fact that  $\Delta\Gamma^{H^\pm \rightarrow W^\pm h}$ , defined according to Eq. (12.6), diverges for  $\Gamma_{H^\pm \rightarrow W^\pm h}^{\text{tree}} \rightarrow 0$ . However, this is not to be regarded as sign of numerical instability but merely reflects the vanishing tree-level decay width. We checked that also  $\Gamma_{H^\pm \rightarrow W^\pm h}^{\mathcal{O}(1\text{-loop})}$  tends to zero for parameter points with vanishing  $\Gamma_{H^\pm \rightarrow W^\pm h}^{\text{tree}}$ . The inflation visible in the plots is due fact that  $\Gamma_{H^\pm \rightarrow W^\pm h}^{\text{tree}}$  is proportional to  $c_{\beta-\alpha}^2$ , while  $\Gamma_{H^\pm \rightarrow W^\pm h}^{\mathcal{O}(1\text{-loop})}$  contains terms which are linear in  $c_{\beta-\alpha}$  (cf. Eqs. B.5 and Eq. (B.7)). Hence  $\Delta\Gamma^{H^\pm \rightarrow W^\pm h}$  behaves like  $1/c_{\beta-\alpha}$  in the limit  $c_{\beta-\alpha} \rightarrow 0$  and thus diverges. Still, we can conclude that the KOSY and the pinched schemes lead to numerically stable results for the decay  $H^\pm \rightarrow W^\pm h$ . Note that we do not show points where the relative corrections exceed  $-100\%$  or  $+300\%$  in the process-dependent scheme. Corrections below  $-100\%$  would lead to negative decay widths. Hence, no physically meaningful result can be obtained within the corresponding scenarios at one-loop order and the inclusion of higher orders would be required. By the same token, it is debatable whether corrections of more than  $+100\%$  are reasonable. We still display positive corrections of up to  $+300\%$  for illustrative purposes. The fact that the process-dependent scheme yields corrections beyond  $100\%$  for many parameter points demonstrates its inappropriateness at one-loop order and hence manifests the preferability of the pinched schemes. Moreover, we have discarded all points leading to tree-level decay widths below  $0.1$  GeV, since the relative corrections defined according to Eq. (12.6) diverge for  $\Gamma_{H^\pm \rightarrow W^\pm h}^{\text{tree}} \rightarrow 0$ . If not stated otherwise, we will proceed in the same manner, i.e. apply the same cuts on the  $\Gamma^{\text{tree}}$ - and the  $\Delta\Gamma$ -range, for all scatter plots shown in the subsequent sections.

To investigate the various renormalization schemes further, we now pick a particular scenario and vary the mass of the charged and of the CP-odd Higgs boson in the allowed ranges, as described in Sec. 12.2. Figs. 12.2 and 12.3 show the relative one-loop corrections for Scenarios 1a and 1b as a function of  $m_{H^\pm}$  and  $m_{A_0}$ , respectively.

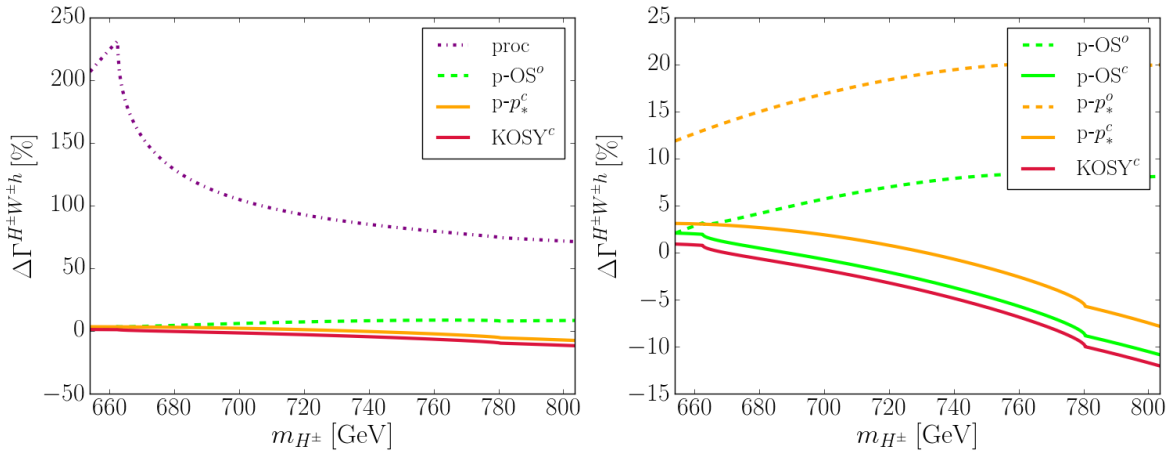


**Figure 12.2.:** Relative one-loop corrections to the decay  $H^\pm \rightarrow W^\pm h$  as a function of  $m_{H^\pm}$ . The input parameters have been chosen according to Scenario 1a. The left plot shows the results for the process-dependent, the KOSY<sup>c</sup>, the p-OS<sup>o</sup> and the p-p<sub>\*</sub><sup>c</sup> schemes. The right plot shows results for the KOSY<sup>c</sup> and all pinched schemes. Similar plots have been shown in our publication [42].

The plots on the left display the results for the process-dependent scheme, the KOSY<sup>c</sup> scheme and one version of each pinched scheme, where we have chosen p-OS<sup>o</sup> and p-p<sub>\*</sub><sup>c</sup> as representatives. In the plots on the right, we display all versions of the pinched schemes together with the KOSY<sup>c</sup> scheme. Note that the kinks appearing in these plots are due to threshold effects in B<sub>0</sub>-functions, entering the amplitude through the scalar WFRCs and the angular

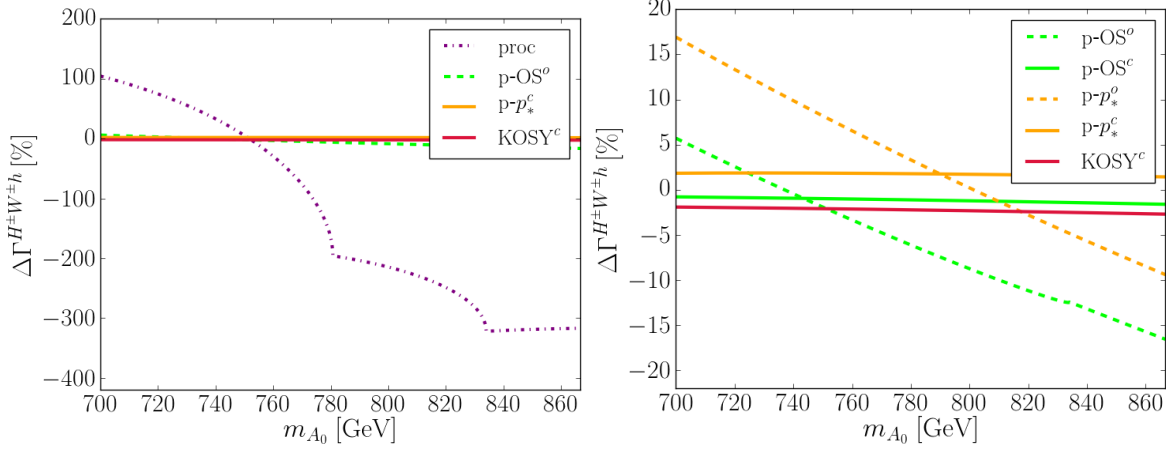


**Figure 12.3.:** Relative one-loop corrections to the decay  $H^\pm \rightarrow W^\pm h$  as a function of  $m_{A_0}$ . The input parameters have been chosen according to Scenario 1b. The left plot shows the results for the process-dependent, the KOSY<sup>c</sup>, the p-OS<sup>o</sup> and the p-p<sub>\*</sub><sup>c</sup> schemes. The right plot shows results for the KOSY<sup>c</sup> and all pinched schemes.

counterterms. They arise when the arguments of  $B_0(m_1^2, m_2^2, m_3^2)$  fulfill the condition

$$m_1 = m_2 + m_3. \quad (12.7)$$

Again, both plots on the left-hand side demonstrate that the process-dependent scheme leads to huge corrections, ranging between 70% and 240% in Scenario 1a (Fig. 12.2) and from 100% to -310% in Scenario 1b (Fig. 12.3), and is thus to be regarded as unsuitable for the process  $H^\pm \rightarrow W^\pm h$ . Note in particular that the results in the process-dependent scheme become meaningless in Scenario 1b for  $m_{A_0} \gtrsim 770$  GeV, where the decay width  $\Gamma_{H^\pm \rightarrow W^\pm h}^{\mathcal{O}(1\text{-loop})}$  turns negative.

The plots on the right-hand side allow for a closer investigation of the pinched schemes. First, by comparing the plots on the right in Figs. 12.2 and 12.3 we can observe that the charged schemes, KOSY<sup>c</sup>, p-OS<sup>c</sup> and p-p<sub>\*</sub><sup>c</sup>, show a stronger dependence on  $m_{H^\pm}$  than the CP-odd ones, whereas the opposite is true for the dependence on  $m_{A_0}$ . This can be traced back to the counterterm  $\delta\beta$ , which in the charged versions depends on

$$\frac{1}{m_{H^\pm}^2} \tilde{\Sigma}_{G^\pm H^\pm}(m_{H^\pm}^2) \quad \text{or} \quad \frac{1}{m_{H^\pm}^2} \tilde{\Sigma}_{G^\pm H^\pm}\left(\frac{m_{H^\pm}^2}{2}\right), \quad (12.8)$$

whereas in the CP-odd versions it involves

$$\frac{1}{m_{A_0}^2} \tilde{\Sigma}_{G_0 A_0}(m_{A_0}^2) \quad \text{or} \quad \frac{1}{m_{A_0}^2} \tilde{\Sigma}_{G_0 A_0}\left(\frac{m_{A_0}^2}{2}\right). \quad (12.9)$$

Due to the strong impact of the angular counterterms on the whole amplitude, this dependence is clearly visible in the final result.

Furthermore, the numerical difference originating from a change between the p-OS and the p-p<sub>\*</sub> scheme is less pronounced for the charged version than for the CP-odd version of  $\delta\beta$  as can be seen by comparing the solid green and orange curves and the green and the orange dashed curves, respectively. This behaviour can be observed for most scenarios we considered. However it is not generic and depends delicately on the input parameters, especially on the masses of the (non-SM) Higgs bosons.

Finally, note that the curve corresponding to the p-OS<sup>c</sup> scheme is very close to the one belonging to the KOSY<sup>c</sup> scheme. This is to be expected, since both schemes incorporate the charged versions of  $\delta\beta$  and in both schemes the angular counterterms are defined in terms of

	Scenario 1a	Scenario 1b
$x, y$	$\Delta_{H^\pm W^\pm h}^{x,y}$	$\Delta_{H^\pm W^\pm h}^{x,y}$
p-OS <sup>o</sup> , p-OS <sup>c</sup>	$\lesssim 11.0\%$	$\lesssim 10.6\%$
p-OS <sup>o</sup> , p- $p_*^o$	$\lesssim 17.6\%$	$\lesssim 17.9\%$
p-OS <sup>c</sup> , p- $p_*^c$	$\lesssim 3.4\%$	$\lesssim 3.1\%$
p- $p_*^o$ , p- $p_*^c$	$\lesssim 23.2\%$	$\lesssim 12.9\%$
p-OS <sup>o</sup> , p- $p_*^c$	$\lesssim 14.7\%$	$\lesssim 21.6\%$
p- $p_*^o$ , p-OS <sup>c</sup>	$\lesssim 25.7\%$	$\lesssim 15.1\%$

**Table 12.4.:** Estimates of the theoretical uncertainty in the decay  $H^\pm \rightarrow W^\pm h$  by a comparison of the results for  $\Gamma_{H^\pm \rightarrow W^\pm h}^{\mathcal{O}(1\text{-loop})}$  obtained in different renormalization schemes.

OS self-energies.

The fact that we have different renormalization schemes at our disposal allows us to estimate the theoretical uncertainty due to missing higher-order corrections. For this purpose we define a measure for the theoretical uncertainty as

$$\Delta_{H^\pm W^\pm h}^{x,y} = \left| \frac{\Gamma_{H^\pm \rightarrow W^\pm h}^{\mathcal{O}(1\text{-loop}),x} - \Gamma_{H^\pm \rightarrow W^\pm h}^{\mathcal{O}(1\text{-loop}),y}}{\Gamma_{H^\pm \rightarrow W^\pm h}^{\mathcal{O}(1\text{-loop}),x}} \right|, \quad (12.10)$$

where  $x$  and  $y$  denote two different renormalization schemes. With the help of this measure we can estimate the uncertainty resulting from the choice of the version for  $\delta\beta$  and from the choice of the scale (OS or  $p_*$ ) for the angular counterterms. Comparing any two schemes, which either differ by the version of  $\delta\beta$  or by the scale, we find for the plotted ranges the values of  $\Delta_{H^\pm W^\pm h}^{x,y}$  shown in Tab. 12.4. Also shown are values which are obtained by comparing schemes that differ in both, the definition of  $\delta\beta$  and the choice of the scale, as these lead to the largest, i.e. most conservative, estimations of the theoretical uncertainty. Note, however, that we do not include the process-dependent scheme, since this scheme is clearly inappropriate. Using these numbers as guideline, we estimate the theoretical uncertainty to be below 26% for Scenario 1a and below 22% for Scenario 1b.

## 12.4. Numerical Analysis of the Decay $H \rightarrow ZZ$

We now turn to the next process of our test set, the decay of the heavy CP-even Higgs boson into two  $Z$ -bosons. Like the process studied in the previous section, its counterterm amplitude comprises the angular counterterms but does not depend on  $\delta m_{12}^2$ . This time, however,  $\delta\beta$  does not enter in its role as mixing angle, but as ratio of the two vevs  $v_1$  and  $v_2$ .

Again, we start the discussion by investigating a scatter plot of the relative corrections  $\Delta\Gamma^{HZZ}$ , defined in analogy to Eq. (12.6), to get a general idea. The conventions used in the corresponding plots in Fig. 12.4 are as explained in the previous section, apart from the fact that this time we do not need to restrict ourselves to the charged version of the KOSY scheme. Hence, the red dots correspond to results of both versions of the KOSY scheme. Similar to the case of the decay  $H^\pm \rightarrow W^\pm h$ , the corrections in the process-dependent scheme can be up to two orders of magnitude larger than those of the other schemes, as the plot on the left-hand side reveals. In contrast to that, the right plot, which concentrates on the central region, shows that all the other schemes lead to corrections of the same size, remaining between  $-40$  and  $+40\%$ . This is true for all parameter points that do not lead to vanishing

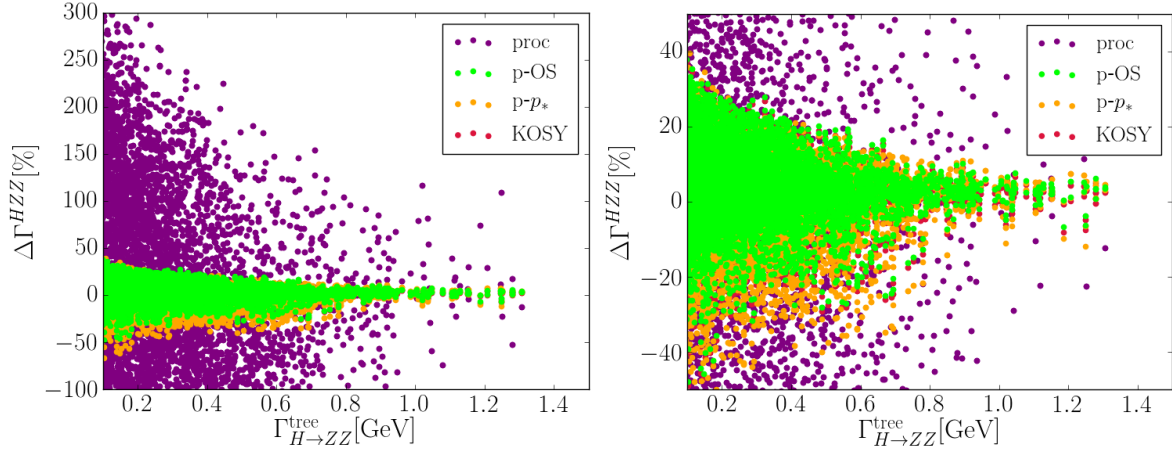


**Figure 12.4.:** Scatter plots for the decay  $H \rightarrow ZZ$ , showing the relative one-loop corrections  $\Delta\Gamma^{HZZ}$  as a function of the tree-level decay width for the parameter points of Scan I. Again we have cut the plots at  $\Gamma_{H \rightarrow ZZ}^{\text{tree}} = 0.1$  GeV and constrained the range for  $\Delta\Gamma^{HZZ}$  to  $-100\% - +300\%$  (see the discussion in Sec. 12.3). In the right plot we have zoomed into the central region.

tree-level amplitudes (cf. the discussion above). Since the tree-level coupling for the decay  $H \rightarrow ZZ$  is proportional to  $c_{\beta-\alpha}$ , whereas the angular counterterms enter with an overall factor  $s_{\beta-\alpha}$ , the situation is identical to the case of the decay  $H^\pm \rightarrow W^\pm h$ . Therefore, the discussion below Fig. 12.1 can directly be transferred to the decay  $H \rightarrow ZZ$  and we can conclude that all process-independent schemes can be regarded as numerically stable, while the process-dependent scheme is not an appropriate choice for this decay.

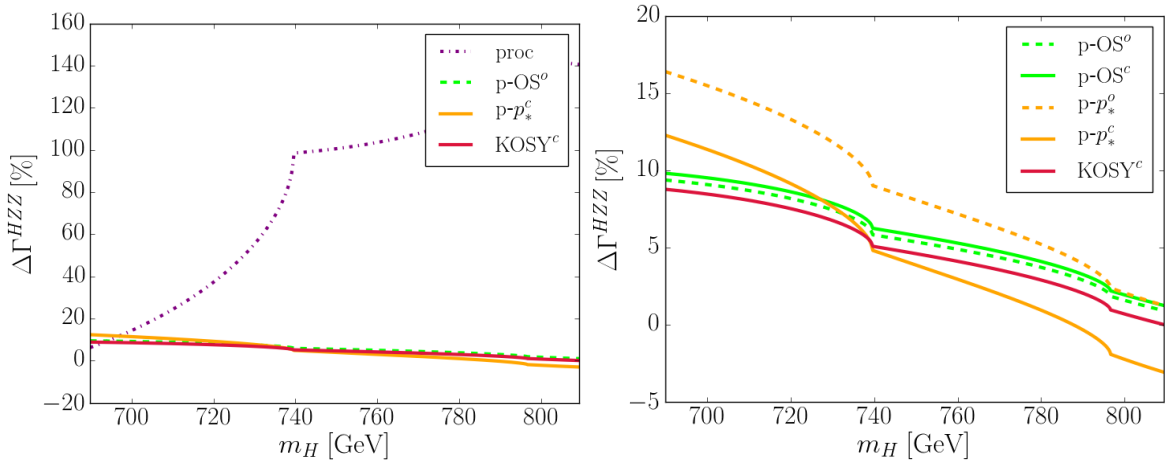


**Figure 12.5.:** Relative one-loop corrections to the decay  $H \rightarrow ZZ$  as a function of  $m_H$ . The input parameters are chosen according to Scenario 2. The left plot shows the results for the process-dependent, the  $\text{KOSY}^c$ , the  $\text{p-OS}^o$  and the  $\text{p-p}_*^c$  schemes. The right plot shows results for the  $\text{KOSY}^c$  and all pinched schemes. Similar plots have been shown in our publication [42].

For a closer investigation, Fig. 12.5 shows the relative corrections  $\Delta\Gamma^{HZZ}$  as a function of  $m_H$  for one specific scenario (Scenario 2). The plot on the left makes apparent the numerical instability of the process dependent scheme, which is found to yield corrections of up to 140% for the chosen scenario. On the right-hand side, we compare again the different versions of pinched schemes among each other and to the  $\text{KOSY}^c$  scheme as reference. Like in the previous section we can use the quantity  $\Delta_{HZZ}^{x,y}$ , defined in analogy to Eq. (12.10), as a measure for the theoretical uncertainty. For the plotted range this estimation yields the results shown in Tab. 12.5, from which the theoretical uncertainty can be estimated to be below about 6.4%

Scenario 2	
$x, y$	$\Delta_{HZZ}^{x,y}$
p-OS <sup>o</sup> , p-OS <sup>c</sup>	$\lesssim 0.4\%$
p-OS <sup>o</sup> , p- $p_*^o$	$\lesssim 6.4\%$
p-OS <sup>c</sup> , p- $p_*^c$	$\lesssim 4.3\%$
p- $p_*^o$ , p- $p_*^c$	$\lesssim 4.3\%$
p-OS <sup>o</sup> , p- $p_*^c$	$\lesssim 3.9\%$
p- $p_*^o$ , p-OS <sup>c</sup>	$\lesssim 5.7\%$

**Table 12.5.:** Estimate of the theoretical uncertainty in the decay  $H \rightarrow ZZ$  by a comparison of the results for  $\Gamma_{H \rightarrow ZZ}^{\mathcal{O}(1\text{-loop})}$  obtained in different renormalization schemes.

for the scenario under consideration.

## 12.5. Numerical Analysis of the Decay $H \rightarrow hh$

The last process we consider is the decay of the heavy CP-even Higgs boson into two lighter ones. As mentioned above, for all scenarios we consider, the light Higgs bosons always corresponds to the SM-like Higgs boson, although in principle scenarios with interchanged roles of the CP-even Higgs bosons are possible. Since the trilinear Higgs coupling  $g_{Hhh}$  depends on  $m_{12}^2$ , this process allows us to study different renormalization schemes for the last parameter of the 2HDM potential. Moreover, we can use it to further test the numerical stability of the renormalization schemes for the angular counterterms, as the coupling shows a complicated dependence on  $\alpha$  and  $\beta$  and hence the cancellation of huge tadpole contributions is non-trivial.

We start with an investigation of the angular counterterms. For this purpose, we display in Fig. 12.6 the relative one-loop corrections  $\Delta\Gamma^{Hhh}$ , defined pursuant to Eq. (12.6), as a function of the corresponding tree-level decay width for the process-dependent, the p-OS, the p- $p_*$  and the KOSY scheme.  $m_{12}^2$  is renormalized according to  $\overline{\text{MS}}$  conditions with the renormalization scale  $\mu_r$  set equal to  $2m_h$ .

In contrast to our observations in the previous sections, this time all schemes lead to huge relative corrections easily reaching beyond 100% in the KOSY and the pinched schemes and even further in the process-dependent scheme. Although striking at first glance, this is not necessarily to be regarded as a sign of numerical instability but can rather be attributed to non-decoupling effects, which generically arise in Higgs-to-Higgs decays in the 2HDM [40,190]. Their occurrence can be explained as follows: In the 2HDM the masses of the heavy Higgs bosons  $m_H$ ,  $m_{A_0}$  and  $m_{H^\pm}$  originate from two sources: the soft- $Z_2$ -breaking parameter  $m_{12}^2$  of the Higgs potential and the vevs  $v_1$  and  $v_2$  of the two Higgs doublets. Thus, schematically they can be written as

$$m_\phi^2 = c_\phi^2 M^2 + L_\phi(\lambda_i) v^2, \quad (12.11)$$

where  $L_\phi(\lambda_i)$  denotes some linear combination of  $\lambda_1$ - $\lambda_5$  and  $\phi$  represents either of  $H$ ,  $A_0$  or  $H^\pm$ . Furthermore, we have introduced the abbreviation  $M^2 = m_{12}^2/c_{\beta s_\beta}$  and the coefficient  $c_\phi$ , given by

$$c_\phi = \begin{cases} 1 & \text{for } \phi \in \{A_0, H^\pm\} \\ s_{\beta-\alpha} & \text{for } \phi = H \end{cases}. \quad (12.12)$$

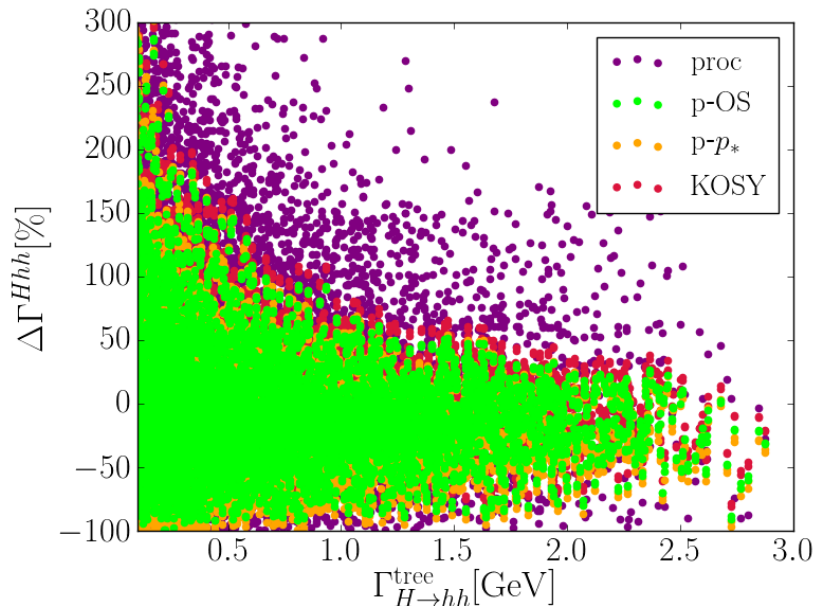


**Figure 12.6.:** Scatter plot for the decay  $H \rightarrow hh$ , showing the relative one-loop corrections  $\Delta\Gamma^{Hhh}$  as a function of the tree-level decay width for the parameter points of Scan I. Again we have cut the plot at  $\Gamma_{H \rightarrow hh}^{\text{tree}} = 0.1$  GeV and constrained the range for  $\Delta\Gamma^{Hhh}$  to  $-100\% - +300\%$  (see the discussion in Sec. 12.3). A similar plot has been shown in our publication [43].

The ratio between these two terms is crucial for the influence of radiative corrections originating from loops with heavy Higgs bosons. If  $c_\phi^2 M^2 \gg L_\phi(\lambda_i)v^2$  holds for all  $\phi \in \{H, A_0, H^\pm\}$ , the masses of the heavy Higgs bosons are determined by the soft- $Z_2$ -breaking parameter  $M^2$  and the second term is negligible. Since the  $\lambda_i$ , appearing in the second term, control the size of the trilinear and quadrilinear Higgs couplings, this limit implies scalar couplings which are small compared to the scalar masses. Therefore, this case corresponds to the *decoupling limit*, where the loop effects of the heavy Higgs bosons vanish for  $m_\phi \rightarrow \infty$  according to the Appelquist-Carazzone decoupling theorem [84]. As a side-remark, note that the MSSM Higgs sector automatically resides in the decoupling regime as the MSSM trilinear and quartic Higgs couplings are determined through the gauge couplings  $g_1$  and  $g_2$ .

The situation is different if instead we have  $c_\phi^2 M^2 \lesssim L_\phi(\lambda_i)v^2$  for at least one of the non-SM Higgs bosons  $\phi$ . In this case, the corresponding mass  $m_\phi$  receives a non-negligible contribution from the coupling parameters  $\lambda_i$  and consequently the limit  $m_\phi \rightarrow \infty$  corresponds to the strong coupling regime. Since in this case the scalar couplings increase in the same proportion as the masses, no decoupling takes place. On the contrary, the contributions of loops with heavy Higgs bosons grow according to  $m_\phi^4$  [40, 190]. For scenarios with heavy non-SM-like Higgs bosons, this power law dependence gives rise to the huge corrections to the decay  $H \rightarrow hh$ , visible in Fig. 12.6.

Due to the large radiative corrections encountered in the decay of the heavy Higgs boson, a meaningful investigation of the numerical stability of the various renormalization schemes can only be conducted in the decoupling limit. In non-decoupled scenarios the large tree-level couplings and the resulting huge radiative corrections necessitate the inclusion of higher-order corrections to achieve reliable predictions. Therefore, a further parameter scan, Scan II, was performed with the additional requirement

$$m_H^2 \approx m_{A_0}^2 \approx m_{H^\pm}^2 \approx M^2. \quad (12.13)$$

This constraint leads to scenarios with non-SM-like Higgs bosons whose masses are approximately degenerate and of the order of the  $Z_2$ -breaking scale. Following the above reasoning,

one would expect all coupling parameters  $\lambda_1$ - $\lambda_5$  to be small and the huge radiative corrections to be absent in these scenarios. However, although this rationale is correct in most cases, there is a subtlety that has to be considered: Even if Eq. (12.13) is fulfilled, decoupling is not automatically guaranteed and actually is found to be impossible in the specific limit  $s_{\beta+\alpha} \rightarrow 1$ . In the context of the 2HDM of type II (and F), this limit is often denoted as the *wrong sign limit*, since in these model types, the Yukawa couplings of the SM-like Higgs boson  $h$  to down-type fermions receive a relative minus sign w.r.t. the couplings to massive gauge bosons and up-type fermions for  $s_{\beta+\alpha} \rightarrow 1$  [159,191–193]. As was shown and discussed in detail in Ref. [191], non-decoupling properties *necessarily* arise in the limit  $s_{\beta+\alpha} \rightarrow 1$  of the 2HDM. Similar observations, were made in Refs. [194–196], focusing like Ref. [191] on the contribution of the charged Higgs boson to the decay  $h \rightarrow \gamma\gamma$ .

In the context of our study, i.e. in the decay  $H \rightarrow hh$ , the emergence of non-decoupling effects in the wrong sign limit can be understood by considering the trigonometric relations that are involved. For these examinations it is useful to treat the cases  $s_{\beta-\alpha} \approx 1$  and  $s_{\beta-\alpha} < 1$  separately.

Let us first consider the second situation, i.e. a scenario where  $s_{\beta-\alpha}$  differs sufficiently much from one. Although the limit  $s_{\beta-\alpha} \rightarrow 1$  corresponds to the SM limit, which is favoured by LHC Higgs data, significant deviations from this limit can appear in the wrong sign regime. This was shown in Refs. [159,192,193], where values of  $s_{\beta-\alpha} \approx 0.55$  (0.62) were found to be compatible at 3 (2) $\sigma$  with the LHC Higgs data and to comply with the other constraints implemented in **ScannerS**. As can directly be inferred from Eq. (12.11), such “small” values of  $s_{\beta-\alpha}$ , however, necessitate a significant contribution of the term  $L_H(\lambda_i)v^2$  to  $m_H^2$  even if the mass of the heavy Higgs boson  $H$  is of the order of the soft- $Z_2$ -breaking scale, i.e. if  $m_H^2 \approx M^2$  holds. This, in turn, brings us back to the non-decoupling regime.

Moreover, also for values of  $s_{\beta-\alpha}$  close to one, corresponding to the first case mentioned above, the corrections to the vertex  $Hhh$  can be huge in the wrong sign limit. Here the situation is similar to the case studied in Ref. [191], that is the non-decoupling of the charged Higgs boson in the decay  $h \rightarrow \gamma\gamma$ . As was shown by the authors of this publication, the ratio  $g_{hH^\pm H^\mp}/m_{H^\pm}^2$  approaches a constant, i.e. mass-independent, value for  $s_{\beta+\alpha} \rightarrow 1$ , viz. in the wrong sign regime. Consequently, the charged Higgs boson does not decouple and contributes significantly to the decay  $h \rightarrow \gamma\gamma$ . An analogous observation can be made in the case of the decay  $H \rightarrow hh$ , where apart from  $H^\pm$  also the other heavy Higgs bosons  $H$  and  $A_0$  show a non-decoupling behaviour in the wrong sign limit. In the following, we briefly exemplify this for the case of the CP-even Higgs boson  $H$ . For this purpose, we consider the ratio  $g_{HHh}/m_H^2$ , which plays an important role in the radiative corrections to the process under consideration. In the limit  $s_{\beta-\alpha} \rightarrow 1$ , this ratio approaches the following values in the wrong sign and in the

correct sign regime, respectively

$$\begin{aligned}
\frac{g_{HHh}}{m_H^2} &= \frac{1}{m_H^2} \frac{1}{v} \frac{s_{\beta-\alpha}}{s_{2\beta}} [s_{2\alpha}(2m_H^2 + m_h^2) - M^2(3s_{2\alpha} + s_{2\beta})] \\
&\stackrel{m_H^2 \approx M^2}{\approx} -\frac{1}{v} \frac{s_{\beta-\alpha}}{s_{2\beta}} [s_{2\alpha} + s_{2\beta}] + \mathcal{O}\left(\frac{m_h^2}{vm_H^2}\right) \\
&= -\frac{1}{v} s_{\beta-\alpha} \left(1 + \frac{s_\alpha c_\alpha}{s_\beta c_\beta}\right) + \mathcal{O}\left(\frac{m_h^2}{vm_H^2}\right) \\
&= -\frac{1}{v} s_{\beta-\alpha} \left(1 - \frac{s_{\beta-\alpha} - c_{\beta-\alpha} t_\beta}{s_{\beta-\alpha} + c_{\beta-\alpha} t_\alpha}\right) + \mathcal{O}\left(\frac{m_h^2}{vm_H^2}\right) \\
&\approx -\frac{1}{v} s_{\beta-\alpha} \left(1 - \frac{s_{\beta-\alpha} - \begin{cases} 0 & \text{correct sign limit} \\ 2 & \text{wrong sign limit} \end{cases}}{s_{\beta-\alpha}}\right) + \mathcal{O}\left(\frac{m_h^2}{vm_H^2}\right) \\
&\begin{cases} \stackrel{s_{\beta-\alpha} \rightarrow 1}{\approx} 0 & \text{correct sign limit} \\ \stackrel{s_{\beta-\alpha} \rightarrow 1}{\approx} -\frac{2}{v} & \text{wrong sign limit} \end{cases} + \mathcal{O}\left(\frac{m_h^2}{vm_H^2}\right), \tag{12.14}
\end{aligned}$$

Here we have used the fact that in the wrong sign limit,  $s_{\beta-\alpha} \rightarrow 1$  is only possible for  $\alpha \rightarrow 0$  and  $\beta \rightarrow \frac{\pi}{2}$ , which in turn implies  $t_\beta \rightarrow \infty$ . Therefore in the wrong sign limit we have  $c_{\beta-\alpha} t_\beta \rightarrow 2$  despite the fact that  $c_{\beta-\alpha}$  approaches zero for  $s_{\beta-\alpha} \rightarrow 1$ . This can directly be obtained from the considerations in Ref. [191]. As can be seen from Eq. (12.14), the ratio  $g_{HHh}/m_H^2$  closes in on a constant value in the wrong sign regime, whereas it vanishes in the correct sign case with growing mass  $m_H^2$  as  $m_h^2/(vm_H^2)$ . Consequently, the heavy CP-even Higgs boson decouples for  $m_H^2 \rightarrow \infty$  in the correct sign regime, but not in the wrong sign limit. Analogous observations can be made for the coupling  $g_{Hhh}$ . Furthermore, a comparable treatment of the ratio  $g_{hA_0A_0}/m_{A_0}^2$  results in

$$\begin{aligned}
\frac{g_{hA_0A_0}}{m_{A_0}^2} &= -\frac{2}{v} \left(c_{\beta-\alpha} \left(\frac{1}{t_\beta} - t_\beta\right)\right) + \mathcal{O}\left(\frac{m_h^2}{vm_{A_0}^2}\right) \\
&\begin{cases} \stackrel{s_{\beta-\alpha} \rightarrow 1}{\approx} 0 & \text{correct sign limit} \\ s_{\beta-\alpha} \rightarrow 1, \\ t_\beta \rightarrow \infty \\ \approx \frac{2}{v} & \text{wrong sign limit} \end{cases} + \mathcal{O}\left(\frac{m_h^2}{vm_{A_0}^2}\right). \tag{12.15}
\end{aligned}$$

Again, decoupling only takes place in the correct sign case. Finally, as far as  $H^\pm$  is concerned, the discussion can directly be taken from [191].

Due to these non-decoupling effects, it is advisable to exclude also all scenarios which reside in the wrong sign regime from the samples in order to reach a conclusion on the numerical stability of the various renormalization schemes. The large tree-level couplings which can arise in non-decoupled settings, lead to huge radiative corrections, such that an inclusion of higher-order effects is recommended and a discussion at one-loop order does not appear sensible.

Therefore, we show in Fig. 12.7 a scatter plot of the relative one-loop corrections  $\Delta\Gamma^{Hhh}$  for the parameter points of Scan II which belong to scenarios in the correct sign regime. We used the sign of  $s_\alpha$  as a discriminator between the two cases, assigning all parameter points with  $s_\alpha < 0 (> 0)$  to the correct (wrong) sign regime<sup>3</sup>. Having excluded all non-decoupling

<sup>3</sup>Note that with  $0 \leq \beta \leq \frac{\pi}{2}$ , as imposed by **ScannerS**, the wrong sign regime with both  $s_{\beta-\alpha} \rightarrow 1$  and  $s_{\beta+\alpha} \rightarrow 1$  can only be obtained for  $s_\alpha > 0$ , while  $s_\alpha < 0$  implies  $s_{\beta+\alpha} < 1$  for  $s_{\beta-\alpha} \rightarrow 1$ .

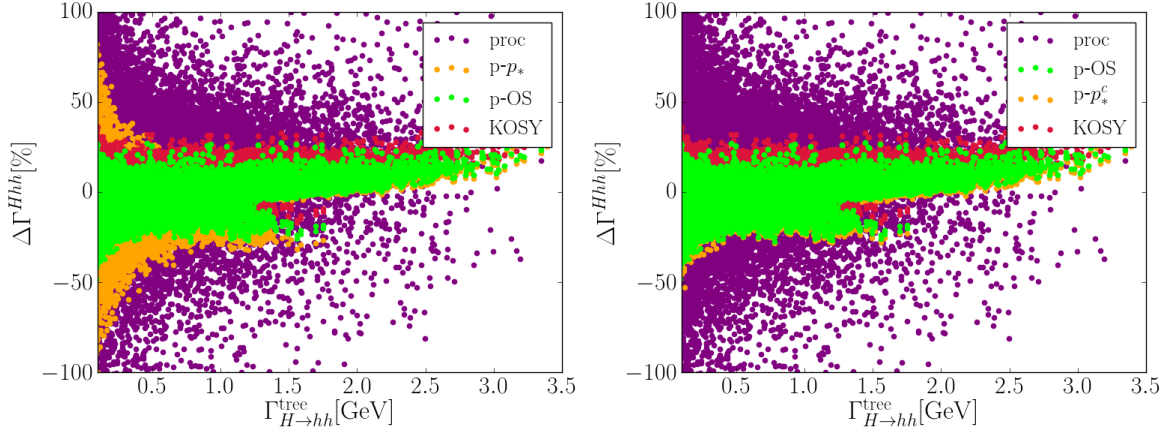


**Figure 12.7.:** Scatter plots for the decay  $H \rightarrow hh$ , showing the relative one-loop corrections  $\Delta\Gamma^{Hhh}$  as a function of the tree-level decay width for the parameter points of Scan II corresponding to scenarios in the correct sign regime. In the right panel we only show the charged version of the  $p$ - $p_*$ -scheme. We have cut the plots at  $\Gamma_{H \rightarrow hh}^{\text{tree}} = 0.1$  GeV and constrained the range for  $\Delta\Gamma^{Hhh}$  to  $-100\%$  -  $+100\%$  (see the discussion in Sec. 12.3 and in the text below). Similar plots have been shown in our publication [43].

effects, we encounter the familiar situation of the previously studied processes. While the process-dependent scheme leads to corrections beyond  $-100\%$  and  $+100\%$  (not shown in the plot, which is restricted to a range between  $\pm 100\%$ <sup>4</sup>), the data points belonging to the KOSY and the  $p$ -OS schemes remain in a range between  $\pm 40\%$ . Unlike before, however, there is a difference visible in the left panel between the OS schemes (the KOSY and the  $p$ -OS scheme) and the  $p$ - $p_*$  scheme. This difference originates from scenarios with comparably light CP-odd Higgs bosons. Its occurrence can be traced back to the top resonance, which appears in the mixed  $A_0$ - $G_0$ -self-energy contributing to  $\delta\beta_0^{p-p_*}$  and results from the diagram shown in Fig. 12.8. In the  $p$ - $p_*^c$ -scheme this resonance is hit for a value of  $m_{A_0}^2/2 = 4m_t^2$ , i.e. for  $m_{A_0} \approx 488$

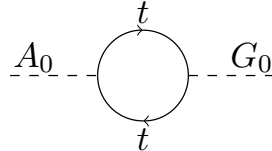


**Figure 12.8.:** Top quark contributing to the mixed  $A_0$ - $G_0$ -self-energy becoming resonant for  $\frac{m_{A_0}^2}{2} = 4m_t^2$  in the  $p$ - $p_*^c$ -scheme.

GeV, however its tail is visible up to values of  $m_{A_0} \approx 700$  GeV. Since all scenarios of Scan I, used for the previously studied processes, do not contain a CP-odd Higgs boson with a mass below 700 GeV, we have not encountered this resonance in our investigations hitherto. Scan II on the other hand, which is utilized for the present analysis, exhibits plenty of scenarios with a pseudoscalar Higgs boson in the mass range  $450 \dots 700$  GeV.

In contrast to  $\delta\beta_0^{p-p_*}$ , the charged version of  $\delta\beta_0^{p-p_*}$  is not affected by the top resonance, as there is no comparable pure top loop contribution in the mixed  $H^\pm$ - $G^\pm$ -self-energy. Indeed, excluding the  $p$ - $p_*^c$ -scheme from the scatter plot, the difference between the  $p$ - $p_*$  and the OS schemes almost disappears, as can be seen in the right panel of Fig. 12.7. We can conclude that the charged version of the  $p$ - $p_*$  scheme is preferable for scenarios with a light CP-odd Higgs boson. Moreover, this plot clearly demonstrates the stable numerical properties of the charged  $p$ - $p_*$  and the  $p$ -OS scheme.

On top of this, the above investigations also illustrate the good numerical behaviour of the

<sup>4</sup>For better visibility, we do not go up to 300% in these plots.

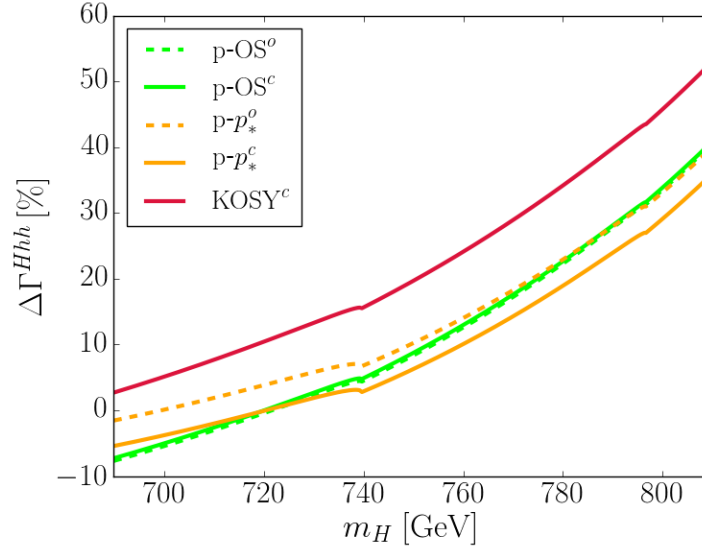


**Figure 12.9.:** Relative one-loop corrections to the decay  $H \rightarrow hh$  as a function of  $m_H$ . The plot shows the results for the decoupled setting of Scenario 2 for the  $\text{KOSY}^c$  and all pinched schemes.

$\overline{\text{MS}}$  scheme for  $m_{12}^2$ , which was applied throughout.

In order to round off the discussion of the angular counterterms, we now examine one specific scenario (Scenario 2), which resides in the decoupling limit. Note that the mass of the pseudoscalar Higgs boson is large enough in this case to evade the top resonance. Fig. 12.9 shows the relative one-loop corrections  $\Delta\Gamma^{Hhh}$  as a function of the mass  $m_H$  for the selected scenario. As can be seen, the corrections in Scenario 2 remain between about  $-8\%$  and  $+50\%$  in all pinched schemes, which confirms the numerical stability of these. Furthermore, it is interesting to note that the decoupling regime is gradually abandoned with growing  $m_H$  such that strict decoupling does not apply any longer towards the right end of the plot. This is also reflected in the increasing radiative corrections.

Employing again the quantity  $\Delta_{Hhh}^{x,y}$ , defined in analogy to Eq. (12.10), as a measure for the theoretical uncertainty in the decay  $H \rightarrow hh$ , we obtain for Scenario 2 the estimates summarized in Tab. 12.6. They imply a theoretical uncertainty below  $6.6\%$  within the plotted

Scenario 2	
$x, y$	$\Delta_{Hhh}^{x,y}$
p-OS <sup>o</sup> , p-OS <sup>c</sup>	$\lesssim 0.4\%$
p-OS <sup>o</sup> , p- $p_*^o$	$\lesssim 6.6\%$
p-OS <sup>c</sup> , p- $p_*^c$	$\lesssim 3.6\%$
p- $p_*^o$ , p- $p_*^c$	$\lesssim 3.9\%$
p-OS <sup>o</sup> , p- $p_*^c$	$\lesssim 5.8\%$
p- $p_*^o$ , p-OS <sup>c</sup>	$\lesssim 3.3\%$

**Table 12.6.:** Estimates of the theoretical uncertainty in the decay  $H \rightarrow hh$  by a comparison of the results for  $\Gamma_{H \rightarrow hh}^{\mathcal{O}(1\text{-loop})}$  obtained in different renormalization schemes.

range.

The last scheme which remains to be tested for numerical stability is the process-dependent

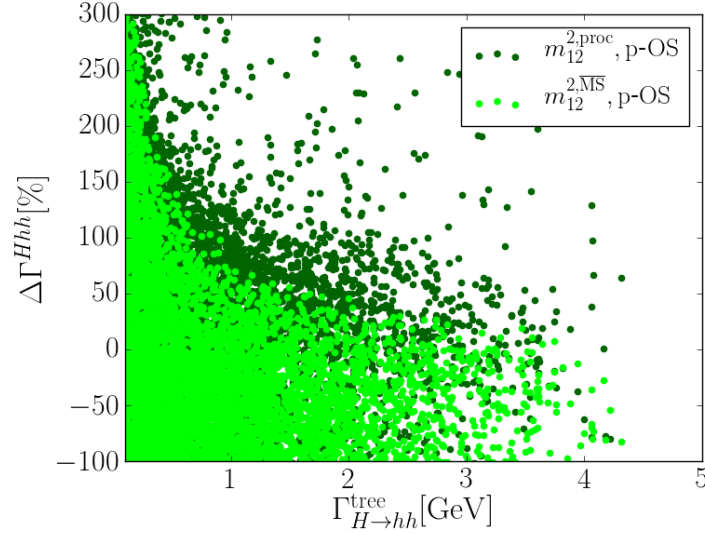


**Figure 12.10.:** Scatter plot for the decay  $H \rightarrow hh$ , showing the relative one-loop corrections  $\Delta\Gamma^{Hhh}$  as a function of the tree-level decay width for the parameter points of Scan III in the correct sign regime for two different renormalization schemes for  $m_{12}^2$ : the process-dependent scheme (dark green) and the  $\overline{\text{MS}}$  scheme (light green), with the renormalization scale fixed at  $\mu_r = 2m_h$ . The angular counterterms are renormalized in the p-OS $^\circ$  scheme. Again we have cut the plot at  $\Gamma_{H \rightarrow hh}^{\text{tree}} = 0.1$  GeV and constrained the range for  $\Delta\Gamma^{Hhh}$  to  $-100\% - +300\%$  (see the discussion in Sec. 12.3). A similar plot has been shown in our publication [43].

renormalization scheme for  $m_{12}^2$ . In order to examine this scheme, a third parameter scan, Scan III, was performed, in which we demanded the scalar masses to obey the relation

$$m_H \geq 2m_{A_0}, \quad (12.16)$$

such that the decay  $H \rightarrow A_0 A_0$  is kinematically allowed. This relation can only be fulfilled in the non-decoupling regime as it requires a mass hierarchy among the non-SM-like Higgs bosons. Therefore we expect to find large radiative corrections in the decay  $H \rightarrow hh$  for the parameter points of Scan III. Fig. 12.10, which displays the relative one-loop corrections for the decay under consideration, confirms this anticipation. In this plot we compare the two proposed renormalization schemes for  $m_{12}^2$ , the process-dependent and the  $\overline{\text{MS}}$  scheme, where the renormalization scale has been fixed at  $\mu_r = 2m_h$ . For both cases, the angles are renormalized in the p-OS $^\circ$  scheme. The relative one-loop corrections are found to be huge in both schemes, however, the better performance of the  $\overline{\text{MS}}$  scheme is still discernible if we disregard the range to the left side of the plot, where the tree-level decay width vanishes (cf. the discussion above). While all corresponding points in the  $\overline{\text{MS}}$  scheme remain below  $\approx 150\%$ , there are outlying points scattered beyond 300% in the process-dependent scheme. This observation suggests a numerical instability of the process-dependent scheme for  $m_{12}^2$ , which on top suffers from a limited applicability due to kinematic restrictions. Therefore, the  $\overline{\text{MS}}$  scheme, whose good performance was verified in the above studies in the decoupling regime, is clearly preferable as renormalization scheme for  $m_{12}^2$ .

As discussed above, the occurrence of radiative corrections as large as those encountered here clearly calls for the inclusion of higher-order contributions to achieve reliable predictions. This, however, is beyond the scope of this thesis.

The purpose of this part of the thesis was the establishment and investigation of various renormalization schemes for the 2HDM. Throughout our considerations the focus was on finding a suitable scheme for the mixing angles  $\alpha$  and  $\beta$  and for the soft- $Z_2$ -breaking parameter  $m_{12}^2$ . As criteria for a good renormalization scheme we employed the three properties of process independence, gauge independence and numerical stability. While process independence is merely a preferable feature for an appropriate renormalization scheme, the latter two criteria are indispensable. Meaningful higher-order predictions for physical observables are only feasible within a renormalization framework leading to gauge-independent and numerically stable results for physical quantities.

In the course of our investigations it has become apparent that the treatment of the tadpoles is crucial for the matter of gauge independence. We proposed and investigated two different tadpole schemes, the first of which, dubbed scheme I, introduces tadpole counterterms such that all tadpole diagrams can be discarded. On the contrary, the second scheme, called scheme II, forgoes tadpole counterterms, which in turn entails a proper inclusion of tadpole diagrams in all Green's functions.

As we have discussed, within the framework of scheme II, all counterterms of physical parameters are manifestly gauge independent. In scheme I, however, gauge-dependent counterterms for physical parameters are necessary in order to achieve gauge-independent expressions for physical observables. We demonstrated that this fact prohibits a straightforward process-independent definition of the angular counterterms in scheme I. In contrast, the gauge independence of the counterterms in scheme II allows, in synergy with the pinch technique, for a process-independent renormalization of the mixing angles, leading to gauge-independent observables.

We investigated various renormalization schemes for the angular counterterms within both tadpole frameworks. Concerning process-independent definitions, we considered the KOSY scheme within tadpole scheme I and the p-OS and p- $p_*$  scheme, relying on the pinch technique in the context of tadpole scheme II. Each of these schemes comes in two versions, depending on whether the CP-odd or the charged Higgs sector is used to define the counterterm  $\delta\beta$ . As can be inferred from our discussion and as was explicitly verified, the KOSY scheme leads to gauge-dependent expressions for physical quantities and therefore is to be regarded as unsustainable. On the other hand, the pinched schemes are manifestly gauge independent.

As a further variant of a process-independent definition, we also briefly inspected an  $\overline{\text{MS}}$

scheme for the mixing angles within both tadpole schemes. Again, this definition turned out to yield gauge-dependent  $\mathcal{S}$ -matrix-elements in tadpole scheme I while being evidently gauge independent in scheme II.

On top of these schemes, we examined a process-dependent definition of the angular counterterms, utilizing the decay processes  $A_0 \rightarrow \tau\tau$  and  $H \rightarrow \tau\tau$  to fix  $\delta\beta$  and  $\delta\alpha$ , respectively. Process-dependent schemes automatically lead to gauge-independent observables, irrespective of the treatment of the tadpoles.

After the investigation of gauge dependence, we performed a thorough numerical analysis of the proposed renormalization schemes, comprising three different test processes. The picture emerging from this clearly showed that the process-dependent scheme for the mixing angles is numerically unstable. Radiative corrections of more than 100% were seen to evolve within this scheme for many of the investigated scenarios, regardless of the tadpole scheme. On the other hand, the p-OS scheme and the charged version of the p- $p_*$  scheme were found to yield numerically stable results in all processes we considered. The CP-odd version of the p- $p_*$  scheme is less favorable in scenarios featuring a light pseudoscalar Higgs bosons, which is due to the emergence of the top resonance in  $\delta\beta$  in this scheme, leading to enhanced radiative corrections.

With regard to the parameter  $m_{12}^2$ , we investigated two renormalization schemes, an  $\overline{\text{MS}}$  definition and a process-dependent scheme, fixing  $\delta m_{12}^2$  in terms of the decay  $H \rightarrow A_0 A_0$ . Since  $m_{12}^2$  is a parameter of the original gauge-independent Lagrangian, gauge dependence is of no concern in the renormalization of  $m_{12}^2$ . Therefore both considered definitions are manifestly gauge independent, irrespective of the tadpole scheme. However, the applicability of the process-dependent scheme is subject to severe kinematic restrictions. Furthermore, the numerical analysis suggests an unstable behaviour of the process-dependent scheme. Contrariwise, the  $\overline{\text{MS}}$  definition of  $m_{12}^2$  leads to numerically stable results.

Summarizing all gained insights, we first of all clearly advocate the usage of tadpole scheme II. Only within this framework, a renormalization scheme for the mixing angles can be found that is at the same time process independent, gauge independent and numerically stable. In the context of scheme II, the p-OS scheme and the charged version of the p- $p_*$  scheme have proven good numerical properties in all processes and scenarios we considered. Therefore we recommend their application in order to renormalize the mixing angles of the 2HDM.

Concerning the parameter  $m_{12}^2$ , we suggest the usage of the  $\overline{\text{MS}}$  scheme, which also fulfills all three criteria established as prerequisites for an appropriate renormalization scheme.

For future research it would certainly be interesting to examine the numerical behaviour of the advocated schemes in further processes and to test whether their numerical stability persists as expected. An affirmative outcome of these investigations would manifest the role of the p-OS and the p- $p_*^c$  scheme as the preferable renormalization schemes for the mixing angles of the 2HDM.

Finally, having set up a suitable renormalization scheme, we are now in the position to proceed with a dedicated study of LHC phenomenology in order to investigate the implications of our findings.

**Part III.**

**The  $\mathcal{O}(\alpha_t\alpha_s)$  Corrections to the  
Trilinear Higgs Self-Couplings in the  
Complex NMSSM**



We now move on to the next extension of the SM, we want to consider in more detail in this thesis. Already in part I, we have emphasized the elegance of SUSY and its capability of providing a solution to many unanswered problems the SM is plagued with. In this part we want to study one specific realization of a SUSY model, the Next-to-Minimal Supersymmetric Standard Model (NMSSM) [30–37]. Our particular interest will be in the Higgs sector of the NMSSM.

Although all evaluated data collected by the two general-purpose particle detectors ATLAS and CMS at the LHC are up to now in good agreement with the Higgs boson discovered in 2012 being the SM Higgs boson [12–15], it is still premature to draw a definite conclusion. More data is required in order to infer the properties and couplings of the Higgs boson with a higher precision, before further insight can be gained. However, even if all measurements turn out to confirm its SM-like behaviour, it is still possible that the discovered particle is a Higgs boson of some BSM model, mimicking the one of the SM. In fact, it is conceivable that a non-SM Higgs boson imitates the one of the SM with such a degree of perfection that a distinction can be made only in high-precision measurements. This in turn necessitates from the theory side predictions of comparable accuracy for physical observables within specific BSM models.

Apart from precision measurements, another possibility of tracking down new physics is to search for additional BSM particles. Since many BSM models feature an enlarged Higgs sector, it is at hand to first look for additional Higgs bosons. In this endeavour, decays of heavy Higgs bosons into lighter ones can play an important role.

For both of these possibilities of detecting new physics, trilinear Higgs self-couplings are of particular importance. They enter prominent processes like Higgs pair production and Higgs-to-Higgs decays and can hence have a significant phenomenological impact.

Moreover, they play a key role in the efforts of gaining further insight into the mechanism of EWSB. In the SM with only one Higgs boson  $h$ , the Higgs potential is completely determined by the mass  $m_h$  of the Higgs boson and its trilinear and quadrilinear self-couplings  $\lambda_{hhh}$  and  $\lambda_{hhhh}$ . Furthermore, there is a unique relation between the self-couplings and the Higgs mass, given by

$$\lambda_{hhh} = \frac{3m_h^2}{v} \quad \text{and} \quad \lambda_{hhhh} = \frac{3m_h^2}{v^2}. \quad (14.1)$$

The last step in the experimental verification of the Higgs mechanism requires the reconstruction of the Higgs potential, and hence the determination of the trilinear and quadrilinear Higgs self-couplings. However, the quartic Higgs coupling is experimentally out of reach in the foreseeable future [197]. Also the determination of the trilinear Higgs self-coupling will be a challenging task, but there is justified reason to assume that it may be accessible at the high-luminosity LHC. At least, it should be feasible to determine, whether the trilinear coupling is non-vanishing, as required for a non-vanishing vev, and thus to perform a first consistency check of the SM Higgs mechanism.

Several groups have performed dedicated studies on the measurability of the trilinear Higgs coupling at present and future colliders and estimated the accuracy, with which we can expect the latter to be extracted. Their analyses resulted in predicted accuracies ranging from  $\sim \mathcal{O}(1)$  to 30% for the high-luminosity LHC at 14 TeV [198–206], from 10 to 20% for the ILC at 1 TeV [204, 207] and from 8 to 30% for a future 100 TeV hadron collider [204, 208, 209]. It should be noted, however, that some of these estimates are probably too optimistic, since they underrate experimental uncertainties [209].

All quoted studies assume the SM as underlying model. For models with enlarged Higgs sectors, the prospects for measuring the trilinear Higgs self-couplings are highly model dependent [204, 210]. However, if in nature a model is realized that features large deviations of the trilinear coupling  $\lambda_{hhh}$  of three SM-like Higgs bosons from the SM prediction, these might be detectable at the LHC or future colliders. In this context it should be noted that  $\lambda_{hhh}$  can still deviate substantially from its SM value without being in contradiction with experiment, even if all other couplings and properties of the Higgs boson are close to the SM predictions [209]. Therefore it is conceivable that new physics will first be detected by means of the trilinear Higgs self-coupling [210, 211]. Furthermore, in case a sign of an extended Higgs sector is found, the trilinear Higgs self-couplings might be used in order to discriminate between different BSM models [212].

Models with an extended Higgs sector do not fulfill the relation between the masses and trilinear couplings of their Higgs bosons stated in Eq. (14.1), as the Higgs potential is more involved and the Higgs mass eigenstates are complicated mixtures of gauge eigenstates. Nevertheless, Higgs masses and trilinear self-couplings are closely entwined, since both derive from the Higgs potential. For that reason, the order of the corrections included in the trilinear couplings should match the precision the Higgs boson masses are calculated with. Only if both, the masses and the trilinear couplings, are known up to the same order in the perturbative expansion, consistent predictions for observables of that order can be made.

A treatment of the Higgs masses and trilinear self-couplings on an equal footing is also important in considerations of decoupling properties [213]. In some SM extension, e.g. the MSSM, the coupling between three SM-like Higgs bosons approaches the SM value and fulfills Eq. (14.1) in the decoupling limit. In the MSSM this limit is attained for  $m_{A_0}^2 \gg M_Z^2$ , where  $m_{A_0}$  is the mass of the MSSM pseudoscalar Higgs boson. The relation remains valid even if higher-order corrections of the same order are included in both the masses and the couplings [214–217]. In the NMSSM on the other hand, the trilinear coupling of three SM-like Higgs bosons does not necessarily approach the SM value in the decoupling limit, not even at tree level, if the SM-like Higgs boson exhibits a substantial admixture of the NMSSM-specific singlet component [46].

Within the NMSSM considerable effort has been devoted in the recent years to the determination of higher-order corrections to the masses of the Higgs bosons. In the CP-conserving NMSSM, featuring purely real parameters and vevs, the first leading corrections have been calculated in Refs. [218–223]. Subsequently the full one-loop mass corrections have been presented in Refs. [224, 225] in the  $\overline{\text{DR}}$  scheme and in Ref. [226] in a scheme with mixed  $\overline{\text{DR}}$  and

OS conditions. Furthermore, the leading two-loop corrections of  $\mathcal{O}(\alpha_t\alpha_s + \alpha_b\alpha_s)$ <sup>1</sup> have been determined in the effective potential approach in Ref. [224] and even first corrections going beyond have been announced in Refs. [227–230].

For the CP-violating NMSSM, where some of the parameters of the scalar potential as well as the vevs can be complex (cf. Sec. 16.2), the first leading one-loop corrections to the Higgs boson masses have been presented in Refs. [231–235]. Moreover, the full one-loop corrections [236] as well as the corrections of  $\mathcal{O}(\alpha_t\alpha_s)$  [44] and beyond [45] in the limit of vanishing external momentum are available by now.

Concerning the trilinear Higgs self-couplings, the research activity with regard to higher-order corrections has been much less pronounced. Until recently only the full one-loop corrections in the framework of the CP-conserving NMSSM, determined in Ref. [46], were known. In their numerical analysis, the authors have found the corrections to the trilinear couplings to be important. Included into Higgs-to-Higgs decays, they were seen to yield deviations of up to 90% in the decay widths compared to tree-level results. The incorporation of these corrections in a program scanning the NMSSM parameter space for allowed parameter points was found to lead to an exclusion of some parameter points that were allowed when only tree-level trilinear couplings were used or the other way around to the admission of some parameter configurations excluded at tree-level. Furthermore, the authors estimated the influence of the corrections on Higgs pair production and concluded it to be substantial.

In view of these phenomenological investigations, the importance of higher-order corrections to the trilinear Higgs self-couplings within the NMSSM becomes obvious. Moreover, the size of the one-loop corrections found in Ref. [46] calls for the inclusion of higher orders to verify the convergence of the perturbative expansion and to reduce the theoretical uncertainty. With regard to the precision available for the masses, it is besides clear that a consistent prediction for physical observables of higher accuracy requires the inclusion of higher-order corrections to the trilinear Higgs self-couplings. The next important higher-order corrections are those of  $\mathcal{O}(\alpha_t\alpha_s)$ , which match the precision in the masses of Ref. [44].

The purpose of this part of the thesis is the determination and presentation of these corrections in the limit of vanishing external momentum. Our results, which we will detail in the following chapters, have been published in [47].

In order to set the scene, we will start in Ch. 15 with some preliminaries concerning notations and conventions. An emphasis will lie on the introduction of the approximations which will be used in the subsequent chapters as well as on the rough structure of the corrections.

Afterwards, in Ch. 16, we will give a brief introduction to the NMSSM, summarizing its particle content and detailing the sectors, which will be important for the following investigations. Ch. 17 will be devoted to the specification of the renormalization scheme, focusing again on those parts of the NMSSM which are relevant for our studies. Concerning the top-stop sector, we will introduce two different renormalization schemes, the OS and the  $\overline{\text{DR}}$  scheme, and give the necessary conversion rules for switching between both. For the Higgs sector we will suggest a hybrid scheme, mixing OS and  $\overline{\text{DR}}$  conditions, in analogy to the one used in Ref. [44].

We will then continue with the presentation of the calculation of the corrections to the trilinear Higgs self-couplings. In Ch. 18 we will first deal with the corrections of  $\mathcal{O}(\alpha_t)$  and illustrate their determination by means of the effective potential approach. They will allow us to define *effective trilinear Higgs self-couplings* and give access to an estimation of the goodness of our approximations.

Subsequently, we will turn to the calculation of the  $\mathcal{O}(\alpha_t\alpha_s)$  corrections in Ch. 19. We will explain our treatment of the two-loop integrals and go into details concerning a proper inclusion of the counterterms at two-loop order.

Finally, we will turn to the numerical investigation of our results. In Ch. 20 we will consider

<sup>1</sup>For an explanation of this notation for the order see Ch. 15.

---

the implications of our corrections, in particular for the trilinear self-coupling of three SM-like Higgs bosons. First, we will discuss the range of validity of our approximations by means of a comparison of the  $\mathcal{O}(\alpha_t)$  corrections to the full one-loop corrections. Afterwards, we will examine the size of the corrections at different orders and estimate the theoretical uncertainty by comparing the results obtained in different renormalization schemes and by a variation of the renormalization scale. Furthermore, we will examine the influence of the complex phases on our results. Eventually, we will investigate the subject of Higgs-to-Higgs decays and discuss the limitation of neglecting the external momentum in the  $\mathcal{O}(\alpha_t\alpha_s)$  corrections in this context. The conclusions will be given in Ch. 21.

---

## Preliminaries on Used Approximations and the Structure of the Corrections

---

Before presenting the details of the calculation, we first want to explain the approximations and limits, which will be used in the subsequent chapters. Furthermore, we want to present the rough structure of the corrections to be calculated in order to make it easier for the reader to follow our discussion.

First of all, let us clarify the meaning of the term  $\mathcal{O}(\alpha_t\alpha_s)$  and similar specifications. Conventionally, these terms are used to indicate the order of loop corrections in terms of the couplings involved. For instance the term  $\mathcal{O}(\alpha_t\alpha_s)$  denotes a proportionality of the corrections to  $\alpha_t\alpha_s$ . Here  $\alpha_s$  is as usual defined as  $\alpha_s = g_s^2/4\pi$ , where  $g_s$  denotes the gauge coupling constant of  $SU(3)_C$ . Analogously,  $\alpha_t$  is given in terms of the top Yukawa coupling  $y_t$  by  $\alpha_t = y_t^2/4\pi$ . Both coupling constants,  $g_s$  and  $y_t$ , are large compared to the electroweak gauge couplings or the Yukawa couplings of other SM fermions, wherefore the corrections of  $\mathcal{O}(\alpha_t\alpha_s)$  are the dominant corrections at two-loop order. It should be noted, however, that the corrections to the trilinear Higgs couplings presented in this thesis are actually proportional to  $y_t\alpha_t$  and  $y_t\alpha_t\alpha_s$ . We will still denote them as the corrections of  $\mathcal{O}(\alpha_t)$  and  $\mathcal{O}(\alpha_t\alpha_s)$  to comply with the convention used in the literature and to emphasize their compatibility with the corrections of  $\mathcal{O}(\alpha_t)$  and  $\mathcal{O}(\alpha_t\alpha_s)$  to the Higgs boson masses.

The  $\mathcal{O}(\alpha_t\alpha_s)$  corrections are obtained in the *gaugeless* limit, where the electroweak gauge couplings  $g_1$  and  $g_2$  are neglected. Accordingly, also the electric charge  $e$  as well as the masses of the gauge bosons are set to zero, as they vanish for  $g_1, g_2 \rightarrow 0$ . However, care has to be taken performing the gaugeless limit correctly in ratios of vanishing quantities. For example, while  $M_W$ ,  $M_Z$  and  $e$  vanish separately, their ratios, e.g.  $M_W/M_Z = c_W \neq 0$  or  $M_W/e = v/2s_W$ , do not. This will be important in particular in the renormalization procedure to be discussed below. Besides the gauge bosons, all SM fermions apart from the top quark will be treated as massless. In particular, we will also consider the bottom quark as massless, which is consistent with neglecting corrections of  $\mathcal{O}(\alpha_b\alpha_s)$ , where  $\alpha_b = y_b^2/4\pi$  and  $y_b$  denotes the bottom Yukawa coupling.

Furthermore, we work in the limit of vanishing external momentum. Although we will use the Feynman diagrammatic approach, the results obtained in this approximation are equivalent to those obtained in the effective potential approach, where the external momenta are neglected by definition. This approximation is justified, if all contributing virtual particles are heavy as compared to the typical external momenta [40, 190, 237, 238]. Above the threshold of on-shell production of the loop particles, however, the loop integrals develop an imaginary

part, which is not captured in the effective potential approach, and the  $p^2 = 0$  approximation breaks down. Below, we will discuss in detail the applicability of this approximation for our purposes and consider its limitations.

In addition to the corrections of  $\mathcal{O}(\alpha_t\alpha_s)$  we will also determine the corrections of  $\mathcal{O}(\alpha_t)$ , which are the leading corrections at one-loop order. We will calculate these corrections subject to the same approximations outlined above, i.e. in the gaugeless limit and for vanishing external momentum. This will allow us to establish *effective trilinear Higgs self-couplings*, that is to say couplings incorporating the leading higher-order corrections defined in the limit of vanishing external momentum. We will use these effective couplings in order to compare the corrections of  $\mathcal{O}(\alpha_t)$  and of  $\mathcal{O}(\alpha_t\alpha_s)$ , calculated under identical approximations, and thus estimate the influence of higher-order corrections and the remaining theoretical uncertainty. This is interesting in particular for the trilinear coupling of three SM-like Higgs bosons, for which the effective couplings of  $\mathcal{O}(\alpha_t)$  are a good approximation of the full one-loop-corrected couplings (cf. Sec. 20.3). The reason behind our restriction to  $\mathcal{O}(\alpha_t)$  in the effective couplings at one-loop order is the fact that, at this order, only top quarks and their supersymmetric partners the stops appear as loop particles. These are sufficiently heavy in order for the  $p^2 = 0$  approximation to be valid for our purposes in Sec. 20.4, where we consider the trilinear Higgs coupling of three SM-like Higgs bosons.

In view of the above discussion, it is clear, however, that the approximation of vanishing external momentum cannot be justified in the calculation of the decay widths of heavy Higgs bosons with masses above the  $t\bar{t}$  threshold, where on-shell top pair production becomes possible. Therefore, we will include the full one-loop corrections with explicit momentum dependence when we discuss Higgs-to-Higgs decays in Sec. 20.5. Furthermore, we will ensure the  $t\bar{t}$ -resonance to be negligible for the two-loop results, such that the approximation of vanishing external momentum remains applicable at  $\mathcal{O}(\alpha_t\alpha_s)$ .

The two-loop-corrected effective trilinear Higgs self-couplings  $\Lambda_{ijk}^{\mathcal{O}(\alpha_t\alpha_s)}$  can be decomposed into three pieces

$$\Lambda_{ijk}^{\mathcal{O}(\alpha_t\alpha_s)} = \lambda_{ijk} + \Delta\lambda_{ijk}^{\mathcal{O}(\alpha_t)} + \Delta\lambda_{ijk}^{\mathcal{O}(\alpha_t\alpha_s)}. \quad (15.1)$$

Since the NMSSM comprises six neutral scalars in the Higgs sector, the indices of the couplings  $i, j, k$  take values  $\in \{1, \dots, 6\}$ . We have not yet specified a particular basis, as the structure of the couplings to be illustrated here is general. Hence, the indices can be interpreted as indicating mass or gauge eigenstates. The first term in Eq. (15.1) represents the tree-level coupling, whereas the second and the third term stand for the corrections of  $\mathcal{O}(\alpha_t)$  and  $\mathcal{O}(\alpha_t\alpha_s)$ , respectively. Both correction terms can be split up further according to

$$\Delta\lambda_{ijk}^{\mathcal{O}(\alpha_t)} = \Delta\lambda_{ijk}^{\mathcal{O}(\alpha_t),\text{virt}} + \Delta\lambda_{ijk}^{\mathcal{O}(\alpha_t),\text{ct}} \quad (15.2)$$

$$\Delta\lambda_{ijk}^{\mathcal{O}(\alpha_t\alpha_s)} = \Delta\lambda_{ijk}^{\mathcal{O}(\alpha_t\alpha_s),\text{virt}} + \Delta\lambda_{ijk}^{\mathcal{O}(\alpha_t\alpha_s),\text{virt}\otimes\text{ct}} + \Delta\lambda_{ijk}^{\mathcal{O}(\alpha_t\alpha_s),\text{ct}}. \quad (15.3)$$

For the  $\mathcal{O}(\alpha_t)$  corrections, the division corresponds to a neat separation into pure counterterm and pure virtual contributions, following the nomenclature introduced in Subs. 3.2.2. However, in the case of the  $\mathcal{O}(\alpha_t\alpha_s)$  corrections a mixed term appears, corresponding to contributions of one-loop diagrams of order  $\mathcal{O}(\alpha_t)$  with the insertion of a counterterm of  $\mathcal{O}(\alpha_s)$ . The other two terms respectively stand for the contributions of genuine two-loop diagrams and of pure counterterm diagrams, where the corresponding counterterms are of  $\mathcal{O}(\alpha_t\alpha_s)$ . Since we will dedicate an own chapter to the corrections of one-loop order, we also define the effective couplings of  $\mathcal{O}(\alpha_t)$

$$\Lambda_{ijk}^{\mathcal{O}(\alpha_t)} = \lambda_{ijk} + \Delta\lambda_{ijk}^{\mathcal{O}(\alpha_t)}. \quad (15.4)$$

The purpose of this chapter is to give a brief introduction to the NMSSM. In Sec. 16.1 we will exhibit its particle content and explain the notation used in the following. Furthermore, we will discuss the main motivations for studying the NMSSM. Afterwards, in Sec. 16.2, we will deal with the Lagrangian of the NMSSM, going into details of the Higgs sector (sections 16.3, 16.4) and the stop sector (Sec. 16.5), which will be needed for the subsequent chapters. Throughout, we will make considerable use of Refs. [36, 37, 48].

## 16.1. Motivations for and Particle Content of the NMSSM

We have already mentioned in Sec. 2.2, that in a supersymmetric model, all SM degrees of freedom have to receive a supersymmetric counterpart, together with which they form a supermultiplet. The members of a supermultiplet agree in all quantum numbers with the exception of the spin, which differs by a unit of  $1/2$  between the SM particles and their superpartners.

In the MSSM, the simplest realization of SUSY, each SM particle receives exactly one superpartner and, with the exception of a second Higgs doublet (cf. Sec. 2.2), no further degrees of freedom are added to the SM particle spectrum. As we will see below, although the MSSM is attractive due to its sparingness, there are strong motivations to extend its particle content by one further complex scalar singlet and its SUSY partner. The resulting model is called the Next-to-Minimal Supersymmetric Standard Model (NMSSM).

Within the NMSSM (and equally in the MSSM), the SM fermions are arranged into *chiral* supermultiplets. Each of the left- and right-handed components that was listed in Tab. 2.1 is assigned a complex scalar as superpartner, whose name is conventionally derived from the name of the SM fermion by prepending an “s”. Equally, the symbols for the superpartner fields are those of the corresponding SM fields decorated with a tilde. Like in the case of the SM fermions, the left-handed sfermions are grouped into  $SU(2)_L$ -doublets, whereas the right-handed sfermions are singlets under  $SU(2)_L$ . An overview of all SM fermions and their superpartners can be found in Tab. 16.1. By convention, the chiral supermultiplets are defined in terms of left-handed Weyl spinors. Following this custom, we list in the table the conjugates of the right-handed fermions, which transform as left-handed spinors. We also assign a handedness to the sfermions in Tab. 16.1. It is important to note, however, that this does not refer to a property of the sfermions themselves, which, as scalar particles, cannot

be allotted a chirality, but derives from their respective SM partners. Furthermore, we introduce a symbol for each of the chiral supermultiplets as a whole, given by the notation of the involved SM field, adorned with a hat.

Also the two Higgs doublets as well as the NMSSM singlet reside in chiral supermultiplets. As they are scalars, their superpartners have to be spin-1/2 Weyl fermions. In the case of the two Higgs doublets, the latter form left-handed  $SU(2)_L$  doublets and are denoted as *higgsinos*. The Higgs doublets are conventionally designated by the type of quark they couple to and thus endow with a mass, i.e. by  $H_u$  and  $H_d$ , and the higgsinos are correspondingly denoted as  $\tilde{H}_u$  and  $\tilde{H}_d$ . In this context, let us remind the reader of the fact, that the Higgs sector of the MSSM constitutes a 2HDM of type II. The singlet, which does not couple to any SM particle outside the Higgs sector, is symbolized by  $S$ , its superpartner, the singlino, by  $\tilde{S}$ .

chiral supermultiplets		spin 0	spin 1/2	$(SU(3)_C \otimes SU(2)_L \otimes U(1)_Y)$
squarks, quarks	$\hat{Q}$	$\tilde{Q}_L = (\tilde{u}_L, \tilde{d}_L)^T$	$Q_L = (u_L, d_L)^T$	$(\mathbf{3}, \mathbf{2}, \frac{1}{6})$
	$\hat{u}$	$\tilde{u}_R^*$	$u_R^\dagger$	$(\bar{\mathbf{3}}, \mathbf{1}, -\frac{2}{3})$
	$\hat{d}$	$\tilde{d}_R^*$	$d_R^\dagger$	$(\bar{\mathbf{3}}, \mathbf{1}, \frac{1}{3})$
sleptons, leptons	$\hat{L}$	$\tilde{L}_L = (\tilde{\nu}_L, \tilde{e}_L)^T$	$L_L = (\nu_L, e_L)^T$	$(\mathbf{1}, \mathbf{2}, -\frac{1}{2})$
	$\hat{e}$	$\tilde{e}_R^*$	$e_R^\dagger$	$(\mathbf{1}, \mathbf{1}, 1)$
Higgs, higgsinos	$\hat{H}_u$	$H_u = (H_u^+, H_u^0)^T$	$\tilde{H}_u = (\tilde{H}_u^+, \tilde{H}_u^0)^T$	$(\mathbf{1}, \mathbf{2}, \frac{1}{2})$
	$\hat{H}_d$	$H_d = (H_d^+, H_d^0)^T$	$\tilde{H}_d = (\tilde{H}_d^+, \tilde{H}_d^0)^T$	$(\mathbf{1}, \mathbf{2}, -\frac{1}{2})$
	$\hat{S}$	$S$	$\tilde{S}$	$(\mathbf{1}, \mathbf{1}, 0)$

**Table 16.1.:** Chiral supermultiplets of the NMSSM. All fermions and sfermions come in three generations. The last column shows the transformation properties of the particles w.r.t. the gauge groups, as introduced in Sec. 2.1.

Unlike the matter particles, the gauge bosons have to be assigned to *vector supermultiplets*. As they transform under the adjoint representation of the corresponding gauge group, their superpartners, which are spin-1/2 Weyl fermions, called *gauginos*, must be vector fermions, i.e. their left- and right-handed components have to behave identical under gauge transformations. This is due to the fact that the adjoint representation of a gauge group is its own conjugate. Like the  $W$  bosons, their superpartners, the *winos* form a triplet under  $SU(2)_L$  whereas the *bino*, the superpartner of the  $B$ -boson, comes as a singlet. The gauge bosons and their superpartners are summarized in Tab. 16.2. Note that in the case of the  $W$ -bosons and winos it is convenient to quote states of definite charge, given by  $W^\pm = \frac{1}{\sqrt{2}}(W_1 \mp iW_2)$ ,  $W^0 = W_3$  and analogous for the winos, instead of the triplet components.

In the discussion of the 2HDM, we have already become acquainted with the fact that particles of identical quantum numbers mix. The NMSSM spectrum comprises a wealth of particles with this property such that the gauge eigenstates listed in Tabs. 16.1 and 16.2 do not correspond to the physical mass eigenstates. A closer look at the tables reveals that the charged higgsinos can combine with the charged winos to form the *charginos*, while the neutral higgsinos can combine with the singlino, the bino and neutral wino to form the *neutralinos*. Due to the additional singlino, the number of neutralinos is enhanced by one compared to the MSSM, resulting in a total of five neutralinos.

Mixing also takes place among the squarks and sleptons. Strictly speaking, all six squark

gauge supermultiplets	spin 1	spin 1/2	$(SU(3)_C \otimes SU(2)_L \otimes U(1)_Y)$
gluons, gluinos	$g$	$\tilde{g}$	$(\bar{\mathbf{8}}, \mathbf{1}, 0)$
$W$ bosons, winos	$W^\pm, W^0$	$\tilde{W}^\pm, \tilde{W}^0$	$(\bar{\mathbf{1}}, \mathbf{3}, 0)$
$B$ bosons, bino	$B$	$\tilde{B}$	$(\bar{\mathbf{1}}, \mathbf{1}, 0)$

**Table 16.2.:** Gauge supermultiplets of the NMSSM. The last column shows the transformation properties of the particles w.r.t. the gauge groups, as introduced in Sec. 2.1.

species of one type, all six charged sleptons and all three sneutrinos respectively share identical quantum numbers and thus are capable of mixing. In practice, however, flavor violation in the squark sector is usually not considered, such that inter-generational mixing does not take place. Furthermore, mixing is often supposed to be negligible for the first two generations and only the third generation sfermions are considered to be strongly mixing in pairs [48]. This approximation is justified, as the mixing between left- and right-handed sfermions is controlled by the Yukawa couplings of the corresponding fermions. Thus, the physical mass eigenstates of e.g. the stops are given by  $(\tilde{t}_1, \tilde{t}_2)$ , where  $\tilde{t}_1$  and  $\tilde{t}_2$  are linear combinations of  $\tilde{t}_L$  and  $\tilde{t}_R$ . Analogous relations hold for the sbottoms and staus.

Yet, most important for our purposes is the mixing in the Higgs sector. This will be dealt with in detail in Sec. 16.3.

The core of any SUSY model is given by its *superpotential*  $\hat{W}$ . Once the superpotential is specified and the particle content and gauge transformation properties of the supermultiplets are known, the supersymmetric gauge-invariant Lagrangian of the model and the corresponding couplings, mass and tadpole terms can be derived. Only those parts of the Lagrangian which explicitly break SUSY (denoted by  $\mathcal{L}_{\text{soft}}$ ) or gauge invariance ( $\mathcal{L}_{\text{gf}}$  and  $\mathcal{L}_{\text{ghost}}$ ) cannot directly be obtained from  $\hat{W}$  and the transformation properties of the supermultiplets.

In order to motivate the study of the NMSSM, we will first consider the MSSM superpotential, as it already reveals one of the major shortcomings of the MSSM. Using the superfield notation defined above, it is given by

$$\hat{W}_{\text{MSSM}} = \hat{u}Y^U \left( \hat{Q}^T \epsilon \hat{H}_u \right) - \hat{d}Y^D \left( \hat{Q}^T \epsilon \hat{H}_d \right) - \hat{e}Y^E \left( \hat{L}^T \epsilon \hat{H}_d \right) + \mu \left( \hat{H}_u^T \epsilon \hat{H}_d \right). \quad (16.1)$$

As in Sec. 5.4, the Yukawa couplings  $Y^J$  are  $3 \times 3$  matrices in flavor space and  $\epsilon$  denotes the totally anti-symmetric tensor in 2 dimensions. For brevity we have suppressed all gauge and family indices. Unlike in the case of the 2HDM, the Yukawa matrices will be considered as diagonal. Furthermore, the quark fields can always be redefined in such a way that the Yukawa couplings are real.

The dimensionful parameter  $\mu$  appearing here is indispensable for the process of EWSB since it assumes the role of the Higgs mass term in the scalar potential, derived from the superpotential. For phenomenological reasons  $\mu$  must be of the order of the electroweak scale. However, since  $\mu$  is a parameter of the symmetric phase and as such unrelated to EWSB, there is no theoretical reason for why this parameter should be so small as compared e.g. to the Planck mass  $M_{\text{Pl}}$ . This so-called  $\mu$ -problem is often considered as the main motivation for the NMSSM. Within the latter, the  $\mu$ -term is replaced by the expression

$$\lambda \hat{S} \left( \hat{H}_u^T \epsilon \hat{H}_d \right), \quad (16.2)$$

where  $\lambda$  is a dimensionless complex coupling. In this way, the introduction of a dimensionful parameter in the superpotential is avoided and the necessary  $\mu$  term in the scalar potential

is generated only when the scalar component of  $\hat{S}$  acquires a vev. Hence, the  $\mu$ -parameter is replaced by the effective parameter  $\mu_{\text{eff}} = \lambda\langle S \rangle$ , which is generated dynamically in the process of EWSB and is therefore automatically of the desired order.

While this replacement of the  $\mu$ -term solves the  $\mu$ -problem, it leads to an invariance of the superpotential under a global phase transformation, i.e. the superpotential gains an accidental Peccei-Quinn (PQ) symmetry  $U(1)_{PQ}$  [239–241]. Once the Higgs bosons acquire their vevs, this PQ symmetry is spontaneously broken, resulting due to the Goldstone theorem in the occurrence of a massless Peccei-Quinn axion. In order to avoid such an axion, whose existence is subject to severe experimental constraints, the PQ symmetry has to be broken explicitly by the introduction of the additional term

$$\frac{1}{3}\kappa\hat{S}^3 \quad (16.3)$$

into the superpotential. Here  $\kappa$  is a complex dimensionless parameter.

In its most general form, the NMSSM superpotential could also include the following non-scale-invariant terms

$$\mu' \left( \hat{H}_u^T \epsilon \hat{H}_d \right) + \tau_S \hat{S} + \mu'' \hat{S}^2. \quad (16.4)$$

However, the additional dimensionful parameters  $\mu'$ ,  $\mu''$  and  $\tau_S$  in these terms would obviously reintroduce the  $\mu$ -problem. Therefore, in most studies of the NMSSM, a  $Z_3$ -symmetry is imposed on the superpotential, which prohibits the occurrence of these terms, resulting in the following NMSSM superpotential

$$\hat{W}_{\text{NMSSM}} = \hat{u}Y^U \left( \hat{Q}^T \epsilon \hat{H}_u \right) - \hat{d}Y^D \left( \hat{Q}^T \epsilon \hat{H}_d \right) - \hat{e}Y^E \left( \hat{L}^T \epsilon \hat{H}_d \right) + \lambda \hat{S} \left( \hat{H}_u^T \epsilon \hat{H}_d \right) + \frac{1}{3}\kappa\hat{S}^3. \quad (16.5)$$

In the subsequent discussion, we will follow the usual convention to refer to the  $Z_3$ -invariant NMSSM as *the NMSSM*. As a side remark, note that an exact  $Z_3$ -symmetry, which is spontaneously broken by the vev of the singlet  $S$ , would lead to the formation of domain walls in the early universe, spoiling the cosmic microwave background. This can be avoided by the introduction of certain higher dimensional operators, which explicitly break the  $Z_3$ -symmetry, whose effect on low energy scales is, however, negligible. We do not go into further details here and will henceforth assume the domain-wall problem to be solved in this way, pointing to Ref. [36] and the references therein for more information.

Although the solution of the  $\mu$ -problem is often referred to as the primary motivation for the NMSSM, there are other benefits coming along with the introduction of a further singlet.

One is connected to the mass of the SM-like Higgs boson. In the MSSM, there is an upper bound on the tree-level mass of the lightest CP-even Higgs boson  $h_1$ , given by

$$(m_{h_1}^{\text{MSSM}})^2 < M_Z^2 c_{2\beta}^2. \quad (16.6)$$

Thus, in order to accommodate a Higgs mass of 125 GeV, huge radiative corrections are necessary. As the dominant corrections to the Higgs mass arise from stop and top loops, this in turn requires rather large stop masses. Yet, a too strong violation of the the degeneracy between tops and stops endangers the main motivation for SUSY itself, which is the solution of the hierarchy problem (cf. Sec. 2.2).

In the NMSSM the upper bound in Eq. (16.6) is alleviated by an additional contribution coming from the coupling  $\lambda$ , which yields

$$(m_{h_1}^{\text{NMSSM}})^2 < M_Z^2 c_{2\beta}^2 + \frac{|\lambda|^2 v^2}{2} s_{2\beta}^2. \quad (16.7)$$

Owing to this additional term, a value of 125 GeV can more easily be realized, requiring less enhancement of the mass through radiative corrections.

Another motivation for studying the NMSSM is the fact that, unlike the MSSM, it allows, in its complex version, for CP-violation in the Higgs sector at tree level. As discussed in the introduction 2.1, a sufficient amount of CP-violation is necessary in order to fulfill one of the three Sakharov criteria for a successful baryogenesis, i.e. the generation of the baryon-antibaryon asymmetry of the universe [50].

Furthermore, the additional cubic terms in the NMSSM Higgs potential, which are absent in the MSSM, allow for an easier realization of a strong electroweak phase transition in the early universe, which constitutes one of the favourite mechanisms to explain baryogenesis (see Ref. [36] and references therein).

Beyond these theoretical advantages, the NMSSM offers a rich and interesting phenomenology. For instance, the NMSSM allows for light Higgs bosons with masses below the LEP bounds, evading the exclusion limits by a substantial singlet admixture [242, 243]. The enlarged Higgs sector also offers a huge variety of possible Higgs-to-Higgs decays, which can result in interesting and exotic final states [243].

In the context of dark matter searches, the NMSSM is often discussed due to its capability of furnishing light neutralino dark matter candidates with masses around 10 GeV [244–247], as favoured by some experiments [248–253]<sup>1</sup>.

All the given examples clearly show that there is a strong motivation to accept the enhancement of the complexity caused by adding further degrees of freedom to the MSSM spectrum.

## 16.2. The Lagrangian of the NMSSM

We now want to have a closer look at the Lagrangian of the NMSSM. As we have mentioned above, its supersymmetric, gauge-invariant part, denoted by  $\mathcal{L}_{\text{SUSY}}$ , directly follows from the superpotential, specified in Eq. (16.5) and the transformation properties of the superfields under gauge transformations. Adding the SUSY and gauge invariance violating terms, the Lagrangian of the NMSSM is given by

$$\mathcal{L}_{\text{NMSSM}} = \mathcal{L}_{\text{SUSY}} + \mathcal{L}_{\text{soft}} + \mathcal{L}_{\text{gf}} + \mathcal{L}_{\text{ghost}}. \quad (16.8)$$

Both  $\mathcal{L}_{\text{gf}}$  and  $\mathcal{L}_{\text{ghost}}$  are identical to the equivalent terms of the 2HDM, stated in Sec. 5.5.  $\mathcal{L}_{\text{SUSY}}$  comprises the kinetic terms for all NMSSM particles, the Yukawa interactions and (part of) the scalar potential. Finally,  $\mathcal{L}_{\text{soft}}$  incorporates all possible soft-SUSY-breaking terms, which are necessary in order to prevent SUSY from being directly excluded by the non-observation of any SM superpartners. Since the mechanism of SUSY breaking is unknown, we have to include in  $\mathcal{L}_{\text{soft}}$  all possible terms which possess couplings of positive mass dimension and are compatible with matter parity (cf. Sec. 2.2). Under these constraints, the soft-SUSY-breaking Lagrangian of the NMSSM takes the form

$$\begin{aligned} -\mathcal{L}_{\text{soft}} = & m_{\tilde{Q}}^2 \tilde{Q}^\dagger \tilde{Q} + m_{\tilde{u}_R}^2 |\tilde{u}_R|^2 + m_{\tilde{d}_R}^2 |\tilde{d}_R|^2 + \left( A_u Y^U \tilde{u}_R^* (\tilde{Q}^T \epsilon H_u) - A_d Y^D \tilde{d}_R^* (\tilde{Q}^T \epsilon H_d) + \text{h.c.} \right) \\ & + m_{\tilde{L}}^2 \tilde{L}^\dagger \tilde{L} + m_{\tilde{e}_R}^2 |\tilde{e}_R|^2 - \left( A_e Y^E \tilde{e}_R^* (\tilde{L}^T \epsilon H_d) + \text{h.c.} \right) \\ & + m_{H_u}^2 H_u^\dagger H_u + m_{H_d}^2 H_d^\dagger H_d + m_S^2 |S|^2 + \left( A_\lambda \lambda (H_u^T \epsilon H_d) S + \frac{1}{3} A_\kappa \kappa S^3 + \text{h.c.} \right) \\ & + \frac{1}{2} \left( M_1 \tilde{B} \tilde{B} + M_2 \tilde{W}^i \tilde{W}^i + M_3 \tilde{g} \tilde{g} \right). \end{aligned} \quad (16.9)$$

<sup>1</sup>Note, however, that there is tension between the results of these experiments and moreover they conflict with the results of LUX XENON [254] and [255].

Many new parameters are introduced by these SUSY violating terms. The first two rows of Eq. (16.9) comprise the soft breaking terms for the squark and slepton sector, containing the soft-SUSY-breaking mass parameters  $m_{\tilde{Q}}, m_{\tilde{u}_R}, m_{\tilde{d}_R}, m_{\tilde{L}}, m_{\tilde{e}_R}$  and trilinear couplings  $A_u, A_d, A_e$ . Analogously, the third row incorporates the soft breaking masses and trilinear couplings  $m_{H_u}, m_{H_d}, m_S$  and  $A_\lambda, A_\kappa$  for the Higgs sector, while the last row holds the soft breaking gaugino masses  $M_1, M_2, M_3$ . In the case of the sfermions, the soft breaking mass terms and trilinear couplings are in general complex  $3 \times 3$  matrices in family space. However, like the Yukawa matrices, they will be considered as diagonal in the following. Due to the hermiticity of the mass matrices, the entries of the resulting diagonal soft-SUSY-breaking mass terms have to be real. By the same token, also the soft-SUSY-breaking masses of the Higgs and the gaugino sectors are real parameters, whereas the trilinear couplings  $A_\lambda$  and  $A_\kappa$  are complex in general.

Together with parts of  $\mathcal{L}_{\text{SUSY}}, \mathcal{L}_{\text{soft}}$  constitutes the scalar potential of the NMSSM. Unlike in the SM or the 2HDM, the scalar sector comprises particles not being part of the Higgs sector, viz. the scalar superpartners of the SM fermions. Yet, in the following we will mainly concentrate on the Higgs sector and therefore only discuss the corresponding Higgs potential in more detail. Concerning the sfermion contributions to the scalar potential, we content ourselves with the remark that the presence of additional charged and colored scalars in the potential poses the danger of the development of charge and color breaking minima, which have to be avoided, imposing limits on the NMSSM parameters [36, 37]. A comprehensive treatment of the full NMSSM scalar potential can be found e.g. in Ref. [36].

### 16.3. The NMSSM Higgs Potential

The NMSSM Higgs potential  $V_H$  is composed of terms derived from the superpotential and of terms entering through  $\mathcal{L}_{\text{soft}}$ . Assembling all pieces,  $V_H$  is given by

$$\begin{aligned} V_H = & |\lambda|^2 |S|^2 \left( H_u^\dagger H_u + H_d^\dagger H_d \right) + |\lambda (H_u^T \epsilon H_d) + \kappa S^2|^2 \\ & + \frac{1}{2} g_2^2 \left| H_u^\dagger H_d \right|^2 + \frac{1}{8} (g_1^2 + g_2^2) \left( H_u^\dagger H_u - H_d^\dagger H_d \right)^2 \\ & + m_{H_u}^2 H_u^\dagger H_u + m_{H_d}^2 H_d^\dagger H_d + m_S^2 |S|^2 + \left( A_\lambda \lambda (H_u^T \epsilon H_d) S + \frac{1}{3} A_\kappa \kappa S^3 + h.c. \right). \end{aligned} \quad (16.10)$$

Like in the case of the 2HDM, we can expand the two Higgs doublets as well as the singlet  $S$  around their vevs and split the neutral components into a CP-even and a CP-odd part

$$H_d = \begin{pmatrix} H_d^0 \\ h_d^- \end{pmatrix} = \begin{pmatrix} \frac{v_d + h_d + ia_d}{\sqrt{2}} \\ h_d^- \end{pmatrix}, \quad H_u = \begin{pmatrix} h_u^+ \\ H_u^0 \end{pmatrix} = e^{i\varphi_u} \begin{pmatrix} h_u^+ \\ \frac{v_u + h_u + ia_u}{\sqrt{2}} \end{pmatrix}, \quad (16.11)$$

$$S = e^{i\varphi_s} \frac{v_s + h_s + ia_s}{\sqrt{2}}. \quad (16.12)$$

Due to the fact that we consider the *complex* NMSSM, we have to account for a possible phase difference between the two doublets and between the doublets and the singlet. Since only relative phases play a role, these can always be adjusted such that one of the scalars,  $H_d$  in our case, comes without a phase. Note that the complex phase  $\varphi_u$  enters the expressions for all up-type quark masses. In order to keep the Yukawa couplings and the quark masses real, we redefine the left- and right-handed up-type quark fields, according to

$$u_L \rightarrow e^{-i\varphi_u/2} u_L, \quad u_R \rightarrow e^{i\varphi_u/2} u_R, \quad (16.13)$$

where as before,  $u$  represents  $u, c,$  and  $t$ . This redefinition leads to the appearance of the phase  $\varphi_u$  in all couplings involving only one up-type quark.

Inserting the expansions in Eqs. 16.11 and 16.12 into Eq. (16.10), the Higgs potential can be cast into the following form (summation over recurring indices implied)

$$V_H = \frac{1}{2} (\mathcal{M}_\phi)_{ij} \phi_i \phi_j + (\mathcal{M}_{\phi^\pm})_{ij} \phi_i^+ \phi_j^- + (t_\phi)_i \phi_i + \lambda_{\phi_i \phi_j \phi_k} \phi_i \phi_j \phi_k + \lambda_{\phi_i^+ \phi_j^- \phi_k}^\pm \phi_i^+ \phi_j^- \phi_k + V_H^{\phi^4} + V_H^{\text{const}}, \quad (16.14)$$

with

$$\phi = (h_d, h_u, h_s, a_d, a_u, a_s)^T \quad \text{and} \quad \phi^\pm = ((h_d^\mp)^*, h_u^\pm)^T. \quad (16.15)$$

In this representation we have collected the neutral scalar components as well as the charged ones in the vectors  $\phi$  and  $\phi^\pm$ , respectively. As a result, the complex coefficients of the terms bilinear in the scalar fields are grouped into the  $6 \times 6$  matrix  $\mathcal{M}_\phi$  and the  $2 \times 2$  matrix  $\mathcal{M}_{\phi^\pm}$ , which constitute the neutral and charged Higgs mass matrices in the gauge basis. Furthermore, the terms linear in the scalar fields, the tree-level tadpoles, are gathered in the vector  $t_\phi$ .  $\lambda_{\phi_i \phi_j \phi_k}$  denotes the trilinear coupling between the three neutral scalars  $\phi_i$ ,  $\phi_j$ ,  $\phi_k$ , while those connecting one neutral scalar and two charged ones are summarized in  $\lambda_{\phi_i^+ \phi_j^- \phi_k}^\pm$ . All quartic scalar couplings are collected in  $V_H^{\phi^4}$  and irrelevant constant terms in  $V_H^{\text{const}}$ .

As in the 2HDM, the terms linear in the scalar fields have to vanish in the minimum of the potential, i.e. it must hold

$$\frac{\partial V_H}{\partial \phi_i} = (t_\phi)_i \Big|_{\langle H_u \rangle = v_u, \langle H_d \rangle = v_d, \langle S \rangle = v_s} = 0, \quad i = 1, \dots, 6. \quad (16.16)$$

These are six equations, one for each of the components of the vector  $\phi$ . Unlike in the 2HDM, the MSSM or the CP-conserving NMSSM, the terms linear in the pseudoscalar components do not vanish trivially and lead to additional tadpole conditions. Due to the important role the tadpoles play in the renormalization procedure, we will again keep the tadpole parameters  $(t_\phi)_i$  explicit and set them to zero only after renormalization has been performed. Expressed in terms of the parameters of the Higgs potential and the vevs, the six tadpole parameters are given by

$$t_{h_d} = \frac{1}{2} |\lambda| \left( -\sqrt{2} v_u v_s |A_\lambda| c_{\varphi_x} + |\lambda| v_d (v_u^2 + v_s^2) - |\kappa| v_s^2 v_u c_{\varphi_y} \right) + \frac{1}{8} (g_1^2 + g_2^2) v_d (v_d^2 - v_u^2) + m_{H_d}^2 v_d, \quad (16.17)$$

$$t_{h_u} = \frac{1}{2} |\lambda| \left( -\sqrt{2} v_d v_s |A_\lambda| c_{\varphi_x} + |\lambda| v_u (v_d^2 + v_s^2) - |\kappa| v_s^2 v_d c_{\varphi_y} \right) + \frac{1}{8} (g_1^2 + g_2^2) v_u (v_u^2 - v_d^2) + m_{H_u}^2 v_u, \quad (16.18)$$

$$t_{h_s} = \frac{1}{2} v_s \left( \sqrt{2} v_s |\kappa| |A_\kappa| c_{\varphi_z} + |\lambda|^2 (v_d^2 + v_u^2) - 2 v_d v_u |\kappa| |\lambda| c_{\varphi_y} + 2 |\kappa|^2 v_s^2 \right) - \frac{1}{\sqrt{2}} v_d v_u |\lambda| |A_\lambda| c_{\varphi_x} + m_S^2 v_s, \quad (16.19)$$

$$t_{a_d} = \frac{1}{\sqrt{2}} v_u v_s |\lambda| |A_\lambda| s_{\varphi_x} + \frac{1}{2} v_s^2 v_u |\kappa| |\lambda| s_{\varphi_y}, \quad (16.20)$$

$$t_{a_u} = \frac{1}{\sqrt{2}} v_d v_s |\lambda| |A_\lambda| s_{\varphi_x} + \frac{1}{2} v_s^2 v_d |\kappa| |\lambda| s_{\varphi_y}, \quad (16.21)$$

$$t_{a_s} = \frac{1}{\sqrt{2}} v_d v_u |\lambda| |A_\lambda| s_{\varphi_x} - \frac{1}{\sqrt{2}} v_s^2 |\kappa| |A_\kappa| s_{\varphi_z} - v_d v_u v_s |\kappa| |\lambda| s_{\varphi_y}, \quad (16.22)$$

where we have used the notation  $(t_\phi)_i \equiv t_{\phi_i}$ . As can directly be read off,  $t_{a_d}$  and  $t_{a_u}$  are not linearly independent, wherefore the total amount of tadpole conditions is reduced to five. Subsequently,  $t_{a_d}$  will be considered as independent,  $t_{a_u}$  as dependent. In the expressions Eqs. 16.17 - 16.22, we have introduced the abbreviations  $\varphi_x$ ,  $\varphi_y$  and  $\varphi_z$  for the following linear combinations of complex phases

$$\varphi_x = \varphi_u + \varphi_s + \varphi_\lambda + \varphi_{A_\lambda}, \quad (16.23)$$

$$\varphi_y = \varphi_u - 2\varphi_s + \varphi_\lambda - \varphi_\kappa, \quad (16.24)$$

$$\varphi_z = 3\varphi_s + \varphi_\kappa + \varphi_{A_\kappa}, \quad (16.25)$$

where the phases of the parameters are defined via  $\lambda = e^{i\varphi_\lambda}|\lambda|$  and analogously for  $\kappa$ ,  $A_\lambda$  and  $A_\kappa$ . These linear combinations turn out to be the only ones appearing in the Higgs sector. The five linearly independent tadpole parameters can be utilized to eliminate the soft-SUSY-breaking masses  $m_{H_d}$ ,  $m_{H_u}$  and  $m_S$  and two of the complex phases, for which we choose  $\varphi_x$  and  $\varphi_z$ .

In the complex NMSSM, all six neutral scalar degrees of freedom collected in  $\phi$  can mix. Therefore,  $\mathcal{M}_\phi$ , the mass matrix in the gauge basis, is a  $6 \times 6$  matrix. Yet, it is instructive to decompose  $\mathcal{M}_\phi$  into four  $3 \times 3$  blocks, according to

$$\mathcal{M}_\phi = \begin{pmatrix} \mathcal{M}_{hh} & \mathcal{M}_{ha} \\ (\mathcal{M}_{ha})^T & \mathcal{M}_{aa} \end{pmatrix}. \quad (16.26)$$

Considering the off-diagonal blocks

$$\mathcal{M}_{ha} = \frac{1}{2}|\kappa||\lambda|s_{\varphi_y} \begin{pmatrix} 0 & 0 & v_u v_s \\ 0 & 0 & v_d v_s \\ -3v_u v_s & -3v_d v_s & 4v_d v_u \end{pmatrix}, \quad (16.27)$$

it becomes obvious, that in the CP-conserving case, where  $\varphi_y = 0$ , the mass matrix decomposes into a purely CP-even  $3 \times 3$ -block and a purely CP-odd  $3 \times 3$ -block and no mixing between CP-even and CP-odd components takes place. Note that the tadpole conditions have already been applied in Eq. (16.27).

Diagonalizing the mass matrix provides us with the rotation matrix  $R$ , which performs the transformation between the gauge basis  $\phi$  and the tree-level mass basis  $\Phi$ , according to

$$\Phi_i = R_{ij}\phi_j, \quad \text{with} \quad \Phi^T = (h_1, h_2, h_3, h_4, h_5, G_0). \quad (16.28)$$

Here and in the following, we implicitly assume summation over recurring indices. Within the vector  $\Phi$ , the five tree-level mass eigenstates  $h_i$  are arranged by their mass in ascending order and the neutral Goldstone boson  $G_0$  has been singled out. For later convenience we split up the rotation into two steps, according to

$$R_{ik} = R_{ij}^{h,6} R_{jk}^{\text{GB}}, \quad (16.29)$$

where  $R_{jk}^{\text{GB}}$  isolates the Goldstone boson in the gauge basis

$$(h_d, h_u, h_s, a, a_s, G_0)^T = R^{\text{GB}}\phi, \quad (16.30)$$

$$\text{with} \quad R^{\text{GB}} = \begin{pmatrix} \mathbb{1}_{3 \times 3} & \mathbb{0}_{3 \times 3} \\ \mathbb{0}_{3 \times 3} & \begin{pmatrix} s_{\beta_n} & c_{\beta_n} & 0 \\ 0 & 0 & 1 \\ -c_{\beta_n} & s_{\beta_n} & 0 \end{pmatrix} \end{pmatrix}.$$

The rotation angle  $\beta_n$  appearing here coincides at tree-level with  $\beta_p$ , defined as  $\tan(\beta_p) = \frac{v_u}{v_d}$ . Furthermore, we introduce the *reduced* gauge and tree-level mass bases  $\phi^{h,T} = (h_d, h_u, h_s, a, a_s)$  and  $\Phi^{h,T} = (h_1, h_2, h_3, h_4, h_5)$ , connected via

$$\Phi_i^h = R_{ij}^h \phi_j^h, \quad \text{with} \quad R^{h,6} = \begin{pmatrix} R^h & 0 \\ 0 & 1 \end{pmatrix}, \quad i, j = 1, \dots, 5. \quad (16.31)$$

We can proceed in the same way for the charged Higgs sector. Diagonalizing the mass matrix  $\mathcal{M}_{\phi^\pm}$  with the rotation matrix

$$R^c = \begin{pmatrix} -c_{\beta_c} & s_{\beta_c} \\ s_{\beta_c} & c_{\beta_c} \end{pmatrix}, \quad (16.32)$$

provides us with an expression for the mass of the charged Higgs boson  $H^\pm$

$$m_{H^\pm}^2 = \frac{1}{2} \frac{|\lambda| v_s}{s_\beta c_\beta} \left( \sqrt{2} |A_\lambda| c_{\varphi_x} + |\kappa| v_s c_{\varphi_y} \right) - \frac{1}{4} v^2 (2|\lambda|^2 - g_2^2) \quad (16.33)$$

and furthermore leads us to the tree-level mass basis

$$\Phi^\pm = \begin{pmatrix} G^\pm \\ H^\pm \end{pmatrix} = R^c \begin{pmatrix} (h_d^\mp)^* \\ h_u^\pm \end{pmatrix}. \quad (16.34)$$

Here  $H^\pm$  and  $G^\pm$  denote the charged Higgs mass eigenstate and Goldstone boson, respectively. Like in the case of  $\beta_n$ , at tree-level the identity  $\beta_c = \beta_p$  holds. In the following, we will not distinguish between  $\beta_p$ ,  $\beta_n$  and  $\beta_c$  and denote all three of them as  $\beta$ . However, it should be kept in mind, that care has to be taken during the renormalization procedure, as only  $\beta_p$  receives a counterterm in our scheme, to be defined below.

The calculations presented in the following sections will throughout be performed either in the mass or in the gauge basis, which are related by the rotation matrices  $R$  and  $R^c$ . We will refer to the (loop-corrected) neutral trilinear Higgs self-couplings in the gauge basis as  $\Lambda_{\phi_i \phi_j \phi_k}$  and to those in the tree-level mass basis as  $\Lambda_{h_i h_j h_k}$ . At tree level, the former can directly be obtained by a differentiation of  $V_H$ , according to

$$\lambda_{\phi_i \phi_j \phi_k} = - \frac{\partial V_H}{\partial \phi_i \partial \phi_j \partial \phi_k}. \quad (16.35)$$

The corresponding couplings in the tree-level mass basis are then found by a transformation with  $R$

$$\lambda_{h_i h_j h_k} = R_{ii'} R_{jj'} R_{kk'} \lambda_{\phi_{i'} \phi_{j'} \phi_{k'}}. \quad (16.36)$$

## 16.4. Independent Parameters of the NMSSM Higgs Potential

In the course of our calculation, we will have to renormalize the whole NMSSM Higgs sector. For this purpose, it is indispensable to determine the number of independent parameters present in the Higgs sector and subsequently to specify a set of parameters, that will be treated as independent during the calculation. Starting from Eq. (16.10), we encounter the following set of parameters in the Higgs sector

$$g_1, g_2, v_d, v_u, v_s, \kappa, \lambda, A_\kappa, A_\lambda, m_{H_d}^2, m_{H_u}^2, m_S^2, \varphi_u, \varphi_s. \quad (16.37)$$

We have already mentioned the fact, that the linear combinations of the complex phases stated in Eqs. 16.23 - 16.25 are the only ones encountered in the Higgs sector and furthermore, two of

them can be eliminated together with  $m_{H_u}^2$ ,  $m_{H_d}^2$  and  $m_S^2$  in favour of five tadpole parameters. Concerning the remaining parameters, we first can trade  $g_1$ ,  $g_2$ ,  $v_u$  and  $v_d$  for  $M_W^2$ ,  $M_Z^2$ ,  $e$  and  $\tan\beta$ , like in the case of the 2HDM. Moreover, Eq. (16.33) can be used to eliminate  $|A_\lambda|$  in terms of  $m_{H^\pm}^2$ . However, due to the complication of five neutral Higgs bosons mixing with each other, it is recommendable not to try and use any of the neutral Higgs masses as independent parameter, but instead adhere to the original parameters of the potential. Altogether, the resulting set of independent parameters is hence given by

$$\boxed{e, M_W^2, M_Z^2, m_{H^\pm}^2, t_{h_d}, t_{h_u}, t_{h_s}, t_{a_d}, t_{a_s}, \tan\beta, v_s, |\kappa|, |\lambda|, |A_\kappa|, \varphi_y}. \quad (16.38)$$

## 16.5. The Stop Sector of the NMSSM

For the calculation of the corrections of order  $\mathcal{O}(\alpha_s\alpha_t)$ , we also need to renormalize the NMSSM top and stop sector. To this end we have to determine the set of independent parameters entering through this sector. The top sector is identical to the one of the SM and introduces only one new parameter, the mass of the top quark  $m_t$ .

Concerning the stop sector, the situation is complicated by the fact, that we have to take into account mixing between the two stop species (cf. Sec. 16.1). In the gaugeless limit, i.e. neglecting all terms proportional to the electroweak gauge couplings, the corresponding stop mass matrix is given by

$$\mathcal{M}_{\tilde{t}} = \begin{pmatrix} m_{\tilde{Q}_3}^2 + m_t^2 & m_t \left( A_t^* e^{-i\varphi_u} - \frac{\mu_{\text{eff}}}{\tan\beta} \right) \\ m_t \left( A_t e^{i\varphi_u} - \frac{\mu_{\text{eff}}^*}{\tan\beta} \right) & m_{\tilde{t}_R}^2 + m_t^2 \end{pmatrix}, \quad (16.39)$$

where  $m_{\tilde{Q}_3}$ ,  $m_{\tilde{t}_R}$  and  $A_t$  are the soft-SUSY-breaking masses and trilinear coupling for the stop sector. Furthermore, we have used the abbreviation

$$\mu_{\text{eff}} = \frac{\lambda v_s e^{i\varphi_s}}{\sqrt{2}}. \quad (16.40)$$

A diagonalization of  $\mathcal{M}_{\tilde{t}}$  with the unitary matrix  $\mathcal{U}_{\tilde{t}}$  leads to the physical stop masses  $m_{\tilde{t}_1}$  and  $m_{\tilde{t}_2}$ . Apart from the parameters present already in the Higgs sector, the top and stop sector comprises four independent parameters, for which we choose

$$m_t, m_{\tilde{t}_1}^2, m_{\tilde{t}_2}^2, A_t. \quad (16.41)$$

Besides top quarks and squarks also bottoms and sbottoms play a role in the calculation of the counterterms for the charged Higgs mass and the mass of the  $W$  boson. According to the approximation described in Sec. 14, we treat the bottom quarks as massless. This in turn renders the mass matrix for the sbottoms, which is similar in form to the one of the stops, diagonal. Therefore, there is no mixing between  $\tilde{b}_L$  and  $\tilde{b}_R$  in our approximation and only the left-handed sbottom and its mass counterterm appear in our calculation. Since the mass of the left-handed sbottom is given by  $m_{\tilde{Q}_3}$  for vanishing bottom quark mass, no new parameter enters through the bottom and sbottom sector.

In this chapter, we will set up the renormalization framework, used throughout the subsequent calculations. We will start with a discussion of two different renormalization schemes for the top-stop sector, the OS and the  $\overline{\text{DR}}$  scheme, in Sec. 17.1. Afterwards, we will introduce WFRCs for the Higgs fields in Sec. 17.2 and present the renormalization conditions for the set of independent parameters of the Higgs potential in Sec. 17.3.

### 17.1. Renormalization of the Top-Stop Sector

At tree level, the trilinear Higgs couplings do not depend on the parameters specific to the top and stop sector, which we have listed in the previous chapter. Therefore, in a calculation of one-loop order, a renormalization of these parameters is not necessary. Starting from the two-loop level, however, loop diagrams appear that feature the insertion of a counterterm originating from the top and stop sector. In our case, these loop diagrams are of  $\mathcal{O}(\alpha_t)$ , wherefore the top-stop-specific counterterms have to be determined up to order  $\alpha_s$ , such that the overall contribution of these *counterterm inserted diagrams* is of  $\mathcal{O}(\alpha_t \alpha_s)$ . We will examine two different renormalization schemes for the top-stop-sector, the OS scheme and the  $\overline{\text{DR}}$  scheme. This will enable us to estimate the theoretical uncertainty due to missing higher orders by a comparison of the result obtained in the two schemes.

The mass of the top quark,  $m_t$ , is a parameter of the SM and can hence be treated as detailed in Sec. 7.3 for the case of the  $\tau$  lepton. This results in the following expression for  $\delta^{(\alpha_s)} m_t$  in the OS scheme

$$\delta^{(\alpha_s)} m_t^{\text{OS}} = \frac{m_t}{2} \widetilde{\text{Re}} \left( \Sigma_{tt}^{L,(\alpha_s)}(m_t^2) + \Sigma_{tt}^{R,(\alpha_s)}(m_t^2) + \Sigma_{tt}^{S,l,(\alpha_s)}(m_t^2) + \Sigma_{tt}^{S,r,(\alpha_s)}(m_t^2) \right). \quad (17.1)$$

The constituents of the top-self-energy  $\Sigma_{tt}^{(\alpha_s)}$  appearing here are defined in the same way as in Sec. 7.3. However, as the superscript indicates, only terms of  $\mathcal{O}(\alpha_s)$  are to be considered in  $\Sigma_{tt}^{(\alpha_s)}$ . Having derived an expression for  $\delta^{(\alpha_s)} m_t$  in the OS scheme, the corresponding counterterm in the  $\overline{\text{DR}}$  scheme is obtained by extracting only the divergences contained in  $\delta^{(\alpha_s)} m_t^{\text{OS}}$ .

Also the OS counterterms for the two stop mass parameters,  $m_{t_1}^2$  and  $m_{t_2}^2$ , can be determined

by the usual OS conditions. For the case of mixing scalar fields, these have been detailed in Sec. 7.1. Adopted to the stop sector, they yield at  $\mathcal{O}(\alpha_s)$

$$\delta^{(\alpha_s)} m_{\tilde{t}_1}^{2,\text{OS}} = \Sigma_{\tilde{t}_1 \tilde{t}_1}^{(\alpha_s)} \left( m_{\tilde{t}_1}^2 \right), \quad (17.2)$$

$$\delta^{(\alpha_s)} m_{\tilde{t}_2}^{2,\text{OS}} = \Sigma_{\tilde{t}_2 \tilde{t}_2}^{(\alpha_s)} \left( m_{\tilde{t}_2}^2 \right). \quad (17.3)$$

Concerning the last parameter of the stop sector, the trilinear stop coupling  $A_t$ , we adhere to the scheme proposed in [91, 256] and subsequently applied in [44], which is suitable for the case of a complex stop sector. Therein,  $\delta A_t$  is fixed by the demixing condition

$$\hat{\Sigma}_{\tilde{t}_1 \tilde{t}_2} \left( m_{\tilde{t}_1}^2 \right) + \hat{\Sigma}_{\tilde{t}_1 \tilde{t}_2} \left( m_{\tilde{t}_2}^2 \right) = 0. \quad (17.4)$$

Solving for  $\delta A_t$  and keeping only terms which are of order  $\alpha_s$ , we find

$$\begin{aligned} \delta^{(\alpha_s)} A_t^{\text{OS}} = \frac{e^{-i\varphi_u}}{m_t} & \left[ \mathcal{U}_{\tilde{t}_{11}} \mathcal{U}_{\tilde{t}_{12}}^* (\delta^{(\alpha_s)} m_{\tilde{t}_1}^{2,\text{OS}} - \delta^{(\alpha_s)} m_{\tilde{t}_2}^{2,\text{OS}}) + \mathcal{U}_{\tilde{t}_{11}} \mathcal{U}_{\tilde{t}_{22}}^* (\delta^{(\alpha_s)} X_t^{\text{OS}})^* \right. \\ & \left. + \mathcal{U}_{\tilde{t}_{21}} \mathcal{U}_{\tilde{t}_{12}}^* \delta^{(\alpha_s)} X_t^{\text{OS}} - \left( A_t e^{i\varphi_u} - \frac{\mu_{\text{eff}}^*}{\tan \beta} \right) \delta^{(\alpha_s)} m_t^{\text{OS}} \right]. \end{aligned} \quad (17.5)$$

Here  $\mathcal{U}_{\tilde{t}}$  denotes the stop mixing matrix defined in Sec. 16.5 and  $\delta X_t^{\text{OS}}$ , the off-diagonal stop mass counterterm in the mass basis, is given by

$$\delta X_t^{\text{OS}} = \left( \mathcal{U}_{\tilde{t}} \delta \mathcal{M}_{\tilde{t}} \mathcal{U}_{\tilde{t}}^\dagger \right)_{12} = \left( \mathcal{U}_{\tilde{t}} \delta \mathcal{M}_{\tilde{t}} \mathcal{U}_{\tilde{t}}^\dagger \right)_{21}^* = \frac{1}{2} \widetilde{\text{Re}} \left( \Sigma_{\tilde{t}_1^* \tilde{t}_2} \left( m_{\tilde{t}_1}^2 \right) + \Sigma_{\tilde{t}_1 \tilde{t}_2^*} \left( m_{\tilde{t}_2}^2 \right) \right). \quad (17.6)$$

Again, the corresponding counterterms in the  $\overline{\text{DR}}$  scheme can be obtained by keeping only the divergent terms of the OS expressions.

In order to perform the translation between the OS and the  $\overline{\text{DR}}$  scheme properly, not only the counterterms but also the input parameters have to be adapted. The correct relation between the parameters in the two schemes can be derived by linking them to the bare parameter. For an arbitrary parameter  $p$ , this yields [44]

$$p^{\text{OS}} + \delta p^{\text{OS}} = p_b = p^{\overline{\text{DR}}} + \delta p^{\overline{\text{DR}}}, \quad (17.7)$$

where  $p_b$ ,  $p^{\text{OS}}$  and  $p^{\overline{\text{DR}}}$  denote the bare, the OS and the  $\overline{\text{DR}}$  parameter, respectively. Furthermore, we have

$$\delta p^{\text{OS}} = \delta p^{\overline{\text{DR}}} + \delta p^{\text{OS}}|_{\text{fin}}, \quad (17.8)$$

which we can insert into Eq. (17.7), leading to the relation

$$p^{\text{OS}} = p^{\overline{\text{DR}}} - \delta p^{\text{OS}}|_{\text{fin}}. \quad (17.9)$$

Taking into account only counterterms of  $\mathcal{O}(\alpha_s)$ , these relations are no longer exact and hold only up to higher orders. Moreover, they exhibit a residual dependence on the renormalization scale  $\mu_r$ , which strictly speaking has to be considered in the transformation. Especially in the case of  $m_t$  this is important, as the OS top mass is determined at a scale  $m_t^{\text{OS}}$ , corresponding to the top quark pole mass, which is far below the renormalization scale  $\mu_r$ . The latter is set equal to the SUSY breaking scale  $M_{\text{SUSY}}$  in our calculation. Therefore, the conversion between the OS top mass and the  $\overline{\text{DR}}$  top mass has to incorporate RGE<sup>1</sup> running from  $m_t^{\text{OS}}$  to  $M_{\text{SUSY}}$ . In order to account for this, we proceed along the lines detailed in App. D.1, which is based on dedicated studies performed in Refs. [257–261]. For all remaining parameters,  $A_t$ ,  $m_{\tilde{t}_1}^2$  and  $m_{\tilde{t}_2}^2$ , corresponding RGE relations have not yet been worked out, wherefore we have to rely on the lowest order linear approximations in Eq. (17.9). Note that the solution of this equation requires an iterative procedure, if  $p^{\overline{\text{DR}}}$  is given as input, since  $\delta p^{\text{OS}}|_{\text{fin}}$  is to be calculated in terms of OS parameters.

<sup>1</sup>The abbreviation RGE stands for Renormalization Group Equation. Details can be found in any text book on QFT, e.g. in [58, 59, 109].

## 17.2. Wave Function Renormalization

Apart from the counterterms for the Lagrangian parameters, we also introduce WFRCs for the Higgs doublets and the singlet  $S$ . In doing so, we proceed along the lines of the minimal scheme, defined in Eq. (6.3), i.e. we introduce exactly one complex WFRC for each doublet and one for the singlet, resulting in

$$H_d \rightarrow \left( 1 + \frac{1}{2} \delta^{(\alpha_t)} Z_{H_d} + \frac{1}{2} \delta^{(\alpha_t \alpha_s)} Z_{H_d} \right) H_d, \quad (17.10)$$

$$H_u \rightarrow \left( 1 + \frac{1}{2} \delta^{(\alpha_t)} Z_{H_u} + \frac{1}{2} \delta^{(\alpha_t \alpha_s)} Z_{H_u} \right) H_u, \quad (17.11)$$

$$S \rightarrow \left( 1 + \frac{1}{2} \delta^{(\alpha_t)} Z_S + \frac{1}{2} \delta^{(\alpha_t \alpha_s)} Z_S \right) S. \quad (17.12)$$

As already discussed in Sec. 6.1, this minimal set of WFRCs is sufficient to render all possible Green's functions finite. However, it does not allow for a proper OS renormalization of all Higgs fields. Hence, we will have to introduce finite wave function correction factors when we consider processes with external Higgs bosons later in this thesis (cf. Sec. 20.5).

Yet, for the moment we content ourselves with an elimination of all UV divergences appearing in the Green's functions, which is achieved by the following  $\overline{\text{DR}}$  definition of the WFRCs

$$\delta^{(\alpha_j)} Z_{H_i} = - \left. \frac{\partial \Sigma_{h_i h_i}^{(\alpha_j)}(p^2)}{\partial p^2} \right|_{\text{div}}, \quad H_i \in \{H_d, H_u, S\}. \quad (17.13)$$

Here  $\Sigma_{h_i h_i}^{(\alpha_j)}$  with  $i \in \{d, u, s\}$  denotes those terms of the self-energy for the respective Higgs field in the gauge basis, which are of the order  $\alpha_j$ . For the purpose of treating both cases simultaneously, we have introduced the symbol  $\alpha_j$ , standing for either of the two orders  $\alpha_t$  and  $\alpha_t \alpha_s$ . We will make extensive use of this notation in the following. Besides, we will denote by  $\delta Z_{H_i}$  (no superscript) the sum of the  $\mathcal{O}(\alpha_t)$  and the  $\mathcal{O}(\alpha_t \alpha_s)$  parts

$$\delta Z_{H_i} = \delta^{(\alpha_t)} Z_{H_i} + \delta^{(\alpha_t \alpha_s)} Z_{H_i}. \quad (17.14)$$

It turns out that only  $\delta Z_{H_u}$  contains terms of  $\mathcal{O}(\alpha_t)$  and  $\mathcal{O}(\alpha_t \alpha_s)$ , while  $\delta Z_{H_d}$  and  $\delta Z_S$  vanish in our approximation. Furthermore, the form of  $\delta^{(\alpha_j)} Z_{H_u}$ , more precisely the distribution of terms among the  $\mathcal{O}(\alpha_t)$  and the  $\mathcal{O}(\alpha_t \alpha_s)$  parts of  $\delta Z_{H_u}$ , is found to depend on the renormalization scheme applied to the top-stop sector. This was derived and shown in detail in Ref. [44], where the following relations were stated

$$\delta Z_{H_u}^{\overline{\text{DR}}} = \underbrace{-\frac{3m_t^{2,\overline{\text{DR}}}}{8\pi^2 v^2 s_\beta^2} \frac{1}{\epsilon}}_{\delta^{(\alpha_t)} Z_{H_u}^{\overline{\text{DR}}}} + \underbrace{\frac{\alpha_s m_t^{2,\overline{\text{DR}}}}{4\pi^3 v^2 s_\beta^2} \left( \frac{1}{\epsilon^2} - \frac{1}{\epsilon} \right)}_{\delta^{(\alpha_t \alpha_s)} Z_{H_u}^{\overline{\text{DR}}}}, \quad (17.15)$$

$$\delta Z_{H_u}^{\text{OS}} = \underbrace{-\frac{3m_t^{2,\text{OS}}}{8\pi^2 v^2 s_\beta^2} \frac{1}{\epsilon}}_{\delta^{(\alpha_t)} Z_{H_u}^{\text{OS}}} + \underbrace{\frac{\alpha_s m_t^{2,\text{OS}}}{4\pi^3 v^2 s_\beta^2} \left( \frac{1}{\epsilon^2} - \frac{1}{\epsilon} \right) - \frac{3m_t^{\text{OS}}}{4\pi^2 v^2 s_\beta^2} \frac{\delta m_t^{\text{OS}}|_{\text{fin}}}{\epsilon}}_{\delta^{(\alpha_t \alpha_s)} Z_{H_u}^{\text{OS}}}. \quad (17.16)$$

Note that the superscripts OS and  $\overline{\text{DR}}$  of the WFRCs refer to the renormalization scheme utilized in the top-stop sector while calculating  $\delta Z_{H_u}$  and not to the scheme for the WFRCs themselves, which are always defined by  $\overline{\text{DR}}$  conditions. The authors of [44] emphasized the fact that, although  $\delta^{(\alpha_t)} Z_{H_u}$  and  $\delta^{(\alpha_t \alpha_s)} Z_{H_u}$  separately differ in the two schemes, their

sum is independent of the treatment of the top-stop sector. This can be seen by inserting  $m_t^{\overline{\text{DR}}} = m_t^{\text{OS}} + \delta m_t^{\text{OS}}|_{\text{fin}}$ , with the finite top mass counterterms  $\delta m_t^{\text{OS}}|_{\text{fin}}$  given by

$$\delta m_t^{\text{OS}}|_{\text{fin}} = \frac{\alpha_s m_t}{3\pi} \left[ 3 \ln \left( \frac{m_t^2}{\mu_r^2} \right) - 5 \right] + dm_t^{\text{SQCD}} \quad (17.17)$$

into Eq. (17.15). Here  $dm_t^{\text{SQCD}}$  denotes the SUSY-QCD corrections, which are stated in App. D.1. Similar results were obtained in Refs. [262, 263], although their definition of the OS top mass counterterm differs from ours by a term proportional to  $\epsilon$  (see the discussion in [263], in [44] and in Sec. 19.2). Moreover, the pure  $\overline{\text{DR}}$  result in Eq. (17.15) can also be extracted from the general formulae stated in Refs. [264, 265].

Up to now, the WFRs have been defined in the gauge basis. Yet, during the course of the calculation, we will also need the WFRs for the physical mass eigenstates. These can be determined by a transformation with the rotation matrices  $R$  and  $R^c$  defined in Sec. 16.3. Arranging the gauge basis WFRs into the matrices

$$\delta Z_\phi = \text{diag}(\delta Z_{H_d}, \delta Z_{H_u}, \delta Z_S, \delta Z_{H_d}, \delta Z_{H_u}, \delta Z_S), \quad (17.18)$$

$$\delta Z_{\phi^\pm} = \text{diag}(\delta Z_{H_d}, \delta Z_{H_u}), \quad (17.19)$$

such that

$$\phi_b = \left( \mathbf{1}_{6 \times 6} + \frac{1}{2} \delta Z_\phi \right) \phi_r \equiv Z_\phi \phi_r, \quad (17.20)$$

$$\phi_b^\pm = \left( \mathbf{1}_{2 \times 2} + \frac{1}{2} \delta Z_{\phi^\pm} \right) \phi_r^\pm \equiv Z_{\phi^\pm} \phi_r^\pm \quad (17.21)$$

holds up to the considered order, the WFRs in the mass basis are obtained via

$$\delta Z_\Phi = R^\dagger \delta Z_\phi R, \quad (17.22)$$

$$\delta Z_{\Phi^\pm} = R^{c\dagger} \delta Z_{\phi^\pm} R^c. \quad (17.23)$$

As before the subscripts  $b$  and  $r$  denote bare and renormalized quantities. For the case of the charged mass eigenstates, we can explicitly state the result

$$\delta Z_{\Phi^\pm} = \begin{pmatrix} s_\beta^2 \delta Z_{H_d} + c_\beta^2 \delta Z_{H_u} & s_\beta c_\beta (\delta Z_{H_u} - \delta Z_{H_d}) \\ s_\beta c_\beta (\delta Z_{H_u} - \delta Z_{H_d}) & c_\beta^2 \delta Z_{H_d} + s_\beta^2 \delta Z_{H_u} \end{pmatrix}, \quad (17.24)$$

which will be needed further down.

### 17.3. Renormalization of the Higgs Potential

In Sec. 16.4 we have specified the set of independent parameters of the Higgs sector. This enables us to introduce counterterms for the chosen parameters and to fix them by suitable renormalization conditions. The order of the counterterms has to match the order of the virtual corrections, wherefore we introduce the counterterms as

On-shell parameters/ tadpole scheme I:

$\overline{\text{DR}}$  parameters:

$$\begin{aligned} e &\rightarrow e \left( 1 + \delta^{(\alpha_t)} Z_e + \delta^{(\alpha_t \alpha_s)} Z_e \right), & \tan \beta &\rightarrow \tan \beta + \delta^{(\alpha_t)} \tan \beta + \delta^{(\alpha_t \alpha_s)} \tan \beta, \\ M_W^2 &\rightarrow M_W^2 + \delta^{(\alpha_t)} M_W^2 + \delta^{(\alpha_t \alpha_s)} M_W^2, & v_s &\rightarrow v_s + \delta^{(\alpha_t)} v_s + \delta^{(\alpha_t \alpha_s)} v_s, \\ M_Z^2 &\rightarrow M_Z^2 + \delta^{(\alpha_t)} M_Z^2 + \delta^{(\alpha_t \alpha_s)} M_Z^2, & |\lambda| &\rightarrow |\lambda| + \delta^{(\alpha_t)} |\lambda| + \delta^{(\alpha_t \alpha_s)} |\lambda|, \\ m_{H^\pm}^2 &\rightarrow m_{H^\pm}^2 + \delta^{(\alpha_t)} m_{H^\pm}^2 + \delta^{(\alpha_t \alpha_s)} m_{H^\pm}^2, & |\kappa| &\rightarrow |\kappa| + \delta^{(\alpha_t)} |\kappa| + \delta^{(\alpha_t \alpha_s)} |\kappa|, \\ t_{\phi_i} &\rightarrow t_{\phi_i} + \delta^{(\alpha_t)} t_{\phi_i} + \delta^{(\alpha_t \alpha_s)} t_{\phi_i}, & |A_\kappa| &\rightarrow |A_\kappa| + \delta^{(\alpha_t)} |A_\kappa| + \delta^{(\alpha_t \alpha_s)} |A_\kappa|, \\ & \text{with } \phi_i \in \{h_d, h_u, h_s, a_d, a_s\}, & \varphi_y &\rightarrow \varphi_y + \delta^{(\alpha_t)} \varphi_y + \delta^{(\alpha_t \alpha_s)} \varphi_y. \end{aligned}$$

We have already arranged the counterterms in two groups according to the renormalization scheme they will be determined in. The corresponding renormalization conditions will be detailed in the following.

Since the treatment of the **tadpoles** has an impact on the whole renormalization scheme, we start by establishing their renormalization conditions. Throughout this part of the thesis, we will apply tadpole scheme I, as specified in Sec. 6.3, i.e. we will introduce tadpole counterterms, which are chosen such that they exactly cancel the tadpole diagrams of  $\mathcal{O}(\alpha_t)$  and  $\mathcal{O}(\alpha_t\alpha_s)$ . Accordingly, the tadpole counterterms are given by

$$\delta^{(\alpha_j)} t_{\phi_i} = T_{\phi_i}^{(\alpha_j)}, \quad \phi_i \in \{h_d, h_u, h_s, a_d, a_s\}, \quad (17.25)$$

where  $T_{\phi_i}^{(\alpha_j)}$  denotes the corresponding tadpole diagram of order  $\alpha_j \in \{\alpha_t, \alpha_t\alpha_s\}$ .

The **elementary charge**  $e$  can be determined in the same way as detailed in Eq. (7.21), taking into account the contributions of the desired order. However, it turns out that, performing the transition to the gaugeless limit, no terms  $\propto \delta Z_e$  remain in our calculation. Hence, we do not need to specify a counterterm  $\delta Z_e$ .

As in the previous part, the counterterms for the **masses of the gauge bosons**,  $\delta M_W^2$  and  $\delta M_Z^2$ , are determined according to OS conditions. However, in order to comply with the gaugeless limit, where  $M_W^2 = M_Z^2 = 0$  holds, and furthermore since we work in the approximation of vanishing external momentum, the corresponding self-energies have to be evaluated at  $p^2 = 0$ , which leads to

$$\delta^{(\alpha_j)} M_W^2 = \Sigma_{WW}^{T,(\alpha_j)}(0), \quad (17.26)$$

$$\delta^{(\alpha_j)} M_Z^2 = \Sigma_{ZZ}^{T,(\alpha_j)}(0). \quad (17.27)$$

As the involved Passarino-Veltman functions are purely real for vanishing external momenta, we can omit the  $\text{Re}()/\widetilde{\text{Re}}()$ -prescriptions we had to consider in Eqs. 7.10 and 7.11. Owing to the fact that the self-energies  $\Sigma_{WW}$  and  $\Sigma_{ZZ}$  are proportional to  $e^2$ , the counterterms  $\delta^{(\alpha_j)} M_W^2$  and  $\delta^{(\alpha_j)} M_Z^2$  only contribute if they appear in ratios proportional to  $\delta^{(\alpha_j)} M_W^2/e^2$  or  $\delta^{(\alpha_j)} M_Z^2/e^2$ . It turns out that the only non-vanishing contributions containing  $\delta^{(\alpha_j)} M_W^2$  and  $\delta^{(\alpha_j)} M_Z^2$  appear in a combination that corresponds to the counterterm of the vev  $v = \sqrt{v_d^2 + v_u^2}$  and is given by

$$\frac{\delta^{(\alpha_j)} v}{v} = \frac{c_W^2}{2s_W^2} \left( \frac{\delta^{(\alpha_j)} M_Z^2}{M_Z^2} - \frac{\delta^{(\alpha_j)} M_W^2}{M_W^2} \right) + \frac{\delta^{(\alpha_j)} M_W^2}{2M_W^2}. \quad (17.28)$$

Extracting only the UV-divergent part of Eq. (17.28), we find in an explicit calculation the following relation between  $\delta^{(\alpha_j)} v|_{\text{div}}$  and  $\delta^{(\alpha_j)} Z_{H_u}$

$$\frac{\delta^{(\alpha_j)} v}{v} \Big|_{\text{div}} = \frac{s_\beta^2}{2} \delta^{(\alpha_j)} Z_{H_u}. \quad (17.29)$$

Similar to the mass counterterms for the gauge bosons, also the **mass of the charged Higgs boson**  $m_{H^\pm}^2$  is fixed by an OS-like conditions with vanishing external momentum, i.e by the requirement

$$\hat{\Sigma}_{H^\pm H^\pm}^{(\alpha_j)}(0) = 0. \quad (17.30)$$

Note that, in contrast to the case of the gauge bosons, this condition is not an OS condition in the strict sense, since  $m_{H^\pm}^2$  does not vanish in the gaugeless limit. As a consequence,

the counterterm  $\delta^{(\alpha_j)} m_{H^\pm}^2$  receives a contribution of the WFRC  $\delta^{(\alpha_j)} Z_{H^\pm H^\pm}$ . This follows directly from the fact that the renormalized self-energy  $\hat{\Sigma}_{H^\pm H^\pm}^{(\alpha_j)}$  comprises a WFRC contribution (cf. Sec. 7.1), given by the term  $(p^2 - m_{H^\pm}^2) \delta^{(\alpha_j)} Z_{H^\pm H^\pm}$ . In a proper OS scheme, where the mass counterterm is defined at an external momentum  $p^2 = m_{H^\pm}^2$ , this contribution would drop out in Eq. (17.30). However, in the OS-like scheme with  $p^2 = 0$  we consider here, the term remains. According to our findings in Sec. 17.2,  $\delta^{(\alpha_j)} Z_{H^\pm H^\pm}$  is given by  $\delta^{(\alpha_j)} Z_{H^\pm H^\pm} = c_\beta^2 \delta^{(\alpha_j)} Z_{H_u}$ . Hence, we arrive at

$$\delta^{(\alpha_j)} m_{H^\pm}^2 = \Sigma_{H^\pm H^\pm}^{(\alpha_j)}(0) - m_{H^\pm}^2 c_\beta^2 \delta^{(\alpha_j)} Z_{H_u}. \quad (17.31)$$

The ratio of the vevs  $v_u$  and  $v_d$ ,  $\tan\beta$ , is renormalized according to  $\overline{\text{DR}}$  conditions, as recommended in Ref. [138]. Following these  $\overline{\text{DR}}$  prescriptions,  $\tan\beta$  can be expressed in terms of the WFRCs as

$$\delta^{(\alpha_j)} \tan\beta = \frac{1}{2} \tan\beta \left( \delta^{(\alpha_j)} Z_{H_u} - \delta^{(\alpha_j)} Z_{h_d} \right) \Big|_{\text{div}} = \frac{1}{2} \tan\beta \left( \delta^{(\alpha_j)} Z_{H_u} \right) \Big|_{\text{div}}, \quad (17.32)$$

where we have used the fact that only the WFRC of the doublet  $H_u$  yields contributions of  $\mathcal{O}(\alpha_t)$  or  $\mathcal{O}(\alpha_t \alpha_s)$ .

Finally, also all remaining parameters  $|\lambda|$ ,  $|\kappa|$ ,  $|A_\kappa|$ ,  $v_s$  and  $\varphi_y$  are renormalized in the  $\overline{\text{DR}}$  scheme, by demanding their counterterms to cancel all remaining divergences in the  $6 \times 6$  matrix of the renormalized neutral Higgs self-energy  $\hat{\Sigma}_{\phi_i, \phi_j}^{(\alpha_j)}$ , i.e. by requiring

$$\hat{\Sigma}_{\phi_i, \phi_j}^{(\alpha_j)} \Big|_{\text{div}} = 0, \quad i, j \in \{h_d, h_u, h_s, a_d, a_u, a_s\}. \quad (17.33)$$

Although not all 36 equations resulting from Eq. (17.33) are linearly independent, the system of equations overdetermines the five counterterms to be established. Hence, the simultaneous finiteness of all elements of Eq. (17.33) constitutes a strong consistency check. Solving for the five counterterms provides us with

$$\delta^{(\alpha_j)} |\lambda| = -\frac{|\lambda|}{2} \left( c_\beta^2 \delta^{(\alpha_j)} Z_{H_u} + 2 \frac{\delta^{(\alpha_j)} v}{v} \Big|_{\text{div}} \right) = -\frac{|\lambda|}{2} \delta^{(\alpha_j)} Z_{H_u}, \quad (17.34)$$

$$\delta^{(\alpha_j)} |\kappa| = -\frac{|\kappa|}{2} \left( -s_\beta^2 \delta^{(\alpha_j)} Z_{H_u} + 2 \frac{\delta^{(\alpha_j)} v}{v} \Big|_{\text{div}} \right) = 0, \quad (17.35)$$

$$\delta^{(\alpha_j)} v_s = -\frac{v_s}{2} \left( -s_\beta^2 \delta^{(\alpha_j)} Z_{H_u} + 2 \frac{\delta^{(\alpha_j)} v}{v} \Big|_{\text{div}} \right) = 0, \quad (17.36)$$

$$\delta^{(\alpha_j)} |A_\kappa| = 0, \quad (17.37)$$

$$\delta^{(\alpha_j)} \varphi_y = 0. \quad (17.38)$$

In the approximation we consider, only  $|\lambda|$  receives a counterterm that contributes at  $\mathcal{O}(\alpha_t)$  or  $\mathcal{O}(\alpha_t \alpha_s)$ . All other parameters need not be renormalized for the purpose of our calculations. This can be understood by considering the expressions derived in [236] for  $\delta|\kappa|$ ,  $\delta|A_\kappa|$ ,  $\delta v_s$  and the counterterms for the complex phases at full one-loop order. In this publication the authors fix the counterterms in question by relating them to the neutralino and chargino sector. The divergences of the resulting counterterms can be checked to vanish in the gaugeless limit at  $\mathcal{O}(\alpha_t)$ . Going one order higher, i.e. to  $\mathcal{O}(\alpha_t \alpha_s)$ , which amounts to adding one further loop containing gluons, gluinos or stops, does not change this statement.

---

The Corrections of  $\mathcal{O}(\alpha_t)$

---

Having set up the renormalization scheme, we can now proceed with the actual calculation of the corrections to the effective trilinear Higgs self-couplings. In this chapter, we will assail this task and determine the corrections of  $\mathcal{O}(\alpha_t)$ . As outlined in the introduction, these consist of a virtual and a counterterm part

$$\Delta\lambda_{ijk}^{\mathcal{O}(\alpha_t)} = \Delta\lambda_{ijk}^{\mathcal{O}(\alpha_t),\text{virt}} + \Delta\lambda_{ijk}^{\mathcal{O}(\alpha_t),\text{ct}}. \quad (18.1)$$

We will first deal with the virtual corrections. In order to calculate these, we will exploit the well-known relation between Feynman diagrammatic calculations in the limit of vanishing external momentum and the *effective potential approach*. This approach relies on the use of an object called the *effective potential*, which is defined to embody all possible momentum-independent radiative corrections to the tree-level scalar potential. With its help, higher-order corrections in the limit of vanishing external momentum to any scalar Green's function can be obtained by simply taking appropriate derivatives of the effective potential. The advantage of this approach is at hand: Once the effective potential has been determined up to some order, radiative corrections of that order to all existing scalar Green's functions are in principle known and their determination reduces to straightforward, although occasionally tedious, algebra.

We will give a brief introduction to the subject in Sec. 18.1, and present the method we use to determine the effective NMSSM Higgs potential of  $\mathcal{O}(\alpha_t)$ . The actual calculation for the NMSSM is carried out in Sec. 18.2, where we also extract the virtual  $\mathcal{O}(\alpha_t)$  corrections to the trilinear Higgs self-couplings. In the last section ( Sec. 18.3), we determine the corresponding counterterms.

In this chapter, we will for convenience work in the gauge basis. The resulting corrections to the couplings  $\lambda_{\phi_i\phi_j\phi_k}$  can, however, easily be transferred to the mass basis by means of the rotation matrix  $R$ , defined in Sec. 16.3, according to

$$\Delta\lambda_{h_i h_j h_k}^{\mathcal{O}(\alpha_t)} = R_{ii'} R_{jj'} R_{kk'} \Delta\lambda_{\phi_{i'} \phi_{j'} \phi_{k'}}^{\mathcal{O}(\alpha_t)} \quad i, i', j, j', k, k' \in \{1, \dots, 6\}, \quad (18.2)$$

where a summation over recurring indices is implied and  $h_i/\phi_i$  represent a member of the tree-level mass/gauge basis defined in 16.3.

## 18.1. The Effective Potential Approach

We begin this chapter with a brief presentation of the effective potential approach. Our treatment does not strive for completeness nor for rigorous derivations but rather has the purpose of introducing the most important notions and concepts. To exemplify the approach, we will first consider the simple case of a theory with only one scalar field  $\rho$ , before we examine the more complicated situation we encounter in the NMSSM.

The effective potential  $V_{\text{eff}}[\bar{\rho}]$  for a scalar field  $\rho(x)$  is defined as the momentum independent part of the *effective action*  $\Gamma[\bar{\rho}]$ . This in turn is given by the Legendre transform of the *generating functional of connected Green's functions*  $\mathcal{W}[J]$ , i.e. by

$$\Gamma[\bar{\rho}] = \mathcal{W}[J] - \int d^4x J(x)\bar{\rho}(x), \quad (18.3)$$

$$\text{with} \quad \bar{\rho}(x) = \frac{\partial \mathcal{W}[J]}{\partial J(x)}. \quad (18.4)$$

Here  $\bar{\rho}(x)$ , conventionally referred to as the *classical field*, denotes the expectation value of the field  $\rho(x)$  in the presence of an external source  $J(x)$  in the vacuum  $|\Omega\rangle$

$$\bar{\rho}(x) = \left. \frac{\langle \Omega | \rho(x) | \Omega \rangle}{\langle \Omega | \Omega \rangle} \right|_{J(x)}. \quad (18.5)$$

Moreover, the functional  $\mathcal{W}[J]$  is directly related to the *generating functional of Green's functions*, introduced in Sec. 3.3, via

$$e^{i\mathcal{W}[J]} = \mathcal{Z}[J] = \int \mathcal{D}\rho e^{i(S[\rho] + \int d^4x \rho(x)J(x))}. \quad (18.6)$$

Being a functional of the classical field, the effective action  $\Gamma[\bar{\rho}]$  can be functionally expanded in powers of  $\bar{\rho}(x)$ , according to

$$\Gamma[\bar{\rho}] = \sum_{n=1}^{\infty} \frac{1}{n!} \int d^4x_1 \dots d^4x_n \Gamma^{(n)}(x_1 \dots x_n) \bar{\rho}(x_1) \dots \bar{\rho}(x_n). \quad (18.7)$$

Here we have labeled the coefficients of the expansion as  $\Gamma^{(n)}$ , hinting to the fact that these objects exactly correspond to the 1PI  $n$ -particle Green's functions, i.e. the sum of all 1PI Feynman diagrams with  $n$  external legs. The  $\Gamma^{(n)}$  are sometimes also referred to as *vertex functions*.

Alternatively, one may expand  $\Gamma[\bar{\rho}]$  around constant (i.e.  $x$ -independent) values of  $\bar{\rho}$ , which corresponds to an expansion in powers of derivatives of  $\bar{\rho}(x)$  [266, 267]

$$\Gamma[\bar{\rho}] = \int d^4x \left( -V_{\text{eff}}[\bar{\rho}] + \frac{1}{2}(\partial_\mu \bar{\rho}(x)\partial^\mu \bar{\rho}(x))Z[\bar{\rho}] + \dots \right). \quad (18.8)$$

The first term in this expansion represents the effective potential  $V_{\text{eff}}$ . In order to clarify its meaning, we introduce the Fourier transform of the vertex functions  $\Gamma^{(n)}$  in Eq. (18.7)

$$\Gamma^{(n)}(x_1 \dots x_n) = \int \frac{d^4p_1}{2\pi^4} \dots \frac{d^4p_n}{2\pi^4} e^{ix_1p_1} \dots e^{ix_np_n} 2\pi^4 \delta^4(p_1 + \dots + p_n) \widetilde{\Gamma}^{(n)}(p_1 \dots p_n), \quad (18.9)$$

which, inserted into Eq. (18.7), leads to [267]

$$\Gamma[\bar{\rho}] = \sum_{n=1}^{\infty} \frac{1}{n!} \int d^4x_1 \dots d^4x_n \bar{\rho}(x_1) \dots \bar{\rho}(x_n) \int \frac{d^4p_1}{2\pi^4} \dots \frac{d^4p_n}{2\pi^4} e^{ix_1p_1} \dots e^{ix_np_n} 2\pi^4 \delta^4(p_1 + \dots + p_n) \widetilde{\Gamma}^{(n)}(p_1 \dots p_n). \quad (18.10)$$

The four-dimensional  $\delta$ -distribution appearing here is a consequence of translational invariance of the vertex functions  $\Gamma^{(n)}$  and naturally incorporates momentum conservation into Eq. (18.10). In the following we will omit the tilde for the Fourier transform, to keep the notation clean. If not stated otherwise, the vertex functions are henceforth assumed to be defined in momentum space. A subsequent expansion of  $\Gamma^{(n)}(p_1 \dots p_n)$  around vanishing external momenta  $\{p_1, \dots, p_n\} = \{0, \dots, 0\}$  and a comparison with Eq. (18.10) shows that  $V_{\text{eff}}$  is given by [267, 268]

$$V_{\text{eff}}[\bar{\rho}] = - \sum_{n=1}^{\infty} \frac{1}{n!} \Gamma^{(n)}(p_i = 0) \bar{\rho}^n, \quad i = 1 \dots n, \quad (18.11)$$

with a constant field  $\bar{\rho}$ . As can be seen from this expression,  $V_{\text{eff}}$  is the momentum-independent part of the effective action. Furthermore, it can directly be inferred that the  $n$ th derivative of  $V_{\text{eff}}$  with respect to  $\bar{\rho}$ , evaluated at  $\bar{\rho} = 0$ , yields the corresponding 1PI  $n$ -point function in the limit of vanishing external momentum

$$- \left. \frac{\partial^n}{\partial \bar{\rho}^n} V_{\text{eff}}[\bar{\rho}] \right|_{\bar{\rho}=0} = \Gamma^{(n)}(p_i = 0), \quad i = 1 \dots n. \quad (18.12)$$

This confirms the statement we made in the introduction: Once the effective potential is known up to some order in the perturbative expansion, all Green's functions of the corresponding order can be extracted from it in the limit of vanishing external momentum by straightforward differentiation.

Hence, the only task to be accomplished is the determination of the effective potential up to the desired order. There are several methods proposed in the literature to calculate the effective potential. In [267, 269] the effective potential is determined by functional integration of the generating functional of Green's functions in Eq. (18.6), using the method of steepest descent. A very different approach is used in [266, 270, 271], where the effective potential is calculated by a summation over an infinite number of Feynman diagrams of fixed loop-order, making explicit use of the definition in Eq. (18.11). For our calculation, we use a third method, advocated in [268, 272, 273]. This approach, called the *tadpole method*, starts from an expansion of the effective potential around some point  $\bar{\rho} = \omega$ . Then instead of Eq. (18.11), where  $V_{\text{eff}}$  is expanded around  $\bar{\rho} = 0$ , we get

$$V_{\text{eff}}[\bar{\rho}] = - \sum_{n=1}^{\infty} \frac{1}{n!} \bar{\Gamma}^{(n)}(p_i = 0) (\bar{\rho} - \omega)^n, \quad i = 1 \dots n. \quad (18.13)$$

It should be noted that here  $\bar{\Gamma}^{(n)}$  stands for the 1PI  $n$ -point function evaluated in the shifted theory. The shift parameter  $\omega$  is most conveniently chosen equal to the vev of the scalar field  $\phi$ , in which case the usual Feynman rules can be used to calculate the  $\bar{\Gamma}^{(n)}$ . However, in principle,  $\omega$  can be chosen freely, as it constitutes merely an auxiliary parameter [268]. Now a differentiation of  $V_{\text{eff}}$  with respect to  $\bar{\rho}$ , evaluated at the point  $\bar{\rho} = \omega$ , yields

$$- \left. \frac{dV_{\text{eff}}[\bar{\rho}]}{d\bar{\rho}} \right|_{\bar{\rho}=\omega} = \bar{\Gamma}^{(1)}, \quad (18.14)$$

where  $\bar{\Gamma}^{(1)}$  is the 1PI one-point function, i.e. the sum of all tadpole diagrams with an external  $\bar{\rho}$  multiplied by  $(-i)$ , of the shifted theory. According to our convention, the latter is denoted by  $\bar{T}_{\bar{\rho}}$ . The idea of the tadpole method now consists in reverting Eq. (18.14), which amounts to calculating the tadpoles of the shifted theory, integrating them w.r.t. the shift parameter  $\omega$  and subsequently replacing  $\omega \rightarrow \bar{\rho}$  [268, 273]. Formally, these steps can be expressed as

$$V_{\text{eff}}[\bar{\rho}] = - \int d\omega \bar{\Gamma}^{(1)} \Big|_{\omega \rightarrow \bar{\rho}} = - \int d\omega \cdot \bar{T}_{\bar{\rho}} \Big|_{\omega \rightarrow \bar{\rho}}. \quad (18.15)$$

We will exemplify this procedure in the following section for the case of the effective NMSSM Higgs potential.

## 18.2. The Virtual $\mathcal{O}(\alpha_t)$ Corrections to the Trilinear Higgs Self-Couplings

Turning towards the case of the NMSSM, we encounter a slightly more complicated situation since the NMSSM Higgs sector comprises a total of six neutral scalars. However, the generalization of Eq. (18.11) is straightforward.

The goal of this chapter is the calculation of the  $\mathcal{O}(\alpha_t)$  corrections to the trilinear Higgs self-couplings by means of the effective potential. For this purpose, the latter has to be determined up to the  $\mathcal{O}(\alpha_t)$ . With the tadpole approach as our method of choice, this implies that we have to calculate all  $\mathcal{O}(\alpha_t)$  contributions to the tadpole diagrams, which entirely originate from top quark and squark loops.

Unlike the simple toy model considered in the previous section, the NMSSM exhibits six tadpoles, one for each of the neutral gauge eigenstates of the Higgs sector, five of which are linearly independent. The corresponding tadpole diagrams differ by the couplings of the gauge eigenstates to the loop particles. As we will see below, the dependence on these couplings drops out completely during our calculation after applying a convenient substitution. Therefore, we can choose any of the six tadpoles as integrand in Eq. (18.15) to determine the effective potential and arrive at the same final result. One subtlety arises however, if the coupling of the chosen gauge eigenstate to any of the loop particles vanishes identically, since in this case, the contribution of the respective loop would be missed and special care would have to be taken to include the absent terms properly [274]. In our case, we are interested only in the contributions of top quarks and squarks. Hence, the  $h_u$  tadpole suggests itself as integrand in Eq. (18.15), since  $h_u$  couples to both tops and stops and therefore all contributions are captured without the need of special measures.

A straightforward calculation of the  $\mathcal{O}(\alpha_t)$  top and stop contributions to the  $h_u$ -tadpole  $T_{h_u}^{(\alpha_t)}$ , using DRRed to regularize the divergences, leads to

$$T_{h_u,t}^{(\alpha_t)} = \frac{3}{4\pi^2} g_{h_u \bar{t} t} m_t^3 \left( \frac{1}{\epsilon} + 1 - \ln \left( \frac{m_t^2}{Q^2} \right) \right) \equiv g_{h_u \bar{t} t} T_t^{(\alpha_t)}, \quad (18.16)$$

$$T_{h_u, \tilde{t}_i}^{(\alpha_t)} = \frac{-3}{16\pi^2} g_{h_u \tilde{t}_i^\dagger \tilde{t}_i} m_{\tilde{t}_i}^2 \left( \frac{1}{\epsilon} + 1 - \ln \left( \frac{m_{\tilde{t}_i}^2}{Q^2} \right) \right) \equiv g_{h_u \tilde{t}_i^\dagger \tilde{t}_i} T_{\tilde{t}_i}^{(\alpha_t)}. \quad (18.17)$$

On the right hand side, we have defined the general top and stop tadpole contributions  $T_t^{(\alpha_t)}$  and  $T_{\tilde{t}_i}^{(\alpha_t)}$ , which, having extracted the couplings to the Higgs boson, are devoid of any dependence on  $h_u$ . Using the vevs as the shift parameters in Eq. (18.13), we next have to integrate these tadpoles with respect to  $v_u$ . In order to guarantee the disappearance of any dependence on the couplings and thus on the gauge eigenstate of the tadpole chosen as integrand, we apply a substitution, such that the integration is performed w.r.t. the masses of the loop particles

$$\begin{aligned} & \int dv_u \left( -g_{h_u \bar{t} t} T_t^{(\alpha_t)} - \sum_{i=1}^2 g_{h_u \tilde{t}_i^\dagger \tilde{t}_i} T_{\tilde{t}_i}^{(\alpha_t)} \right) \\ &= \int dm_t \underbrace{\left( \frac{\partial m_t}{\partial v_u} \right)^{-1}}_{(-g_{h_u \bar{t} t})^{-1}} \left( -g_{h_u \bar{t} t} T_t^{(\alpha_t)} \right) + \sum_{i=1}^2 \int dm_{\tilde{t}_i} 2m_{\tilde{t}_i} \underbrace{\left( \frac{\partial m_{\tilde{t}_i}^2}{\partial v_u} \right)^{-1}}_{(-g_{h_u \tilde{t}_i^\dagger \tilde{t}_i})^{-1}} \left( -g_{h_u \tilde{t}_i^\dagger \tilde{t}_i} T_{\tilde{t}_i}^{(\alpha_t)} \right) \\ &= \int dm_t T_t^{(\alpha_t)} + \sum_{i=1}^2 \int dm_{\tilde{t}_i} 2m_{\tilde{t}_i} T_{\tilde{t}_i}^{(\alpha_t)}. \end{aligned} \quad (18.18)$$

Note that the substitution is crucial for a complete cancellation of any dependence on the chosen tadpole component. Without performing it, the result of the integration would depend

on the chosen gauge eigenstate and we would have to consider and determine integration constants to account for this (cf. e.g. citeBobrowski:2014dla,MILLER198359).

The remaining integrals can be evaluated by elementary calculus, yielding

$$V_{\text{eff}}^{\mathcal{O}(\alpha_t)} = \frac{3}{16\pi^2} \left[ \overline{m}_t^4 \left[ \frac{1}{\epsilon} + \frac{3}{2} - \ln \left( \frac{\overline{m}_t^2}{Q^2} \right) \right] - \frac{1}{2} [(\overline{m}_t \leftrightarrow \overline{m}_{\tilde{t}_1}) + (\overline{m}_t \leftrightarrow \overline{m}_{\tilde{t}_2})] \right]. \quad (18.19)$$

In this expression the replacement  $v_i \rightarrow H_i^0$ ,  $v_s \rightarrow S$ , demanded by the prescription in Eq. (18.15), has already been performed, wherefore the overlined masses appearing here have to be interpreted as the *field dependent* masses

$$\overline{m}_t^2 = |y_t H_u^0|^2, \quad (18.20)$$

$$\overline{m}_{\tilde{t}_{1,2}}^2 = \frac{1}{2} \left( m_{\tilde{Q}_3}^2 + m_{\tilde{t}_R}^2 + 2\overline{m}_t^2 \mp \sqrt{\left( m_{\tilde{Q}_3}^2 - m_{\tilde{t}_R}^2 \right)^2 + 4|\tilde{X}|^2} \right), \quad (18.21)$$

$$\text{with } \tilde{X} = y_t |A_t H_u^0 - \lambda S^* H_d^{0*}|.$$

Furthermore, the last two terms in Eq. (18.19) are to be perceived as being identical to the first one, with  $\overline{m}_t$  exchanged by  $\overline{m}_{\tilde{t}_1}$  or  $\overline{m}_{\tilde{t}_2}$ , respectively. As can directly be inferred from Eq. (18.19), the effective potential contains UV divergences, which become manifest as poles in the limit  $\epsilon \rightarrow 0$ . These will be propagated into any quantity extracted from it and have to be cancelled by suitably chosen counterterms.

It is now a matter of straightforward algebra to determine the corrections of  $\mathcal{O}(\alpha_t)$  to all trilinear Higgs self-couplings, according to

$$\Delta\lambda_{\phi_i\phi_j\phi_k}^{\mathcal{O}(\alpha_t),\text{virt}} = -\frac{\partial^3 V_{\text{eff}}^{\mathcal{O}(\alpha_t)}}{\partial\phi_i\partial\phi_j\partial\phi_k}. \quad (18.22)$$

Explicit expressions can be found in App. B.2. Our result is in accordance with the one obtained in [275] for the case of the MSSM, if the necessary modifications for the NMSSM are taken into account.

### 18.3. The Counterterm of $\mathcal{O}(\alpha_t)$

After the calculation of all virtual corrections, only the counterterm contributions  $\Delta\lambda_{ijk}^{\mathcal{O}(\alpha_t),\text{ct}}$  remain to be determined. To that end, the tree-level couplings have to be expressed in terms of the parameters  $p_i$  we chose in Sec. 16.4 as independent parameters. A subsequent replacement  $p_i \rightarrow p_i + \delta^{(\alpha_t)} p_i$  of all parameters  $p_i$  and an extraction of the terms linear in the renormalization constants  $\delta^{(\alpha_t)} p_i$  yields the counterterm for the respective coupling. Taking into account WFRCs, the coupling counterterms can schematically be expressed as (summation over repeated indices implied)

$$\begin{aligned} & \lambda_{\phi_i\phi_j\phi_k}(p_1, \dots, p_n) \\ & \rightarrow Z_{\phi_i, i' i} Z_{\phi_j, j' j} Z_{\phi_k, k' k} \lambda_{\phi_{i'}\phi_{j'}\phi_{k'}}(p_1 + \delta p_1, \dots, p_n + \delta p_n) \Big|_{\mathcal{O}(\alpha_t)} \\ & = \lambda_{\phi_i\phi_j\phi_k}(p_1, \dots, p_n) + \frac{\partial\lambda_{\phi_i\phi_j\phi_k}}{\partial p_l} \delta^{(\alpha_t)} p_l \\ & \quad + \frac{1}{2} \left( \delta^{(\alpha_t)} Z_{\phi_i, i' i} \lambda_{\phi_{i'}\phi_j\phi_k} + \delta^{(\alpha_t)} Z_{\phi_j, j' j} \lambda_{\phi_i\phi_{j'}\phi_k} + \delta^{(\alpha_t)} Z_{\phi_k, k' k} \lambda_{\phi_i\phi_j\phi_{k'}} \right) + \mathcal{O}(\delta^2) \\ & = \lambda_{\phi_i\phi_j\phi_k}(p_1, \dots, p_n) + \Delta\lambda_{\phi_i\phi_j\phi_k}^{\mathcal{O}(\alpha_t),\text{ct}} + \mathcal{O}(\delta^2). \end{aligned} \quad (18.23)$$

Explicit expressions for  $\Delta\lambda_{\phi_i\phi_j\phi_k}^{\mathcal{O}(\alpha_t),\text{ct}}$  in terms of the parameter counterterms and WFRCs can be found in App. B.3. We have already defined the counterterms for all independent parameters as well as the WFRCs in sections 17.3 and 17.2, respectively. At this point, we only want to emphasize the fact that both the tadpoles and the elements of the  $\mathcal{O}(\alpha_t)$  Higgs self-energies at vanishing external momentum, which are necessary in order to determine all counterterms according to our renormalization program, can be obtained from the effective potential. To be specific, the tadpoles are given by

$$T_{\phi_i}^{(\alpha_t)} = -\frac{\partial V_{\text{eff}}^{(\alpha_t)}}{\partial \phi_i} \quad (18.24)$$

and the elements of the self-energies by

$$\Sigma_{ij}^{(\alpha_t)}(0) = -\frac{\partial^2 V_{\text{eff}}^{(\alpha_t)}}{\partial \phi_i \partial \phi_j}. \quad (18.25)$$

The resulting expressions can be used in Eqs. 17.25 and 17.30 for the determination of the  $\mathcal{O}(\alpha_t)$  counterterms.

We have checked explicitly that the coupling counterterms, determined pursuant to Eq. (18.23) with the WFRCs and parameter counterterms defined according to Secs. 17.2 and 17.3, cancel all divergences that appear in the trilinear Higgs self-couplings calculated as specified in Eq. (18.22).

---

The Corrections of  $\mathcal{O}(\alpha_t\alpha_s)$

---

We can now proceed to the next loop-order and determine the  $\mathcal{O}(\alpha_t\alpha_s)$  corrections to the effective trilinear Higgs self-couplings. Due to the existence of sophisticated and well-tested software tools for the evaluation of higher-order Feynman diagrams, we switch to the Feynman diagrammatic approach for this undertaking. As already mentioned, there is a complete equivalence between the effective potential approach and Feynman diagrammatic calculations in the limit of vanishing external momentum. Therefore, the results of this chapter are compatible with those obtained in the previous one, although the adopted approaches differ. Furthermore, we will perform the calculation in the tree-level mass basis  $\Phi = (h_1, \dots, h_5, G)$  defined in Eq. (16.28).

The  $\mathcal{O}(\alpha_t\alpha_s)$  corrections can be split into three parts, as outlined in the introduction to Part III

$$\Delta\lambda_{ijk}^{\mathcal{O}(\alpha_t\alpha_s)} = \Delta\lambda_{ijk}^{\mathcal{O}(\alpha_t\alpha_s),\text{virt}} + \Delta\lambda_{ijk}^{\mathcal{O}(\alpha_t\alpha_s),\text{virt}\otimes\text{ct}} + \Delta\lambda_{ijk}^{\mathcal{O}(\alpha_t\alpha_s),\text{ct}}, \quad (19.1)$$

which we will successively determine in this chapter.

We will start in Sec. 19.1 with the genuine two-loop contributions and explain in detail how the two-loop integrals, appearing in the course of the calculation, can be coped with.

The second term in Eq. (19.1), which comprises contributions of one-loop diagrams with inserted counterterms from the top-stop sector, will be treated in Sec. 19.2. We will close this chapter in Sec. 19.3 with the discussion of the  $\mathcal{O}(\alpha_t\alpha_s)$  counterterms to the trilinear Higgs self-couplings.

### 19.1. The Genuine Two-Loop Corrections to the Trilinear Higgs Self-Couplings

In order to determine the corrections of  $\mathcal{O}(\alpha_t\alpha_s)$  to the trilinear Higgs self-couplings, we first have to identify the relevant diagrams leading to contributions of the desired order. As before the  $\alpha_t$  is procured by top quarks and squarks, coupling to the external Higgs bosons. The additional corrections of  $\mathcal{O}(\alpha_s)$  can arise in two different ways: Either they can originate from additional gluons or their superpartners, the gluinos, coupled to the tops and stops, or they can emerge from four-stop vertices. Some generic representative diagrams contributing at  $\mathcal{O}(\alpha_t\alpha_s)$  are shown in Fig. 19.1. As these diagrams lead to UV-divergent two-loop integrals,

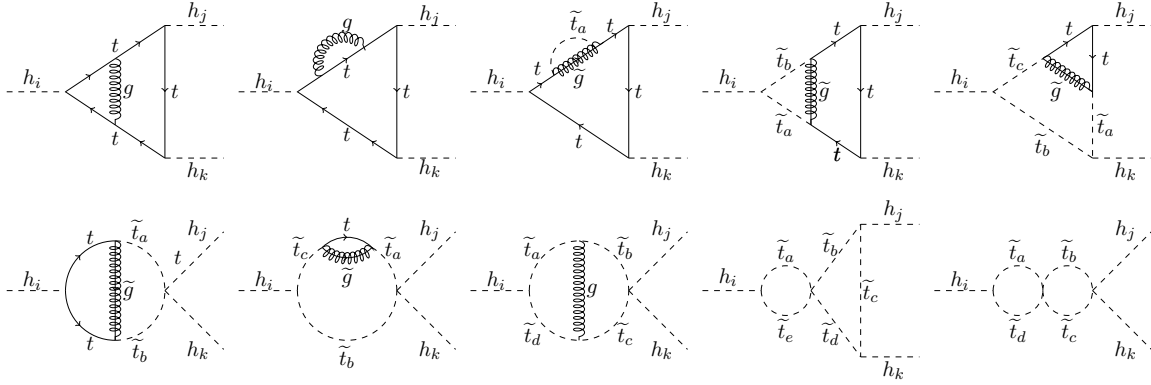


**Figure 19.1.:** Generic representative diagrams contributing to the  $\mathcal{O}(\alpha_t\alpha_s)$  corrections to the trilinear Higgs self-couplings between the Higgs bosons  $h_i, h_j, h_k, i, j, k \in \{1, 2, 3, 4, 5\}$  in the tree-level mass basis. The particles running in the loops are top quarks ( $t$ ), top squarks ( $\tilde{t}_{a/b/c/d/e}$ , with  $a, b, c, d, e \in \{1, 2\}$ ), gluons ( $g$ ) and gluinos ( $\tilde{g}$ ).

we need to define a regularization procedure, i.e. a method to isolate and extract the UV divergences of these integrals. In the previous chapter, we have applied DRed without further comment. Here however we have to be more careful. We have already mentioned in Subs. 3.1.1 that, unlike DReg, DRed is known to respect SUSY at full one-loop order. Yet, at two-loop level no general proof of SUSY non-violation under DRed has been conducted so far and only a few dedicated studies for certain special cases have been performed. In Ref. [76] the authors have verified that DRed does not violate SUSY in  $\mathcal{O}(\alpha_t\alpha_s)$  corrections to the Higgs boson masses in the MSSM. Their results also hold for the NMSSM as explained in Ref. [44]. Moreover, their arguments are not changed by adding one further external Higgs boson, as is required for our calculation. Hence, we conclude that we can apply DRed for our purposes without the need for SUSY restoring counterterms.

For the calculation of the two-loop integrals, we availed ourselves of well-tested and widely-used computer tools. `FeynArts 3.7` [152] was employed to generate all diagrams and the corresponding amplitudes. Subsequently, the Dirac and Lorentz indices were contracted and the Dirac traces evaluated with the help of `FeynCalc 8.2` [276, 277]. After this step, we encountered integrals of the generic form

$$\begin{aligned}
 & I_{\nu_1, \nu_2, \nu_3, \nu_4, \nu_5}^{D, \alpha, \beta, \gamma}(m_1^2, m_2^2, m_3^2, m_4^2, m_5^2) \\
 &= C^2 \int \frac{d^D q_1 d^D q_2 (q_1^2)^\alpha (q_2^2)^\beta (q_1 q_2)^\gamma}{(q_1^2 - m_1^2)^{\nu_1} (q_2 - m_2^2)^{\nu_2} ((q_1 - q_2)^2 - m_3^2)^{\nu_3} (q_1^2 - m_4^2)^{\nu_4} (q_2^2 - m_5^2)^{\nu_5}}, \quad (19.2) \\
 &\text{with } C = \left( \frac{(2\pi\mu_r)^{2\epsilon}}{i\pi^2} \right).
 \end{aligned}$$

These can further be manipulated and reduced to a set of basic integrals, the so-called *master integrals*, which was accomplished by means of the `Mathematica` [278] package `TARCER` [279]. This package was designed for the reduction of an even more general type of integrals and can handle the case of up to five different propagators and two external legs with non-vanishing external momenta. It is based on an algorithm devised by Tarasov [280, 281], called the *Tarasov algorithm*.

In our case all integrals can be reduced to only two master integrals, the one- and the two-loop

one-point function  $A_0^D(m^2)$  [282] and  $K_0^D(m_1^2, m_2^2, m_3^2)$  [283–289], given by

$$A_0^D(m^2) = C \int \frac{d^D q}{q^2 - m^2} = m^2 \frac{1}{\epsilon} + A_{\text{fin}}(m^2) + \epsilon A_\epsilon(m^2) + \mathcal{O}(\epsilon^2), \quad (19.3)$$

$$\begin{aligned} K_0^D(m_1^2, m_2^2, m_3^2) &= C^2 \int \frac{d^D q_1 d^D q_2}{(q_1^2 - m_1^2)(q_2 - m_2^2)((q_1 - q_2)^2 - m_3^2)} \\ &= K_{\text{div}_2}(m_1^2, m_2^2, m_3^2) \frac{1}{\epsilon^2} + K_{\text{div}_1}(m_1^2, m_2^2, m_3^2) \frac{1}{\epsilon} + K_{\text{fin}}(m_1^2, m_2^2, m_3^2) + \mathcal{O}(\epsilon). \end{aligned} \quad (19.4)$$

With their help all integrals  $I_{\nu_1, \nu_2, \nu_3, \nu_4, \nu_5}^{D, \alpha, \beta, \gamma}(m_1^2, m_2^2, m_3^2, m_4^2, m_5^2)$ , and thus all diagrams, can be expressed in the following form

$$\begin{aligned} &I_{\nu_1, \nu_2, \nu_3, \nu_4, \nu_5}^{D, \alpha, \beta, \gamma}(m_1^2, m_2^2, m_3^2, m_4^2, m_5^2) \\ &= \sum_{j, k=1}^5 c_{jk}^A(D, \{m_i\}) A_0^D(m_j^2) A_0^D(m_k^2) + \sum_{l, m, n=1}^5 c_{lmn}^K(D, \{m_i\}) K_0^D(m_l^2, m_m^2, m_n^2). \end{aligned} \quad (19.5)$$

The coefficients  $c_{jk}^A$  and  $c_{lmn}^K$  in general depend on the set of masses  $\{m_i\} = \{m_1, \dots, m_5\}$ , appearing in the integrand, and on the dimension  $D$  and are specific to the particular integral  $I_{\nu_1, \nu_2, \nu_3, \nu_4, \nu_5}^{D, \alpha, \beta, \gamma}$  under consideration.

For the final result, only the finite,  $\epsilon$ -independent terms of Eq. (19.5) are relevant. However, in order to check for a proper cancellation of all divergences, we also have to consistently extract the overall coefficients of the single and the double pole. To that end, Eq. (19.5) has to be expanded in a series in the regulator  $\epsilon$ .

In Eqs. 19.3 and 19.4, we have already performed the required expansion for the loop functions  $A_0^D$  and  $K_0^D$ . Being a two-loop function,  $K_0^D$  comprises, apart from a term  $\propto 1/\epsilon$ , also a double pole  $\propto 1/\epsilon^2$ . Furthermore, a term  $\propto \epsilon$  has to be considered in the expansion of  $A_0^D$ . Although this term vanishes for  $D \rightarrow 4$ , it leads to a non-vanishing finite part in Eq. (19.5), when multiplied with the pole term of the second  $A_0^D$ . Finally, for a complete expansion also the dependence of the coefficients  $c_{jk}^A$  and  $c_{lmn}^K$  on  $\epsilon$  has to be considered. These can contain terms  $\propto \epsilon$  but are free of poles. Inserting all expansions into Eq. (19.5), the coefficients of the single and double pole as well as the finite terms can be extracted.

## 19.2. Diagrams with Counterterms from the Top-Stop Sector

Apart from the genuine two-loop diagrams considered in the previous section, corrections of  $\mathcal{O}(\alpha_t \alpha_s)$  also arise from one-loop diagrams of  $\mathcal{O}(\alpha_t)$  containing the insertion of an  $\mathcal{O}(\alpha_s)$  counterterm from the top-stop sector. Generic representatives of these *counterterm inserted diagrams* are shown in Fig. 19.2.

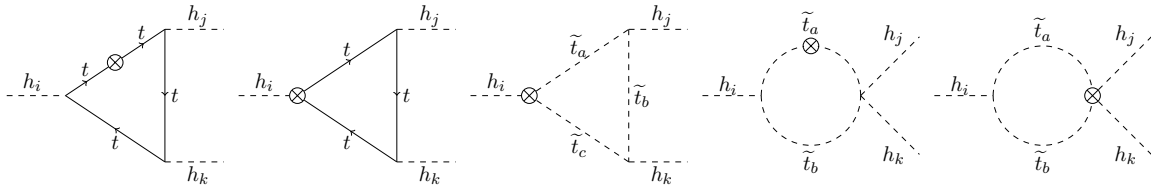


**Figure 19.2.:** Generic one-loop diagrams with the insertion of a counterterm from the top-stop sector contributing to the  $\mathcal{O}(\alpha_t \alpha_s)$  corrections to the trilinear Higgs self-couplings between the Higgs bosons  $h_i, h_j, h_k$ ,  $i, j, k \in \{1, 2, 3, 4, 5\}$  in the tree-level mass basis. The particles running in the loops are top quarks ( $t$ ) and top squarks ( $\tilde{t}_{a/b/c}$ , with  $a, b, c \in \{1, 2\}$ ).

Being of one-loop order, these diagrams do not require special treatment and can straightforwardly be calculated with the help of the usual chain `FeynArts 3.7 - FormCalc 8.2` [152,153].

The results for the one-loop diagrams can be expressed in terms of the scalar Passarino-Veltman functions  $A_0^D$ ,  $B_0^D$ ,  $C_0^D$  and  $D_0^D$  with vanishing external momenta, while the inserted top-stop counterterms also contain  $B_1^D$  and  $B_0^D$ -functions at finite momentum. All occurring loop functions with vanishing external momenta can be reduced to  $A_0^D$  functions, however special care has to be taken to properly include terms proportional to the regulator  $\epsilon$ . Multiplied with the poles of the inserted top-stop counterterms these can yield finite contributions to the final result. We quote the relevant relations in App. C.1.

Furthermore, the two-point function  $B_1^D(q^2, m_1^2, m_2^2)$ , appearing in the OS counterterms of the top-stop sector, can be reduced to  $A_0^D$  functions and the scalar two-point function  $B_0^D(q^2, m_1^2, m_2^2)$  at finite external momentum (cf. App. C.1). In our convention the latter is given by

$$B_0^D(p^2, m_1^2, m_2^2) = C \int \frac{d^D q}{(q^2 - m_1^2)((q+p)^2 - m_2^2)} \quad (19.6)$$

$$= \frac{1}{\epsilon} + B_{\text{fin}}(p^2, m_1^2, m_2^2) + \mathcal{O}(\epsilon), \quad (19.7)$$

where as before, an expansion in the regulator  $\epsilon$  has to be performed as indicated. Note, however, that we have not quoted a terms  $\propto \epsilon$  in this expansion. This is due to the fact that we do not include any terms proportional to  $\epsilon$  in the OS counterterms of the top-stop sector (cf. Sec. 17.1). Although their inclusion would lead to additional finite contributions to the counterterm inserted diagrams, they would not have any net effect on the final result. This can be attributed to the fact that the  $\epsilon$ -terms, if included, would also enter the Higgs WFRCs via the top mass counterterm (cf. Eq. (17.15)), as discussed in [44, 290]. It was explicitly checked that the effect of the thereby generated additional finite terms in the WFRCs exactly cancel those of the counterterm inserted diagrams. Hence, we can make use of our freedom to choose the finite parts of the counterterms in a convenient way and not incorporate the  $\epsilon$ -terms into the OS top-stop counterterms.

Like the results of the genuine two-loop diagrams, the expression for the counterterm inserted diagrams have to be expanded in  $\epsilon$  such that the coefficients of the single and double pole as well as the finite terms can be extracted.

### 19.3. The Counterterm of $\mathcal{O}(\alpha_t\alpha_s)$

In order to achieve a complete cancellation of all UV divergences, we also have to include the  $\mathcal{O}(\alpha_t\alpha_s)$  counterterms of the Higgs sector. The coupling counterterms  $\Delta\lambda_{ijk}^{\mathcal{O}(\alpha_t\alpha_s),\text{ct}}$  in the gauge basis have the same form as those derived in Eq. (18.23), where now instead of the  $\mathcal{O}(\alpha_t)$  parameter counterterms and WFRCs those of  $\mathcal{O}(\alpha_t\alpha_s)$  have to be inserted. Explicit expressions for the coupling counterterms in the gauge basis are given in App. B.3. Again, the corresponding counterterms in the mass basis are attained via a rotation with the matrix  $R$ . After an expansion of the resulting coupling counterterms in  $\epsilon$ , the cancellation of all UV divergences can be checked. We verified the finiteness of every component of  $\Delta\lambda_{h_i h_j h_k}^{\mathcal{O}(\alpha_t\alpha_s)}$ , which provides a strong consistency check for our procedure.

The final result for the effective trilinear Higgs self-couplings of  $\mathcal{O}(\alpha_t\alpha_s)$  can now be obtained by assembling all pieces determined in the previous sections. We cross-checked our results with an independent calculation performed by Dr. Dao Thi Nhung and found full agreement within numerical uncertainties in all steps. Furthermore, we considered our results in the limit of the real MSSM, which is achieved by  $\lambda, \kappa \rightarrow 0$ , while keeping  $\mu_{\text{eff}} = \lambda v_s / \sqrt{2}$  as well as  $A_\lambda$  and  $A_\kappa$  fixed and setting all complex phases to zero. This allowed us to compare our results to those obtained by the authors of Ref. [275], who determined the  $\mathcal{O}(\alpha_t\alpha_s)$  corrections to the trilinear Higgs self-couplings in the real MSSM. Again complete accordance could be verified.

---

## Numerical Analysis of the Corrections

---

Having completed the calculation of the corrections of  $\mathcal{O}(\alpha_t)$  and  $\mathcal{O}(\alpha_t\alpha_s)$ , we can now continue with the numerical analysis of our findings. Beforehand, however, in Sec. 20.1 we will go into details concerning the Higgs mass bases at different loop orders and dwell on the necessity of external leg corrections.

Afterwards, in Sec. 20.2, we will present the software tools that are applied for the numerical study and state all input parameters entering our calculations.

In Sec. 20.3 we will then first consider the corrections of  $\mathcal{O}(\alpha_t)$ . A comparison to the complete one-loop results with full momentum dependence will allow us to assess the reliability of our approximations.

Subsequently, we will study in Sec. 20.4 the impact of the corrections of  $\mathcal{O}(\alpha_t\alpha_s)$  on the trilinear Higgs self-couplings and investigate the convergence of the perturbative series and the theoretical uncertainty due to missing higher-order corrections. We will also consider the influence of the complex phases.

Sec. 20.5 will finally be dedicated to an examination of the effect of the  $\mathcal{O}(\alpha_t\alpha_s)$  corrections on Higgs-to-Higgs decays. We will add a discussion on the reliability of the approximation of vanishing external momentum in this context before we draw our conclusions.

### 20.1. Different Mass Bases

Up to now we have been working either in the gauge basis or in the tree-level mass basis. In order to examine and interpret physical results, however, neither of both is the proper choice. Instead, we have to introduce yet another basis  $\Phi^H$ , the physical mass basis at  $\mathcal{O}(\alpha_t\alpha_s)$ . In part II of this thesis, we chose our renormalization scheme of the 2HDM Higgs sector in such a way that the tree-level mass basis corresponds to the physical mass basis to all loop orders. Hence, the whole calculation could be carried out in terms of properly OS renormalized fields. However, in the NMSSM the much more involved situation with five mixing neutral Higgs bosons renders such a procedure virtually impossible and calls for performing the calculation in terms of  $\overline{\text{DR}}$  renormalized fields instead. This comes at the expense of working in a basis, that does not correspond to the physical basis. Consequently, when we calculate processes with external Higgs bosons, we have to take into account external leg corrections (cf Subs. 3.2.1), which we will incorporate in terms of finite *wave function correction factors*  $\hat{Z}$ .

The matrix  $\hat{Z}$ , which is in general complex and non-unitary, can be decomposed as [91, 291]

$$\hat{Z}_{ij} = \sqrt{\hat{z}_i \hat{z}_{ij}}, \quad i, j = 1, \dots, 5, \quad (20.1)$$

with

$$\hat{z}_i = \left( \left( \frac{\partial}{\partial p^2} \frac{i}{\hat{G}_{ii}(p^2)} \right) \Big|_{p^2=\mathcal{M}_{H_i}^2} \right)^{-1} \quad \text{and} \quad \hat{z}_{ij} = \frac{\hat{G}_{ij}(p^2)}{\hat{G}_{ii}(p^2)} \Big|_{p^2=\mathcal{M}_{H_i}^2}. \quad (20.2)$$

Again, summation over recurring indices is assumed throughout this section.  $\hat{G}(p^2)$  denotes the renormalized propagator matrix, i.e. the inverse of the renormalized two-point function

$$\hat{G}(p^2) = i\hat{\Gamma}^{-1}(p^2), \quad (20.3)$$

defined in analogy to Eq. (6.40). Here  $\hat{\Gamma}(p^2)$  includes the complete one-loop corrections with full momentum dependence and the  $\mathcal{O}(\alpha_t \alpha_s)$  corrections at  $p^2 = 0$ . Moreover,  $\mathcal{M}_{H_i}$  denotes the mass of the Higgs boson  $H_i$  in the  $\mathcal{O}(\alpha_t \alpha_s)$  mass basis  $\Phi^H$ , which is related to the reduced tree-level mass basis  $\Phi^h$  by

$$\Phi_i^H = \hat{Z}_{ij} \Phi_j^h, \quad \text{with} \quad (\Phi^H)^T = (H_1, H_2, H_3, H_4, H_5). \quad (20.4)$$

Calculating a process with external Higgs bosons in the tree-level mass basis, the properly OS renormalized quantity is obtained by multiplication with a factor of  $\hat{Z}$  for each external Higgs boson. For instance, the properly normalized partial width  $\Gamma_{H_i H_j H_k}$  for the Higgs-to-Higgs decay  $H_i \rightarrow H_j H_k$  is given by

$$\Gamma_{H_i H_j H_k} = \hat{Z}_{ii'} \hat{Z}_{jj'} \hat{Z}_{kk'} \Gamma_{h_{i'} h_{j'} h_{k'}}. \quad (20.5)$$

The matrix  $\hat{Z}$  yields the proper relation between the tree-level and the  $\mathcal{O}(\alpha_t \alpha_s)$  mass basis and diagonalizes the loop-corrected Higgs mass matrix in the reduced tree-level mass basis. However, it is not unitary and can hence not be treated as a rotation matrix. Consequently,  $\hat{Z}$  can also not be utilized to define *effective tree-level Higgs couplings*<sup>1</sup>. These are conveniently employed to incorporate higher-order effects into an observable and are obtained by rotating the tree-level Higgs couplings with a loop-corrected rotation matrix.

In order to arrive at the unitary loop-corrected rotation matrix required for this purpose, the  $p^2 = 0$  approximation has to be applied in the calculation of the Higgs mass matrix. That is, the external momentum has to be neglected both in the one-loop corrections and in the  $\mathcal{O}(\alpha_t \alpha_s)$  corrections to the Higgs mass matrix. In the  $p^2 = 0$  approximation, the loop-corrected mass matrix in the tree-level mass basis is hermitian such that its diagonalization is achieved by an orthogonal matrix  $\hat{Z}^0$ . It was shown in Ref. [290] that the absolute values of the elements of the matrices  $\hat{Z} R^h$  and  $\hat{Z}^0 R^h$  differ by less than 10%. Here  $R^h$  is the reduced rotation matrix introduced in Eq. (16.31), such that  $\hat{Z} R^h$  and  $\hat{Z}^0 R^h$  diagonalize the  $\mathcal{O}(\alpha_t \alpha_s)$  mass matrix in the gauge basis with or without full momentum dependence, respectively.

We will use the matrix  $\hat{Z}^0$  in the following sections, where we discuss the effective trilinear Higgs self-couplings  $\Lambda_{ijk}$  of  $\mathcal{O}(\alpha_t)$  and  $\mathcal{O}(\alpha_t \alpha_s)$  as defined in Ch. 15. Hence, these couplings will be given in a basis

$$\Phi_i^{H,0} = \hat{Z}_{ij}^0 \Phi_j^h, \quad (20.6)$$

which does not exactly correspond to the proper  $\mathcal{O}(\alpha_t \alpha_s)$  mass basis. However, in order to keep the notation clean, we will omit the index 0.

<sup>1</sup>Note that the notion of the term *effective* in this context differs slightly from the one in the remaining thesis, where we use this terms to denote the  $\mathcal{O}(\alpha_t)$ - or  $\mathcal{O}(\alpha_t \alpha_s)$ -corrected couplings at  $p^2 = 0$ .

When we discuss Higgs-to-Higgs decays in Sec. 20.5 on the other hand, we will apply Eq. (20.5) with full momentum dependence taken into account in  $\hat{Z}$  at one-loop order to guarantee proper OS renormalized external fields.

All rotation matrices and wave function correction factors discussed here can be obtained by means of the program package `NMSSMCALC` [292], which we will detail in the following section.

## 20.2. Software Tools and Numerical Setup

In order to perform the numerical analysis, we implemented all described corrections of  $\mathcal{O}(\alpha_t)$  and  $\mathcal{O}(\alpha_t\alpha_s)$  in the approximation of vanishing external momentum into a Fortran program. Furthermore, one of the authors<sup>2</sup> of Ref. [46] provided us with a Fortran code for the calculation of the full one-loop corrections to the trilinear Higgs self-couplings, as described in their publication, but extended to include the case of the CP-violating NMSSM.

Both were linked to the program package `NMSSMCALC` [292], which calculates corrections to the NMSSM Higgs boson masses up to  $\mathcal{O}(\alpha_t\alpha_s)$  as well as decay widths and branching ratios of all Higgs bosons for the CP-conserving and the CP-violating NMSSM. As in our calculation of the trilinear couplings, the  $\mathcal{O}(\alpha_t\alpha_s)$  corrections to the masses are determined for two different renormalization schemes in the top-stop sector, the OS and the  $\overline{\text{DR}}$  scheme. `NMSSMCALC` contains a routine performing the conversion of the relevant parameters between the two schemes (cf. Sec. 17.1), necessary for a meaningful comparison of the OS and the  $\overline{\text{DR}}$  results. Furthermore, the running of the top mass is implemented as described in App. D.1. The decay widths of the NMSSM Higgs bosons are calculated by a routine based on the Fortran code `HDECAY` [183, 184], which was extended to the case of the NMSSM. All decays include the dominant QCD corrections, augmented by SUSY corrections for the fermionic decays. Details can be found in [292].

We used `NMSSMCALC` for the calculation of the Higgs boson masses up to  $\mathcal{O}(\alpha_t\alpha_s)$  and for the conversion of the parameters, to guarantee a consistent treatment of the latter in the corrections to the masses and the trilinear self-couplings. Furthermore, we employed the program to determine the partial decay widths and branching ratios of Higgs-to-Higgs decays, subject to higher-order corrections. For this purpose we extended the relevant routine in `NMSSMCALC` such that the corresponding decay widths include the full one-loop corrections and the newly determined  $\mathcal{O}(\alpha_t\alpha_s)$  corrections to the trilinear Higgs self-couplings.

On the other hand, `NMSSMCALC` was employed in a parameter scan over the NMSSM parameter space to find input parameter configurations which are consistent with current LHC Higgs and SUSY data as well as theoretical constraints. To that end, `NMSSMCALC` was linked to the program packages `HiggsBounds` [186–188] and `HiggsSignals` [189] (cf. Sec. 12.2). All effective couplings, masses, widths and branching ratios of the Higgs bosons, required as input to these programs, were provided by `NMSSMCALC`. The effective couplings to gluons and photons, normalized to the respective SM couplings, were obtained by taking the ratio of the partial decay widths of the Higgs bosons into gluons and photons in the NMSSM and those in the SM for a Higgs boson of the corresponding mass. For the relevant widths, higher-order QCD and EW corrections were taken into account as far as they are known for the NMSSM. Corrections which are not available for the NMSSM were neglected consistently also in the SM decay widths. Again we refer to Ref. [292] for further details. Moreover, accordance with theoretical constraints from perturbativity and from color or charge breaking minima mentioned in [36, 37] as well as with experimental constraints from SUSY searches [293] available at that time was guaranteed by choosing the range of the soft SUSY breaking masses and trilinear couplings and of  $\lambda$  and  $\kappa$  appropriately. Our scanning routine is based on the one developed for Ref. [290]<sup>3</sup>, where more information can be found.

<sup>2</sup>We are grateful to Dr. Dao Thi Nhung.

<sup>3</sup>We thank Dr. Kathrin Walz for sharing her code.

	Scenario 1	Scenario 2	Scenario 3
$m_{\tilde{f}_R} = m_{\tilde{F}}$	3000 GeV	3000 GeV	3000 GeV
$m_{\tilde{t}_R}$	1909 GeV	1170 GeV	1940 GeV
$m_{\tilde{Q}_3}$	2764 GeV	1336 GeV	2480 GeV
$m_{\tilde{b}_R}$	1108 GeV	1029 GeV	1979 GeV
$m_{\tilde{L}_3}$	472 GeV	2465 GeV	2667 GeV
$m_{\tilde{\tau}_R}$	1855 GeV	301 GeV	1689 GeV
$m_{\tilde{t}_1}^{\text{OS}}$	1992 GeV	1145 GeV	1996 GeV
$m_{\tilde{t}_2}^{\text{OS}}$	2820 GeV	1421 GeV	2528 GeV
$m_{H^\pm}$	1491 GeV	788 GeV	613 GeV
$\tan \beta$	7.52	4.02	8.97
$\varphi_u$	0	0	0
$ A_{u,c,t} $ $\varphi_{A_{u,c,t}}$	1283 GeV $\pi$	1824 GeV 0	1192 GeV $\pi$
$ A_{d,s,b} $ $\varphi_{A_{d,s,b}}$	1020 GeV $\pi$	16539 GeV $\pi$	685 GeV 0
$ A_{e,\mu,\tau} $ $\varphi_{A_{e,\mu,\tau}}$	751 GeV $\pi$	1503 GeV $\pi$	778 GeV 0
$ M_1 $ $\varphi_{M_1}$	908 GeV 0	862 GeV 0	517 GeV 0
$ M_2 $ $\varphi_{M_2}$	237 GeV 0	211 GeV 0	239 GeV 0
$ M_3 $ $\varphi_{M_3}$	1966 GeV 0	2285 GeV 0	1544 GeV 0
$ A_\kappa $ $\varphi_{A_\kappa}$	178 GeV $\pi$	180 GeV 0	810 GeV $\pi$
$ \mu_{\text{eff}} $ $\varphi_{\mu_{\text{eff}}}$	184 GeV 0	174 GeV 0	104 GeV 0
$ \lambda $ $\varphi_\lambda$	0.374 0	0.629 0	0.267 0
$ \kappa $ $\varphi_\kappa$	0.162 0	0.208 $\pi$	0.539 0

**Table 20.1.:** Input parameters for the scenarios studied in the following.  $m_{\tilde{f}_R}/m_{\tilde{F}}$  denotes the mass of all right-/left-handed first and second generation sfermions. We also give the values for the OS stop masses  $m_{\tilde{t}_1}^{\text{OS}}$  and  $m_{\tilde{t}_2}^{\text{OS}}$ . All scenarios have been obtained by means of a scan of the NMSSM parameter space as described in the text.

In the following numerical analysis, we will consider three different scenarios, resulting from the parameter scan. All SUSY parameters for the three scenarios are summarized in Tab. 20.1. Following SLHA [294, 295] conventions, we treat the soft-SUSY-breaking parameters as well as  $\lambda$ ,  $\kappa$ ,  $A_\kappa$ ,  $\mu_{\text{eff}}$  and  $\tan \beta$  as  $\overline{\text{DR}}$  parameters at the SUSY breaking scale  $M_{\text{SUSY}}$ , which we set to

$$M_{\text{SUSY}} = \sqrt{m_{\tilde{Q}_3} m_{\tilde{t}_R}}. \quad (20.7)$$

As a result, all parameters entering the stop sector have to be converted to OS parameters, if the OS scheme is chosen for the top-stop sector.  $m_{H^\pm}$  on the other hand is treated as OS parameter, in accordance with our renormalization conditions. The mass values for all SM particles that enter the calculation can be found in Tab. 20.2. In case  $\overline{\text{DR}}$  conditions are

$M_Z$ [GeV]	$M_W$ [GeV]	$m_t$ [GeV]	$m_b^{\overline{\text{MS}}}(m_b^{\overline{\text{MS}}})$ [GeV]	$m_s$ [MeV]	$m_c$ [GeV]
91.1876	80.385	173.5	4.18	100	1.42
$m_u$ [MeV]	$m_d$ [MeV]	$m_e$ [keV]	$m_\mu$ [MeV]	$m_\tau$ [GeV]	
2.5	4.95	510.99891	105.658367	1.77684	

**Table 20.2.:** Masses of the SM particles used in the calculation. All values were taken from Ref. [54]. Note that the light quark masses have only a small impact on the higher-order corrections.

applied for the top-stop sector, a conversion of the quoted OS top mass to its  $\overline{\text{DR}}$  value is necessary. Moreover, we use as input for the coupling constants [54, 141]

$$\alpha(M_Z) = \frac{1}{128.962} \quad \text{and} \quad \alpha_s^{\overline{\text{MS}}}(M_Z) = 0.1184. \quad (20.8)$$

For  $\alpha_s$  we take into account SM two-loop RGE evolution [296] up to  $M_{\text{SUSY}}$ , where a conversion to  $\alpha_s^{\overline{\text{DR}}}$  [297] is performed.

Using the input parameters specified above, `NMSSMCALC` determines the physical mass spectrum for the Higgs bosons and all SUSY particles. For our purposes, especially the masses of the Higgs bosons and the composition of the Higgs mass eigenstates in terms of gauge eigenstates will be important. Therefore we summarize the masses of the five physical Higgs bosons, calculated up to  $\mathcal{O}(\alpha_t\alpha_s)$ , in Tab. 20.3, where we also state the main component of the respective mass eigenstates. Furthermore, we quote the tree-level mass values, since these will be needed for the calculation of the full one-loop corrections to the trilinear Higgs self-couplings.

	$H_1$	$H_2$	$H_3$	$H_4$	$H_5$
Scenario 1					
$m_{H_i}^{\text{tree}}$ [GeV]	71.14 ( $h_u$ )	117.49 ( $h_s$ )	211.12 ( $a_s$ )	1491.05 ( $a$ )	1491.61 ( $h_d$ )
$m_{H_i}^{\mathcal{O}(\alpha_t\alpha_s),\text{OS}}$ [GeV]	94.68 ( $h_s$ )	125.06 ( $h_u$ )	217.32 ( $a_s$ )	1490.47 ( $a$ )	1491.70 ( $h_d$ )
$m_{H_i}^{\mathcal{O}(\alpha_t\alpha_s),\overline{\text{DR}}}$ [GeV]	94.41 ( $h_s$ )	124.24 ( $h_u$ )	217.33 ( $a_s$ )	1490.49 ( $a$ )	1491.07 ( $h_d$ )
Scenario 2					
$m_{H_i}^{\text{tree}}$ [GeV]	79.15 ( $h_s$ )	103.55 ( $h_u$ )	146.78 ( $a_s$ )	796.62 ( $h_d$ )	803.86 ( $a$ )
$m_{H_i}^{\mathcal{O}(\alpha_t\alpha_s),\text{OS}}$ [GeV]	102.99 ( $h_s$ )	126.09 ( $h_u$ )	128.94 ( $a_s$ )	796.45 ( $h_d$ )	803.07 ( $a$ )
$m_{H_i}^{\mathcal{O}(\alpha_t\alpha_s),\overline{\text{DR}}}$ [GeV]	103.09 ( $h_s$ )	124.55 ( $h_u$ )	128.91 ( $a_s$ )	796.36 ( $h_d$ )	803.03 ( $a$ )
Scenario 3					
$m_{H_i}^{\text{tree}}$ [GeV]	49.17 ( $h_s$ )	99.83 ( $h_u$ )	608.21 ( $a$ )	611.77 ( $h_d$ )	715.92 ( $a_s$ )
$m_{H_i}^{\mathcal{O}(\alpha_t\alpha_s),\text{OS}}$ [GeV]	83.66 ( $h_s$ )	124.95 ( $h_u$ )	608.73 ( $a$ )	611.37 ( $h_d$ )	694.76 ( $a_s$ )
$m_{H_i}^{\mathcal{O}(\alpha_t\alpha_s),\overline{\text{DR}}}$ [GeV]	83.03 ( $h_s$ )	124.34 ( $h_u$ )	608.71 ( $a$ )	611.36 ( $h_d$ )	694.78 ( $a_s$ )

**Table 20.3.:** Masses of the five physical NMSSM Higgs bosons within the Scenario 1, 2 and 3 at tree level and at  $\mathcal{O}(\alpha_t\alpha_s)$  for the two renormalization schemes in the top-stop sector. In parentheses we quote the main components of the respective mass eigenstates.

All three scenarios, to be investigated below, feature an SM-like Higgs boson<sup>4</sup>, i.e. a Higgs boson with a mass of  $m_h = 125 \pm 3$  GeV, which is capable of reproducing the Higgs signals observed at the LHC within current uncertainties. In the following sections, we will denote a Higgs boson featuring these properties by  $h$ . Note that the comparatively large uncertainty range of  $\pm 3$  GeV, which is considered in the scan for  $m_h$ , accounts for typical theoretical uncertainties in SUSY Higgs mass calculations [298]. The LHC constraints force the SM-like Higgs boson to be dominated by the  $h_u$  gauge eigenstate. This is due to the fact that Higgs

<sup>4</sup>In principle also scenarios are possible, in which two Higgs bosons, that are close in mass, account for the Higgs signals observed at the LHC [46, 242, 243]. We will, however, not consider such scenarios in the following.

production mainly proceeds via gluon fusion, which is mostly mediated by top loops for the small to moderate values of  $\tan\beta$  of our scenarios. Hence, sufficiently large production rates can only be accommodated by a substantial  $h_u$  admixture.

Subsequently, we will denote the mass eigenstate with the largest  $h_u$  component as SM-like.

### 20.3. Comparison between Full One-Loop-Corrected and Effective $\mathcal{O}(\alpha_t)$ Couplings

In Sec. 15 we have defined the effective trilinear Higgs self-couplings as the sum of the tree-level couplings and the  $\mathcal{O}(\alpha_t)$  and  $\mathcal{O}(\alpha_t\alpha_s)$  corrections at vanishing external momentum. We will use these effective couplings in the subsequent section to investigate the numerical impact of the  $\mathcal{O}(\alpha_t\alpha_s)$  corrections on the trilinear couplings of three SM-like Higgs bosons, on the theoretical uncertainty and on the convergence of the perturbative expansion. First, however, we want to examine the goodness of the  $\mathcal{O}(\alpha_t)$  corrections as compared to the full one-loop results. This will allow us to estimate the reliability of the approximations made in calculating the effective trilinear Higgs self-couplings.

There are two important points to be considered. On the one hand, we have to investigate the influence of corrections originating from outside the top-stop sector, which are neglected in the  $\mathcal{O}(\alpha_t)$  and the  $\mathcal{O}(\alpha_t\alpha_s)$  approximation. On the other hand, we must examine the goodness of the approximation of vanishing external momentum. As mentioned in Ch. 15, the approximation of vanishing external momentum is known to be applicable if the typical external momentum remains below the threshold of on-shell production of the loop particles. The  $\mathcal{O}(\alpha_t)$  corrections are hence expected to yield reliable results below the top resonance at  $p^2 = (2m_t)^2$ . We can explicitly check this as well as the influence of non- $\mathcal{O}(\alpha_t)$  corrections since we have the complete one-loop corrections with full momentum dependence at our disposal.

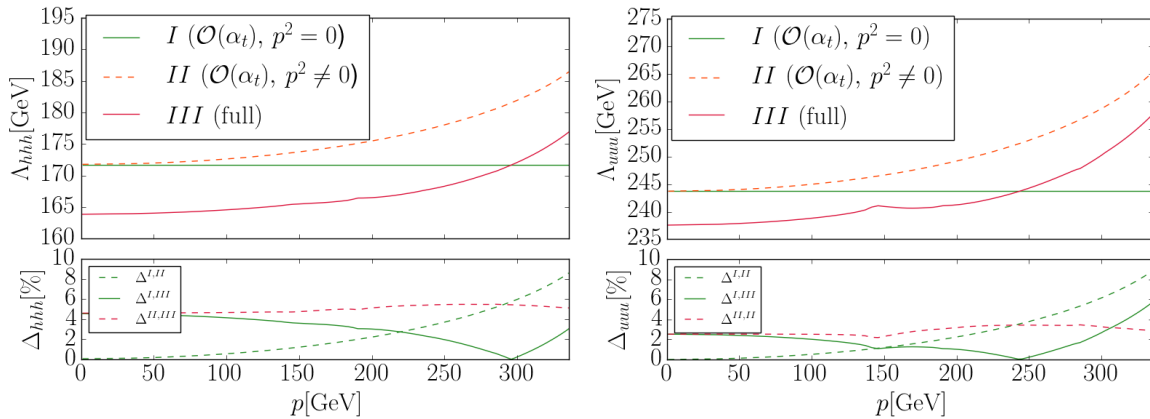


**Figure 20.1.:** Comparison of different approximations for the couplings  $\Lambda_{hhh}$  and  $\Lambda_{uuu} \equiv \Lambda_{h_u h_u h_u}$  at one-loop order. The upper panels show the couplings  $\Lambda_{hhh}$  (left) and  $\Lambda_{h_u h_u h_u}$  (right) with full one-loop corrections (red), momentum dependent  $\mathcal{O}(\alpha_t)$  corrections (orange dashed) and  $\mathcal{O}(\alpha_t)$  corrections at vanishing external momentum (green), as a function of the external momentum  $p$ . The lower panels display the relative corrections as defined in Eq. (20.9). All input parameters are chosen according to Scenario 1.

Fig. 20.1 shows a comparison of three different one-loop approximations of the trilinear Higgs self-couplings of three SM-like Higgs bosons in the mass eigenstates (left plot) and of three  $h_u$  gauge eigenstates (right plot). All couplings are depicted as a function of the absolute value of the external momentum below the top resonance. For the displayed results, we have chosen the input parameters according to Scenario 1 and fixed the top and stop masses at their OS values.

The red curve represents the full one-loop-corrected trilinear couplings (*III*), whereas the dashed orange and the green curves display the results including only  $\mathcal{O}(\alpha_t)$  corrections. For the dashed orange curve, we have taken into account a non-vanishing external momentum (*II*), while the green curve shows the results obtained in the effective potential approach (*I*), as described in Sec. 18.2. In the lower panel we show the normalized differences

$$\Delta^{a,b} = \left| \frac{\Lambda_{ijk}^a - \Lambda_{ijk}^b}{\Lambda_{ijk}^a} \right| \quad (20.9)$$

expressed as a percentage, where  $a$  and  $b$  denote the approximation applied for the couplings, abbreviated by *I*, *II* and *III*.

An estimation for the goodness of the approximation of vanishing external momentum in the  $\mathcal{O}(\alpha_t)$  corrections can be obtained from the dashed green curve in the lower panels, which represents the relative difference between curves *I* and *II*. In both bases the influence of the external momentum  $p$  on the  $\mathcal{O}(\alpha_t)$  corrections remains below 10% for  $p \lesssim 340$  GeV. Since we are considering here the coupling of three SM-like Higgs bosons or of three  $h_u$  eigenstates, which constitute the main component of the SM-like Higgs boson (cf. Sec. 20.2), a typical external momentum is of the order of  $p \approx 2m_h \approx 250$  GeV, corresponding to the threshold of on-shell  $h$  pair production. For this value of  $p$ , the relative difference between the two  $\mathcal{O}(\alpha_t)$  curves approximately amounts to 4%, which demonstrates the validity of the effective potential approximation for the  $\mathcal{O}(\alpha_t)$  corrections in the typical momentum range.

Concerning the applicability of the  $\mathcal{O}(\alpha_t)$  approximation itself, i.e. the neglect of all particles apart from top quarks and squarks in the loops, we can compare the orange dashed and the red curve in the upper panels, whose relative difference is displayed as red-dashed curve in the lower panels. As this curve reflects, the non- $\mathcal{O}(\alpha_t)$  corrections give rise to a nearly constant off-set amounting to 3% and 5% in the mass and gauge eigenstates, respectively, modulated only by tiny resonances. The latter are caused by virtual contributions of the light Higgs mass eigenstates  $h_1$  and  $h_2$ , which exhibit tree-level masses of 71 GeV and 117 GeV in the chosen scenario<sup>5</sup>. As it shows, the resonances completely drown in the huge corrections resulting from top and stop loops. Furthermore, in view of the corresponding tree-level couplings of  $\lambda_{hhh} = 76.2$  GeV and  $\lambda_{h_u h_u h_u} = 101.7$  GeV, it becomes obvious that the  $\mathcal{O}(\alpha_t)$  corrections by far dominate the one-loop corrections, amounting to 90% and 94% of the full corrections, respectively.

Finally, we can compare directly our effective couplings of  $\mathcal{O}(\alpha_t)$  to the full one-loop-corrected ones. From the solid green curve in the lower panel, we can deduce a relative difference below 4% (mass eigenstates) and 6% (gauge eigenstates) over the whole plotted momentum range for the chosen scenario. This demonstrates the effective  $\mathcal{O}(\alpha_t)$  corrections to capture the dominant corrections at one-loop order and the external momentum to be negligible in the shown range.

Up to now we have discussed only the trilinear Higgs couplings of three  $h_u$  gauge eigenstates and of three SM-like Higgs bosons  $h$ , which are mainly  $h_u$ -like. For other gauge eigenstates (apart from  $a_u$ ), the  $\mathcal{O}(\alpha_t)$  corrections are less pronounced, due to a vanishing coupling of the doublet  $H_d$  and the singlet  $S$  to top quarks. As a consequence, for these components the influence of other contributions, e.g. of bottoms, sbottoms and especially of light Higgs bosons, gain importance. Hence, the  $\mathcal{O}(\alpha_t)$ -approximation deteriorates, most notably in the considered range below the  $t\bar{t}$  threshold, where the contributions of light Higgs loops become resonant. This can be seen in Fig. 20.2, which shows the full one-loop corrections together with the momentum dependent  $\mathcal{O}(\alpha_t)$  corrections for different couplings in the gauge basis in Scenario 2 (left) and Scenario 3 (right) as function of the external momentum. The resonances resulting from light Higgs bosons are clearly visible and a comparison with Tab. 20.3 shows

<sup>5</sup>Note, that we use the tree-level masses for all particles appearing in loops.

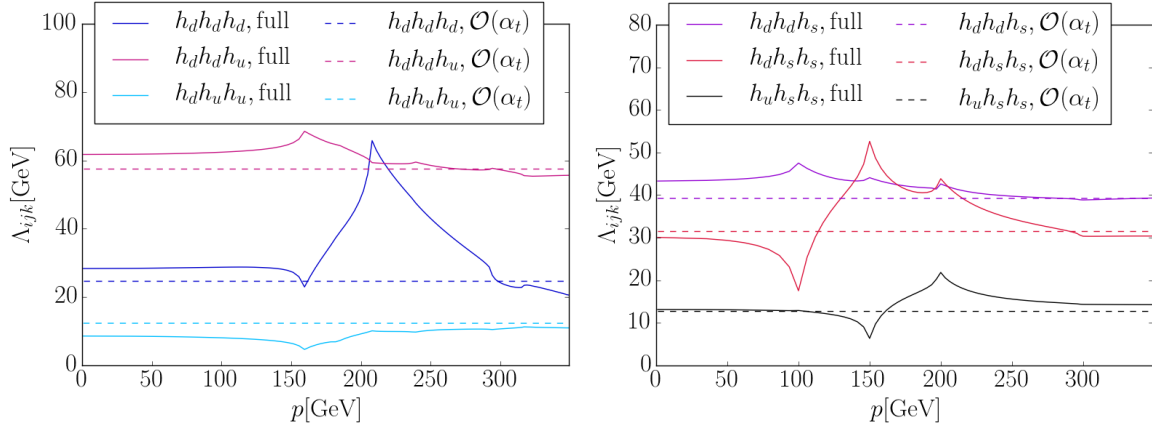


**Figure 20.2.:** Comparison of full one-loop and momentum dependent  $\mathcal{O}(\alpha_t)$ -corrected couplings in the gauge basis for components as specified in the legend as a function of the external momentum. The left plot contains results for Scenario 2, the right one shows results for Scenario 3.

that they appear at momenta corresponding to linear combinations of the three (Scenario 2) or two (Scenario 3) lightest tree-level Higgs masses. These resonances are particularly important for all scenarios with large  $A_\lambda$  or  $A_\kappa$ , leading to increased tree-level couplings  $\lambda_{h_d h_u h_s}$  or  $\lambda_{h_s h_s h_s}$ , respectively (cf. App. A.3). For the trilinear couplings with external  $h_d$ -dominated Higgs bosons, a large coupling  $\lambda_{h_d h_u h_s}$  implies enhanced contributions of loops with  $h_u$  and  $h_s$  dominated mass eigenstates. An increased coupling  $\lambda_{h_s h_s h_s}$ , in turn, leads to heightened contributions of loops with  $h_s$ -dominated states to the trilinear couplings with external  $h_s$ -like Higgs bosons. Since  $h_u$  and  $h_s$  are the main constituents of the light Higgs mass eigenstates  $h_1$  and  $h_2$  in the considered scenarios, this corresponds to an increased influence of light Higgs boson loops on the respective trilinear couplings.

Within Scenario 2, which exhibits a relatively large value of  $A_\lambda$ , this increased influence becomes particularly visible in the coupling  $\Lambda_{h_d h_d h_d}^{\mathcal{O}(\alpha_t)}$  (dark blue curve), where the loops containing the light Higgs bosons  $h_1$  and  $h_2$  are proportional to  $\lambda_{h_d h_u h_s}^3$ , i.e.  $A_\lambda^3$ . Near the resonances, the difference between the full one-loop and the  $\mathcal{O}(\alpha_t)$ -corrected couplings can become as large as 165%. For the other two curves, corresponding to  $\Lambda_{h_d h_d h_u}^{\mathcal{O}(\alpha_t)}$  (pink curve) and  $\Lambda_{h_d h_u h_u}^{\mathcal{O}(\alpha_t)}$  (light blue curve), the resonances are still clearly visible but suppressed since one or two external  $h_d$ s are replaced by  $h_u$ s, such that the light Higgs loops are enhanced only by factors of  $A_\lambda^2$  or  $A_\lambda$ .

Scenario 3 features a comparatively large value of  $A_\kappa$ , hence couplings with external  $h_s$ -like Higgs bosons, like  $\Lambda_{h_d h_s h_s}^{\mathcal{O}(\alpha_t)}$  (red curve) or  $\Lambda_{h_u h_s h_s}^{\mathcal{O}(\alpha_t)}$  (black curve) are particularly affected by the resonances, since for these the diagrams with light Higgs bosons are proportional to  $\lambda_{h_s h_s h_s}^2$ , i.e.  $A_\kappa^2$ . Here the deviation of the full-one loop from the  $\mathcal{O}(\alpha_t)$  result can become as large as 71% for  $\Lambda_{h_u h_s h_s}^{\mathcal{O}(\alpha_t)}$  and 66% for  $\Lambda_{h_d h_s h_s}^{\mathcal{O}(\alpha_t)}$  near the resonances. For the purple curve, corresponding to  $\Lambda_{h_d h_d h_s}^{\mathcal{O}(\alpha_t)}$ , the deviation is reduced to less than 21% due to the replacement of one external  $h_s$  by  $h_d$ .

Note, however, that a large value of  $A_\lambda$ , i.e. an enhanced coupling  $\lambda_{h_d h_u h_s}$ , does not at the same time have a huge effect on the corrections to the trilinear  $h_u$ -couplings. This is due to the fact that for an external  $h_u$ , the coupling  $\lambda_{h_d h_u h_s}$  only appears in diagrams containing at least one virtual  $h_d$  dominated state, which corresponds to a heavy Higgs boson in all considered scenarios. Hence the contributions of these diagrams are suppressed.

We conclude that the restriction to the corrections of  $\mathcal{O}(\alpha_t)$  is reliable for  $h_u$  dominated Higgs bosons, while for  $h_d$  and  $h_s$  dominated mass eigenstates it is recommended to include the full one-loop corrections, in particular in the region where the resonances of light Higgs bosons

are important.

In the following sections, we will hence examine the effective couplings as defined in Ch. 15 only for the  $h_u$  gauge eigenstates or for the  $h_u$  dominated SM-like mass eigenstates  $h$ . As argued above, for these the  $\mathcal{O}(\alpha_t)$  corrections capture the dominant contributions and furthermore the approximation of vanishing external momentum is justified for typical momenta around  $p \approx 2m_h$ .

Once we go beyond the momentum range considered in this section, the approximation of vanishing external momentum no longer needs to be reliable. Therefore, we will take into account the full one-loop corrections to the trilinear Higgs self-couplings when we investigate the decays of heavy Higgs bosons with masses above 350 GeV in Sec. 20.5.

## 20.4. Numerical Analysis of the $\mathcal{O}(\alpha_t\alpha_s)$ Corrections

Having defined the range of validity of our approximations, we are now in the position to examine and discuss the effective trilinear Higgs self-couplings of  $\mathcal{O}(\alpha_t\alpha_s)$ . Our particular interest is in investigating the stability of the perturbative expansion and in estimating the theoretical uncertainty due to missing higher-order corrections. Furthermore, we want to consider the influence of the complex phases, entering through radiative corrections, on the trilinear Higgs self-couplings.

One possibility to estimate the theoretical uncertainty entails comparing the results obtained in two different renormalization schemes. As mentioned in Subs. 3.1.2, every renormalization scheme must eventually lead to the same final answer, if all terms in the perturbative series are summed up. At finite orders, however, the results differ due to missing higher-order terms, which can be exploited to estimate the size of the latter. In order for the perturbative expansion to be meaningful, both the size of the additional corrections and the remaining theoretical uncertainty have to decrease at higher orders.

We investigate these issues in Fig. 20.3, showing the effective coupling  $\Lambda_{hhh}$  for three SM-like Higgs bosons at  $\mathcal{O}(\alpha_t)$  (blue curves) and  $\mathcal{O}(\alpha_t\alpha_s)$  (red curves) within Scenario 1. Depending on the choice of the renormalization scheme for the top-stop sector, the curves are labelled as  $\overline{\text{DR}}$  (dashed curves) or OS (solid curves). In the following, the designation OS and  $\overline{\text{DR}}$  will always refer to the renormalization of the top-stop sector. Furthermore, we illustrate for comparison the effective trilinear Higgs self-coupling of the SM  $\Lambda_{\text{SM}}^{\mathcal{O}(\alpha_t\alpha_s)}$  (magenta curves), calculated within the same approximations, i.e. including corrections of  $\mathcal{O}(\alpha_t)$  and  $\mathcal{O}(\alpha_t\alpha_s)$  at vanishing external momentum. This time, the dashed/solid curve represents the result for  $\overline{\text{DR}}$ /OS renormalization of the top sector only. All couplings are shown as a function of the soft-SUSY-breaking parameter  $A_t^{\overline{\text{DR}}}$ , which enters the calculation as input parameter and is varied for illustrative purposes in a range from  $-3000$  to  $+3000$  GeV. Note that we demand the constraints of the parameter scan to be fulfilled only at  $A_t^{\overline{\text{DR}}} = -1283$  GeV, corresponding to the value of  $A_t^{\overline{\text{DR}}}$  quoted in Tab. 20.1.

The corrections, both those of  $\mathcal{O}(\alpha_t)$  and those of  $\mathcal{O}(\alpha_t\alpha_s)$ , are found to be large in the chosen scenario. A comparison at the Scenario 1 value  $A_t^{\overline{\text{DR}}} = -1283$  GeV reveals that the  $\mathcal{O}(\alpha_t)$  corrections enhance the tree-level coupling  $\lambda_{hhh}^{\text{OS}} = 76.2$  GeV or  $\lambda_{hhh}^{\overline{\text{DR}}} = 71.8^6$  GeV by 123% in the OS and by 53% in the  $\overline{\text{DR}}$  scheme, while the  $\mathcal{O}(\alpha_t\alpha_s)$  corrections lead to a reduction of the one-loop results by 21% in the OS scheme and to a further increase by 8% in the  $\overline{\text{DR}}$  scheme. This indicates on the one hand that, although the corrections are huge, especially in the OS scheme, they decline with growing loop order such that our confidence in the convergence of the perturbative series is corroborated. Note in this context that the better convergence of the  $\overline{\text{DR}}$  scheme is due to the fact that the coupling  $\Lambda_{hhh}^{\mathcal{O}(\alpha_t),\overline{\text{DR}}}$  already

<sup>6</sup>The scheme dependence of the tree-level coupling results from the rotation with the loop-corrected matrix  $\hat{Z}^0$  to the  $\mathcal{O}(\alpha_t\alpha_s)$  mass basis  $\Phi^{H,0}$ .

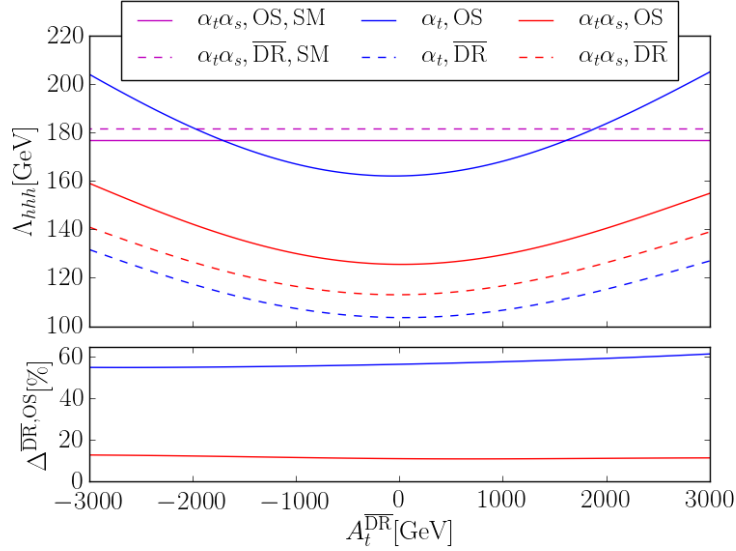


**Figure 20.3.:** Effective trilinear Higgs self-couplings for three SM(-like) Higgs bosons as a function of the input parameter  $A_t^{\overline{\text{DR}}}$ . The blue (red) curves show the results for the couplings in the complex NMSSM at  $\mathcal{O}(\alpha_t)$  ( $\mathcal{O}(\alpha_t\alpha_s)$ ), the magenta curves illustrate the couplings in the SM at  $\mathcal{O}(\alpha_t\alpha_s)$ . The solid (dashed) curves display the results for the OS ( $\overline{\text{DR}}$ ) scheme. In the lower panel we show an estimation for the theoretical uncertainty, defined according to Eq. (20.10), at  $\mathcal{O}(\alpha_t)$  (blue) and  $\mathcal{O}(\alpha_t\alpha_s)$  (red). A similar plot was published in [47].

includes part of the corrections which in the OS scheme enter only at  $\mathcal{O}(\alpha_t\alpha_s)$ . This is caused by the conversion of the OS top mass used as input parameter to its  $\overline{\text{DR}}$  value, as discussed in [44].

On the other hand, it shows that the results in the two different schemes, which are far apart at  $\mathcal{O}(\alpha_t)$ , approach each other when the corrections of  $\mathcal{O}(\alpha_t\alpha_s)$  are added. This can be seen in the lower panel, where we display the quantity  $\Delta^{\overline{\text{DR}},\text{OS}}$ , defined as the normalized difference

$$\Delta^{\overline{\text{DR}},\text{OS}} = \left| \frac{\Lambda_{hhh}^{a,\text{OS}} - \Lambda_{hhh}^{a,\overline{\text{DR}}}}{\Lambda_{hhh}^{a,\overline{\text{DR}}}} \right|, \quad \text{with } a \in \{\mathcal{O}(\alpha_t), \mathcal{O}(\alpha_t\alpha_s)\}. \quad (20.10)$$

Using the thus defined  $\Delta^{\overline{\text{DR}},\text{OS}}$  as a measure for the theoretical uncertainty, we find the latter to be reduced from about 55% at  $\mathcal{O}(\alpha_t)$  to 12% at  $\mathcal{O}(\alpha_t\alpha_s)$  (for  $A_t^{\overline{\text{DR}}} = -1283$  GeV).

Another interesting investigation is the comparison between the NMSSM and the SM results. At  $A_t^{\overline{\text{DR}}} = -1283$  GeV we find

$$\Lambda_{hhh}^{\mathcal{O}(\alpha_t\alpha_s),\text{OS}} = 0.75 \cdot \Lambda_{\text{SM}}^{\mathcal{O}(\alpha_t\alpha_s),\text{OS}}, \quad (20.11)$$

$$\Lambda_{hhh}^{\mathcal{O}(\alpha_t\alpha_s),\overline{\text{DR}}} = 0.66 \cdot \Lambda_{\text{SM}}^{\mathcal{O}(\alpha_t\alpha_s),\overline{\text{DR}}}. \quad (20.12)$$

Hence, within the chosen scenario we encounter a reduction of the trilinear Higgs self-coupling with respect to the corresponding SM value. Note in particular that the inclusion of the  $\mathcal{O}(\alpha_t\alpha_s)$  corrections has a large influence on these findings. Taking into account only  $\mathcal{O}(\alpha_t)$  corrections both in the NMSSM and the SM, we arrive at  $\Lambda_{hhh}^{\mathcal{O}(\alpha_t),\text{OS}} = 0.98\Lambda_{\text{SM}}^{\mathcal{O}(\alpha_t),\text{OS}}$  and  $\Lambda_{hhh}^{\mathcal{O}(\alpha_t),\overline{\text{DR}}} = 0.59\Lambda_{\text{SM}}^{\mathcal{O}(\alpha_t),\overline{\text{DR}}}$ , whereas at tree-level we get  $\lambda_{hhh}^{\text{OS}} = 0.39\lambda_{\text{SM}}$  and  $\lambda_{hhh}^{\overline{\text{DR}}} = 0.37\lambda_{\text{SM}}$ . So, while the tree-level results suggest a strong reduction of the coupling  $\lambda_{hhh}$  in Scenario 1, at  $\mathcal{O}(\alpha_t)$  it depends on the choice of the renormalization scheme whether or not we obtain a decrease of the trilinear Higgs self-coupling. Only at  $\mathcal{O}(\alpha_t\alpha_s)$  a clear picture, predicting a reduction of  $\Lambda_{hhh}^{\mathcal{O}(\alpha_t\alpha_s)}$  by 25%-34% within Scenario 1, emerges<sup>7</sup>.

<sup>7</sup>Note that within other scenarios, the trilinear coupling can also be increased w.r.t. the SM.

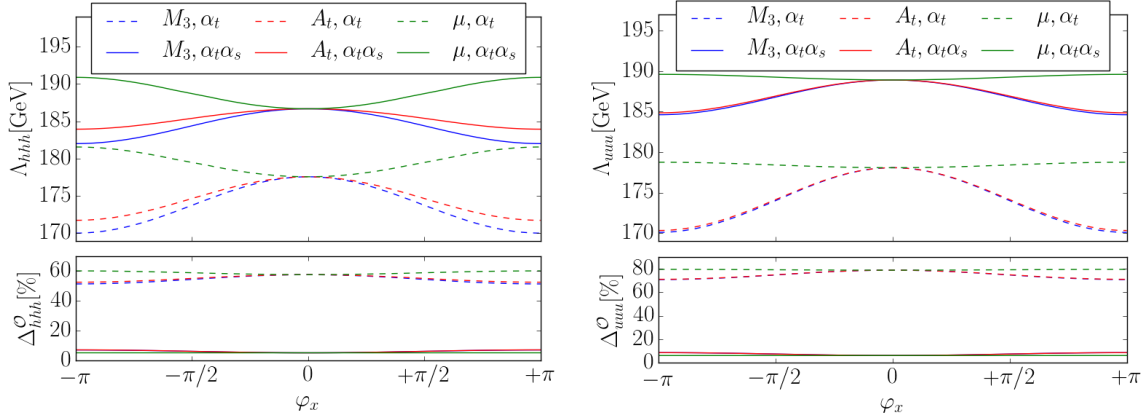


**Figure 20.4.:** Upper panels: Effective trilinear Higgs self-couplings of three SM-like Higgs bosons (left plot) or three  $h_u$  components (right plot) as a function of the complex phases  $\varphi_{M_3}$  (blue),  $\varphi_{A_t}$  (red) and  $\varphi_\mu$  (green) at  $\mathcal{O}(\alpha_t)$  (dashed) and  $\mathcal{O}(\alpha_t\alpha_s)$  (solid) for Scenario 1 for  $\overline{\text{DR}}$  renormalization in the top-stop sector. Lower panels: Relative size of the corrections as defined in Eq. (20.13), with  $(a, b) = (\text{tree}, \alpha_t)$  (dashed) and  $(a, b) = (\alpha_t, \alpha_t\alpha_s)$  (solid). Similar plots were published in [47].

According to most studies, such a reduction will probably escape detection at the LHC [201–203, 205, 206, 208, 209]. Of course, we have to be careful in drawing any conclusions on experimental observability of our findings. In practice the trilinear Higgs self-coupling is in most studies extracted from the Higgs pair production cross section, whose invariant mass distribution features a maximum at  $m_{hh} \approx 400$  GeV [206, 208], i.e. above the top resonance, where the external momentum is no longer negligible. One might, in a very first estimation, assume the leading momentum dependent corrections, dominated by the top resonance, to be universal in the SM and the NMSSM for stops with masses far above 400 GeV. This would allow investigating the influence of an NMSSM-specifically modified trilinear coupling  $\Lambda_{hhh}^{\mathcal{O}(\alpha_t\alpha_s)}$  on the SM Higgs pair production cross section. However, without having calculated the full momentum dependent corrections for the NMSSM we can not verify this assumption. Furthermore, it is clear that a consistent examination would have to take into account further NMSSM-specific corrections, apart from the corrections to the trilinear Higgs self-coupling, playing a role in Higgs pair production. Hence, any considerations concerning the observability of deviations from the SM have to be regarded as a very rough estimate giving merely a hint of possible deviations.

Still, our results show that the difference between the trilinear Higgs self-coupling in the SM and the NMSSM can be sizeable. In particular, however, our findings emphasize the importance of including the corrections of  $\mathcal{O}(\alpha_t\alpha_s)$ , seeing that without them, no useful statement can be made at all in the inspected scenario.

Since we consider the complex NMSSM, we next want to study the impact of the CP-violating phases on the trilinear Higgs self-couplings. For this purpose we start from Scenario 2, which resides in the CP-conserving limit, and successively vary the three phases  $\varphi_{A_t}$ ,  $\varphi_{M_3}$  and  $\varphi_{\mu_{\text{eff}}}$  of the trilinear stop coupling  $A_t$ , the soft-SUSY-breaking gluino mass parameter  $M_3$  and the effective  $\mu$ -parameter  $\mu_{\text{eff}}$ . In the following we will omit the subscript “eff” keeping in mind that  $\mu \equiv \mu_{\text{eff}} = \lambda v_s e^{i\varphi_s} / \sqrt{2}$ . Furthermore, while varying  $\varphi_\mu = \varphi_s + \varphi_\lambda$ , we will make sure that  $\varphi_y = \varphi_u - 2\varphi_s + \varphi_\lambda - \varphi_\kappa$ , which is the only phase entering at tree-level, remains at zero. This is achieved by a simultaneous variation of  $\varphi_s$  and  $\varphi_\lambda$  in such a way that  $\varphi_\lambda = 2\varphi_s = 2/3\varphi_\mu$ , keeping  $\varphi_u = \varphi_\kappa = 0$ . In this way, our investigations are sensitive to CP-violating effects entering only through radiative corrections. Fig. 20.4 illustrates the behaviour of the couplings  $\Lambda_{hhh}$  (left plot) and  $\Lambda_{uuu} \equiv \Lambda_{h_u h_u h_u}$  (right plot) at  $\mathcal{O}(\alpha_t)$  (dashed) and  $\mathcal{O}(\alpha_t\alpha_s)$  (solid) under the variations of  $\varphi_{M_3}$  (blue),  $\varphi_{A_t}$  (red) and  $\varphi_\mu$  (green). Note that we vary all phases for illustrative purposes in the range  $[-\pi, \pi]$ , although part of these values may be excluded

	$\delta_{hhh}^{\varphi_x, \mathcal{O}(\alpha_t)}$	$\delta_{hhh}^{\varphi_x, \mathcal{O}(\alpha_t \alpha_s)}$	$\delta_{h_u h_u h_u}^{\varphi_x, \mathcal{O}(\alpha_t)}$	$\delta_{h_u h_u h_u}^{\varphi_x, \mathcal{O}(\alpha_t \alpha_s)}$
$\varphi_{A_t}$	-3.2%	-1.5%	-4.3%	-2.1%
$\varphi_\mu$	2.3%	2.1%	0.4%	0.4%
$\varphi_{M_3}$	-4.2%	-2.5%	-4.5%	-2.3%

**Table 20.4.:** Influence of the complex phases on the couplings  $\Lambda_{hhh}$  and  $\Lambda_{h_u h_u h_u}$  at  $\mathcal{O}(\alpha_t)$  and  $\mathcal{O}(\alpha_t \alpha_s)$  in Scenario 2, defined according to Eq. (20.14).

by constraints coming from LHC Higgs data and measurements of electric dipole moments (EDMs) [299]. In the lower panels we display the relative size of the corrections, i.e.

$$\Delta_{h_i h_i h_i}^{\mathcal{O}} = \left| \frac{\Lambda_{h_i h_i h_i}^{\mathcal{O}(a)} - \Lambda_{h_i h_i h_i}^{\mathcal{O}(b)}}{\Lambda_{h_i h_i h_i}^{\mathcal{O}(a)}} \right|, \quad \text{with } h_i \in \{h, h_u\} \quad (20.13)$$

and  $(a, b) \in \{(\text{tree}, \alpha_t), (\alpha_t, \alpha_t \alpha_s)\}$ .

All results have been obtained with a  $\overline{\text{DR}}$ -renormalized top-stop sector.

At first sight it might be surprising that an influence of  $\varphi_{M_3}$  is visible already at  $\mathcal{O}(\alpha_t)$ , although gluinos only enter at  $\mathcal{O}(\alpha_t \alpha_s)$ . However, this can be explained by the fact that  $\varphi_{M_3}$  enters through the conversion of the OS top mass to the  $\overline{\text{DR}}$  mass  $m_t^{\overline{\text{DR}}}$  along the lines detailed in App. D.1. In order to estimate the impact of the phases, we define the quantity  $\delta_{h_i h_i h_i}^{\varphi_x, \mathcal{O}(a)}$

$$\delta_{h_i h_i h_i}^{\varphi_x, \mathcal{O}(a)} = \frac{\Lambda_{h_i h_i h_i}^{\mathcal{O}(a)}(\varphi_x = 0) - \Lambda_{h_i h_i h_i}^{\mathcal{O}(a)}(\varphi_x = \pi)}{\Lambda_{h_i h_i h_i}^{\mathcal{O}(a)}(\varphi_x = 0)}, \quad h_i \in \{h, h_u\}, a \in \{\alpha_t, \alpha_t \alpha_s\}, \quad (20.14)$$

which compares the value of a particular coupling at  $\varphi_x = 0$  to its value at  $\varphi_x = \pi$ . The corresponding results for all three phases are summarized in Tab. 20.4. Concentrating first on the  $\mathcal{O}(\alpha_t)$  couplings, we see that the impact of  $\varphi_{A_t}$  and  $\varphi_{M_3}$  is slightly more pronounced in the gauge basis. This is due to the fact that  $\varphi_{A_t}$  enters at  $\mathcal{O}(\alpha_t)$  mostly through the coupling  $g_{h_u \tilde{t}_i \tilde{t}_j}$ ,  $i, j = 1, 2$ , of the  $h_u$  component to stops. Similarly,  $\varphi_{M_3}$  contributes via  $m_t^{\overline{\text{DR}}}$  and hence mainly through top quarks, which couple only to  $h_u$  (and  $a_u$ ). As the SM-like Higgs boson  $h$  contains apart from  $h_u$  an admixture of the  $h_s$  component, the influence of the phases on  $\Lambda_{hhh}^{\mathcal{O}(\alpha_t)}$  is diluted as compared to  $\Lambda_{h_u h_u h_u}^{\mathcal{O}(\alpha_t)}$ . The opposite is true for  $\varphi_\mu$ , which appears in the couplings of  $h_d$ ,  $h_s$ ,  $a_d$  and  $a_s$  to stops. Hence,  $\varphi_\mu$  shows only a tiny effect on  $\Lambda_{h_u h_u h_u}^{\mathcal{O}(\alpha_t)}$ , caused by the stop mass matrix, while the admixture of  $h_s$  to  $h$  leads to a more pronounced influence on  $\Lambda_{hhh}^{\mathcal{O}(\alpha_t)}$ . At  $\mathcal{O}(\alpha_t \alpha_s)$  the impact of the phases is reduced, however, since the two-loop corrections are generally smaller than those of one-loop order, the overall trend visible at  $\mathcal{O}(\alpha_t)$  is preserved.

Altogether, the influence of the phases is seen to be very small, amounting to less than 4.5% at  $\mathcal{O}(\alpha_t)$  and less than 2.5% at  $\mathcal{O}(\alpha_t \alpha_s)$ . Comparing this to the typical size of the remaining theoretical uncertainty, estimated above, we conclude their impact to be negligible. Note again, however, that, having chosen the tree-level phase  $\varphi_y$  to remain zero, we only investigate the influence of phases entering through radiative corrections, wherefore the smallness of their effect was to be expected. Allowing for CP violation already at tree-level, the impact of the phases would be more pronounced.

The lower panels again demonstrate the convergence of the perturbative expansion, showing that the radiative corrections decrease from 50-60% and 70-80% at  $\mathcal{O}(\alpha_t)$  to less than 10%

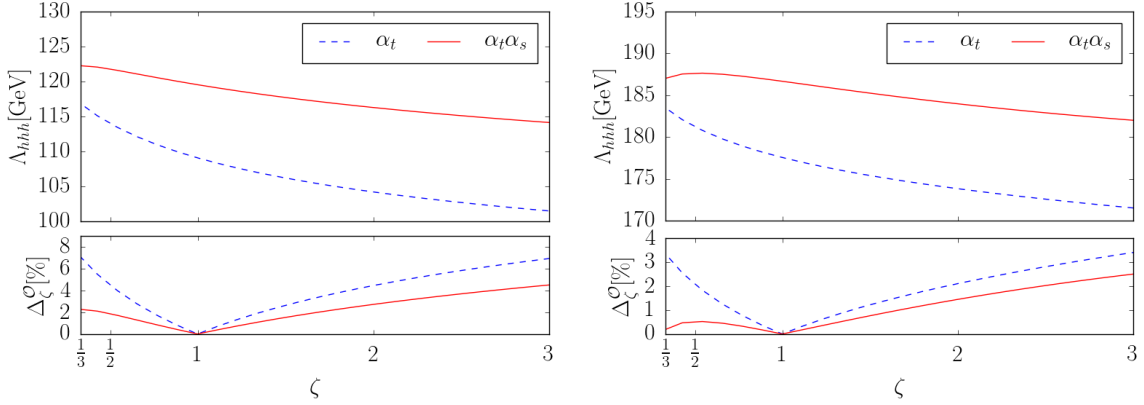


**Figure 20.5.:** Upper panel: Dependence of the couplings  $\Lambda_{hhh}^{\mathcal{O}(\alpha_t)}$  (blue dashed) and  $\Lambda_{hhh}^{\mathcal{O}(\alpha_t\alpha_s)}$  (red solid) on the renormalization scale  $\mu$  for Scenario 1 (left) and 2 (right) and a  $\overline{\text{DR}}$ -renormalized top-stop sector. The curves are plotted as functions of  $\zeta = \mu_r/\mu_0$ . Lower panel: Relative deviation from the central scale  $\mu_0$  as defined in Eq. (20.15) with the same color code as in the upper panel. Similar plots were published in [47].

at  $\mathcal{O}(\alpha_t\alpha_s)$  in the mass and the gauge eigenstates, respectively.

Before, we have estimated the theoretical uncertainty due to missing higher-order corrections by comparing the results obtained in different renormalization schemes. Another possibility, available in  $\overline{\text{MS}}$ - and  $\overline{\text{DR}}$ -like schemes, which exhibit a dependence on the renormalization scale  $\mu_r$ , is to investigate the behaviour of the results under a variation of this unphysical scale. Summing up all orders of the perturbative series, the scale dependence has to vanish. Hence, the  $\mu_r$ -dependence remaining at finite orders can be interpreted as a measure for missing higher-order corrections. A dedicated study of the renormalization scale dependence would require two-loop RGEs for all  $\overline{\text{DR}}$  parameters of the Higgs sector and one-loop RGEs for the top-stop sector within the complex NMSSM. However, since we are interested here only in a rough estimate of the scale uncertainty and do not strive for rigorous derivations, we content ourselves with a linear approximation of the RGEs, similar to our treatment of the top-stop parameters in Sec. 17.1. Due to the more involved situation at  $\mathcal{O}(\alpha_t\alpha_s)$ , we detail our procedure in App. D.2.

Fig. 20.5 shows the result of a  $\mu_r$ -variation in this vein within a range of  $[1/3\mu_0, 3\mu_0]$  around the central scale  $\mu_0 = M_{\text{SUSY}}$  for Scenario 1 (left plot) and 2 (right plot). In the upper panel we illustrate the impact of the variation on the absolute size of the coupling  $\Lambda_{hhh}$  at  $\mathcal{O}(\alpha_t)$  (blue dashed) and  $\mathcal{O}(\alpha_t\alpha_s)$  (red solid) as a function of  $\zeta = \mu_r/\mu_0$  for a  $\overline{\text{DR}}$ -renormalized top-stop sector. One can readily recognize the flattening of the curve when going from  $\mathcal{O}(\alpha_t)$  to  $\mathcal{O}(\alpha_t\alpha_s)$ , which indicates a reduction of the theoretical uncertainty. This can even more clearly be seen in the lower panels, where we display the relative deviation from the central scale, i.e.

$$\Delta_\zeta^{\mathcal{O}} = \left| \frac{\Lambda_{hhh}^{\mathcal{O}(a)}(\mu_0) - \Lambda_{hhh}^{\mathcal{O}(a)}(\zeta\mu_0)}{\Lambda_{hhh}^{\mathcal{O}(a)}(\mu_0)} \right|, \quad \text{with } a \in \{\mathcal{O}(\alpha_t), \mathcal{O}(\alpha_t\alpha_s)\}. \quad (20.15)$$

Using  $\Delta_\zeta$  as a measure for the theoretical uncertainty, we conclude the latter to be reduced from  $\approx 7\%$  (Scenario 1) and  $\approx 3.5\%$  (Scenario 2) at  $\mathcal{O}(\alpha_t)$  to  $\approx 4.5\%$  and  $\approx 2.5\%$  at  $\mathcal{O}(\alpha_t\alpha_s)$ . These findings further consolidate the conclusions drawn above, when estimating the theoretical uncertainty from a comparison of different schemes. Note that the estimates resulting from the scale variation are smaller than those obtained from a scheme comparison. This is due to the fact that we consider only the  $\overline{\text{DR}}$  scheme in the scale variation analysis, which shows better convergence properties, as discussed above. However, let us emphasize again that the results from the scale variation can be considered as a rough estimate only, owing to our simplistic approximation of the RGE evolution.

## 20.5. Higgs-to-Higgs Decays

Before closing this chapter, we want to have a brief glance at possible applications of our findings. For this purpose, we will now turn to the subject of Higgs-to-Higgs decays and investigate the decay of a heavier Higgs boson into two SM-like Higgs bosons.

The partial width  $\Gamma_{H_i \rightarrow H_j H_k}$  for the decay  $H_i \rightarrow H_j H_k$  can be obtained along the lines described in Subs. 3.2.2. Making use of the general formulae Eqs. 3.22 and 3.23 stated there, we arrive at the following expression for the width

$$\Gamma_{H_i \rightarrow H_j H_k}^{(a)} = \frac{\sigma}{16\pi m_{H_i}^3} \lambda(m_{H_i}^2, m_{H_j}^2, m_{H_k}^2) \left| \mathcal{A}_{H_i \rightarrow H_j H_k}^{(a)} \right|^2, \quad \sigma = \begin{cases} \frac{1}{2} & j = k \\ 1 & \text{else} \end{cases}, \quad (20.16)$$

with  $(a) \in \{(1\text{-loop}), (\alpha_t \alpha_s)\}$ . According to this definition, the width  $\Gamma_{H_i \rightarrow H_j H_k}^{(a)}$  comprises the squared amplitude  $\mathcal{A}_{H_i \rightarrow H_j H_k}^{(a)}$  of the respective Higgs-to-Higgs decay, which in turn is given by

$$\mathcal{A}_{H_i \rightarrow H_j H_k}^{(a)} = \sum_{i', j', k'=1}^5 \hat{Z}_{ii'} \hat{Z}_{jj'} \hat{Z}_{kk'} \Lambda_{h_i' h_j' h_k'}^{\mathcal{O}(a)} + \mathcal{A}_{H_i \rightarrow H_j H_k}^{G_0, Z}. \quad (20.17)$$

Here  $\Lambda_{h_i' h_j' h_k'}^{\mathcal{O}(a)}$  denotes the trilinear Higgs self-coupling in the reduced tree-level mass basis, including the complete one-loop corrections with full momentum dependence and for  $a = \alpha_t \alpha_s$  also the corrections of  $\mathcal{O}(\alpha_t \alpha_s)$  at  $p^2 = 0$ . Furthermore, as previously announced, the  $\hat{Z}$ -factors now comprise the full momentum dependence at one-loop order, such that the resulting decay widths are defined in the proper  $\mathcal{O}(\alpha_t \alpha_s)$  mass basis  $\Phi^H$  (cf. Sec. 20.1). Note at this point that we define both, the decay widths comprising the one-loop corrections and those containing on top the  $\mathcal{O}(\alpha_t \alpha_s)$  corrections, in the same basis  $\Phi^H$ . Likewise, the Higgs masses appearing in Eq. (20.16) are always to be interpreted as those calculated at  $\mathcal{O}(\alpha_t \alpha_s)$ . The last term in Eq. (20.17) accounts for external leg corrections which arise from mixing between the pseudoscalar components of the Higgs bosons and the Goldstone or  $Z$  boson. In order to preserve gauge invariance, the external momenta for these contributions have to be set equal to the tree-level masses of the external scalars [46, 91, 291]. For this reason, we consider mixing with Goldstone and  $Z$  bosons only at one-loop order. However, since these mixing contributions are found to be small, we expect the corresponding two-loop terms to be safely negligible.

Both the external leg corrections expressed through the wave function correction factors and those incorporating mixing with Goldstone and  $Z$  bosons are a consequence of our non-OS renormalization of the scalar fields (cf. Subs. 3.2.1).

As becomes obvious from the above definitions, neither  $\Gamma_{H_i \rightarrow H_j H_k}^{(a)}$  nor  $\mathcal{A}_{H_i \rightarrow H_j H_k}^{(a)}$  can be assigned a strict loop order, since the incorporation of the  $\hat{Z}$ -factors leads to contributions, which are formally of higher order. Hence, the superscript  $(a)$  merely refers to the order of the corrections included in  $\Lambda_{h_i' h_j' h_k'}^{\mathcal{O}(a)}$ .

In order to examine the impact of the  $\mathcal{O}(\alpha_t \alpha_s)$  corrections on Higgs-to-Higgs decays, we now turn to a specific example, given by the decay  $H_4 \rightarrow H_2 H_2$  within Scenario 2. Fig. 20.6 shows the partial decay widths (left plot) and the branching ratios (right plot) for the chosen decay at one-loop order (blue) and two-loop order (red) within the DR (dashed) and the OS (solid) scheme. All curves are shown as a function of the input parameter  $A_t^{\text{DR}}$ , which was varied in a range from  $-3000$  to  $+3000$  GeV. Again, we demand the constraints of the parameter scan to be fulfilled only at  $A_t^{\text{DR}} = 1824$  GeV, corresponding to the value quoted in Tab. 20.1. The Higgs masses,  $\hat{Z}$ -factors, all partial widths as well as the total width  $\Gamma_{H_4, \text{tot}}^{(a)}$  of the fourth Higgs mass eigenstate have been calculated with NMSSMCALC, extended

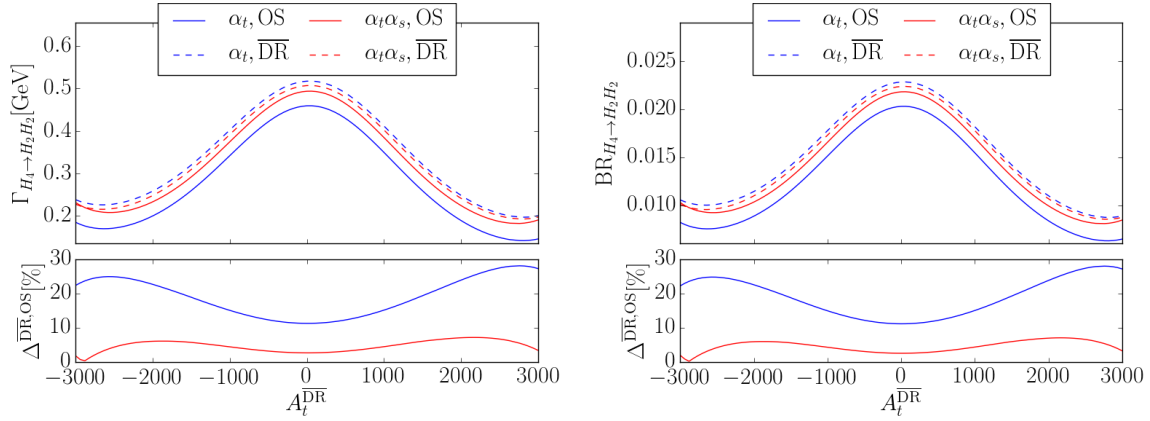


**Figure 20.6.:** Upper panel: Partial decay width (left) and branching ratio (right) for the decay  $H_4 \rightarrow H_2 H_2$  in Scenario 2 in dependence of the input parameter  $A_t^{\overline{\text{DR}}}$  at  $\mathcal{O}(\alpha_t)$  (blue) and  $\mathcal{O}(\alpha_t \alpha_s)$  (red) in the OS (solid) and  $\overline{\text{DR}}$  (dashed) scheme. Lower panel: Estimation of the theoretical uncertainty, defined according to Eq. (20.10), at  $\mathcal{O}(\alpha_t)$  (blue) and  $\mathcal{O}(\alpha_t \alpha_s)$  (red).

by our corrections to the trilinear Higgs self-couplings as described in Sec. 20.2.  $\Gamma_{H_4, \text{tot}}^{(a)}$ , which includes the corrections to the trilinear Higgs couplings of  $\mathcal{O}(a)$ , is needed in order to determine the branching ratio

$$\text{BR}_{H_4 \rightarrow H_2 H_2}^{(a)} = \frac{\Gamma_{H_4 \rightarrow H_2 H_2}^{(a)}}{\Gamma_{H_4, \text{tot}}^{(a)}}. \quad (20.18)$$

In the lower panels we display the relative difference  $\Delta^{\overline{\text{DR}}, \text{OS}}$  between the results obtained in the OS and in the  $\overline{\text{DR}}$  scheme, as defined in Eq. (20.10).

A comparison to the partial width at tree-level, corresponding to 0.34 GeV in the OS and 0.35 GeV in the  $\overline{\text{DR}}$  scheme at  $A_t^{\overline{\text{DR}}} = 1824$  GeV, shows that the one-loop corrections lead to a reduction of the width by 37.1% and 22.1%, respectively. In the  $\overline{\text{DR}}$  scheme the  $\mathcal{O}(\alpha_t \alpha_s)$  corrections further reduce the partial width by another 2.8% while they enhance the one-loop width by 16.3% in the OS scheme. Consequently, we can again observe an approach of the results in the two schemes when adding the corrections of  $\mathcal{O}(\alpha_t \alpha_s)$  resulting in a reduction of the theoretical uncertainty  $\Delta^{\overline{\text{DR}}, \text{OS}}$  from 22% to 6.7%. As the plot on the right-hand side reveals, the branching ratio for the decay of the heavy Higgs boson  $H_4$  is very small in the considered scenario, staying below 2.3% over the whole plotted range and corresponding to 1.2% at  $A_t^{\overline{\text{DR}}} = 1824$  GeV. The scenario has been chosen for illustrative purposes rather than to derive phenomenological implications, since it clearly features the relevance of the  $\mathcal{O}(\alpha_t \alpha_s)$  corrections and the reduction of the theoretical uncertainty.

One important comment is in order concerning the applicability of the approximation of vanishing external momentum in the  $\mathcal{O}(\alpha_t \alpha_s)$  corrections. As discussed in Sec. 20.3, the  $p^2 = 0$  approximation is applicable if the external momentum does not exceed the threshold of on-shell production of the loop particles. Above this threshold, the loop integrals develop an imaginary part, which is not captured in the effective potential approximation, wherefore the latter is no longer reliable.

Regarding the decay under consideration, it is obvious that, with a mass of the decaying Higgs boson of  $m_{H_4} = 796$  GeV, we are far above the  $t\bar{t}$ -threshold. Thus, the top quarks which appear in some diagrams contributing to the  $\mathcal{O}(\alpha_t \alpha_s)$  corrections can go on-shell and the approximation of vanishing external momentum is strictly speaking not applicable. However, as we will show in the following, for the chosen decay and scenario, the dangerous contributions of internal top quarks are small compared to the remaining corrections of  $\mathcal{O}(\alpha_t \alpha_s)$ . Hence, we estimate the error made by neglecting the external momenta in these diagrams, to be of

minor importance in our specific case.

There are two groups of diagrams at  $\mathcal{O}(\alpha_t\alpha_s)$  featuring potentially dangerous top contributions. The first precarious type is represented by the first to third diagram in Fig. 19.1 and the first two diagrams in Fig. 19.2, containing a top triangle with an intermediate gluon or stop-gluino exchange or a counterterm insertion. For the decay under consideration, these diagrams exhibit a  $H_4 t \bar{t}$ -coupling on the left, which strongly suppresses the contribution of these topologies. The suppression is due to the fact that  $H_4$  is mostly  $h_d$ -like in Scenario 2 and hence barely couples to top quarks. We can assess the negligibility of the momentum dependence, entering through these contributions, by considering the one-loop corrections of  $\mathcal{O}(\alpha_t)$ , where the same diagram without the gluon or the stop-gluino supplement or without the counterterm appears. A comparison of the width  $\Gamma_{H_4 \rightarrow H_2 H_2}^{(\alpha_t)}$ , comprising the one-loop corrections of  $\mathcal{O}(\alpha_t)$  with full momentum dependence, to the one including the same corrections in the  $p^2 = 0$  approximation, shows the relative difference between both to be less than 5.4% in the OS and 4% in the  $\overline{\text{DR}}$  scheme. We assume the additional gluons, stops and gluinos or counterterms entering at  $\mathcal{O}(\alpha_t\alpha_s)$  not to change this behaviour drastically and hence the error made by neglecting the external momentum in diagrams of this type to be of minor significance.

The second group of diagrams, potentially invalidating the  $p^2 = 0$  approximation, is representatively depicted by the fourth to seventh diagram in Fig. 19.1. In this case the incoming  $H_4$  couples to stops and the dangerous top propagator appears on the right, coupling to the mostly  $h_u$ -like mass eigenstates  $H_2$ , or in a loop<sup>8</sup>. Hence, we cannot rely on a suppression of this contribution by a small top coupling. However, the diagrams still turn out to yield only a minor contribution to the corrections of  $\mathcal{O}(\alpha_t\alpha_s)$ , amounting to less than 6.6% within the considered scenario. This can be traced back to the fact that the contribution of these diagrams are proportional to the ratio  $\mu_{\text{eff}}/m_{\tilde{t}}$ , which is small ( $\approx 0.15$ ) in Scenario 2. Therefore, we estimate the influence of neglecting the external momentum in the diagrams of the second type on the full  $\mathcal{O}(\alpha_t\alpha_s)$  corrections to be small.

It is important to note, however, that in particular the last statement is highly scenario dependent. In scenarios featuring a ratio of  $\mu_{\text{eff}}/m_{\tilde{t}} \sim \mathcal{O}(1)$ , the relative importance of diagrams of the second type can be enhanced. Varying  $\mu_{\text{eff}}$ , we found the contributions to rise up to 30 % of the  $\mathcal{O}(\alpha_t\alpha_s)$  corrections. Therefore, we clearly cannot rely on the approximation of vanishing external momentum in general scenarios and its applicability has to be checked on a case-by-case basis.

Nonetheless, for the scenario and the decay discussed here, the neglect of the external momentum is well-motivated and we hence consider our results as trustworthy.

<sup>8</sup>For the sixth diagram, a flipping between initial and final states of the external Higgs bosons has to be considered in order to obtain a contribution as described in the text. In the form shown in Fig. 19.1, the diagram is even more suppressed, due to the coupling  $H_4 t \bar{t}$  appearing on the left.

---

Conclusion of Part III

---

The goal of this part of the thesis was the determination and investigation of the  $\mathcal{O}(\alpha_t\alpha_s)$  corrections to the trilinear Higgs self-couplings of the complex NMSSM in the approximation of vanishing external momentum and in the gaugeless limit.

These corrections are required in order to match the precision reached in the calculation of the NMSSM Higgs boson masses. Due to the entwinement of the Higgs boson masses and trilinear self-couplings, which both derive from the Higgs potential, a consistent description of the NMSSM Higgs sector demands the corrections to both to be of the same order. Furthermore, also the huge size of the corrections to the trilinear Higgs self-couplings as well as the theoretical uncertainty found at one-loop level call for the inclusion of higher orders.

In this thesis we presented the calculation of the corrections of  $\mathcal{O}(\alpha_t\alpha_s)$  to the trilinear NMSSM Higgs self-couplings in the Feynman diagrammatic approach. All necessary steps were exposed in detail. Restricting ourselves to the limit of vanishing external momentum, the occurring two-loop integrals could be reduced with the help of the Tarasov algorithm, implemented in the `Mathematica` package `TARCER`, to two known master integrals. These were expanded in a series in  $\epsilon$ , the regulator of dimensional reduction, such that all divergences could be extracted and cancelled by a suitable renormalization procedure.

The latter was explained thoroughly. For the Higgs sector, which has to be renormalized up to  $\mathcal{O}(\alpha_t\alpha_s)$ , we introduced a hybrid scheme, mixing OS and  $\overline{\text{DR}}$  conditions. Concerning the top-stop sector, contributing counterterms of  $\mathcal{O}(\alpha_s)$ , we applied two separate schemes, the OS and the  $\overline{\text{DR}}$  scheme. A comparison of the results obtained in the two different renormalization schemes allows us to assess the theoretical uncertainty of our results.

Apart from the corrections of  $\mathcal{O}(\alpha_t\alpha_s)$ , we also presented the calculation of the  $\mathcal{O}(\alpha_t)$  corrections in the effective potential approach, subject to the same approximations as the former. With their help we defined effective trilinear Higgs self-couplings, comprising the  $\mathcal{O}(\alpha_t)$  and  $\mathcal{O}(\alpha_t\alpha_s)$  corrections at  $p^2 = 0$ . Including only top quarks and squarks in the loops, these effective couplings can be used as an approximation, as long as the external momentum remains below the threshold of on-shell  $t\bar{t}$  production. As further benefit, the  $\mathcal{O}(\alpha_t)$  corrections allow us to estimate the goodness of our approximations. This can be achieved by comparing the couplings of  $\mathcal{O}(\alpha_t)$  to those including the complete one-loop corrections with full momentum dependence.

A corresponding comparison was subject of the first part of our numerical investigations, where we contrasted three different one-loop approximations of the trilinear Higgs self-couplings:

the full one-loop-corrected ones, those including  $\mathcal{O}(\alpha_t)$  corrections with full momentum dependence and the effective  $\mathcal{O}(\alpha_t)$  couplings at  $p^2 = 0$ . Concerning the coupling of three SM-like, i.e.  $h_u$ -dominated, Higgs bosons, we found the effective  $\mathcal{O}(\alpha_t)$  corrections to approximate well the full one-loop corrections for external momenta below the  $t\bar{t}$ -threshold. Both the neglect of contributions outside the top-stop sector and of the external momentum were found to be applicable in this case. However, we also demonstrated that non- $\mathcal{O}(\alpha_t)$  contributions can be significant for the couplings of Higgs bosons dominated by  $h_d$  and  $h_s$  components. These can receive large contributions from loops with light Higgs bosons, which are relevant in particular in the range of small external momenta.

In the subsequent study of the effective trilinear Higgs self-couplings, including corrections of  $\mathcal{O}(\alpha_t)$  and  $\mathcal{O}(\alpha_t\alpha_s)$ , we hence restricted ourselves to the coupling of three SM-like Higgs bosons  $h$  or three  $h_u$  gauge eigenstates, where the investigations at one-loop order support the applicability of our approximations. As we demonstrated, the  $\mathcal{O}(\alpha_t\alpha_s)$  corrections are important for several reasons. On the one hand, they can have a significant impact on the absolute size of the effective trilinear couplings. We exemplified this by means of a specific scenario, where the  $\mathcal{O}(\alpha_t\alpha_s)$  corrections were found to lead to an enhancement (reduction) of 21% (8%) of the results at  $\mathcal{O}(\alpha_t)$  in the OS ( $\overline{\text{DR}}$ ) scheme. On the other hand, they lead to a considerable reduction of the theoretical uncertainty. We estimated the latter in two different ways: by a comparison of the results obtained in the OS and in the  $\overline{\text{DR}}$  scheme and by a variation of the renormalization scale. Both methods of assessing the theoretical uncertainty due to missing higher-order corrections demonstrated the  $\mathcal{O}(\alpha_t\alpha_s)$  corrections to reduce the latter noticeably.

We demonstrated the importance of this reduction by a comparison of the NMSSM trilinear coupling of three SM-like Higgs bosons to the one of the SM, calculated in the same approximation. Within the chosen scenario, the large theoretical uncertainty remaining at  $\mathcal{O}(\alpha_t)$  precludes any statement on whether or not the effective NMSSM trilinear Higgs coupling is altered significantly w.r.t. the corresponding SM coupling. At  $\mathcal{O}(\alpha_t\alpha_s)$  the ambiguity is resolved and a clear picture emerges, showing in the presented case a reduction of the effective coupling by 25-34% as compared to the SM.

We also investigated the influence of the complex phases, entering the effective trilinear Higgs couplings through radiative corrections. However, their impact was found to be small.

In the last section, we studied the effect of the  $\mathcal{O}(\alpha_t\alpha_s)$  corrections on partial widths of Higgs-to-Higgs decays. As an example we considered the decay of the heavy fourth Higgs mass eigenstate  $H_4$  into two SM-like Higgs bosons. For the purpose of this investigation, we included at one-loop order the complete electroweak corrections with full momentum dependence. Again, we found the  $\mathcal{O}(\alpha_t\alpha_s)$  corrections to be non-negligible and ascertained a reduction of the theoretical uncertainty from 22% at one-loop order to 6.7% at  $\mathcal{O}(\alpha_t\alpha_s)$  in the considered scenario. We furthermore discussed the applicability of the approximation of vanishing external momentum in the  $\mathcal{O}(\alpha_t\alpha_s)$  corrections. We argued that, although the external momentum is far above the  $t\bar{t}$  threshold in the considered decay, we estimate the error made by neglecting the external momentum to be small for the chosen scenario. This estimation was justified by the fact that the diagrams containing possibly resonant top quark contributions are suppressed in the studied case.

Still, these investigations clearly exhibit the limitations of the  $p^2 = 0$  approximation. For other scenarios and other decays, the impact of the external momentum can be significant. The same is true for the process of Higgs pair production, where the external momentum is known to be non-negligible. Furthermore, from our investigations of the one-loop corrections, it is presumable that other corrections, e.g. Higgs loops or bottom-sbottom contributions, become important in processes featuring external non- $h_u$ -like Higgs bosons.

Hence, it would be interesting to include these contributions as well and to perform the calculation with full momentum dependence. Especially the latter is, however, clearly beyond

the scope of this thesis.

If in the future the trilinear Higgs self-coupling can be determined with higher accuracy, an inclusion of the momentum dependent effects in the corrections of  $\mathcal{O}(\alpha_t\alpha_s)$  and beyond is advisable. Our analysis has shown that the one-loop corrections alone may not be sufficient to make a conclusive statement about the size of the trilinear Higgs couplings of the NMSSM compared to the one of the SM. In this case the corrections of  $\mathcal{O}(\alpha_t\alpha_s)$  and beyond will be required to gain a clear picture. Due to the limitations of the approximation of vanishing external momentum, however, a thorough study is possible only if the latter are determined with full momentum dependence. Also for a dedicated investigation of Higgs-to-Higgs decays, an inclusion of momentum dependent effects at two-loop order as well as of corrections going beyond  $\mathcal{O}(\alpha_t\alpha_s)$  are mandatory. We consider an endeavour in this direction as very interesting and rewarding, should the trilinear Higgs self-coupling be measured at a future collider with adequate precision, in particular if on top, other observations hint to a possible realization of SUSY in nature.



Despite its tremendous success in predicting numerous observables and processes of elementary particle physics with high precision, the Standard Model of particle physics leaves unanswered many fundamental questions concerning the true nature of our universe. It can hence not be considered as the ultimate description of nature, but rather has to be regarded as low-energy approximation of some underlying theory. Huge efforts are therefore constantly being undertaken in developing and investigating possible extensions of the SM.

The discovery of the Higgs boson in 2012 might have opened the door to a more complete description of nature. Since many extensions of the SM feature an enlarged Higgs sector, its observation has encouraged an enhanced activity in research trying to use the Higgs sector as an entrance to physics beyond the SM.

In this thesis, we examined two specific extensions of the SM with enlarged Higgs sectors, the 2HDM and the NMSSM. Our focus was on the calculation of higher-order corrections to observables connected to the Higgs sectors of the respective models. As the measurements of Higgs properties at the LHC more and more seem to converge towards the SM expectations, the importance of higher-order corrections grows, since deviations from the SM might be small, calling for precise theoretical predictions.

A suitable renormalization scheme is an important prerequisite for higher-order corrections. For this reason, we pursued in part II of this thesis the goal of developing an appropriate renormalization scheme for the 2HDM. In doing so, we concentrated our attention in particular on the three 2HDM-specific parameters, the mixing angles  $\alpha$  and  $\beta$  and the soft- $Z_2$ -breaking scale  $m_{12}^2$ , for which no well-proven renormalization scheme had been established so far. Throughout our study, the three criteria of gauge independence, process independence and numerical stability served us as guideline to a suitable renormalization scheme.

Our investigations revealed that, in particular with regard to gauge dependence, the treatment of the tadpoles plays a key role. Having examined two different tadpole schemes and various renormalization prescriptions for the mixing angles, we clearly advocate the usage of what we baptized *tadpole scheme II*. Within this scheme no tadpole counterterms are introduced. As a consequence, tadpole diagrams have to be taken into account in all Green's functions. Only this treatment of the tadpoles enables, in combination with the pinch technique, the formulation of a gauge-independent renormalization scheme for the mixing angles. We performed a dedicated numerical study, comprising three test processes, for the various renormalization

schemes introduced in this thesis. From our examinations we concluded that the p-OS<sup>c,o</sup> and the  $p_*^c$  scheme, which are versions of gauge- and process-independent renormalization prescriptions for the mixing angles, lead to numerically stable results. Hence, these schemes comply with all three criteria of a suitable renormalization scheme.

Regarding the parameter  $m_{12}^2$ , gauge dependence is of no concern and our studies suggest an  $\overline{\text{MS}}$  definition of  $m_{12}^2$  to be the best choice, fulfilling likewise all three criteria.

In conclusion, we were able to develop a complete, suitable renormalization scheme for the 2HDM, which is at the same time process and gauge independent and numerically stable. This scheme can henceforth be applied in higher-order calculations and thus in a thorough investigation of LHC phenomenology in the framework of the 2HDM.

Part III of this thesis dealt with the calculation of the  $\mathcal{O}(\alpha_t\alpha_s)$  corrections to the trilinear Higgs self-couplings of the complex NMSSM in the approximation of vanishing external momentum and in the gaugeless limit. Trilinear Higgs self-couplings play an important role in the intentions of gaining more insight into the mechanism of electroweak symmetry breaking. Furthermore, they enter interesting processes like Higgs pair production and Higgs-to-Higgs decays. Due to the close connection between the trilinear couplings and the masses of the Higgs bosons, a consistent description of the NMSSM Higgs sector requires both to be calculated with comparable precision. As the masses are known up to  $\mathcal{O}(\alpha_t\alpha_s)$  in the complex NMSSM, this implies the necessity of corrections of this order to the trilinear Higgs self-couplings.

We presented all steps of the calculation, which entails a reduction of the contributing two-loop integrals to master integrals, in detail. Moreover, we illustrated the renormalization of the Higgs sector up to  $\mathcal{O}(\alpha_t\alpha_s)$  and of the top-stop sector up to  $\mathcal{O}(\alpha_s)$ . To allow for an estimation of the theoretical uncertainty due to missing higher-order corrections, we applied two different renormalization schemes to the top-stop sector, the OS and the  $\overline{\text{DR}}$  scheme.

Our subsequent numerical analysis demonstrated the importance of the  $\mathcal{O}(\alpha_t\alpha_s)$  corrections to the trilinear Higgs self-couplings. Depending on the scenario, they can have a large impact on the size of the couplings. Furthermore, they can lead to a drastic reduction of the theoretical uncertainty. The latter was estimated by a comparison of the results obtained in the OS and the DR scheme and also by a variation of the renormalization scale.

The same picture emerged when we investigated the effect of the  $\mathcal{O}(\alpha_t\alpha_s)$  corrections on the partial widths of Higgs-to-Higgs decays.

However, our examinations also revealed the limitation of the used approximations. More dedicated studies of Higgs-to-Higgs decays and investigations of Higgs pair production should definitely include both, contributions beyond  $\mathcal{O}(\alpha_t\alpha_s)$  and effects of non-vanishing external momenta.

Currently, the second run is ongoing at the LHC, which is operating at a center of mass energy of 13 TeV. The data collected in the course of this run will allow for a more precise determination of the properties of the Higgs boson and thus lead to a better assessment of its nature. Furthermore, the new data might contain first signals of physics beyond the SM. Therefore, Higgs sectors of models beyond the SM are currently an exciting object of research and we are expectantly looking forward to future insights. We hope, our work has contributed to the endeavour of unveiling the nature of the Higgs boson and of exploring new physics beyond the SM.

### A.1. Shifts in the 2HDM Parameters

In Sec. 8.2 we dealt with the shifts, which are induced in the mass parameters by the vev shifts  $\Delta v_1$  and  $\Delta v_2$ . Apart from the masses, also the parameters  $\alpha_p$  and  $\beta_p$  receive shifts  $\Delta\alpha_p$  and  $\Delta\beta_p$ . These can directly be obtained by performing the shifts  $v_i \rightarrow v_i + \Delta v_i$ ,  $i = 1, 2$ , in the definitions of  $\alpha_p$  and  $\beta_p$  in dependence of  $v_1$  and  $v_2$ . Using Eqs. 8.11 and 8.12, these shifts can at one-loop order be expressed in terms of the tadpoles  $T_h^{(1)}$  and  $T_H^{(1)}$ . We find

$$\begin{aligned}\Delta \tan(\beta_p) &= \Delta \left( \frac{v_2}{v_1} \right) = \tan(\beta_p) \left( \frac{\Delta v_2}{v_2} - \frac{\Delta v_1}{v_1} \right) \\ &= \frac{1}{c_{\beta_p}^2} \left( \frac{c_{\beta-\alpha} T_h^{(1)}}{v m_h^2} - \frac{s_{\beta-\alpha} T_H^{(1)}}{v m_H^2} \right) \\ \Rightarrow \Delta \beta_p &= c_{\beta_p}^2 \Delta \tan(\beta_p) = \left( \frac{c_{\beta-\alpha} T_h^{(1)}}{v m_h^2} - \frac{s_{\beta-\alpha} T_H^{(1)}}{v m_H^2} \right),\end{aligned}\tag{A.1}$$

$$\begin{aligned}\Delta \tan(2\alpha_p) &= \Delta \left( \frac{4(m_{12}^2 - (\lambda_{345})v_1 v_2)}{-2m_{11}^2 + 2m_{22}^2 - 3\lambda_1 v_1^2 + \lambda_{345} v_1^2 + 3\lambda_2 v_2^2 - \lambda_{345} v_2^2} \right) \\ \Rightarrow \Delta \alpha_p &= \frac{c_{2\alpha_p}^2}{2} \Delta \tan(2\alpha_p) \\ &= \frac{c_{\beta-\alpha}((2m_h^2 + m_H^2)s_{2\beta} - 6m_{12}^2)s_{2\alpha} + 2m_{12}^2 s_{2\beta}}{s_{2\beta}^2 m_h^2 (m_H^2 - m_h^2)v} T_h^{(1)} \\ &\quad - \frac{s_{\beta-\alpha}((2m_H^2 + m_h^2)s_{2\beta} - 6m_{12}^2)s_{2\alpha} - 2m_{12}^2 s_{2\beta}}{s_{2\beta}^2 m_H^2 (m_H^2 - m_h^2)v} T_H^{(1)} \\ &= - \frac{g_{Hhh}}{(m_H^2 - m_h^2)} \frac{T_h^{(1)}}{m_h^2} - \frac{g_{HHh}}{(m_H^2 - m_h^2)} \frac{T_H^{(1)}}{m_H^2},\end{aligned}\tag{A.2}$$

where we have applied the transformation rules between the parameter sets 1 and 2 in Eqs. 5.33 - 5.37 and afterwards dropped a differentiation between  $\alpha_p$ ,  $\beta_p$  and  $\alpha_{\text{rot}}$ ,  $\beta_{\text{rot}}$ . Furthermore, we have used the couplings in Eqs. Eqs. A.9 and A.10. These shifts lead, together with the shifts in the mass parameters and with additional shifts entering by means of the

translation between the sets 1 and 2, to a restoration of the tadpole diagrams in all vertices, the latter can be attached to. In order to properly account for the shifts entering via the parameter translation rules, all tadpole terms have to be kept explicit in these. Instead of the relations Eqs. 5.33 - 5.37, where the tadpole terms have already been set to zero, the following rules have to be applied for that purpose

$$\lambda_1 = \frac{1}{v^2 c_\beta^2} (s_\alpha^2 m_h^2 + c_\alpha^2 m_H^2 - t_\beta m_{12}^2) - \frac{T_1^0}{v^3 c_\beta^3}, \quad (\text{A.3})$$

$$\lambda_2 = \frac{1}{v^2 s_\beta^2} \left( c_\alpha^2 m_h^2 + s_\alpha^2 m_H^2 - \frac{m_{12}^2}{t_\beta} \right) - \frac{T_2^0}{v^3 s_\beta^3}, \quad (\text{A.4})$$

$$\lambda_3 = 2 \frac{m_{H^\pm}^2}{v^2} + \frac{1}{v^2} \frac{s_{2\alpha}}{s_{2\beta}} (m_H^2 - m_h^2) - \frac{2m_{12}^2}{v^2 s_{2\beta}} - \frac{2T_1^0 s_\beta^2}{v^3 c_\beta} - \frac{2T_2^0 c_\beta^2}{v^3 s_\beta}, \quad (\text{A.5})$$

$$\lambda_4 = \frac{m_{A_0}^2 - 2m_{H^\pm}^2}{v^2} + \frac{2m_{12}^2}{v^2 s_{2\beta}} + \frac{T_1^0 s_\beta^2}{v^3 c_\beta} + \frac{T_2^0 c_\beta^2}{v^3 s_\beta}, \quad (\text{A.6})$$

$$\lambda_5 = -\frac{m_{A_0}^2}{v^2} + \frac{2m_{12}^2}{v^2 s_{2\beta}} + \frac{T_1^0 s_\beta^2}{v^3 c_\beta} + \frac{T_2^0 c_\beta^2}{v^3 s_\beta}. \quad (\text{A.7})$$

## A.2. Couplings of the 2HDM

We state here the 2HDM Higgs couplings needed in Sec. 8.2, to derive the relations Eq. (8.33) to Eq. (8.37), and in Ch. 10:

$$g_{HHH} = \frac{3}{vs_{2\beta}^2} (4m_{12}^2 s_{\alpha+\beta} s_{\beta-\alpha}^2 + m_H^2 (c_{\beta-\alpha} s_{2\alpha} - 2s_{\alpha+\beta}) s_{2\beta}), \quad (\text{A.8})$$

$$g_{HHh} = \frac{s_{\beta-\alpha}}{vs_{2\beta}^2} ((m_h^2 + 2m_H^2) s_{2\alpha} s_{2\beta} - 2m_{12}^2 (3s_{2\alpha} + s_{2\beta})), \quad (\text{A.9})$$

$$g_{Hhh} = -\frac{c_{\beta-\alpha}}{vs_{2\beta}^2} ((2m_h^2 + m_H^2) s_{2\alpha} s_{2\beta} - 2m_{12}^2 (3s_{2\alpha} - s_{2\beta})), \quad (\text{A.10})$$

$$g_{hhh} = \frac{3}{vs_{2\beta}^2} (4m_{12}^2 c_{\alpha+\beta} c_{\beta-\alpha}^2 - m_h^2 (2c_{\alpha+\beta} + s_{2\alpha} s_{\beta-\alpha}) s_{2\beta}), \quad (\text{A.11})$$

$$g_{hA_0A_0} = -\frac{1}{v} \left( (2m_{A_0}^2 - m_h^2) s_{\beta-\alpha} + \left( 2m_h^2 - \frac{2m_{12}^2}{s_\beta c_\beta} \right) \frac{c_{\alpha+\beta}}{s_{2\beta}} \right), \quad (\text{A.12})$$

$$g_{HA_0A_0} = -\frac{1}{v} \left( (2m_{A_0}^2 - m_H^2) c_{\beta-\alpha} + \left( 2m_H^2 - \frac{2m_{12}^2}{s_\beta c_\beta} \right) \frac{s_{\alpha+\beta}}{s_{2\beta}} \right), \quad (\text{A.13})$$

$$g_{hA_0G_0} = \frac{c_{\beta-\alpha}}{v} (m_{A_0}^2 - m_h^2), \quad g_{HA_0G_0} = -\frac{s_{\beta-\alpha}}{v} (m_{A_0}^2 - m_H^2), \quad (\text{A.14})$$

$$g_{hWW} = \frac{M_W e s_{\beta-\alpha}}{s_W}, \quad g_{HWW} = \frac{M_W e c_{\beta-\alpha}}{s_W}, \quad (\text{A.15})$$

$$g_{h\tau\tau} = -\frac{y_\tau Y_1}{\sqrt{2}}, \quad g_{H\tau\tau} = -\frac{y_\tau Y_2}{\sqrt{2}}. \quad (\text{A.16})$$

The Yukawa coupling modifiers  $Y_1$ ,  $Y_2$  and  $Y_3$ , parametrizing the couplings between the fermions and the Higgs bosons in the 2HDM, depend on the type of 2HDM under consideration. For type I and II they are summarized in Tab. A.1:

2HDM type	$Y_1$	$Y_2$	$Y_3$
I	$\frac{c_\alpha}{s_\beta}$	$\frac{s_\alpha}{s_\beta}$	$-\frac{1}{t_\beta}$
II	$-\frac{s_\alpha}{c_\beta}$	$\frac{c_\alpha}{c_\beta}$	$t_\beta$

**Table A.1.:** The Yukawa coupling modifiers  $Y_1$ ,  $Y_2$  and  $Y_3$ , parametrizing the couplings between the fermions and the Higgs bosons in the 2HDM of type I and II.

### A.3. Trilinear Higgs Self-Couplings of the NMSSM at Tree Level

In this appendix we quote the tree-level trilinear Higgs couplings of the NMSSM in the gauge basis  $\phi$ , introduced in Eq. (16.15). The complex phases  $\varphi_x$ ,  $\varphi_y$  and  $\varphi_z$  were defined in Eqs. 16.23 - 16.25. The couplings are symmetric in the indices. All couplings, which do not appear here, vanish at tree level.

$$\begin{aligned}
\lambda_{111} &= -\frac{3c_\beta M_Z^2}{v}, & \lambda_{112} &= \frac{s_\beta M_Z^2}{v} - |\lambda|^2 s_\beta v, & \lambda_{113} &= -|\lambda|^2 v_s, & \lambda_{122} &= \frac{c_\beta M_Z^2}{v} - |\lambda|^2 c_\beta v, \\
\lambda_{123} &= \frac{|A_\lambda| |\lambda| c_{\varphi_x}}{\sqrt{2}} - |\lambda| |\kappa| v_s c_{\varphi_y}, & \lambda_{126} &= \frac{3}{2} |\lambda| |\kappa| v_s s_{\varphi_y}, & \lambda_{133} &= -|\lambda|^2 v c_\beta + |\kappa| |\lambda| v s_\beta c_{\varphi_y}, \\
\lambda_{135} &= -\frac{1}{2} |\lambda| |\kappa| v_s s_{\varphi_y}, & \lambda_{136} &= |\lambda| |\kappa| v s_{\varphi_y} s_\beta, & \lambda_{144} &= \frac{c_\beta M_Z^2}{v}, & \lambda_{155} &= \frac{c_\beta M_Z^2}{v} - |\lambda|^2 c_\beta v, \\
\lambda_{156} &= -\frac{|A_\lambda| |\lambda| c_{\varphi_x}}{\sqrt{2}} + |\lambda| |\kappa| v_s c_{\varphi_y}, & \lambda_{166} &= -|\lambda|^2 c_\beta v - |\kappa| |\lambda| v s_\beta c_{\varphi_y}, & \lambda_{222} &= -\frac{3M_Z^2 s_\beta}{v}, \\
\lambda_{223} &= -|\lambda|^2 v_s, & \lambda_{233} &= |\lambda| |\kappa| v c_\beta c_{\varphi_y} - |\lambda|^2 s_\beta v, & \lambda_{234} &= \frac{1}{2} |\kappa| |\lambda| v_s s_{\varphi_y}, & \lambda_{236} &= |\kappa| |\lambda| v c_\beta s_{\varphi_y}, \\
\lambda_{244} &= \frac{M_Z^2 s_\beta}{v} - |\lambda|^2 v s_\beta, & \lambda_{246} &= \frac{|A_\lambda| |\lambda| c_{\varphi_x}}{\sqrt{2}} - |\lambda| |\kappa| v_s c_{\varphi_y}, & \lambda_{255} &= -\frac{M_Z^2 s_\beta}{v}, \\
\lambda_{266} &= -|\lambda| |\kappa| v c_\beta c_{\varphi_y} - |\lambda|^2 s_\beta v, & \lambda_{333} &= -6|\kappa|^2 v_s - \sqrt{2} |A_\kappa| |\kappa| c_{\varphi_z}, & \lambda_{334} &= -|\kappa| |\lambda| v s_\beta s_{\varphi_y}, \\
\lambda_{335} &= -|\kappa| |\lambda| v c_\beta s_{\varphi_y}, & \lambda_{336} &= \frac{3|\lambda| |\kappa| s_\beta c_\beta s_{\varphi_y} v^2}{v_s}, & \lambda_{344} &= -|\lambda|^2 v_s, \\
\lambda_{345} &= \frac{|A_\lambda| |\lambda| c_{\varphi_x}}{\sqrt{2}} - |\kappa| |\lambda| v_s c_{\varphi_y}, & \lambda_{346} &= |\kappa| |\lambda| v s_\beta c_{\varphi_y}, & \lambda_{355} &= -|\lambda|^2 v_s, \\
\lambda_{356} &= |\kappa| |\lambda| v c_\beta c_{\varphi_y}, & \lambda_{366} &= \sqrt{2} |A_\kappa| |\kappa| c_{\varphi_z} - 2|\kappa|^2 v_s, & \lambda_{456} &= -\frac{3}{2} |\kappa| |\lambda| v_s s_{\varphi_y}, \\
\lambda_{466} &= |\kappa| |\lambda| v s_\beta s_{\varphi_y}, & \lambda_{566} &= |\kappa| |\lambda| v c_\beta s_{\varphi_y}, & \lambda_{666} &= \frac{3|\kappa| |\lambda| c_\beta s_\beta s_{\varphi_y} v^2}{v_s}.
\end{aligned} \tag{A.17}$$

These expressions are also given in our publication [47].



---

Explicit Expressions for Selected Loop Corrections

---

**B.1. The Width  $\Gamma_{H^+ \rightarrow W^+ h}^{\mathcal{O}(1\text{-loop})}$**

In this appendix we state the expression for the decay width  $\Gamma_{H^+ \rightarrow W^+ h}^{\mathcal{O}(1\text{-loop})}$ , which comprises the tree-level, virtual and counterterm contributions. We do not give an explicit expression for the real corrections  $\Gamma_{H^+ \rightarrow W^+ h \gamma}^{\text{soft},(1)}$ , which have to be added incoherently to  $\Gamma_{H^+ \rightarrow W^+ h}^{\mathcal{O}(1\text{-loop})}$  in order to arrive at the physically meaningful, IR finite result  $\Gamma_{H^+ \rightarrow W^+ h}^{\mathcal{O}(1\text{-loop}),\text{phys}}$  (cf. Subs. 3.2.2). An expression for  $\Gamma_{H^+ \rightarrow W^+ h \gamma}^{\text{soft},(1)}$  can be found in Refs. [100, 148]. To obtain  $\Gamma_{H^+ \rightarrow W^+ h}^{\mathcal{O}(1\text{-loop})}$  we can make use of the general formulae stated in Eqs. 3.22 - 3.25, leading us to

$$\Gamma_{H^+ \rightarrow W^+ h}^{\mathcal{O}(1\text{-loop})} = \frac{1}{16\pi m_{H^+}^3} \lambda(m_{H^\pm}^2, M_W^2, m_h^2) \sum_{\lambda_{W^+}} |\mathcal{A}_{H^+ \rightarrow W^+ h}|_{\mathcal{O}(1\text{-loop})}^2. \quad (\text{B.1})$$

Here the sum runs over all possible polarizations  $\lambda_{W^+}$  of the outgoing  $W$ -boson. Furthermore we have

$$|\mathcal{A}_{H^+ \rightarrow W^+ h}|_{\mathcal{O}(1\text{-loop})}^2 = |\mathcal{A}_{H^+ \rightarrow W^+ h}^{\text{tree}}|^2 + 2\text{Re} \left[ \mathcal{A}_{H^+ \rightarrow W^+ h}^{\text{tree}*} \left( \mathcal{A}_{H^+ \rightarrow W^+ h}^{\text{virt}(1)} + \mathcal{A}_{H^+ \rightarrow W^+ h}^{\text{ct}(1)} \right) \right]. \quad (\text{B.2})$$

The tree-level amplitude  $\mathcal{A}_{H^+ \rightarrow W^+ h}^{\text{tree}}$  for this process is given by

$$\begin{aligned} \mathcal{A}_{H^+ \rightarrow W^+ h}^{\text{tree}} &= \frac{-g c_{\beta-\alpha}}{2} g_{\mu\nu} (p_{H^+} + p_h)^\mu \epsilon_{W^+}^{*,\nu} \\ &= -g c_{\beta-\alpha} (p_{H^+} \epsilon_{W^+}^*), \end{aligned} \quad (\text{B.3})$$

where  $p_{H^+}$  denotes the momentum of the incoming  $H^+$ ,  $p_h$  the one of the outgoing  $h$  and  $\epsilon_{W^+}^{*,\nu} \equiv \epsilon_{W^+}^{*,\nu}(p_{W^+})$  stands for the polarization vector of the outgoing  $W^+$  with momentum  $p_{W^+}$ . In the last row we have used momentum conservation,  $p_{H^+} = p_h + p_{W^+}$ , and the transversality of the external  $W$ -boson, yielding  $p_{W^+} \epsilon_{W^+}^* = 0$ .

Both the virtual amplitude  $\mathcal{A}_{H^+ \rightarrow W^+ h}^{\text{virt}(1)}$  and the counterterm amplitude  $\mathcal{A}_{H^+ \rightarrow W^+ h}^{\text{ct}(1)}$  can be written in a factorized form by extracting a factor of  $\mathcal{A}_{H^+ \rightarrow W^+ h}^{\text{tree}}$ . Omitting from now on the superscript (1), we have

$$\mathcal{A}_{H^+ \rightarrow W^+ h}^{\mathcal{O}(1\text{-loop})} = \left( \mathcal{A}_{H^+ \rightarrow W^+ h}^{\text{virt}} + \mathcal{A}_{H^+ \rightarrow W^+ h}^{\text{ct}} \right) = \mathcal{A}_{H^+ \rightarrow W^+ h}^{\text{tree}} \left( \mathcal{F}_{H^+ \rightarrow W^+ h}^{\text{virt}} + \mathcal{F}_{H^+ \rightarrow W^+ h}^{\text{ct}} \right), \quad (\text{B.4})$$

where we introduced the scalar form factors  $\mathcal{F}_{H^+ \rightarrow W^+ h}^{\text{virt}}$  and  $\mathcal{F}_{H^+ \rightarrow W^+ h}^{\text{ct}}$ . The virtual amplitude comprises all possible virtual corrections of one-loop order. As there exists no vertex connecting one gauge boson and three Higgs bosons and hence no tadpole can be attached to the vertex  $H^+ W^+ h$ ,  $\mathcal{A}_{H^+ \rightarrow W^+ h}^{\text{virt}}$  is identical in both tadpole schemes. Furthermore,  $\mathcal{A}_{H^+ \rightarrow W^+ h}^{\text{virt}}$  does not receive contributions from mixing on the external legs since we have renormalized all particles on-shell (cf. Subs. 3.2.2).

The counterterm amplitude  $\mathcal{A}_{H^+ \rightarrow W^+ h}^{\text{ct}}$  is given by

$$\begin{aligned} \mathcal{A}_{H^+ \rightarrow W^+ h}^{\text{ct}} &= \mathcal{A}_{H^+ \rightarrow W^+ h}^{\text{tree}} \left[ \mathcal{F}_{H^+ \rightarrow W^+ h}^{\text{ct}} \right] \\ &= \mathcal{A}_{H^+ \rightarrow W^+ h}^{\text{tree}} \left[ \frac{\delta g_2}{g_2} + \frac{\delta Z_{WW}}{2} + \frac{\delta Z_{H^+ H^+}}{2} + \frac{\delta Z_{hh}}{2} \right. \\ &\quad \left. + \frac{s_{\beta-\alpha}}{c_{\beta-\alpha}} \left( \frac{\delta Z_{G^+ H^+}}{2} - \frac{\delta Z_{Hh}}{2} + \delta\alpha - \delta\beta \right) \right]. \end{aligned} \quad (\text{B.5})$$

All counterterms appearing in the last two rows of Eq. (B.5) individually depend on the treatment of the tadpoles. However, their sum is invariant under a change of the tadpole scheme, which is due to the fact that all contributions of tadpole counterterms (scheme I) or diagrams (scheme II) cancel among  $\delta Z_{G^+ H^+}$  and  $\delta\beta$  or  $\delta Z_{Hh}$  and  $\delta\alpha$ . Of course,  $\delta\alpha$  and  $\delta\beta$  and therefore also  $\mathcal{A}_{H^+ \rightarrow W^+ h}^{\text{ct}}$  depend on the renormalization scheme used to fix the angular counterterms.

As can directly be seen from the factorizability of the virtual and the counterterm amplitude, the polarization sum contains only one term, determined by the Lorentz structure of the tree-level amplitude

$$\begin{aligned} \sum_{\lambda_{W^+}} (p_{H^+} \epsilon_{W^+}) (p_{H^+} \epsilon_{W^+}^*) &= p_{H^+}^\mu p_{H^+}^\nu \sum_{\lambda_{W^+}} \epsilon_{W^+, \mu} \epsilon_{W^+, \nu}^* \\ &= p_{H^+}^\mu p_{H^+}^\nu \left( -g_{\mu\nu} + \frac{p_{W^+, \mu} p_{W^+, \nu}}{M_W^2} \right) \\ &= \frac{1}{4M_W^2} \lambda^2 (m_{H^\pm}^2, M_W^2, m_h^2). \end{aligned} \quad (\text{B.6})$$

Assembling all ingredients, Eq. (B.1) becomes

$$\Gamma_{H^+ \rightarrow W^+ h}^{\mathcal{O}(1\text{-loop})} = \frac{g_2^2 c_{\beta-\alpha}^2}{64\pi m_{H^+}^3 M_W^2} \lambda^3 (m_{H^+}^2, m_{W^+}^2, m_h^2) (1 + 2\text{Re} [\mathcal{F}_{H^+ \rightarrow W^+ h}^{\text{virt}} + \mathcal{F}_{H^+ \rightarrow W^+ h}^{\text{ct}}]). \quad (\text{B.7})$$

The physically meaningful decay width is then obtained as

$$\Gamma_{H^+ \rightarrow W^+ h}^{\mathcal{O}(1\text{-loop}), \text{phys}} = \Gamma_{H^+ \rightarrow W^+ h}^{\mathcal{O}(1\text{-loop})} + \Gamma_{H^+ \rightarrow W^+ h \gamma}^{\text{soft}, (1)}. \quad (\text{B.8})$$

## B.2. Trilinear Higgs Self-Couplings of the NMSSM at $\mathcal{O}(\alpha_t)$

In this appendix we quote the virtual  $\mathcal{O}(\alpha_t)$  corrections  $\Delta\lambda_{ijk}^{\mathcal{O}(\alpha_t), \text{virt}}$ ,  $i, j, k \in 1, \dots, 6$  as defined in Eq. (18.22), in the gauge basis  $\phi$ , introduced in Eq. (16.15).

$$\begin{aligned} \Delta\lambda_{ijk}^{\mathcal{O}(\alpha_t), \text{virt}} &= 2C_F m_t y_t^3 [F_{1x} ((h_i^t)^* h_j^t h_k^t + h_i^t (h_j^t)^* h_k^t + h_i^t h_j^t (h_k^t)^*) + h_i^t h_j^t h_k^t + \text{c.c.}] \\ &\quad + C_F y_t^3 \left[ \left( -F_{3x} y_{h_i \tilde{t}_2 \tilde{t}_1} y_{h_j \tilde{t}_1 \tilde{t}_2} y_{h_k \tilde{t}_1 \tilde{t}_1} + F_{2x} y_{h_i \tilde{t}_2 \tilde{t}_2} y_{h_j \tilde{t}_2 \tilde{t}_1} y_{h_k \tilde{t}_1 \tilde{t}_2} + \text{Permutation}[i, j, k] \right) \right. \\ &\quad \left. - \frac{y_{h_i \tilde{t}_1 \tilde{t}_1} y_{h_j \tilde{t}_1 \tilde{t}_1} y_{h_k \tilde{t}_1 \tilde{t}_1}}{m_{\tilde{t}_1}^2} - \frac{y_{h_i \tilde{t}_2 \tilde{t}_2} y_{h_j \tilde{t}_2 \tilde{t}_2} y_{h_k \tilde{t}_2 \tilde{t}_2}}{m_{\tilde{t}_2}^2} \right] \\ &\quad + C_F y_t^2 \left[ F_{4x} \left( y_{h_k \tilde{t}_2 \tilde{t}_1} y_{h_i h_j \tilde{t}_1 \tilde{t}_2} + y_{h_k \tilde{t}_1 \tilde{t}_2} y_{h_i h_j \tilde{t}_2 \tilde{t}_1} \right) - \ln \frac{m_{\tilde{t}_1}^2}{\mu_r^2} y_{h_k \tilde{t}_1 \tilde{t}_1} y_{h_i h_j \tilde{t}_1 \tilde{t}_1} \right. \\ &\quad \left. - \ln \frac{m_{\tilde{t}_2}^2}{\mu_r^2} y_{h_k \tilde{t}_2 \tilde{t}_2} y_{h_i h_j \tilde{t}_2 \tilde{t}_2} + (k \leftrightarrow i) + (k \leftrightarrow j) \right], \end{aligned} \quad (\text{B.9})$$

where and  $\mu_r$  denotes the renormalization scale and we have used the following abbreviations

$$C_F = \frac{3}{16\pi^2}, \quad y_t = \frac{\sqrt{2}m_t}{vs_\beta}, \quad F_{1x} = 2\ln\frac{m_t^2}{\mu_r^2} + 1, \quad F_{2x} = \frac{m_{\tilde{t}_1}^2 - m_{\tilde{t}_2}^2 - m_{\tilde{t}_1}^2 \ln\frac{m_{\tilde{t}_1}^2}{m_{\tilde{t}_2}^2}}{(m_{\tilde{t}_1}^2 - m_{\tilde{t}_2}^2)^2}, \quad (\text{B.10})$$

$$F_{3x} = \frac{m_{\tilde{t}_1}^2 - m_{\tilde{t}_2}^2 - m_{\tilde{t}_2}^2 \ln\frac{m_{\tilde{t}_1}^2}{m_{\tilde{t}_2}^2}}{(m_{\tilde{t}_1}^2 - m_{\tilde{t}_2}^2)^2}, \quad F_{4x} = \frac{m_{\tilde{t}_1}^2 - m_{\tilde{t}_2}^2 - m_{\tilde{t}_1}^2 \ln\frac{m_{\tilde{t}_1}^2}{\mu_r^2} + m_{\tilde{t}_2}^2 \ln\frac{m_{\tilde{t}_2}^2}{\mu_r^2}}{(m_{\tilde{t}_1}^2 - m_{\tilde{t}_2}^2)}. \quad (\text{B.11})$$

The non-vanishing couplings appearing in Eq. (B.9) are given by

$$\begin{aligned} h_2^t &= \frac{1}{\sqrt{2}}, \quad h_5^t = \frac{i}{\sqrt{2}}, \quad y_{h_1\tilde{t}_n\tilde{t}_m} = -\frac{1}{\sqrt{2}}\mu^* \mathcal{U}_{\tilde{t}_{n1}}^* \mathcal{U}_{\tilde{t}_{m2}} - \frac{1}{\sqrt{2}}\mu \mathcal{U}_{\tilde{t}_{n2}}^* \mathcal{U}_{\tilde{t}_{m1}}, \quad (\text{B.12}) \\ y_{h_2\tilde{t}_n\tilde{t}_m} &= \frac{A_t e^{i\varphi_u} \mathcal{U}_{\tilde{t}_{m2}} \mathcal{U}_{\tilde{t}_{n1}}^*}{\sqrt{2}} + \frac{A_t^* e^{-i\varphi_u} \mathcal{U}_{\tilde{t}_{m1}} \mathcal{U}_{\tilde{t}_{n2}}^*}{\sqrt{2}} + \sqrt{2}m_t \mathcal{U}_{\tilde{t}_{m1}} \mathcal{U}_{\tilde{t}_{n1}}^* + \sqrt{2}m_t \mathcal{U}_{\tilde{t}_{m2}} \mathcal{U}_{\tilde{t}_{n2}}^*, \\ y_{h_3\tilde{t}_n\tilde{t}_m} &= -\frac{\lambda^* c_\beta v e^{-i\varphi_s} \mathcal{U}_{\tilde{t}_{m,2}} \mathcal{U}_{\tilde{t}_{n,1}}^*}{2} - \frac{\lambda c_\beta v e^{i\varphi_s} \mathcal{U}_{\tilde{t}_{m,1}} \mathcal{U}_{\tilde{t}_{n,2}}^*}{2}, \\ y_{h_4\tilde{t}_n\tilde{t}_m} &= \frac{1}{\sqrt{2}}i\mu^* \mathcal{U}_{\tilde{t}_{m2}} \mathcal{U}_{\tilde{t}_{n1}}^* - \frac{1}{\sqrt{2}}i\mu \mathcal{U}_{\tilde{t}_{m1}} \mathcal{U}_{\tilde{t}_{n2}}^*, \\ y_{h_5\tilde{t}_n\tilde{t}_m} &= \frac{iA_t e^{i\varphi_u} \mathcal{U}_{\tilde{t}_{m2}} \mathcal{U}_{\tilde{t}_{n1}}^*}{\sqrt{2}} - \frac{iA_t^* e^{-i\varphi_u} \mathcal{U}_{\tilde{t}_{m1}} \mathcal{U}_{\tilde{t}_{n2}}^*}{\sqrt{2}}, \\ y_{h_6\tilde{t}_n\tilde{t}_m} &= \frac{i\lambda^* c_\beta v e^{-i\varphi_s} \mathcal{U}_{\tilde{t}_{m2}} \mathcal{U}_{\tilde{t}_{n1}}^*}{2} - \frac{i\lambda c_\beta v e^{i\varphi_s} \mathcal{U}_{\tilde{t}_{m1}} \mathcal{U}_{\tilde{t}_{n2}}^*}{2}, \\ y_{h_1 h_3 \tilde{t}_n \tilde{t}_m} &= -\frac{1}{2}\lambda^* e^{-i\varphi_s} \mathcal{U}_{\tilde{t}_{m2}} \mathcal{U}_{\tilde{t}_{n1}}^* - \frac{1}{2}\lambda e^{i\varphi_s} \mathcal{U}_{\tilde{t}_{m1}} \mathcal{U}_{\tilde{t}_{n2}}^*, \\ y_{h_1 h_6 \tilde{t}_n \tilde{t}_m} &= \frac{1}{2}i\lambda^* e^{-i\varphi_s} \mathcal{U}_{\tilde{t}_{m2}} \mathcal{U}_{\tilde{t}_{n1}}^* - \frac{1}{2}i\lambda e^{i\varphi_s} \mathcal{U}_{\tilde{t}_{m1}} \mathcal{U}_{\tilde{t}_{n2}}^*, \\ y_{h_2 h_2 \tilde{t}_n \tilde{t}_m} &= y_t \mathcal{U}_{\tilde{t}_{m1}} \mathcal{U}_{\tilde{t}_{n1}}^* + y_t \mathcal{U}_{\tilde{t}_{m2}} \mathcal{U}_{\tilde{t}_{n2}}^*, \\ y_{h_3 h_4 \tilde{t}_n \tilde{t}_m} &= \frac{1}{2}i\lambda^* e^{-i\varphi_s} \mathcal{U}_{\tilde{t}_{m2}} \mathcal{U}_{\tilde{t}_{n1}}^* - \frac{1}{2}i\lambda e^{i\varphi_s} \mathcal{U}_{\tilde{t}_{m1}} \mathcal{U}_{\tilde{t}_{n2}}^*, \\ y_{h_4 h_6 \tilde{t}_n \tilde{t}_m} &= \frac{1}{2}\lambda^* e^{-i\varphi_s} \mathcal{U}_{\tilde{t}_{m2}} \mathcal{U}_{\tilde{t}_{n1}}^* + \frac{1}{2}\lambda e^{i\varphi_s} \mathcal{U}_{\tilde{t}_{m1}} \mathcal{U}_{\tilde{t}_{n2}}^*, \\ y_{h_5 h_5 \tilde{t}_n \tilde{t}_m} &= y_t \mathcal{U}_{\tilde{t}_{m1}} \mathcal{U}_{\tilde{t}_{n1}}^* + y_t \mathcal{U}_{\tilde{t}_{m2}} \mathcal{U}_{\tilde{t}_{n2}}^*, \end{aligned}$$

where  $\mathcal{U}$  denotes the stop rotation matrix defined in Sec. 16.5. These expressions are also given in our publication [47].

### B.3. The Coupling Counterterms $\Delta\lambda_{\phi_i\phi_j\phi_k}^{\mathcal{O}(\alpha_t),ct}$ and $\Delta\lambda_{\phi_i\phi_j\phi_k}^{\mathcal{O}(\alpha_t\alpha_s),ct}$

In this appendix we quote the counterterm  $\Delta\lambda_{\phi_i\phi_j\phi_k}^{\mathcal{O}(a),ct}$ ,  $a \in \{\mathcal{O}(\alpha_t), \mathcal{O}(\alpha_t\alpha_s)\}$ , for the trilinear Higgs self-coupling in the gauge basis. The superscript  $a$  denotes the order of the coupling

counterterm and of the parameter counterterms to be inserted in the following expressions.

$$\Delta\lambda_{112}^{O(a),ct} = -2vs_\beta|\lambda|\delta^{(a)}|\lambda| - vc_\beta^3|\lambda|^2\delta^{(a)}\tan\beta - s_\beta|\lambda|^2\delta^{(a)}v - \frac{1}{2}vs_\beta|\lambda|^2\delta^{(a)}Z_{h_u}, \quad (\text{B.13})$$

$$\Delta\lambda_{113}^{O(a),ct} = -2v_s|\lambda|\delta^{(a)}|\lambda|,$$

$$\Delta\lambda_{122}^{O(a),ct} = -2vc_\beta|\lambda|\delta^{(a)}|\lambda| + vc_\beta^2s_\beta|\lambda|^2\delta^{(a)}\tan\beta - c_\beta|\lambda|^2\delta^{(a)}v - vc_\beta|\lambda|^2\delta^{(a)}Z_{h_u},$$

$$\begin{aligned} \Delta\lambda_{123}^{O(a),ct} = & -\left(\frac{1}{2}v_s c_{\varphi_y}|\kappa| + \frac{v^2 c_\beta s_\beta |\lambda|}{v_s}\right)\delta^{(a)}|\lambda| + \frac{c_{2\beta}c_\beta^2(2m_{H^\pm}^2 + v^2|\lambda|^2)\delta^{(a)}\tan\beta}{2v_s} \\ & - \frac{s_\beta^3\delta^{(a)}t_{h_d} + c_\beta^3\delta^{(a)}t_{h_u}}{vv_s} + \frac{c_\beta s_\beta \delta^{(a)}M_{H^\pm}^2}{v_s} + \frac{vc_\beta s_\beta |\lambda|^2 \delta^{(a)}v}{v_s} \\ & + \frac{(s_{2\beta}m_{H^\pm}^2 + v_s^2 c_{\varphi_y}|\kappa||\lambda| + v^2 c_\beta s_\beta |\lambda|^2)\delta^{(a)}Z_{h_u}}{4v_s}, \end{aligned}$$

$$\Delta\lambda_{126}^{O(a),ct} = \frac{3}{2}v_s s_{\varphi_y}|\kappa|\delta^{(a)}|\lambda| + \frac{3}{4}v_s s_{\varphi_y}|\kappa||\lambda|\delta^{(a)}Z_{h_u} - \frac{\delta^{(a)}t_{ad}}{vv_s s_\beta},$$

$$\begin{aligned} \Delta\lambda_{133}^{O(a),ct} = & v(c_{\varphi_y}s_\beta|\kappa| - 2c_\beta|\lambda|)\delta^{(a)}|\lambda| + vc_\beta^2|\lambda|(c_\beta c_{\varphi_y}|\kappa| + s_\beta|\lambda|)\delta^{(a)}\tan\beta \\ & + |\lambda|(c_{\varphi_y}s_\beta|\kappa| - c_\beta|\lambda|)\delta^{(a)}v, \end{aligned}$$

$$\Delta\lambda_{135}^{O(a),ct} = -\frac{1}{2}v_s|\kappa|s_{\varphi_y}\delta^{(a)}|\lambda| - \frac{1}{4}v_s|\kappa||\lambda|s_{\varphi_y}\delta^{(a)}Z_{h_u} - \frac{\delta^{(a)}t_{ad}}{vv_s s_\beta},$$

$$\Delta\lambda_{136}^{O(a),ct} = vs_\beta s_{\varphi_y}|\kappa|\delta^{(a)}|\lambda| + vc_\beta^3 s_{\varphi_y}|\kappa||\lambda|\delta^{(a)}\tan\beta + s_\beta s_{\varphi_y}|\kappa||\lambda|\delta^{(a)}v,$$

$$\Delta\lambda_{155}^{O(a),ct} = \Delta\lambda_{122}^{O(a),ct}, \quad \Delta\lambda_{156}^{O(a),ct} = -\Delta\lambda_{123}^{O(a),ct},$$

$$\begin{aligned} \Delta\lambda_{166}^{O(a),ct} = & -v(c_{\varphi_y}s_\beta|\kappa| + 2c_\beta|\lambda|)\delta^{(a)}|\lambda| - vc_\beta^2|\lambda|(c_\beta c_{\varphi_y}|\kappa| - s_\beta|\lambda|)\delta^{(a)}\tan\beta \\ & - |\lambda|(c_{\varphi_y}s_\beta|\kappa| + c_\beta|\lambda|)\delta^{(a)}v, \end{aligned}$$

$$\Delta\lambda_{223}^{O(a),ct} = -2v_s|\lambda|\delta^{(a)}|\lambda| - v_s|\lambda|^2\delta^{(a)}Z_{h_u},$$

$$\begin{aligned} \Delta\lambda_{233}^{O(a),ct} = & (vc_\beta c_{\varphi_y}|\kappa| - 2vs_\beta|\lambda|)\delta^{(a)}|\lambda| - vc_\beta^2|\lambda|(c_{\varphi_y}s_\beta|\kappa| + c_\beta|\lambda|)\delta^{(a)}\tan\beta \\ & + |\lambda|(c_\beta c_{\varphi_y}|\kappa| - s_\beta|\lambda|)\delta^{(a)}v + \frac{1}{2}v|\lambda|(c_\beta c_{\varphi_y}|\kappa| - s_\beta|\lambda|)\delta^{(a)}Z_{h_u}, \end{aligned}$$

$$\Delta\lambda_{234}^{O(a),ct} = \Delta\lambda_{135}^{O(a),ct},$$

$$\Delta\lambda_{236}^{O(a),ct} = vc_\beta|\kappa|s_{\varphi_y}\delta^{(a)}|\lambda| - vc_\beta^2s_\beta|\kappa||\lambda|s_{\varphi_y}\delta^{(a)}\tan\beta + c_\beta|\kappa||\lambda|s_{\varphi_y}\delta^{(a)}v + \frac{1}{2}vc_\beta|\kappa||\lambda|s_{\varphi_y}\delta^{(a)}Z_{h_u},$$

$$\Delta\lambda_{244}^{O(a),ct} = \Delta\lambda_{112}^{O(a),ct},$$

$$\begin{aligned} \Delta\lambda_{246}^{O(a),ct} = & \left(\frac{3}{2}v_s c_{\varphi_y}|\kappa| - \frac{v^2 c_\beta s_\beta |\lambda|}{v_s}\right)\delta^{(a)}|\lambda| - \frac{c_{2\beta}c_\beta^2(2m_{H^\pm}^2 + v^2|\lambda|^2)\delta^{(a)}\tan\beta}{2v_s} \\ & + \frac{s_\beta^3\delta^{(a)}t_{h_d} - c_\beta^3\delta^{(a)}t_{h_u}}{vv_s} - \frac{vc_\beta s_\beta |\lambda|^2 \delta^{(a)}v}{v_s} - \frac{c_\beta s_\beta \delta^{(a)}M_{H^\pm}^2}{v_s} \\ & - \frac{(s_{2\beta}m_{H^\pm}^2 - 3v_s^2 c_{\varphi_y}|\kappa||\lambda| + v^2 c_\beta s_\beta |\lambda|^2)\delta^{(a)}Z_{h_u}}{4v_s}, \end{aligned}$$

$$\begin{aligned} \Delta\lambda_{266}^{O(a),ct} = & -v(c_\beta c_{\varphi_y}|\kappa| + 2s_\beta|\lambda|)\delta^{(a)}|\lambda| + vc_\beta^2|\lambda|(c_{\varphi_y}s_\beta|\kappa| - c_\beta|\lambda|)\delta^{(a)}\tan\beta \\ & - |\lambda|(c_\beta c_{\varphi_y}|\kappa| + s_\beta|\lambda|)\delta^{(a)}v - \frac{1}{2}v|\lambda|(c_\beta c_{\varphi_y}|\kappa| + s_\beta|\lambda|)\delta^{(a)}Z_{h_u}, \end{aligned}$$

$$\Delta\lambda_{333}^{O(a),ct} = -\frac{3v^2 c_\beta s_\beta s_{\varphi_y} t_{\varphi_z} |\kappa| \delta^{(a)} |\lambda|}{v_s} - \frac{3v^2 c_\beta^2 c_{2\beta} s_{\varphi_y} t_{\varphi_z} |\kappa| |\lambda| \delta^{(a)} \tan\beta}{v_s} - \frac{6vc_\beta s_\beta s_{\varphi_y} t_{\varphi_z} |\kappa| |\lambda| \delta^{(a)} v}{v_s},$$

$$\Delta\lambda_{334}^{O(a),ct} = -vs_\beta s_{\varphi_y}|\kappa|\delta^{(a)}|\lambda| - vc_\beta^3 s_{\varphi_y}|\kappa||\lambda|\delta^{(a)}\tan\beta - s_\beta s_{\varphi_y}|\kappa||\lambda|\delta^{(a)}v,$$

$$\begin{aligned}
 \Delta\lambda_{335}^{\mathcal{O}(a),ct} &= -vc_\beta s_{\varphi_y} |\kappa| \delta^{(a)} |\lambda| + vc_\beta^2 s_\beta s_{\varphi_y} |\kappa| |\lambda| \delta^{(a)} \tan\beta - c_\beta s_{\varphi_y} |\kappa| |\lambda| \delta^{(a)} v - \frac{1}{2} vc_\beta s_{\varphi_y} |\kappa| |\lambda| \delta^{(a)} Z_{h_u}, \\
 \Delta\lambda_{336}^{\mathcal{O}(a),ct} &= -\frac{3v^2 c_\beta s_\beta s_{\varphi_y} |\kappa| \delta^{(a)} |\lambda|}{v_s} - \frac{3v^2 c_\beta^2 c_{2\beta} s_{\varphi_y} |\kappa| |\lambda| \delta^{(a)} \tan\beta}{v_s} - \frac{6vc_\beta s_\beta s_{\varphi_y} |\kappa| |\lambda| \delta^{(a)} v}{v_s}, \\
 \Delta\lambda_{344}^{\mathcal{O}(a),ct} &= \Delta\lambda_{113}^{\mathcal{O}(a),ct}, \quad \Delta\lambda_{345}^{\mathcal{O}(a),ct} = -\Delta\lambda_{123}^{\mathcal{O}(a),ct}, \quad \Delta\lambda_{346}^{\mathcal{O}(a),ct} = \frac{c_{\varphi_y}}{s_{\varphi_y}} \Delta\lambda_{136}^{\mathcal{O}(a),ct}, \\
 \Delta\lambda_{355}^{\mathcal{O}(a),ct} &= \Delta\lambda_{223}^{\mathcal{O}(a),ct}, \quad \Delta\lambda_{356}^{\mathcal{O}(a),ct} = \frac{c_{\varphi_y}}{s_{\varphi_y}} \Delta\lambda_{335}^{\mathcal{O}(a),ct}, \quad \Delta\lambda_{366}^{\mathcal{O}(a),ct} = -\Delta\lambda_{333}^{\mathcal{O}(a),ct}, \\
 \Delta\lambda_{456}^{\mathcal{O}(a),ct} &= -\Delta\lambda_{126}^{\mathcal{O}(a),ct}, \quad \Delta\lambda_{466}^{\mathcal{O}(a),ct} = -\Delta\lambda_{334}^{\mathcal{O}(a),ct}, \quad \Delta\lambda_{566}^{\mathcal{O}(a),ct} = -\Delta\lambda_{335}^{\mathcal{O}(a),ct}, \\
 \Delta\lambda_{666}^{\mathcal{O}(a),ct} &= -\Delta\lambda_{336}^{\mathcal{O}(a),ct}.
 \end{aligned}$$

All couplings not stated in this list do not receive a counterterm at  $\mathcal{O}(\alpha_t)$  and  $\mathcal{O}(\alpha_t\alpha_s)$  respectively. These expressions are also given in our publication [47].



### C.1. Reduction of the Scalar Loop Functions

In this appendix we state the conventions for all Passarino-Veltman functions appearing in this thesis and give important relations, which are used in our calculation.

Defining

$$C = \left( \frac{(2\pi\mu_r)^{2\epsilon}}{i\pi^2} \right), \quad (\text{C.1})$$

we use the following conventions

$$A_0^D(m_1^2) = C \int d^D q \frac{1}{q^2 - m_1^2}, \quad (\text{C.2})$$

$$B_0^D(p^2, m_1^2, m_2^2) = C \int d^D q \frac{1}{(q^2 - m_1^2)((q+p)^2 - m_2^2)}, \quad (\text{C.3})$$

$$p_1^\mu B_1^D(p^2, m_1^2, m_2^2) = C \int d^D q \frac{q^\mu}{(q^2 - m_1^2)((q+p)^2 - m_2^2)}, \quad (\text{C.4})$$

$$C_0^D(0, 0, 0, m_1^2, m_2^2, m_3^2) = C \int d^D q \frac{1}{(q^2 - m_1^2)(q^2 - m_2^2)(q^2 - m_3^2)}, \quad (\text{C.5})$$

$$D_0^D(0, 0, 0, 0, m_1^2, m_2^2, m_3^2, m_4^2) = C \int d^D q \frac{1}{(q^2 - m_1^2)(q^2 - m_2^2)(q^2 - m_3^2)(q^2 - m_4^2)}, \quad (\text{C.6})$$

$$K_0^D(m_1^2, m_2^2, m_3^2) = C^2 \int d^D q_1 d^D q_2 \frac{1}{(q_1^2 - m_1^2)(q_2 - m_2^2)((q_1 - q_2)^2 - m_3^2)}. \quad (\text{C.7})$$

The explicit expressions for the D-dimensional scalar one- and two-point functions are given by

$$\begin{aligned} A_0^D(m_1^2) &= m_1^2 \left( \frac{1}{\epsilon} + 1 - \ln \left( \frac{m_1^2}{Q^2} \right) \right) \\ &+ m_1^2 \epsilon \left( 1 + \frac{\pi^2}{12} - \ln \left( \frac{m_1^2}{Q^2} \right) + \frac{1}{2} \ln \left( \frac{m_1^2}{Q^2} \right)^2 \right) + \mathcal{O}(\epsilon^2) \\ &\equiv A_0(m_1^2) + \epsilon A_\epsilon(m_1^2) + \mathcal{O}(\epsilon^2), \end{aligned} \quad (\text{C.8})$$

$$B_0^D(p^2, m_1^2, m_2^2) = \frac{1}{\epsilon} - \ln\left(\frac{p^2}{Q^2}\right) - f_B(x_-) - f_B(x_+) + \mathcal{O}(\epsilon), \quad (\text{C.9})$$

$$\equiv B_0(p^2, m_1^2, m_2^2) + \mathcal{O}(\epsilon),$$

$$\text{with } f_B(x) = \ln(1-x) - x \ln(1-x^{-1}) - 1, \quad (\text{C.10})$$

$$x_{\pm} = \frac{s \pm \sqrt{s^2 - 4p^2(m_1^2 - i\epsilon)}}{2p^2}, \quad s = p^2 - m_2^2 + m_1^2. \quad (\text{C.11})$$

Here  $Q^2$  is defined as

$$Q^2 = 4\pi e^{-\gamma_E} \mu_r^2, \quad (\text{C.12})$$

with the renormalization scale  $\mu_r$  and the Euler–Mascheroni constant  $\gamma_E$ . Note that in Part II, where we remain at one-loop order, we do not need the terms proportional to  $\epsilon$  in Eq. (C.8) but can restrict ourselves to  $A_0$  and  $B_0$ . Furthermore, note that the following relations are valid

$$A_0(m_1^2) = m_1^2 \left( \frac{1}{\epsilon} + 1 - \ln\left(\frac{m_1^2}{Q^2}\right) \right) = m_1^2 \left( \Delta^{\overline{\text{MS}}} + 1 - \ln\left(\frac{m_1^2}{\mu_r^2}\right) \right), \quad (\text{C.13})$$

$$\begin{aligned} B_0(p^2, m_1^2, m_2^2) &= \frac{1}{\epsilon} - \ln\left(\frac{p^2}{Q^2}\right) - f_B(x_-) - f_B(x_+), \quad (\text{C.14}) \\ &= \Delta^{\overline{\text{MS}}} - \ln\left(\frac{p^2}{\mu_r^2}\right) - f_B(x_-) - f_B(x_+), \end{aligned}$$

with  $\Delta^{\overline{\text{MS}}} = \frac{1}{\epsilon} - \gamma_E + \ln(4\pi)$  as defined in Eq. (3.4).

The tensor coefficient  $B_1^D(p^2, m_1^2, m_2^2) = B_1(p^2, m_1^2, m_2^2) + \mathcal{O}(\epsilon)$  can be related to  $B_0^D(p^2, m_1^2, m_2^2)$  and  $A_0^D$  functions via

$$B_1^D(p^2, m_1^2, m_2^2) = \frac{1}{2p^2} [A_0^D(m_1^2) - A_0^D(m_2^2) - (p^2 + m_1^2 - m_2^2) B_0^D(p^2, m_1^2, m_2^2)]. \quad (\text{C.15})$$

Moreover, all scalar functions with vanishing external momenta we need in Sec. 19.2 can be expressed in terms of  $A_0^D$  functions. The following representations for all scalar functions appearing in our calculation were achieved by partial differentiation and partial fraction decomposition as described e.g. in [291]

$$B_0^D(0, m_1^2, m_1^2) = -1 + \frac{1}{m_1^2} A_0^D(m_1^2) - \epsilon \left( 1 - \ln\left(\frac{m_1^2}{Q^2}\right) \right), \quad (\text{C.16})$$

$$B_0^D(0, m_1^2, m_2^2) = \frac{1}{m_1^2 - m_2^2} (A_0^D(m_1^2) - A_0^D(m_2^2)), \quad (\text{C.17})$$

$$C_0^D(\{0\}, m_1^2, m_1^2, m_1^2) = -\frac{1}{2m_1^2} + \frac{\epsilon}{2} \frac{1}{m_1^2} \ln\left(\frac{m_1^2}{Q^2}\right), \quad (\text{C.18})$$

$$C_0^D(\{0\}, m_1^2, m_1^2, m_2^2) = \frac{1}{m_1^2 - m_2^2} (B_0^D(0, m_1^2, m_1^2) - B_0^D(0, m_1^2, m_2^2)), \quad (\text{C.19})$$

$$D_0^D(\{0\}, m_1^2, m_1^2, m_1^2, m_1^2) = \frac{1}{6m_1^4} + \frac{\epsilon}{6} \left( \frac{1}{m_1^4} - \frac{1}{m_1^4} \ln\left(\frac{m_1^2}{Q^2}\right) \right), \quad (\text{C.20})$$

$$D_0^D(\{0\}, m_1^2, m_1^2, m_1^2, m_2^2) = \frac{1}{m_1^2 - m_2^2} (C_0^D(\{0\}, m_1^2, m_1^2, m_1^2) - C_0^D(\{0\}, m_1^2, m_1^2, m_2^2)), \quad (\text{C.21})$$

$$D_0^D(\{0\}, m_1^2, m_1^2, m_2^2, m_2^2) = \frac{1}{m_1^2 - m_2^2} (C_0^D(\{0\}, m_1^2, m_1^2, m_2^2) - C_0^D(\{0\}, m_1^2, m_2^2, m_2^2)). \quad (\text{C.22})$$

The symbol  $\{0\}$  collectively denotes all external momenta.

We refrain from giving explicit expression for the two-loop vacuum function  $K^D(m_1^2, m_2^2, m_3^2)$ , which can, however, be found in the literature [283–289].

## C.2. Splitting of Gauge-Dependent $A_0$ and $B_0$ Functions

In this appendix we demonstrate the non-uniqueness of the gauge-dependent terms, appearing e.g. in  $\delta\alpha^K$  and  $\delta\beta^K$  in Sec. 7.4.2. There, we expressed the terms containing gauge fixing parameters in terms of the Passarino-Veltman functions  $A_0(\xi_V M_V^2)$ ,  $B_0(m_{S_1}^2, m_{S_2}^2, \xi_V M_V^2)$  and  $B_0(m_{S_1}^2, \xi_V M_V^2, \xi_V M_V^2)$ , with  $S_1, S_2 \in \{h, H, A_0, H^\pm\}$  and  $V \in \{Z, W\}$ . These functions can, however, not be regarded as a unique representation of the gauge-dependent parts of the counterterms. Further gauge-independent terms can be split off these  $A_0$  and  $B_0$  functions as we demonstrate explicitly for the case of  $A_0$ , consistently omitting terms of  $\mathcal{O}(\epsilon)$ .

$$\begin{aligned} A_0(\xi_V M_V^2) &= C \int d^D q \frac{1}{q^2 - \xi_V M_V^2} = C \int d^D q \frac{(q^2 - M_V^2) + \xi_V M_V^2 - \xi_V M_V^2}{(q^2 - \xi_V M_V^2)(q^2 - M_V^2)} \quad (\text{C.23}) \\ &= A_0(M_V^2) - (1 - \xi_V) M_V^2 C \int d^D q \frac{1}{(q^2 - \xi_V M_V^2)(q^2 - M_V^2)}, \end{aligned}$$

where we have expanded by a term  $(q^2 - M_V^2)$  and added a zero in the form  $\xi_V M_V^2 - \xi_V M_V^2$  in the first line. By means of this rearrangement, we have split off a gauge-independent  $A_0$  function, appearing as first term in the second line. The same procedure can be repeated for the second term in the second line, such that further gauge-independent pieces can be split off. This demonstrates that the gauge-parameter-dependent terms quoted in Eq. (7.38) and Eq. (7.39) cannot be regarded as *the* unique gauge-dependent part of the counterterms. It also shows the impossibility of defining the truly gauge-independent parts without a suitable technique like the pinch technique.



### D.1. The Running of $m_t^{\overline{\text{DR}}}$

In this appendix we state the formulae needed for the proper transformation of the OS top mass  $m_t^{\text{OS}}$  to the  $\overline{\text{DR}}$  top mass  $m_t^{\overline{\text{DR}}}$ . We closely follow the appendix A of [44]. In order to make the distinction between the OS and the  $\overline{\text{DR}}$  and  $\overline{\text{MS}}$  top mass more clearly, we introduce the notation  $M_t$  for the OS top mass (i.e. the pole mass). Starting from  $M_t$ , we first have to perform the transformation to the  $\overline{\text{MS}}$  top mass  $m_t^{\overline{\text{MS}}}(M_t)$  at the scale  $M_t$ , which is achieved by means of the two-loop SM relation, to be found e.g. in [259],

$$m_t^{\overline{\text{MS}}}(M_t) = \left( 1 - \frac{4}{3} \left( \frac{\alpha_s(M_t)}{\pi} \right) - 9.1253 \left( \frac{\alpha_s(M_t)}{\pi} \right)^2 \right) M_t. \quad (\text{D.1})$$

Subsequently, the SM renormalization group equations are utilized in order to evolve  $m_t^{\overline{\text{MS}}}$  to the scale  $M_{\text{SUSY}}$ , where the influence of SUSY particles becomes relevant. The resulting relation between the two values of  $m_t^{\overline{\text{MS}}}$  at the two different scales is given by [258]

$$m_t^{\overline{\text{MS}}}(\mu_r) = U_6(\mu_r, M_t) m_t^{\overline{\text{MS}}}(M_t), \quad \text{for } \mu_r > M_t, \quad (\text{D.2})$$

with

$$U_n(Q_2, Q_1) = \left( \frac{\alpha_s(Q_2)}{\alpha_s(Q_1)} \right)^{d_n} \left[ 1 + \frac{\alpha_s(Q_1) - \alpha_s(Q_2)}{4\pi} J_n \right], \quad Q_2 > Q_1 \quad (\text{D.3})$$

$$d_n = \frac{12}{33 - 2n}, \quad J_n = -\frac{8982 - 504n + 40n^2}{3(33 - 2n)^2}. \quad (\text{D.4})$$

Here  $n$  denotes the number of active flavours, which has to be set to  $n = 6$  for  $\mu_r > M_t$ . Above  $M_{\text{SUSY}}$ , the  $\overline{\text{MS}}$  mass has to be converted to the  $\overline{\text{DR}}$  mass in order to respect SUSY, wherefore the two-loop formula

$$m_t^{\overline{\text{DR,SM}}}(M_{\text{SUSY}}) = m_t^{\overline{\text{MS}}}(M_{\text{SUSY}}) \left[ 1 - \frac{\alpha_s(M_{\text{SUSY}})}{3\pi} - \frac{\alpha_s^2(M_{\text{SUSY}})}{144\pi^2} (73 - 3n) \right], \quad (\text{D.5})$$

stated in Ref. [257, 260, 261], can be applied. Note that above  $M_{\text{SUSY}}$  no distinction between the evanescent coupling  $\alpha_e$  and  $\alpha_s^{\overline{\text{DR}}}$  is necessary, as detailed in [260, 261]. To arrive at the

correct NMSSM  $\overline{\text{DR}}$  top mass, we still have to include SUSY-QCD corrections, which we denote by  $dm_t^{\text{SQCD}}$

$$m_t^{\overline{\text{DR}},\text{NMSSM}} = m_t^{\overline{\text{DR}},\text{SM}}(M_{\text{SUSY}}) + dm_t^{\text{SQCD}}. \quad (\text{D.6})$$

For completeness, we also state  $dm_t^{\text{SQCD}}$  [44]

$$dm_t^{\text{SQCD}} = \frac{\alpha_s(M_{\text{SUSY}})}{6\pi} \left[ -2m_t \text{Re} \left( B_1(m_t^2, m_{\tilde{g}}^2, m_{\tilde{t}_1}^2) + B_1(m_t^2, m_{\tilde{g}}^2, m_{\tilde{t}_2}^2) \right) \right. \quad (\text{D.7})$$

$$\left. + 2m_{\tilde{g}} \text{Re} \left( B_0(m_t^2, m_{\tilde{g}}^2, m_{\tilde{t}_1}^2) - B_0(m_t^2, m_{\tilde{g}}^2, m_{\tilde{t}_2}^2) \right) \right. \quad (\text{D.8})$$

$$\left. \times \left( e^{i(\varphi_3 + \varphi_u)} \mathcal{U}_{t_{22}}^* \mathcal{U}_{t_{21}}^* + e^{-i(\varphi_3 + \varphi_u)} \mathcal{U}_{t_{21}}^* \mathcal{U}_{t_{22}}^* \right) \right], \quad (\text{D.9})$$

where the convention we use for the  $B_1$  and  $B_0$  functions are given in App. C.1 and  $\varphi_{M_3}$  denotes the phase of the soft-SUSY-breaking gluino mass parameter  $M_3$ .

## D.2. Approximation of the Two-Loop RGEs for the Parameters of the NMSSM Higgs Sector

In this appendix we illustrate the approximation of the renormalization scale dependence of the  $\overline{\text{DR}}$  parameters, which we apply in Sec. 20.4. We demonstrate the procedure using the example of the parameter  $\tan \beta$ . As starting point, we employ the relation

$$p^{\text{OS}} + \delta p^{\text{OS}}(\mu_r) = p^{\overline{\text{DR}}}(\mu_r) + \delta p^{\overline{\text{DR}}}(\mu_r), \quad (\text{D.10})$$

outlined in Sec. 17.1, where  $p^{\text{OS}}$  ( $p^{\overline{\text{DR}}}$ ) is a parameter renormalized in the OS ( $\overline{\text{DR}}$ ) scheme,  $\delta p^{\text{OS}}$  ( $\delta p^{\overline{\text{DR}}}$ ) the corresponding counterterm and  $\mu_r$  the renormalization scale. Note that the scale dependence of the  $\overline{\text{DR}}$  counterterm, which is defined to be purely divergent, is solely due to the scale dependence of other parameters, e.g.  $\alpha_s(\mu_r)$ , entering  $\delta p^{\overline{\text{DR}}}$ . In the following we will consider the parameter  $\tan \beta^{\text{OS}}$  as parameter fixed by OS conditions while applying the OS scheme in the top-stop sector. Equally,  $\tan \beta^{\overline{\text{DR}}}$  is to be regarded as a parameter defined in the  $\overline{\text{DR}}$  scheme, using at the same time  $\overline{\text{DR}}$  conditions for tops and stops. At two-loop order, the following relation between both holds (up to terms of higher order)

$$\tan \beta^{\text{OS}} + \delta^{(1)} \tan \beta^{\text{OS}} + \delta^{(2)} \tan \beta^{\text{OS}} = \tan \beta^{\overline{\text{DR}}} + \delta^{(1)} \tan \beta^{\overline{\text{DR}}} + \delta^{(2)} \tan \beta^{\overline{\text{DR}}}, \quad (\text{D.11})$$

where the superscripts indicate the loop order of the respective counterterms. In the OS scheme, the counterterms can schematically be expressed as

$$\delta^{(1)} \tan \beta^{\text{OS}} = \mu_r^{2\epsilon} \left( \frac{a_1(m_t^{\text{OS}})}{\epsilon} + f_1(m_t^{\text{OS}}) \right), \quad (\text{D.12})$$

$$\delta^{(2)} \tan \beta^{\text{OS}} = \mu_r^{4\epsilon} \left( \frac{b_2(m_t^{\text{OS}}, \alpha_s^{\overline{\text{DR}}}(\mu_r))}{\epsilon^2} + \frac{a_2(m_t^{\text{OS}}, \alpha_s^{\overline{\text{DR}}}(\mu_r))}{\epsilon} + f_2(m_t^{\text{OS}}, \alpha_s^{\overline{\text{DR}}}(\mu_r)) \right). \quad (\text{D.13})$$

The functions  $a_1$ ,  $f_1$ ,  $a_2$ ,  $b_2$  and  $f_2$  do not explicitly depend on  $\mu_r$ , however an implicit dependence enters  $a_2$ ,  $b_2$  and  $f_2$  via  $\alpha_s(\mu_r)^{\overline{\text{DR}}}$ . Furthermore, note that Eqs. D.12 and D.13 hold in this form only in the context of our calculation, where  $\delta \tan \beta$  is proportional to  $\delta Z_{h_u}$  and only corrections from the top-stop sector are taken into account. For  $\epsilon \rightarrow 0$ , we can expand these equations in terms of  $\epsilon$ , leading to

$$\delta^{(1)} \tan \beta^{\text{OS}} = \frac{a_1(m_t^{\text{OS}})}{\epsilon} + a_1(m_t^{\text{OS}}) \ln(\mu_r^2) + f_1(m_t^{\text{OS}}), \quad (\text{D.14})$$

$$\begin{aligned} \delta^{(2)} \tan \beta^{\text{OS}} &= \frac{b_2(m_t^{\text{OS}}, \alpha_s^{\overline{\text{DR}}}(\mu_r))}{\epsilon^2} + \frac{a_2(m_t^{\text{OS}}, \alpha_s^{\overline{\text{DR}}}(\mu_r)) + 2b_2(m_t^{\text{OS}}, \alpha_s^{\overline{\text{DR}}}(\mu_r)) \ln(\mu_r^2)}{\epsilon} \\ &\quad + 2a_2(m_t^{\text{OS}}, \alpha_s^{\overline{\text{DR}}}(\mu_r)) \ln(\mu_r^2) + 2b_2(m_t^{\text{OS}}, \alpha_s^{\overline{\text{DR}}}(\mu_r)) \ln^2(\mu_r^2) \\ &\quad + f_2(m_t^{\text{OS}}, \alpha_s^{\overline{\text{DR}}}(\mu_r)). \end{aligned} \quad (\text{D.15})$$

The corresponding relation in the pure  $\overline{\text{DR}}$  scheme takes the following form

$$\delta^{(1)} \tan \beta^{\overline{\text{DR}}} = \frac{a_1(m_t^{\overline{\text{DR}}})}{\epsilon}, \quad (\text{D.16})$$

$$\delta^{(2)} \tan \beta^{\overline{\text{DR}}} = \frac{b_2(m_t^{\overline{\text{DR}}}, \alpha_s^{\overline{\text{DR}}}(\mu_r))}{\epsilon^2} + \frac{a_2(m_t^{\overline{\text{DR}}}, \alpha_s^{\overline{\text{DR}}}(\mu_r))}{\epsilon}. \quad (\text{D.17})$$

Using the relation

$$m_t^{\overline{\text{DR}}} = m_t^{\text{OS}} + \delta m_t^{\text{OS}}|_{\text{fin}}, \quad (\text{D.18})$$

where  $\delta m_t^{\text{OS}}|_{\text{fin}}$  denotes the finite part of the OS top-mass counterterm, and furthermore exploiting the explicit forms of  $a_1$  and  $b_2$  in the context of our calculation, one can show the following equality

$$a_1(m_t^{\text{OS}}) \delta m_t^{\text{OS}}|_{\mu_r\text{-term}} = b_2(m_t^{\text{OS}}, \alpha_s^{\overline{\text{DR}}}(\mu_r)) \ln(\mu_r^2), \quad (\text{D.19})$$

where  $\delta m_t^{\text{OS}}|_{\mu_r\text{-term}}$  denotes the term  $\propto \ln(\mu_r^2)$  in  $\delta m_t^{\text{OS}}|_{\text{fin}}$ . Inserting Eqs. D.14 - D.16 into Eq. (D.11), taking advantage of Eq. (D.19), we can solve for  $\tan \beta^{\overline{\text{DR}}}(\mu_r)$ . Doing so at two different scales  $\mu_1$  and  $\mu_2$  and taking the difference between the resulting  $\tan \beta^{\overline{\text{DR}}}(\mu_1)$  and  $\tan \beta^{\overline{\text{DR}}}(\mu_2)$ , we arrive at

$$\begin{aligned} \tan \beta^{\overline{\text{DR}}}(\mu_1) - \tan \beta^{\overline{\text{DR}}}(\mu_2) = & \\ & a_1(m_t^{\text{OS}}) \ln \left( \frac{\mu_1^2}{\mu_2^2} \right) \\ & + 2a_2(m_t^{\text{OS}}, \alpha_s^{\overline{\text{DR}}}(\mu_1)) \ln(\mu_1^2) - 2a_2(m_t^{\text{OS}}, \alpha_s^{\overline{\text{DR}}}(\mu_2)) \ln(\mu_2^2) \\ & + 2b_2(m_t^{\text{OS}}, \alpha_s^{\overline{\text{DR}}}(\mu_1)) \ln^2(\mu_1^2) - 2b_2(m_t^{\text{OS}}, \alpha_s^{\overline{\text{DR}}}(\mu_2)) \ln^2(\mu_2^2). \end{aligned} \quad (\text{D.20})$$

We utilize this relation in Sec. 20.4 in order to obtain an approximation for the value of  $\tan \beta^{\overline{\text{DR}}}$  at a scale  $\mu_r$ , starting from the central scale  $\mu_0$ . Apart from  $\tan \beta$ , we apply an analogous relation at  $\mathcal{O}(\alpha_t \alpha_s)$  for  $\lambda$ , which is like  $\tan \beta$  proportional to  $\delta Z_{h_u}$ . In our calculation, these are the only  $\overline{\text{DR}}$  parameters receiving a counterterm at  $\mathcal{O}(\alpha_t \alpha_s)$ .

For all other  $\overline{\text{DR}}$  parameters, the simpler one-loop relation

$$p^{\overline{\text{DR}}}(\mu_1) - p^{\overline{\text{DR}}}(\mu_2) = a_1^p \ln \left( \frac{\mu_1^2}{\mu_2^2} \right) \quad (\text{D.21})$$

is applied, where the coefficient of the logarithm  $a_1^p$  is specific for the parameter  $p$  under consideration.



# Acknowledgments

First of all, I would like to express my deep gratitude to my supervisor Prof. Dr. Margarete Mühlleitner. Not only she gave me the possibility to work on interesting projects, but she also offered constant support and encouragement. Furthermore, she gave me the opportunity to broaden my horizons by taking part in conferences and schools. In particular my involvement in the DAAD collaboration with scientists in Lisbon and Aveiro, which she launched together with Prof. Dr. Rui Santos from the university of Lisbon, was a very enriching experience.

I also want to sincerely thank Prof. Dr. Rui Santos, who agreed to act as second reviewer of this thesis and who showed great hospitality to our group during our stays in Lisbon and Aveiro.

Furthermore, I am grateful to my collaborators Dao Thi Nhung, Marcel Krause and Robin Lorenz for the fruitful cooperation and many interesting discussions. They were always ready to share their knowledge and experience and I learned a lot from them.

At this point I also want to express a million thanks to Marco Sampaio for a million parameter points.

I appreciate very much the efforts made by Marcel Krause, Robin Roth, Juraj Streicher, Alexander Wlotzka and Sebastian Ziesche in reading and correcting my manuscript.

Thanks also goes to all members of the institute for the nice time I enjoyed here during the last three years.

In particular, I am grateful to the admins Robin Roth, Pascal Nagel, Johannes Bellm, Christian Röhr and Bastian Feigl, who did a great job maintaining the IT infrastructure. Without their endless efforts a smooth running of everyday work would not have been possible.

Also my room mates Juraj Streicher and Ramona Gröber deserve special mentioning for their preparedness to discuss all these quick questions arising during daily business and for the pleasant atmosphere they helped create in our office.

A project like a PhD thesis is hardly conceivable without personal and emotional support, which I received from my friends and family.

I am deeply grateful to my husband Sebastian Ziesche for backing me and keeping me grounded. I cannot imagine the past few years without his patience, his imperturbable optimism and his love.

Finally, I want to thank my parents Andrea and Thomas Hoffmann, who have supported me in every imaginable concern during all my life. I cannot rate high enough their caring love and patience. This thesis is dedicated to you!



# Bibliography

- [1] S. L. Glashow *Nuclear Physics* **22** no. 4, (1961) 579 – 588.  
<http://www.sciencedirect.com/science/article/pii/0029558261904692>.
- [2] N. Cabibbo *Phys. Rev. Lett.* **10** (Jun, 1963) 531–533.  
<http://link.aps.org/doi/10.1103/PhysRevLett.10.531>.
- [3] M. Gell-Mann *Physics Letters* **8** no. 3, (1964) 214 – 215.  
<http://www.sciencedirect.com/science/article/pii/S0031916364920013>.
- [4] F. Englert and R. Brout *Phys. Rev. Lett.* **13** (Aug, 1964) 321–323.  
<http://link.aps.org/doi/10.1103/PhysRevLett.13.321>.  
  
P. Higgs *Physics Letters* **12** no. 2, (1964) 132 – 133.  
<http://www.sciencedirect.com/science/article/pii/0031916364911369>.  
  
P. W. Higgs *Phys. Rev. Lett.* **13** (Oct, 1964) 508–509.  
<http://link.aps.org/doi/10.1103/PhysRevLett.13.508>.  
  
P. W. Higgs *Phys. Rev.* **145** (May, 1966) 1156–1163.  
<http://link.aps.org/doi/10.1103/PhysRev.145.1156>.  
  
T. W. B. Kibble *Phys. Rev.* **155** (Mar, 1967) 1554–1561.  
<http://link.aps.org/doi/10.1103/PhysRev.155.1554>.
- [5] S. Weinberg *Phys. Rev. Lett.* **19** (Nov, 1967) 1264–1266.  
<http://link.aps.org/doi/10.1103/PhysRevLett.19.1264>.
- [6] A. Salam, “Weak and electromagnetic interactions,” in *Elementary particle theory*, N. Svartholm, ed., pp. 367–377. Almquist & Wiksell.
- [7] S. L. Glashow, J. Iliopoulos, and L. Maiani *Phys. Rev. D* **2** (Oct, 1970) 1285–1292.  
<http://link.aps.org/doi/10.1103/PhysRevD.2.1285>.
- [8] M. Kobayashi and T. Maskawa *Progress of Theoretical Physics* **49** no. 2, (1973) 652–657.
- [9] H. Fritzsch, M. Gell-Mann, and H. Leutwyler *Physics Letters B* **47** no. 4, (1973) 365 – 368. <http://www.sciencedirect.com/science/article/pii/0370269373906254>.
- [10] **ATLAS Collaboration** Collaboration, G. Aad *et al.* *Phys.Lett.* **B716** (2012) 1–29, [arXiv:1207.7214](https://arxiv.org/abs/1207.7214) [hep-ex].
- [11] **CMS Collaboration** Collaboration, S. Chatrchyan *et al.* *Phys.Lett.* **B716** (2012) 30–61, [arXiv:1207.7235](https://arxiv.org/abs/1207.7235) [hep-ex].
- [12] **CMS Collaboration**, V. Khachatryan *et al.* *Phys. Rev.* **D92** no. 1, (2015) 012004, [arXiv:1411.3441](https://arxiv.org/abs/1411.3441) [hep-ex].

- [13] **CMS** Collaboration, V. Khachatryan *et al.* *Eur. Phys. J.* **C75** no. 5, (2015) 212, [arXiv:1412.8662 \[hep-ex\]](#).
- [14] **ATLAS** Collaboration, G. Aad *et al.* *Eur. Phys. J.* **C75** no. 10, (2015) 476, [arXiv:1506.05669 \[hep-ex\]](#). [Erratum: *Eur. Phys. J.* **C76**,no.3,152(2016)].
- [15] **ATLAS** Collaboration, G. Aad *et al.* [arXiv:1507.04548 \[hep-ex\]](#).
- [16] T. D. Lee *Phys. Rev. D* **8** (Aug, 1973) 1226–1239.  
<http://link.aps.org/doi/10.1103/PhysRevD.8.1226>.
- [17] J. F. Gunion, H. E. Haber, G. L. Kane, and S. Dawson *Front.Phys.* **80** (2000) 1–448.
- [18] G. C. Branco, P. M. Ferreira, L. Lavoura, M. N. Rebelo, M. Sher, and J. P. Silva *Phys. Rept.* **516** (2012) 1–102, [arXiv:1106.0034 \[hep-ph\]](#).
- [19] D. Volkov and V. Akulov *Phys.Lett.* **B46** (1973) 109–110.
- [20] J. Wess and B. Zumino *Nucl.Phys.* **B70** (1974) 39–50.
- [21] P. Fayet *Phys.Lett.* **B64** (1976) 159.  
P. Fayet *Phys.Lett.* **B69** (1977) 489.  
P. Fayet *Phys.Lett.* **B84** (1979) 416.
- [22] G. R. Farrar and P. Fayet *Phys.Lett.* **B76** (1978) 575–579.
- [23] E. Witten *Nucl.Phys.* **B188** (1981) 513.
- [24] H. P. Nilles *Phys.Rept.* **110** (1984) 1–162.
- [25] H. E. Haber and G. L. Kane *Phys.Rept.* **117** (1985) 75–263.
- [26] M. Sohnius *Phys.Rept.* **128** (1985) 39–204.
- [27] J. Gunion and H. E. Haber *Nucl.Phys.* **B272** (1986) 1.
- [28] J. Gunion and H. E. Haber *Nucl.Phys.* **B278** (1986) 449.
- [29] A. Lahanas and D. V. Nanopoulos *Phys.Rept.* **145** (1987) 1.
- [30] J. Derendinger and C. A. Savoy *Nucl.Phys.* **B237** (1984) 307.
- [31] J. R. Ellis, J. Gunion, H. E. Haber, L. Roszkowski, and F. Zwirner *Phys.Rev.* **D39** (1989) 844.
- [32] M. Drees *Int.J.Mod.Phys.* **A4** (1989) 3635.  
U. Ellwanger, M. Rausch de Traubenberg, and C. A. Savoy *Phys.Lett.* **B315** (1993) 331–337, [arXiv:hep-ph/9307322 \[hep-ph\]](#).  
U. Ellwanger, M. Rausch de Traubenberg, and C. A. Savoy *Z.Phys.* **C67** (1995) 665–670, [arXiv:hep-ph/9502206 \[hep-ph\]](#).  
U. Ellwanger, M. Rausch de Traubenberg, and C. A. Savoy *Nucl.Phys.* **B492** (1997) 21–50, [arXiv:hep-ph/9611251 \[hep-ph\]](#).
- [33] T. Elliott, S. King, and P. White *Phys.Lett.* **B351** (1995) 213–219, [arXiv:hep-ph/9406303 \[hep-ph\]](#).
- [34] S. King and P. White *Phys.Rev.* **D52** (1995) 4183–4216, [arXiv:hep-ph/9505326 \[hep-ph\]](#).

- [35] F. Franke and H. Fraas *Int.J.Mod.Phys.* **A12** (1997) 479–534, arXiv:hep-ph/9512366 [hep-ph].
- [36] M. Maniatis *Int.J.Mod.Phys.* **A25** (2010) 3505–3602, arXiv:0906.0777 [hep-ph].
- [37] U. Ellwanger, C. Hugonie, and A. M. Teixeira *Phys.Rept.* **496** (2010) 1–77, arXiv:0910.1785 [hep-ph].
- [38] R. Santos and A. Barroso *Phys. Rev.* **D56** (1997) 5366–5385, arXiv:hep-ph/9701257 [hep-ph].
- [39] D. López-Val and J. Solà *Phys. Rev. D* **81** (Feb, 2010) 033003.  
<http://link.aps.org/doi/10.1103/PhysRevD.81.033003>.
- [40] S. Kanemura, Y. Okada, E. Senaha, and C. P. Yuan *Phys. Rev.* **D70** (2004) 115002, arXiv:hep-ph/0408364 [hep-ph].
- [41] A. Denner, L. Jenniches, J.-N. Lang, and C. Sturm arXiv:1607.07352 [hep-ph].
- [42] M. Krause, R. Lorenz, M. Muhlleitner, R. Santos, and H. Ziesche *JHEP* **09** (2016) 143, arXiv:1605.04853 [hep-ph].
- [43] M. Krause, M. Muhlleitner, R. Santos, and H. Ziesche arXiv:1609.04185 [hep-ph].
- [44] M. Muhlleitner, D. T. Nhung, H. Rzehak, and K. Walz *JHEP* **1505** (2015) 128, arXiv:1412.0918 [hep-ph].
- [45] M. D. Goodsell and F. Staub arXiv:1604.05335 [hep-ph].
- [46] D. T. Nhung, M. Muhlleitner, J. Streicher, and K. Walz *JHEP* **1311** (2013) 181, arXiv:1306.3926 [hep-ph].
- [47] M. Muhlleitner, D. T. Nhung, and H. Ziesche *JHEP* **12** (2015) 034, arXiv:1506.03321 [hep-ph].
- [48] S. P. Martin *Adv.Ser.Direct.High Energy Phys.* **21** (2010) 1–153, arXiv:hep-ph/9709356 [hep-ph].
- [49] **Planck** Collaboration, P. A. R. Ade *et al.* arXiv:1502.01589 [astro-ph.CO].
- [50] A. Sakharov *Pisma Zh.Eksp.Teor.Fiz.* **5** (1967) 32–35.
- [51] **ATLAS, CMS** Collaboration, G. Aad *et al.* *Phys. Rev. Lett.* **114** (2015) 191803, arXiv:1503.07589 [hep-ex].
- [52] S. Coleman and J. Mandula *Phys. Rev.* **159** (Jul, 1967) 1251–1256.  
<http://link.aps.org/doi/10.1103/PhysRev.159.1251>.
- [53] R. Haag, J. T. Łopuszański, and M. Sohnius *Nuclear Physics B* **88** no. 2, (1975) 257 – 274. <http://www.sciencedirect.com/science/article/pii/0550321375902795>.
- [54] **Particle Data Group** Collaboration, K. Olive *et al.* *Chin.Phys.* **C38** (2014) 090001.
- [55] P. Langacker *Physics Reports* **72** no. 4, (1981) 185 – 385.  
<http://www.sciencedirect.com/science/article/pii/0370157381900594>.
- [56] E. Ma *Phys. Rev.* **D73** (2006) 077301, arXiv:hep-ph/0601225 [hep-ph].
- [57] R. Barbieri, L. J. Hall, and V. S. Rychkov *Phys. Rev.* **D74** (2006) 015007, arXiv:hep-ph/0603188 [hep-ph].

- [58] M. Peskin and D. Schroeder, *An Introduction to Quantum Field Theory*. Advanced book classics. Addison-Wesley Publishing Company, 1995.  
<https://books.google.de/books?id=i35LALNOGosC>.
- [59] M. Bohm, A. Denner, and H. Joos, *Gauge theories of strong and electroweak interactions; 3rd ed.* B. G. Teubner, Stuttgart, 2001.  
<https://cds.cern.ch/record/1333727>. Trans. of 3rd ed.: Eichtheorien der starken und elektroschwachen Wechselwirkung. Stuttgart, Teubner, 2001.
- [60] T. Kinoshita *Journal of Mathematical Physics* **3** no. 4, (1962) 650–677.  
<http://scitation.aip.org/content/aip/journal/jmp/3/4/10.1063/1.1724268>.
- [61] T. D. Lee and M. Nauenberg *Phys. Rev.* **133** (Mar, 1964) B1549–B1562.  
<http://link.aps.org/doi/10.1103/PhysRev.133.B1549>.
- [62] C. G. Bollini and J. J. Giambiagi *Nuovo Cim.* **B12** (1972) 20–26.
- [63] G. 't Hooft and M. J. G. Veltman *Nucl. Phys.* **B44** (1972) 189–213.
- [64] D. Kreimer [arXiv:hep-ph/9401354](https://arxiv.org/abs/hep-ph/9401354) [hep-ph].
- [65] F. Jegerlehner *Eur. Phys. J.* **C18** (2001) 673–679, [arXiv:hep-th/0005255](https://arxiv.org/abs/hep-th/0005255) [hep-th].
- [66] R. Delbourgo and V. B. Prasad *Journal of Physics G: Nuclear Physics* **1** no. 4, (1975) 377. <http://stacks.iop.org/0305-4616/1/i=4/a=001>.
- [67] W. Beenakker, R. Hopker, and P. M. Zerwas *Phys. Lett.* **B378** (1996) 159–166, [arXiv:hep-ph/9602378](https://arxiv.org/abs/hep-ph/9602378) [hep-ph].
- [68] W. Hollik, E. Kraus, and D. Stockinger *Eur. Phys. J.* **C11** (1999) 365–381, [arXiv:hep-ph/9907393](https://arxiv.org/abs/hep-ph/9907393) [hep-ph].
- [69] W. Hollik and D. Stockinger *Eur. Phys. J.* **C20** (2001) 105–119, [arXiv:hep-ph/0103009](https://arxiv.org/abs/hep-ph/0103009) [hep-ph].
- [70] I. Fischer, W. Hollik, M. Roth, and D. Stockinger *Phys. Rev.* **D69** (2004) 015004, [arXiv:hep-ph/0310191](https://arxiv.org/abs/hep-ph/0310191) [hep-ph].
- [71] W. Siegel *Phys.Lett.* **B84** (1979) 193.
- [72] W. Siegel *Physics Letters B* **94** no. 1, (1980) 37 – 40.  
<http://www.sciencedirect.com/science/article/pii/0370269380908199>.
- [73] D. Stockinger *JHEP* **0503** (2005) 076, [arXiv:hep-ph/0503129](https://arxiv.org/abs/hep-ph/0503129) [hep-ph].
- [74] I. Jack and D. R. T. Jones [arXiv:hep-ph/9707278](https://arxiv.org/abs/hep-ph/9707278) [hep-ph]. [Adv. Ser. Direct. High Energy Phys.21,494(2010)].
- [75] D. Capper, D. Jones, and P. V. Nieuwenhuizen *Nuclear Physics B* **167** no. 3, (1980) 479 – 499.  
<http://www.sciencedirect.com/science/article/pii/0550321380902448>.
- [76] W. Hollik and D. Stockinger *Phys.Lett.* **B634** (2006) 63–68, [arXiv:hep-ph/0509298](https://arxiv.org/abs/hep-ph/0509298) [hep-ph].
- [77] A. Denner *Fortsch. Phys.* **41** (1993) 307–420, [arXiv:0709.1075](https://arxiv.org/abs/0709.1075) [hep-ph].
- [78] D. Ross and J. Taylor *Nuclear Physics B* **51** (1973) 125 – 144.  
<http://www.sciencedirect.com/science/article/pii/0550321373905051>.
- [79] A. Sirlin *Phys. Rev. D* **22** (Aug, 1980) 971–981.  
<http://link.aps.org/doi/10.1103/PhysRevD.22.971>.

- [80] K. I. Aoki, Z. Hioki, M. Konuma, R. Kawabe, and T. Muta *Prog. Theor. Phys. Suppl.* **73** (1982) 1–225.
- [81] G. 't Hooft *Nuclear Physics B* **61** (1973) 455 – 468.  
<http://www.sciencedirect.com/science/article/pii/0550321373903763>.
- [82] W. A. Bardeen, A. J. Buras, D. W. Duke, and T. Muta *Phys. Rev. D* **18** (Dec, 1978) 3998–4017. <http://link.aps.org/doi/10.1103/PhysRevD.18.3998>.
- [83] R. E. Kallosh and I. V. Tyutin *Yad. Fiz.* **17** (1973) 190–209. [Sov. J. Nucl. Phys.17,98(1973)].
- [84] T. Appelquist, J. Carazzone, T. Goldman, and H. R. Quinn *Phys. Rev. D* **8** (Sep, 1973) 1747–1756. <http://link.aps.org/doi/10.1103/PhysRevD.8.1747>.
- [85] G. Costa and T. M. *La Rivista del Nuovo Cimento (1971-1977)* **5** (2007) 29–107.  
<http://dx.doi.org/10.1007/BF02748108>.
- [86] B. W. Lee, “Gauge theories. Course 3,” 1976.  
[http://lss.fnal.gov/cgi-bin/find\\_paper.pl?pub-76-034-T](http://lss.fnal.gov/cgi-bin/find_paper.pl?pub-76-034-T).
- [87] E. Kazes, T. Feuchtwang, P. Cutler, and H. Grotch *Annals of Physics* **142** no. 1, (1982) 80 – 94.  
<http://www.sciencedirect.com/science/article/pii/0003491682902299>.
- [88] P. Gambino and P. A. Grassi *Phys. Rev.* **D62** (2000) 076002, arXiv:hep-ph/9907254 [hep-ph].
- [89] W. Kummer *Eur. Phys. J.* **C21** (2001) 175–179, arXiv:hep-th/0104123 [hep-th].
- [90] H. Lehmann, K. Symanzik, and W. Zimmermann *Nuovo Cimento* **1** (1955) 205.
- [91] K. E. Williams, H. Rzehak, and G. Weiglein *Eur.Phys.J.* **C71** (2011) 1669, arXiv:1103.1335 [hep-ph].
- [92] L. Faddeev and V. Popov *Physics Letters B* **25** no. 1, (1967) 29 – 30.  
<http://www.sciencedirect.com/science/article/pii/0370269367900676>.
- [93] V. Mathieu, “Introduction to the Pinch Technique,” 2008. arXiv:0801.4249 [hep-ph]. <http://inspirehep.net/record/778254/files/arXiv:0801.4249.pdf>.
- [94] D. Binosi and J. Papavassiliou *Phys. Rept.* **479** (2009) 1–152, arXiv:0909.2536 [hep-ph].
- [95] J. M. Cornwall and J. Papavassiliou *Phys. Rev.* **D40** (1989) 3474.
- [96] J. Papavassiliou *Phys. Rev.* **D41** (1990) 3179.
- [97] G. Degrassi and A. Sirlin *Nuclear Physics B* **383** no. 1, (1992) 73 – 92.  
<http://www.sciencedirect.com/science/article/pii/055032139290671W>.
- [98] J. Papavassiliou *Phys. Rev. D* **50** (Nov, 1994) 5958–5970.  
<http://link.aps.org/doi/10.1103/PhysRevD.50.5958>.
- [99] A. Pilaftsis *Nucl. Phys.* **B487** (1997) 467–491, arXiv:hep-ph/9607451 [hep-ph].
- [100] M. Krause, “On the Renormalization of the Two-Higgs-Doublet Model,” Master’s thesis, Karlsruher Institut für Technologie, 2016.  
[https://www.itp.kit.edu/\\_media/publications/masterthesismarcel.pdf](https://www.itp.kit.edu/_media/publications/masterthesismarcel.pdf).
- [101] M. Böhm, H. Spiesberger, and W. Hollik *Fortschritte der Physik* **34** no. 11, (1986) 687–751. <http://dx.doi.org/10.1002/prop.19860341102>.

- [102] J. Fleischer and F. Jegerlehner *Phys. Rev. D* **23** (May, 1981) 2001–2026.  
<http://link.aps.org/doi/10.1103/PhysRevD.23.2001>.
- [103] P. H. Chankowski, S. Pokorski, and J. Rosiek *Nucl. Phys.* **B423** (1994) 437–496,  
[arXiv:hep-ph/9303309](https://arxiv.org/abs/hep-ph/9303309) [hep-ph].
- [104] A. Dabelstein *Z. Phys.* **C67** (1995) 495–512, [arXiv:hep-ph/9409375](https://arxiv.org/abs/hep-ph/9409375) [hep-ph].
- [105] W. Hollik, E. Kraus, M. Roth, C. Rupp, K. Sibold, and D. Stöckinger *Nuclear Physics B* **639** no. 1–2, (2002) 3 – 65.  
<http://www.sciencedirect.com/science/article/pii/S0550321302005382>.
- [106] J. F. Gunion and H. E. Haber *Phys. Rev.* **D67** (2003) 075019,  
[arXiv:hep-ph/0207010](https://arxiv.org/abs/hep-ph/0207010) [hep-ph].
- [107] A. Akeroyd and W. Stirling *Nuclear Physics B* **447** no. 1, (1995) 3 – 17.  
<http://www.sciencedirect.com/science/article/pii/055032139500173P>.
- [108] P. M. Ferreira, L. Lavoura, and J. P. Silva *Phys. Lett.* **B688** (2010) 341–344,  
[arXiv:1001.2561](https://arxiv.org/abs/1001.2561) [hep-ph].
- [109] J.-B. Zuber and C. Itzykson, *Quantum Field Theory*. McGraw-Hill, Inc., 1980.
- [110] K. Fujikawa *Phys. Rev. D* **7** (Jan, 1973) 393–398.  
<http://link.aps.org/doi/10.1103/PhysRevD.7.393>.
- [111] J. Zinn-Justin *Nuclear Physics B* **246** no. 2, (1984) 246 – 252.  
<http://www.sciencedirect.com/science/article/pii/0550321384902955>.
- [112] S. Kanemura, M. Kikuchi, and K. Yagyu *Nucl. Phys.* **B896** (2015) 80–137,  
[arXiv:1502.07716](https://arxiv.org/abs/1502.07716) [hep-ph].
- [113] M. Frank, *Strahlungskorrekturen im Higgs-Sektor des Minimalen Supersymmetrischen Standardmodells mit CP-Verletzung*. PhD thesis, Berlin, 2003.  
<http://swbplus.bsz-bw.de/bsz107705591abs.htm>. Zugl.: Karlsruhe, Univ., Diss., 2002.
- [114] K. Williams and G. Weiglein *Phys.Lett.* **B660** (2008) 217–227, [arXiv:0710.5320](https://arxiv.org/abs/0710.5320) [hep-ph].
- [115] Y. Yamada, “Definition of tan beta beyond tree level,” in *DPF ’96, The Minneapolis Meeting*. 1996. [arXiv:hep-ph/9608382](https://arxiv.org/abs/hep-ph/9608382) [hep-ph].  
<http://www.slac.stanford.edu/spires/find/books/www?cl=QCD161:A6:1996>.
- [116] Y. Yamada *Phys. Lett.* **B530** (2002) 174–178, [arXiv:hep-ph/0112251](https://arxiv.org/abs/hep-ph/0112251) [hep-ph].
- [117] R. Hempfling and B. A. Kniehl *Phys. Rev. D* **51** (Feb, 1995) 1386–1394.  
<http://link.aps.org/doi/10.1103/PhysRevD.51.1386>.
- [118] P. H. Chankowski and P. Wasowicz *Eur. Phys. J.* **C23** (2002) 249–258,  
[arXiv:hep-ph/0110237](https://arxiv.org/abs/hep-ph/0110237) [hep-ph].
- [119] A. Denner and T. Hahn *Nucl. Phys.* **B525** (1998) 27–50, [arXiv:hep-ph/9711302](https://arxiv.org/abs/hep-ph/9711302) [hep-ph].
- [120] A. Denner, S. Dittmaier, M. Roth, and L. H. Wieders *Nucl. Phys.* **B724** (2005) 247–294, [arXiv:hep-ph/0505042](https://arxiv.org/abs/hep-ph/0505042) [hep-ph]. [Erratum: *Nucl. Phys.* **B854**,504(2012)].
- [121] A. Bredenstein, S. Dittmaier, and M. Roth *Eur. Phys. J.* **C44** (2005) 27–49,  
[arXiv:hep-ph/0506005](https://arxiv.org/abs/hep-ph/0506005) [hep-ph].

- [122] A. Denner and S. Dittmaier *Nucl. Phys. Proc. Suppl.* **160** (2006) 22–26, arXiv:hep-ph/0605312 [hep-ph]. [,22(2006)].
- [123] L. Baulieu *Physics Reports* **129** no. 1, (1985) 1 – 74.  
<http://www.sciencedirect.com/science/article/pii/0370157385900912>.
- [124] P. Gambino, P. A. Grassi, and F. Madricardo *Phys. Lett.* **B454** (1999) 98–104, arXiv:hep-ph/9811470 [hep-ph].
- [125] B. A. Kniehl, F. Madricardo, and M. Steinhauser *Phys. Rev.* **D62** (2000) 073010, arXiv:hep-ph/0005060 [hep-ph].
- [126] A. Barroso, L. Brucher, and R. Santos *Phys. Rev.* **D62** (2000) 096003, arXiv:hep-ph/0004136 [hep-ph].
- [127] Y. Yamada *Phys. Rev.* **D64** (2001) 036008, arXiv:hep-ph/0103046 [hep-ph].
- [128] A. Pilaftsis *Phys. Rev.* **D65** (2002) 115013, arXiv:hep-ph/0203210 [hep-ph].
- [129] A. Denner, E. Kraus, and M. Roth *Phys. Rev.* **D70** (2004) 033002, arXiv:hep-ph/0402130 [hep-ph].
- [130] J. R. Espinosa and I. Navarro *Phys. Rev.* **D66** (2002) 016004, arXiv:hep-ph/0109126 [hep-ph].
- [131] J. R. Espinosa and Y. Yamada *Phys. Rev.* **D67** (2003) 036003, arXiv:hep-ph/0207351 [hep-ph].
- [132] N. Baro and F. Boudjema *Phys. Rev.* **D80** (2009) 076010, arXiv:0906.1665 [hep-ph].
- [133] A. Denner and T. Sack *Nuclear Physics B* **347** no. 1, (1990) 203 – 216.  
<http://www.sciencedirect.com/science/article/pii/055032139090557T>.
- [134] C. Becchi, A. Rouet, and R. Stora *Physics Letters B* **52** no. 3, (1974) 344 – 346.  
<http://www.sciencedirect.com/science/article/pii/0370269374900586>.  
C. Becchi, A. Rouet, and R. Stora *Commun. Math. Phys.* **42** (1975) 127–162.  
C. Becchi, A. Rouet, and R. Stora *Annals Phys.* **98** (1976) 287–321.
- [135] I. V. Tyutin arXiv:0812.0580 [hep-th].
- [136] K. P. O. Diener and B. A. Kniehl *Nucl. Phys.* **B617** (2001) 291–307, arXiv:hep-ph/0109110 [hep-ph].
- [137] Y. Zhou *Phys. Lett.* **B577** (2003) 67–70, arXiv:hep-ph/0304003 [hep-ph].
- [138] A. Freitas and D. Stockinger *Phys. Rev.* **D66** (2002) 095014, arXiv:hep-ph/0205281 [hep-ph].
- [139] M. Steinhauser *Phys. Lett.* **B429** (1998) 158–161, arXiv:hep-ph/9803313 [hep-ph].
- [140] K. Hagiwara, A. D. Martin, D. Nomura, and T. Teubner *Phys. Rev.* **D69** (2004) 093003, arXiv:hep-ph/0312250 [hep-ph].
- [141] F. Jegerlehner *Nuovo Cim.* **C034S1** (2011) 31–40, arXiv:1107.4683 [hep-ph].
- [142] G. Passarino and M. Veltman *Nuclear Physics B* **160** no. 1, (1979) 151 – 207.  
<http://www.sciencedirect.com/science/article/pii/0550321379902347>.
- [143] F. Jegerlehner, M. Yu. Kalmykov, and B. A. Kniehl *Phys. Lett.* **B722** (2013) 123–129, arXiv:1212.4319 [hep-ph].

- [144] F. Jegerlehner, M. Yu. Kalmykov, and O. Veretin *Nucl. Phys.* **B641** (2002) 285–326, [arXiv:hep-ph/0105304](https://arxiv.org/abs/hep-ph/0105304) [hep-ph].
- [145] M. Hirsch, M. A. Díaz, W. Porod, J. C. Romão, and J. W. F. Valle *Phys. Rev. D* **62** (Nov, 2000) 113008. <http://link.aps.org/doi/10.1103/PhysRevD.62.113008>.
- [146] R. Tarrach *Nuclear Physics B* **183** no. 3, (1981) 384 – 396. <http://www.sciencedirect.com/science/article/pii/0550321381901401>.
- [147] A. S. Kronfeld *Phys. Rev.* **D58** (1998) 051501, [arXiv:hep-ph/9805215](https://arxiv.org/abs/hep-ph/9805215) [hep-ph].
- [148] R. Lorenz, “Full One-Loop Electroweak Corrections to the Decays  $H^+ \rightarrow W^+ h/H$  in the Two-Higgs-Doublet Model,” Master’s thesis, Karlsruhe Institut für Technologie, Jun, 2015. <https://www.itp.kit.edu/prep/diploma/PSFiles/MasterRobinL.pdf>.
- [149] R. Santos, A. Barroso, and L. Brucher *Phys. Lett.* **B391** (1997) 429–433, [arXiv:hep-ph/9608376](https://arxiv.org/abs/hep-ph/9608376) [hep-ph].
- [150] J. A. Coarasa Perez, D. Garcia, J. Guasch, R. A. Jimenez, and J. Sola *Eur. Phys. J.* **C2** (1998) 373–392, [arXiv:hep-ph/9607485](https://arxiv.org/abs/hep-ph/9607485) [hep-ph].
- [151] T. Hahn, *FormCalc 9.2 User’s Guide*. Thomas Hahn, 2016. [www.feynarts.de/formcalc/FC8Guide.pdf](http://www.feynarts.de/formcalc/FC8Guide.pdf).
- [152] T. Hahn *Comput.Phys.Commun.* **140** (2001) 418–431, [arXiv:hep-ph/0012260](https://arxiv.org/abs/hep-ph/0012260) [hep-ph].
- [153] T. Hahn and M. Perez-Victoria *Comput. Phys. Commun.* **118** (1999) 153–165, [arXiv:hep-ph/9807565](https://arxiv.org/abs/hep-ph/9807565) [hep-ph].
- [154] T. Hahn and M. Perez-Victoria *Comput.Phys.Commun.* **118** (1999) 153–165, [arXiv:hep-ph/9807565](https://arxiv.org/abs/hep-ph/9807565) [hep-ph].
- [155] **LHC Higgs Cross Section Working Group** Collaboration, S. Dittmaier *et al.* [arXiv:1101.0593](https://arxiv.org/abs/1101.0593) [hep-ph].
- [156] A. Denner, S. Dittmaier, M. Grazzini, R. V. Harlander, R. S. Thorne, M. Spira, and M. Steinhauser. <https://cds.cern.ch/record/2047636>.
- [157] HXSWG, “<https://twiki.cern.ch/twiki/bin/view/lhcphysics/lhchxswgsminputparameter>.”
- [158] R. Coimbra, M. O. P. Sampaio, and R. Santos *Eur. Phys. J.* **C73** (2013) 2428, [arXiv:1301.2599](https://arxiv.org/abs/1301.2599) [hep-ph].
- [159] P. M. Ferreira, R. Guedes, M. O. P. Sampaio, and R. Santos *JHEP* **12** (2014) 067, [arXiv:1409.6723](https://arxiv.org/abs/1409.6723) [hep-ph].
- [160] A. Barroso, P. M. Ferreira, I. P. Ivanov, and R. Santos *JHEP* **06** (2013) 045, [arXiv:1303.5098](https://arxiv.org/abs/1303.5098) [hep-ph].
- [161] A. G. Akeroyd, A. Arhrib, and E.-M. Naimi *Phys. Lett.* **B490** (2000) 119–124, [arXiv:hep-ph/0006035](https://arxiv.org/abs/hep-ph/0006035) [hep-ph].
- [162] S. Kanemura, T. Kubota, and E. Takasugi *Phys. Lett.* **B313** (1993) 155–160, [arXiv:hep-ph/9303263](https://arxiv.org/abs/hep-ph/9303263) [hep-ph].
- [163] M. E. Peskin and T. Takeuchi *Phys. Rev.* **D46** (1992) 381–409.
- [164] C. D. Froggatt, R. G. Moorhouse, and I. G. Knowles *Phys. Rev. D* **45** (Apr, 1992) 2471–2481. <http://link.aps.org/doi/10.1103/PhysRevD.45.2471>.

- [165] W. Grimus, L. Lavoura, O. M. Ogreid, and P. Osland *Nucl. Phys.* **B801** (2008) 81–96, arXiv:0802.4353 [hep-ph].
- [166] H. E. Haber and D. O’Neil *Phys. Rev.* **D83** (2011) 055017, arXiv:1011.6188 [hep-ph].
- [167] **Tevatron Electroweak Working Group, CDF, DELPHI, SLD Electroweak and Heavy Flavour Groups, ALEPH, LEP Electroweak Working Group, SLD, OPAL, D0, L3** Collaboration, L. E. W. Group arXiv:1012.2367 [hep-ex].
- [168] M. Baak, M. Goebel, J. Haller, A. Hoecker, D. Ludwig, K. Moenig, M. Schott, and J. Stelzer *Eur. Phys. J.* **C72** (2012) 2003, arXiv:1107.0975 [hep-ph].
- [169] M. Baak, M. Goebel, J. Haller, A. Hoecker, D. Kennedy, R. Kogler, K. Moenig, M. Schott, and J. Stelzer *Eur. Phys. J.* **C72** (2012) 2205, arXiv:1209.2716 [hep-ph].
- [170] F. Mahmoudi and O. Stal *Phys. Rev.* **D81** (2010) 035016, arXiv:0907.1791 [hep-ph].
- [171] O. Deschamps, S. Descotes-Genon, S. Monteil, V. Niess, S. T’Jampens, and V. Tisserand *Phys. Rev.* **D82** (2010) 073012, arXiv:0907.5135 [hep-ph].
- [172] T. Hermann, M. Misiak, and M. Steinhauser *JHEP* **11** (2012) 036, arXiv:1208.2788 [hep-ph].
- [173] A. Denner, R. J. Guth, W. Hollik, and J. H. Kuhn *Z. Phys.* **C51** (1991) 695–705.
- [174] A. K. Grant *Phys. Rev.* **D51** (1995) 207–217, arXiv:hep-ph/9410267 [hep-ph].
- [175] H. E. Haber and H. E. Logan *Phys. Rev.* **D62** (2000) 015011, arXiv:hep-ph/9909335 [hep-ph].
- [176] A. Freitas and Y.-C. Huang *JHEP* **08** (2012) 050, arXiv:1205.0299 [hep-ph]. [Erratum: JHEP10,044(2013)].
- [177] M. Misiak *et al.* *Phys. Rev. Lett.* **114** no. 22, (2015) 221801, arXiv:1503.01789 [hep-ph].
- [178] **LEP, DELPHI, OPAL, ALEPH, L3** Collaboration, G. Abbiendi *et al.* *Eur. Phys. J.* **C73** (2013) 2463, arXiv:1301.6065 [hep-ex].
- [179] **ATLAS** Collaboration, G. Aad *et al.* *JHEP* **03** (2015) 088, arXiv:1412.6663 [hep-ex].
- [180] **CMS** Collaboration, V. Khachatryan *et al.* *JHEP* **11** (2015) 018, arXiv:1508.07774 [hep-ex].
- [181] **ATLAS** Collaboration, G. Aad *et al.* *JHEP* **03** (2016) 127, arXiv:1512.03704 [hep-ex].
- [182] R. V. Harlander, S. Liebler, and H. Mantler *Comput. Phys. Commun.* **184** (2013) 1605–1617, arXiv:1212.3249 [hep-ph].
- [183] A. Djouadi, J. Kalinowski, and M. Spira *Computer Physics Communications* **108** no. 1, (1998) 56 – 74.  
<http://www.sciencedirect.com/science/article/pii/S0010465597001239>.
- [184] J. M. Butterworth *et al.*, “THE TOOLS AND MONTE CARLO WORKING GROUP Summary Report from the Les Houches 2009 Workshop on TeV Colliders,” in *Physics*

- at TeV colliders. *Proceedings, 6th Workshop, dedicated to Thomas Binoth, Les Houches, France, June 8-26, 2009*. 2010. arXiv:1003.1643 [hep-ph].  
<https://inspirehep.net/record/848006/files/arXiv:1003.1643.pdf>.
- [185] HXSWG, “<https://twiki.cern.ch/twiki/bin/view/lhcphysics/crosssections>.”
- [186] P. Bechtle, O. Brein, S. Heinemeyer, G. Weiglein, and K. E. Williams *Comput.Phys.Commun.* **181** (2010) 138–167, arXiv:0811.4169 [hep-ph].
- [187] P. Bechtle, O. Brein, S. Heinemeyer, G. Weiglein, and K. E. Williams *Comput.Phys.Commun.* **182** (2011) 2605–2631, arXiv:1102.1898 [hep-ph].
- [188] P. Bechtle, O. Brein, S. Heinemeyer, O. Stål, T. Stefaniak, *et al.* *Eur.Phys.J.* **C74** (2014) 2693, arXiv:1311.0055 [hep-ph].
- [189] P. Bechtle, S. Heinemeyer, O. Stål, T. Stefaniak, and G. Weiglein *Eur.Phys.J.* **C74** (2014) 2711, arXiv:1305.1933 [hep-ph].
- [190] S. Kanemura, S. Kiyoura, Y. Okada, E. Senaha, and C.-P. Yuan *Physics Letters B* **558** no. 3–4, (2003) 157 – 164.  
<http://www.sciencedirect.com/science/article/pii/S0370269303002685>.
- [191] P. M. Ferreira, R. Santos, J. F. Gunion, and H. E. Haber *Phys. Rev. D* **89** (Jun, 2014) 115003. <http://link.aps.org/doi/10.1103/PhysRevD.89.115003>.
- [192] P. M. Ferreira, R. Guedes, J. F. Gunion, H. E. Haber, M. O. P. Sampaio, and R. Santos, “The CP-conserving 2HDM after the 8 TeV run,” in *Proceedings, 22nd International Workshop on Deep-Inelastic Scattering and Related Subjects (DIS 2014)*. 2014. arXiv:1407.4396 [hep-ph].
- [193] P. M. Ferreira, R. Guedes, J. F. Gunion, H. E. Haber, M. O. P. Sampaio, and R. Santos, “The Wrong Sign limit in the 2HDM,” in *Proceedings, 2nd Conference on Large Hadron Collider Physics Conference (LHCP 2014)*. 2014. arXiv:1410.1926 [hep-ph].
- [194] B. Dumont, J. F. Gunion, Y. Jiang, and S. Kraml *Phys. Rev.* **D90** (2014) 035021, arXiv:1405.3584 [hep-ph].
- [195] D. Fontes, J. C. Romão, and J. P. Silva *Phys. Rev.* **D90** no. 1, (2014) 015021, arXiv:1406.6080 [hep-ph].
- [196] D. Fontes, J. C. Romão, and J. P. Silva *JHEP* **12** (2014) 043, arXiv:1408.2534 [hep-ph].
- [197] T. Plehn and M. Rauch *Phys. Rev.* **D72** (2005) 053008, arXiv:hep-ph/0507321 [hep-ph].
- [198] A. Djouadi, W. Kilian, M. Mühlleitner, and P. Zerwas *Eur.Phys.J.* **C10** (1999) 27–43, arXiv:hep-ph/9903229 [hep-ph].
- [199] A. Djouadi, W. Kilian, M. Mühlleitner, and P. Zerwas *Eur.Phys.J.* **C10** (1999) 45–49, arXiv:hep-ph/9904287 [hep-ph].
- [200] M. M. Mühlleitner arXiv:hep-ph/0101262 [hep-ph]. [AIP Conf. Proc.578,253(2001)].
- [201] M. J. Dolan, C. Englert, and M. Spannowsky *JHEP* **10** (2012) 112, arXiv:1206.5001 [hep-ph].

- [202] J. Baglio, A. Djouadi, R. Gröber, M. Mühlleitner, J. Quevillon, and M. Spira *Journal of High Energy Physics* **2013** no. 4, (2013) 1–40.
- [203] F. Goertz, A. Papaefstathiou, L. L. Yang, and J. Zurita *JHEP* **06** (2013) 016, [arXiv:1301.3492 \[hep-ph\]](#).
- [204] S. Dawson *et al.*, “Working Group Report: Higgs Boson,” in *Community Summer Study 2013: Snowmass on the Mississippi (CSS2013) Minneapolis, MN, USA, July 29-August 6, 2013*. 2013. [arXiv:1310.8361 \[hep-ex\]](#).  
<https://inspirehep.net/record/1262795/files/arXiv:1310.8361.pdf>.
- [205] V. Barger, L. L. Everett, C. Jackson, and G. Shaughnessy *Physics Letters B* **728** (2014) 433 – 436.  
<http://www.sciencedirect.com/science/article/pii/S037026931300988X>.
- [206] D. E. Ferreira de Lima, A. Papaefstathiou, and M. Spannowsky *JHEP* **08** (2014) 030, [arXiv:1404.7139 \[hep-ph\]](#).
- [207] K. Fujii *et al.* [arXiv:1506.05992 \[hep-ex\]](#).
- [208] W. Yao, “Studies of measuring Higgs self-coupling with  $HH \rightarrow b\bar{b}\gamma\gamma$  at the future hadron colliders,” in *Community Summer Study 2013: Snowmass on the Mississippi (CSS2013) Minneapolis, MN, USA, July 29-August 6, 2013*. 2013. [arXiv:1308.6302 \[hep-ph\]](#).  
<https://inspirehep.net/record/1251544/files/arXiv:1308.6302.pdf>.
- [209] A. Azatov, R. Contino, G. Panico, and M. Son *Phys. Rev.* **D92** no. 3, (2015) 035001, [arXiv:1502.00539 \[hep-ph\]](#).
- [210] R. S. Gupta, H. Rzehak, and J. D. Wells *Phys. Rev.* **D88** (2013) 055024, [arXiv:1305.6397 \[hep-ph\]](#).
- [211] R. Grober, M. Mühlleitner, and M. Spira *JHEP* **06** (2016) 080, [arXiv:1602.05851 \[hep-ph\]](#).
- [212] R. Costa, M. Mühlleitner, M. O. P. Sampaio, and R. Santos *JHEP* **06** (2016) 034, [arXiv:1512.05355 \[hep-ph\]](#).
- [213] A. Agostini, G. Degrassi, R. Gröber, and P. Slavich *JHEP* **04** (2016) 106, [arXiv:1601.03671 \[hep-ph\]](#).
- [214] W. Hollik and S. Penaranda *Eur.Phys.J.* **C23** (2002) 163–172, [arXiv:hep-ph/0108245 \[hep-ph\]](#).
- [215] F. Boudjema and A. Semenov *Phys. Rev.* **D66** (2002) 095007, [arXiv:hep-ph/0201219 \[hep-ph\]](#).
- [216] A. Dobado, M. J. Herrero, W. Hollik, and S. Penaranda *Phys. Rev.* **D66** (2002) 095016, [arXiv:hep-ph/0208014 \[hep-ph\]](#).
- [217] A. Dobado, M. J. Herrero, W. Hollik, and S. Penaranda, “Quantum effects to the Higgs boson selfcouplings in the SM and in the MSSM,” in *Supersymmetry and unification of fundamental interactions. Proceedings, 10th International Conference, SUSY’02, Hamburg, Germany, June 17-23, 2002*, pp. 784–790. 2002.  
[arXiv:hep-ph/0210315 \[hep-ph\]](#). [http://www-library.desy.de/preparch/desy/proc/proc02-02/Proceedings/pa.1a/penaranda\\_pr.pdf](http://www-library.desy.de/preparch/desy/proc/proc02-02/Proceedings/pa.1a/penaranda_pr.pdf).
- [218] U. Ellwanger *Phys.Lett.* **B303** (1993) 271–276, [arXiv:hep-ph/9302224 \[hep-ph\]](#).

- [219] T. Elliott, S. King, and P. White *Phys.Lett.* **B305** (1993) 71–77, [arXiv:hep-ph/9302202](#) [hep-ph].
- [220] T. Elliott, S. King, and P. White *Phys.Lett.* **B314** (1993) 56–63, [arXiv:hep-ph/9305282](#) [hep-ph].
- [221] P. Pandita *Z.Phys.* **C59** (1993) 575–584.
- [222] T. Elliott, S. King, and P. White *Phys.Rev.* **D49** (1994) 2435–2456, [arXiv:hep-ph/9308309](#) [hep-ph].
- [223] U. Ellwanger and C. Hugonie *Phys.Lett.* **B623** (2005) 93–103, [arXiv:hep-ph/0504269](#) [hep-ph].
- [224] G. Degrassi and P. Slavich *Nucl.Phys.* **B825** (2010) 119–150, [arXiv:0907.4682](#) [hep-ph].
- [225] F. Staub, W. Porod, and B. Herrmann *JHEP* **1010** (2010) 040, [arXiv:1007.4049](#) [hep-ph].
- [226] K. Ender, T. Graf, M. Mühlleitner, and H. Rzehak *Phys.Rev.* **D85** (2012) 075024, [arXiv:1111.4952](#) [hep-ph].
- [227] M. D. Goodsell, K. Nickel, and F. Staub *Eur. Phys. J.* **C75** no. 1, (2015) 32, [arXiv:1411.0675](#) [hep-ph].
- [228] M. D. Goodsell, K. Nickel, and F. Staub *Phys.Rev.* **D91** no. 3, (2015) 035021, [arXiv:1411.4665](#) [hep-ph].
- [229] M. Goodsell, K. Nickel, and F. Staub *Eur. Phys. J.* **C75** no. 6, (2015) 290, [arXiv:1503.03098](#) [hep-ph].
- [230] P. Drechsel, L. Galeta, S. Heinemeyer, and G. Weiglein [arXiv:1601.08100](#) [hep-ph].
- [231] S. Ham, J. Kim, S. Oh, and D. Son *Phys.Rev.* **D64** (2001) 035007, [arXiv:hep-ph/0104144](#) [hep-ph].
- [232] S. Ham, S. Oh, and D. Son *Phys.Rev.* **D65** (2002) 075004, [arXiv:hep-ph/0110052](#) [hep-ph].
- [233] S. Ham, Y. Jeong, and S. Oh [arXiv:hep-ph/0308264](#) [hep-ph].
- [234] S. Ham, S. Kim, S. OH, and D. Son *Phys.Rev.* **D76** (2007) 115013, [arXiv:0708.2755](#) [hep-ph].
- [235] K. Funakubo and S. Tao *Prog.Theor.Phys.* **113** (2005) 821–842, [arXiv:hep-ph/0409294](#) [hep-ph].
- [236] T. Graf, R. Grober, M. Mühlleitner, H. Rzehak, and K. Walz *JHEP* **1210** (2012) 122, [arXiv:1206.6806](#) [hep-ph].
- [237] V. Barger, M. S. Berger, A. L. Stange, and R. J. N. Phillips *Phys. Rev. D* **45** (Jun, 1992) 4128–4147. <http://link.aps.org/doi/10.1103/PhysRevD.45.4128>.
- [238] A. Brignole and F. Zwirner *Physics Letters B* **299** no. 1, (1993) 72 – 82. <http://www.sciencedirect.com/science/article/pii/037026939390885L>.
- [239] P. Fayet *Nucl.Phys.* **B90** (1975) 104–124.
- [240] R. D. Peccei and H. R. Quinn *Phys. Rev. Lett.* **38** (Jun, 1977) 1440–1443. <http://link.aps.org/doi/10.1103/PhysRevLett.38.1440>.

- [241] R. D. Peccei and H. R. Quinn *Phys. Rev. D* **16** (Sep, 1977) 1791–1797.  
<http://link.aps.org/doi/10.1103/PhysRevD.16.1791>.
- [242] S. King, M. Mühlleitner, R. Nevzorov, and K. Walz *Nuclear Physics B* **870** no. 2, (2013) 323 – 352.  
<http://www.sciencedirect.com/science/article/pii/S0550321313000576>.
- [243] S. King, M. Mühlleitner, R. Nevzorov, and K. Walz *Phys.Rev.* **D90** no. 9, (2014) 095014, [arXiv:1408.1120](https://arxiv.org/abs/1408.1120) [hep-ph].
- [244] J. Kozaczuk and S. Profumo *Phys. Rev.* **D89** no. 9, (2014) 095012, [arXiv:1308.5705](https://arxiv.org/abs/1308.5705) [hep-ph].
- [245] J. Cao, C. Han, L. Wu, P. Wu, and J. M. Yang *JHEP* **05** (2014) 056, [arXiv:1311.0678](https://arxiv.org/abs/1311.0678) [hep-ph].
- [246] C. Cheung, M. Papucci, D. Sanford, N. R. Shah, and K. M. Zurek *Phys. Rev.* **D90** no. 7, (2014) 075011, [arXiv:1406.6372](https://arxiv.org/abs/1406.6372) [hep-ph].
- [247] R. Enberg, S. Munir, C. Pérez de los Heros, and D. Werder [arXiv:1506.05714](https://arxiv.org/abs/1506.05714) [hep-ph].
- [248] **DAMA** Collaboration, R. Bernabei *et al.* *Eur. Phys. J.* **C56** (2008) 333–355, [arXiv:0804.2741](https://arxiv.org/abs/0804.2741) [astro-ph].
- [249] **CoGeNT Collaboration** Collaboration, C. E. Aalseth *et al.* *Phys. Rev. Lett.* **106** (Mar, 2011) 131301. <http://link.aps.org/doi/10.1103/PhysRevLett.106.131301>.
- [250] **CoGeNT Collaboration** Collaboration, C. E. Aalseth *et al.* *Phys. Rev. Lett.* **107** (Sep, 2011) 141301. <http://link.aps.org/doi/10.1103/PhysRevLett.107.141301>.
- [251] **Fermi-LAT** Collaboration, M. Ackermann *et al.* *Phys. Rev.* **D86** (2012) 022002, [arXiv:1205.2739](https://arxiv.org/abs/1205.2739) [astro-ph.HE].
- [252] G. e. a. Angloher *The European Physical Journal C* **72** no. 4, (2012) 1–22.  
<http://dx.doi.org/10.1140/epjc/s10052-012-1971-8>.
- [253] **CDMS** Collaboration, R. Agnese *et al.* *Phys. Rev. Lett.* **111** no. 25, (2013) 251301, [arXiv:1304.4279](https://arxiv.org/abs/1304.4279) [hep-ex].
- [254] **XENON100 Collaboration** Collaboration, E. e. a. Aprile *Phys. Rev. Lett.* **109** (Nov, 2012) 181301. <http://link.aps.org/doi/10.1103/PhysRevLett.109.181301>.
- [255] **LUX** Collaboration, D. S. Akerib *et al.* *Phys. Rev. Lett.* **112** (2014) 091303, [arXiv:1310.8214](https://arxiv.org/abs/1310.8214) [astro-ph.CO].
- [256] S. Heinemeyer, H. Rzehak, and C. Schappacher *Phys.Rev.* **D82** (2010) 075010, [arXiv:1007.0689](https://arxiv.org/abs/1007.0689) [hep-ph].
- [257] L. V. Avdeev and M. Yu. Kalmykov *Nucl. Phys.* **B502** (1997) 419–435, [arXiv:hep-ph/9701308](https://arxiv.org/abs/hep-ph/9701308) [hep-ph].
- [258] M. Carena, D. Garcia, U. Nierste, and C. E. M. Wagner *Nucl. Phys.* **B577** (2000) 88–120, [arXiv:hep-ph/9912516](https://arxiv.org/abs/hep-ph/9912516) [hep-ph].
- [259] K. Melnikov and T. v. Ritbergen *Phys. Lett.* **B482** (2000) 99–108, [arXiv:hep-ph/9912391](https://arxiv.org/abs/hep-ph/9912391) [hep-ph].
- [260] R. Harlander, P. Kant, L. Mihaila, and M. Steinhauser *JHEP* **09** (2006) 053, [arXiv:hep-ph/0607240](https://arxiv.org/abs/hep-ph/0607240) [hep-ph].

- [261] R. V. Harlander, L. Mihaila, and M. Steinhauser *Phys. Rev.* **D76** (2007) 055002, [arXiv:0706.2953 \[hep-ph\]](#).
- [262] S. Borowka, T. Hahn, S. Heinemeyer, G. Heinrich, and W. Hollik *Eur. Phys. J.* **C74** no. 8, (2014) 2994, [arXiv:1404.7074 \[hep-ph\]](#).
- [263] G. Degrassi, S. Di Vita, and P. Slavich *Eur. Phys. J.* **C75** no. 2, (2015) 61, [arXiv:1410.3432 \[hep-ph\]](#).
- [264] M. Sperling, D. Stöckinger, and A. Voigt *JHEP* **07** (2013) 132, [arXiv:1305.1548 \[hep-ph\]](#).
- [265] M. Sperling, D. Stöckinger, and A. Voigt *JHEP* **01** (2014) 068, [arXiv:1310.7629 \[hep-ph\]](#).
- [266] S. Coleman and E. Weinberg *Phys. Rev. D* **7** (Mar, 1973) 1888–1910. <http://link.aps.org/doi/10.1103/PhysRevD.7.1888>.
- [267] J. Iliopoulos, C. Itzykson, and A. Martin *Rev. Mod. Phys.* **47** (Jan, 1975) 165–192. <http://link.aps.org/doi/10.1103/RevModPhys.47.165>.
- [268] M. Sher *Phys.Rept.* **179** (1989) 273–418.
- [269] R. Jackiw *Phys. Rev. D* **9** (Mar, 1974) 1686–1701. <http://link.aps.org/doi/10.1103/PhysRevD.9.1686>.
- [270] S. P. Martin *Phys.Rev.* **D65** (2002) 116003, [arXiv:hep-ph/0111209 \[hep-ph\]](#).
- [271] S. P. Martin *Phys. Rev.* **D66** (2002) 096001, [arXiv:hep-ph/0206136 \[hep-ph\]](#).
- [272] S. Weinberg *Phys. Rev. D* **7** (May, 1973) 2887–2910. <http://link.aps.org/doi/10.1103/PhysRevD.7.2887>.
- [273] S. Lee and A. M. Sziacaluga *Nucl.Phys.* **B96** (1975) 435.
- [274] M. Bobrowski, G. Chalons, W. G. Hollik, and U. Nierste *Phys. Rev.* **D90** no. 3, (2014) 035025, [arXiv:1407.2814 \[hep-ph\]](#). [Erratum: *Phys. Rev.* **D92**,no.5,059901(2015)].
- [275] M. Brucherseifer, R. Gavin, and M. Spira *Phys.Rev.* **D90** no. 11, (2014) 117701, [arXiv:1309.3140 \[hep-ph\]](#).
- [276] R. Mertig, M. Bohm, and A. Denner *Computer Physics Communications* **64** no. 3, (1991) 345 – 359. <http://www.sciencedirect.com/science/article/pii/001046559190130D>.
- [277] V. Shtabovenko, R. Mertig, and F. Orellana [arXiv:1601.01167 \[hep-ph\]](#).
- [278] I. Wolfram Research *Wolfram Research, Inc., Champaign, Illinois* (2010) .
- [279] R. Mertig and R. Scharf *Comput.Phys.Commun.* **111** (1998) 265–273, [arXiv:hep-ph/9801383 \[hep-ph\]](#).
- [280] O. Tarasov *Phys.Rev.* **D54** (1996) 6479–6490, [arXiv:hep-th/9606018 \[hep-th\]](#).
- [281] O. Tarasov *Nucl.Phys.* **B502** (1997) 455–482, [arXiv:hep-ph/9703319 \[hep-ph\]](#).
- [282] G. 't Hooft and M. Veltman *Nuclear Physics B* **153** (1979) 365 – 401. <http://www.sciencedirect.com/science/article/pii/0550321379906059>.
- [283] C. Ford, I. Jack, and D. Jones *Nucl.Phys.* **B387** (1992) 373–390, [arXiv:hep-ph/0111190 \[hep-ph\]](#).

- [284] A. I. Davydychev and J. Tausk *Nucl.Phys.* **B397** (1993) 123–142.
- [285] R. Scharf and J. Tausk *Nucl.Phys.* **B412** (1994) 523–552.
- [286] G. Weiglein, R. Scharf, and M. Bohm *Nucl.Phys.* **B416** (1994) 606–644, [arXiv:hep-ph/9310358](https://arxiv.org/abs/hep-ph/9310358) [hep-ph].
- [287] F. A. Berends and J. Tausk *Nucl.Phys.* **B421** (1994) 456–470.
- [288] S. P. Martin *Phys.Rev.* **D65** (2002) 116003, [arXiv:hep-ph/0111209](https://arxiv.org/abs/hep-ph/0111209) [hep-ph].
- [289] S. P. Martin and D. G. Robertson *Comput.Phys.Commun.* **174** (2006) 133–151, [arXiv:hep-ph/0501132](https://arxiv.org/abs/hep-ph/0501132) [hep-ph].
- [290] K. Walz, *The Higgs Sector of the (Complex) NMSSM - Higher Order Corrections and Phenomenological Discussions*. PhD thesis, Karlsruher Institut für Technologie, 2015. <http://digbib.ubka.uni-karlsruhe.de/volltexte/1000047996>.
- [291] K. E. Williams, *The Higgs Sector of the Complex Minimal Supersymmetric Standard Model*. PhD thesis, Durham University, 2008. <http://etheses.dur.ac.uk/2129/>.
- [292] J. Baglio, R. Grober, M. Mühlleitner, D. Nhung, H. Rzehak, *et al.* *Comput.Phys.Commun.* **185** no. 12, (2014) 3372–3391, [arXiv:1312.4788](https://arxiv.org/abs/1312.4788) [hep-ph].
- [293] **ATLAS Collaboration** Collaboration, G. Aad *et al.* *Phys.Lett.* **B720** (2013) 13–31, [arXiv:1209.2102](https://arxiv.org/abs/1209.2102) [hep-ex].
- CMS Collaboration** Collaboration, S. Chatrchyan *et al.* *Eur.Phys.J.* **C73** no. 12, (2013) 2677, [arXiv:1308.1586](https://arxiv.org/abs/1308.1586) [hep-ex].
- ATLAS Collaboration**, G. Aad *et al.* *JHEP* **1310** (2013) 189, [arXiv:1308.2631](https://arxiv.org/abs/1308.2631) [hep-ex].
- CMS Collaboration** Collaboration, S. Chatrchyan *et al.* *JHEP* **1401** (2014) 163, [arXiv:1311.6736](https://arxiv.org/abs/1311.6736).
- CMS Collaboration** Collaboration, S. Chatrchyan *et al.* *Phys.Rev.Lett.* **112** (2014) 161802, [arXiv:1312.3310](https://arxiv.org/abs/1312.3310) [hep-ex].
- ATLAS Collaboration** Collaboration, G. Aad *et al.* *JHEP* **1406** (2014) 124, [arXiv:1403.4853](https://arxiv.org/abs/1403.4853) [hep-ex].
- ATLAS Collaboration** Collaboration, G. Aad *et al.* *JHEP* **1409** (2014) 176, [arXiv:1405.7875](https://arxiv.org/abs/1405.7875) [hep-ex].
- ATLAS Collaboration** Collaboration, G. Aad *et al.* *JHEP* **1409** (2014) 015, [arXiv:1406.1122](https://arxiv.org/abs/1406.1122) [hep-ex].
- ATLAS Collaboration** Collaboration, G. Aad *et al.* [arXiv:1407.0583](https://arxiv.org/abs/1407.0583) [hep-ex].
- ATLAS Collaboration**, G. Aad *et al.* *JHEP* **11** (2014) 056, [arXiv:1409.6064](https://arxiv.org/abs/1409.6064) [hep-ex].
- [294] P. Z. Skands, B. Allanach, H. Baer, C. Balazs, G. Belanger, *et al.* *JHEP* **0407** (2004) 036, [arXiv:hep-ph/0311123](https://arxiv.org/abs/hep-ph/0311123) [hep-ph].
- [295] B. Allanach, C. Balazs, G. Belanger, M. Bernhardt, F. Boudjema, *et al.* *Comput.Phys.Commun.* **180** (2009) 8–25, [arXiv:0801.0045](https://arxiv.org/abs/0801.0045) [hep-ph].
- [296] K. G. Chetyrkin, J. H. Kuhn, and M. Steinhauser *Comput. Phys. Commun.* **133** (2000) 43–65, [arXiv:hep-ph/0004189](https://arxiv.org/abs/hep-ph/0004189) [hep-ph].

- 
- [297] H. Baer, J. Ferrandis, K. Melnikov, and X. Tata *Phys. Rev.* **D66** (2002) 074007, [arXiv:hep-ph/0207126](#) [hep-ph].
- [298] F. Staub, P. Athron, U. Ellwanger, R. Gröber, M. Mühlleitner, P. Slavich, and A. Voigt *Comput. Phys. Commun.* **202** (2016) 113–130, [arXiv:1507.05093](#) [hep-ph].
- [299] S. F. King, M. Mühlleitner, R. Nevzorov, and K. Walz *Nucl. Phys.* **B901** (2015) 526–555, [arXiv:1508.03255](#) [hep-ph].